Phosphorylation of Olig2 and the control of stem cell fate choice in the developing spinal cord

Alexander Sinclair-Wilson

A thesis submitted to University College London for the degree of Doctor of Philosophy

DECLARATION

I, Alexander Sinclair-Wilson, confirm that the work presented in this thesis is my own. Where information has been derived from other sources, I confirm that this has been indicated in the thesis.

ACKNOWLEDGEMENTS

I would like to thank Prof. William D. Richardson, in whose lab I have worked for the last four years. The support and guidance I have received has been vital and I am extremely grateful for his outstanding supervision. I am also indebted to all the members – past and present – of the Richardson Lab. In particular, Dr Huiliang Li and Dr Ursula Grazini have been wonderful teachers and I have learnt a tremendous amount working alongside them both. Matthew Grist and Ulla Dennehy have provided excellent technical support in the lab and BSU, respectively. Finally, Paul, Eleni, Sarah, Marcio, Alex and Alejandra each deserve a mention for the huge part they have all played in making the time I have spent at UCL so interesting and enjoyable.

At Yale, Prof. Anne Eichmann and Prof. Jean-Leon Thomas provided the unique opportunity to work in the United States. The engaging research I did and attentive supervision I received as a member of the Eichmann and Thomas Labs made the time I spent at Yale brilliant. Of the many people I worked alongside so easily and enjoyably, Jinah Han deserves a special thank you for looking after me and making me feel so welcome.

Finally, I would like to thank my dad, Jonathan, my mum, Charlotte and my little sister, Rosa, as well as my close friends (Yas, Rohin, Jamie, Charlie, Steve, Tom, Suni, Cian, Ollie, Will and Anya) for their support and encouragement over the years.

ABSTRACT

Oligodendrocytes (OLs) are the myelinating cells of the central nervous system (CNS), ensheathing axons and enabling the rapid conduction of nerve impulses. In CNS development, lineage-restricted OL precursors (OLPs) arise in discrete regions of the ventricular zone under strict spatial and temporal control. In the embryonic spinal cord, for example, the majority of OLPs derive from a subpopulation of neural stem cells (NSCs) residing in the ventral progenitor of motor neurons (pMN) domain. These pMN domain NSCs are characterized by expression of the basic helix-loop-helix (HLH) transcription factor Olig2 and are also responsible for the generation of all spinal motor neurons (MNs). MN generation precedes OLP generation and it has been shown that phosphorylation of serine 147 (S147) in the HLH domain of Olig2 is a key modulator of the MN-OLP fate switch. During MN production, Olig2 is phosphorylated at S147 and forms Olig2:Olig2 homodimers. Dephosphorylation at S147 induces Olig2 homodimer dissociation and formation of heterodimers, and activates the MN-OLP fate switch. In this Thesis, I present the results of my research into the mechanisms that regulate the dephosphorylation of Olig2 and mediate the impact this has on stem cell fate choice. Analysing the genomic binding sites of phosphorylated wild-type Olig2 and a constitutively dephosphorylated mutant form of Olig2 (Olig2-S147A), I have revealed that S147 phosphorylation has a major impact on Olig2 gene target choice. I have also explored the role of angiogenesis in regulation of the fate switch – both in vitro and in vivo using mouse and zebrafish models of development – and I have identified an inhibitory phosphatase component that is down-regulated over the period of the fate switch and is a candidate regulator of Olig2 S147 dephosphorylation. Finally, I have performed computational analysis of Olig2 phosphorylation and designed and

constructed genetic tools for studying the regulation and function of an additional Olig2 phospho-acceptor site at S263.

TABLE OF CONTENTS

LIST OF FIGURES AND TABLES

CHAPTER 1: INTRODUCTION

CHAPTER 2: MATERIALS & METHODS

CHAPTER 3: SPINAL CORD ANGIOGENESIS AND THE MN-OLP FATE SWITCH

CHAPTER 4: OLIG2 S147 DEPHOSPHORYLATION: IDENTIFYING THE PHOSPHATASE

CHAPTER 5: OLIG2 S147 PHOSPHORYLATION AND GENE TARGET CHOICE

CHAPTER 6: OLIG2 S263 PHOSPHORYLATION

LIST OF ABBREVIATIONS

4-OHT	4-hydroxytamoxifen
AEP	Anterior entopeduncular area
Ani	Anisomycin
AP	Alkaline phosphatase
ATF1	Activating transcription factor 1
B-Tub	Beta-Tubulin
BDNF	Brain-derived neurotrophic factor
bHLH	Basic helix-loop-helix
BMP	Bone morphogenetic protein
bp	Base pairs
BSA	Bovine serum albumin
Casp3	Caspase 3
Cdh5	VE Cadherin
CDK5	Cyclin dependent kinase 5
cDNA	Complementary DNA
CGE	Caudal ganglionic eminence
ChAT	Choline acetyltransferase
ChIP	Chromatin immunoprecipitation
ChlorR	Chloramphenicol resistance
CK2	Casein kinase 2
CNP	2’,3’-cyclic-nucleotide 3’-phosphodiesterase
CNS	Central nervous system
CNTF	Ciliary neurotrophic factor
CREB	Cyclic AMP response element binding protein
DA	Dorsal aorta
DAPI	4',6-diamidino-2-phenylindole
DEPC	Diethylpyrocarbonate
DIG	Digoxigenin
dKO	Double knockout
DLAV	Dorsal longitudinal anastomotic vessel
dn	Dominant negative
DTT	Dithiothreitol
Dusp	Dual-specificity phosphatase-like
E(...)	Embryonic day
EC	Endothelial cell
EGF	Epidermal growth factor
EMS	Electromobility shift
EtOH	Ethanol
EUCOMM	International knockout mouse consortium

FBS	Fetal bovine serum
FGF	Fibroblast growth factor
FGFR	Fibroblast growth factor receptor
FITC	Fluorescein isothiocyanate
fl/fl	flox/flox
FP	Floorplate
GABA	Gamma-amino butyric acid
GFAP	Glial fibrillary acidic protein
GO	Gene ontology
GR	Glucocorticoid receptor
GSK3	Glycogen synthase kinase 3
Hb9	Homeobox gene 9
HDAC	Histone deacetylase
HIF	Hypoxia inducible factor
HLH	Helix-loop-helix
HMG	High mobility group
IAA	Isoamylalcohol
IB4	Isolectin B4
ICAM	Intracellular adhesion molecule
ICD	Intra-cellular domain
ID	Inhibitor of differentiation
IGF	Insulin-like growth factor
IHC	Immunohistochemistry
iOL	Immature oligodendrocyte
IP	Immunoprecipitation
ISH	In situ hybridization
ISV	Intersegmental vessel
JAG2	Jagged 2
KO	Knockout
KS	Kolmogorov-Smirnov
LB	Luria-Bertani
LGE	Lateral ganglionic eminence
MAPK	Mitogen activated protein kinase
Mash1	Mouse Achaete-scute homolog 1
MBP	Myelin basic protein
MGE	Medial ganglionic eminence
MN	Motor neuron
mOL	Mature oligodendrocyte
MS	Mass spectrometry
NEAA	Non-essential amino acids
NEB	New England Biolabs
NES	Nuclear export signal
NG2	Neural/glial antigen 2
Ngn2	Neurogenin 2
Nrp1	Neuropilin 1

NSC	Neural stem cell
o/n	Overnight
O2	Oxygen
OCT	Optimal cutting temperature
OD^{600}	Optical density at 600 nm
OL	Oligodendrocyte
OLP	Oligodendrocyte precursor
ORF	Open reading frame
P(…)	Post-natal day
P(I/II/III)	PAC Solution I/II/III
PAC	P1 artificial chromosome
PAGE	Polyacrylamide gel electrophoresis
PBS	Phosphate buffered saline
PBT	Tween(20) in PBS
PBX	TritonX-100 in PBS
PCA	Principal component analysis
PCR	Polymerase chain reaction
PCV	Posterior cardinal vein
PDGFAA	Platelet derived growth factor AA
PDGFRA	Platelet derived growth factor receptor alpha
PFGE	Pulse field gel electrophoresis
ph-HH3	Phosphorylated Histone H3
Phospho	Phosphorylated
PI(3)K	Phosphatidylinositol-3-kinase
PKA	Protein kinase A
PLP	Proteolipid protein
pMN	Progenitor of motor neurons
PNS	Peripheral nervous system
PP	Protein phosphatase
PTM	Post-translational modification
PTU	Phenylthiourea
PVDF	Polyvinylidene fluoride
qPCR	Quantitative PCR
RNAi	RNA interference
RP	Roofplate
rpm	Rotations per minute
RT	Room temperature
RT-PCR	Reverse transcription PCR
S(…)A	Serine(…) to Alanine mutation
SDS	Sodium dodecyl sulphate
Seq	Sequencing
Shh	Sonic hedgehog
Sip1	Smad interacting protein
Sox10	(Sex determining region Y)-Box 10
SRC-1	Steroid receptor co-activator

STR	Serine/threonine-rich
TF	Transcription factor
Tg	Transgenic
TSM	Triple-serine motif
UTR	Untranslated region
VEGF	Vascular endothelial growth factor
VEGFR	Vascular endothelial growth factor receptor
VZ	Ventricular zone
WB	Western blot
WMI	White matter injury
WT	Wild-type

CHAPTER 1

INTRODUCTION

1.1 BACKGROUND

The mammalian central nervous system (CNS) is composed of two major neural cell classes: neurons and glia. Neurons receive, process and transmit electrical and chemical signals as part of an extensive network of interacting cells. Glia provide the necessary metabolic, structural and functional support for development and maintenance of the integrated neuronal system (Verkhratsky & Butt, 2007). Despite making up more than 80% of the cells in the CNS, the role of glia was, throughout most of the twentieth century, considered to be static and not to contribute to the activity of the neuronal network other than in a supporting role. Improvements in our understanding of glia have, however, demonstrated critical functions in dynamically regulating neural circuitry, raising awareness of these cells and provoking an intense interest in glial cell biology.

CNS glia are subdivided into microglia – CNS-resident immune cells derived from the embryonic mesoderm – and macroglia – a variety of cell types that, like neurons, are derived from the neuroectoderm (Jessen & Richardson, 2001). Macroglia are principally comprised of astrocytes and oligodendrocytes. Oligodendrocytes (OLs) are the specialized cells responsible for ensheathing axons of CNS neurons in multilayered myelin (De Robertis et al., 1958). Oligodendrocytes (literally 'cells with several branches') extend processes to axons of different proximate neurons and elaborate multiple myelin sheaths (Figure 1). Bundles of

myelinated axons form the major component of CNS "white matter" tissue, visibly different from "grey matter" (primarily unmyelinated neuronal cell bodies) (Fields, 2008). The lipid-rich myelin sheath electrically insulates the myelinated axon fibre and allows rapid saltatory transmission of action potentials along the axon (Moore et al., 1978). Briefly, action potentials are conducted almost instantaneously between nodes of Ranvier, the unmyelinated segments of axon between myelinated internodes, where activation of clusters of voltage-gated sodium channels depolarizes the axon and regenerates the action potential.

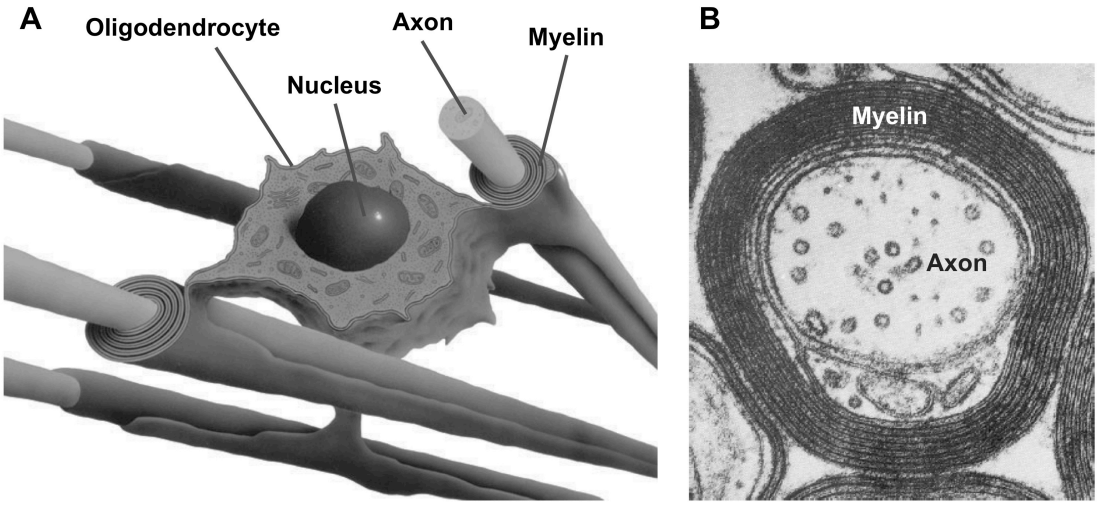

(Image courtesy of *http://the-scientist.com*) (Image courtesy of *http://med.harvard.edu*)

Figure 1. Myelinating oligodendrocytes. A. Schematic representation of a myelinating oligodendrocyte. B. Electron micrograph of the cross-section through a myelinated axon.

Evolution of myelin

In an evolutionary context, accelerated transmission of electrical signals along nerve fibres – enabling a quicker, more sophisticated stimulus-response – would have conferred an obvious selective advantage for both primitive predators and their potential prey. Over the course of evolution, two principal mechanisms have developed for increasing the speed of nerve impulse conduction: expansion of axon diameter and myelination (reviewed by Hartline & Coleman, 2007). Increasing the axon diameter accelerates conduction speed by reducing the

internal resistance of the fibre (conduction speed increases proportionally with the square root of axon diameter) (Hodgkin, 1954). Giant axons are found across a range of different taxa, often in time-critical neural circuits. In the Annelids or ringed worms, for example, signaling along longitudinal giant axons is necessary for eliciting a rapid escape response but is not involved in normal movement. Despite increasing conduction speed, however, giant axons are spatially inefficient and extremely metabolically costly.

Myelin and pseudo-myelin sheaths, the alternative evolutionary mechanism for boosting conduction speeds, have been described in both vertebrates and invertebrates, respectively (Gunther, 1976; Bullock et al., 1984). The different myelinated taxa are widely separated phylogenetically, suggesting that superficially similar myelin structures have evolved independently in different lineages. Vertebrate myelin may have arisen in the first Gnathostomes (jawed fish) (Bullock et al., 1984). Absent in jawless fish (lampreys and hagfish), the co-emergence of myelinated cranial nerves and hinged jaws might underlie the evolution of predation. An alternative hypothesis is that OL myelin first evolved to insulate the axons of motor neurons (MNs) and enable rapid escape behaviour (Li & Richardson, 2008). In support of this hypothesis is the intimate developmental relationship between MNs and OLs in the vertebrate CNS and the fact that pseudo-myelin in invertebrate lineages is primarily associated with circuits involved in rapid escape or startle reactions (see *Oligodendrocyte Development* below).

The myelin sheath reduces the transverse capacitance across the axon plasma membrane. Typically, myelin insulation improves conduction speeds by at least a factor of 10 (equivalent to a ~100-fold increase in unmyelinated axon diameter), and significantly reduces the energy cost of neuronal activity (Harris & Attwell, 2012). Fast and efficient signal transmission enables coordination of more complex neuronal networks in physically larger nervous

systems, with much greater information processing capacity, and ultimately proved critical for the evolution of intelligence.

CNS myelin and disease

In humans, OL loss and demyelination are hallmark pathologies of a variety of neurodegenerative diseases (including multiple sclerosis and leukodystrophies) and white matter injuries.

Multiple sclerosis (MS). MS is a chronic inflammatory degenerative disease of the CNS characterized by demyelination, OL death and axonal degeneration (Compston & Coles, 2002). MS is believed to be triggered by autoimmune attack on OLs and myelin, although whether the immune involvement is the cause or a result of demyelination is still unclear. MS affects over two million people worldwide, predominantly in North America, Europe and Australia, and is a leading cause of disability among young adults. Patients typically present with a relapsing-remitting course of the disease characterized by acute neurological symptoms (days to several months) followed by periods of complete or partial recovery (Milo & Kahana, 2010). Between 10 and 15% of patients follow a primary progressive disease course in which neurological symptoms accumulate steadily from the point of onset (Compston & Coles, 2008). Over time, relapsing-remitting MS frequently develops a secondary-progressive character, with neurological disabilities accumulating in the patient in a manner similar to the primary-progressive form. Although widely considered an autoimmune disease directed against CNS myelin or OLs, the underlying causes of MS are unknown.

The hallmark feature of MS is the formation of numerous white matter lesions (or sclerotic plaques), the direct consequence of oligodendrocyte death and the loss of myelin. One particularly interesting pathophysiology – one very relevant to glial biologists – is the limited capacity in MS sufferers to remyelinate axons and repair lesions (Chandran, 2008). Myelination remains dynamic in the mature CNS, and although the poor OL response in the disease context is not fully understood, inducing effective remyelination in MS lesions has major therapeutic potential.

Leukodystrophies. Leukodystrophies are a large and divergent family of genetic disorders characterized by progressive disturbances in white matter development (Costello et al., 2009). The symptoms of different leukodystrophies vary greatly, reflecting the wide range of underlying genetic causes. Most commonly, delayed cognitive development presents in infants and children and progressively deteriorates, often affecting movement, speech and behaviour. Similarly to MS, myelin repair is an attractive therapeutic target (Kondo & Duncan, 2009). Indeed, in a mouse model of congenital dysmyelination, engrafted OL lineage cells derived from human embryonic stem cells robustly myelinated the deficient brain and significantly extended the survival of hypomyelinated mice (Wang et al., 2013).

White matter injury (WMI). White matter injury can occur as a consequence of different traumatic episodes typically involving a diminished oxygen/blood supply to all or part of the brain (Volpe, 2003; Khwaja & Volpe, 2008). In periventricular leukomalacia (PVL), preterm newborns suffer major OL damage around the lateral ventricles. The cerebral white matter injury is commonly associated with neurodevelopmental impairment and cerebral palsy or epilepsy later in life.

The severity and incidence of OL/white matter diseases is associated with an enormous social and economic burden. Improving our understanding of OL biology in both normal and disease contexts will enable the essential generation of new diagnostic and therapeutic tools.

1.2 OLIGODENDROCYTE SPECIFICATION

Oligodendrocyte lineage and markers

OL lineage cells derive from the neuroepithelium of the developing CNS (Kessaris et al., 2001). The first OL precursors (OLPs) appear late in embryonic neurogenesis from multipotent neuroepithelial stem cells in the ventral ventricular zone of the embryonic spinal cord (Rowitch, 2004; Richardson et al., 2006). OLPs transition through a number of distinct intermediate progenitor stages on the way to becoming mature, myelinating OLs (Figure 2) (Nishiyama et al., 2009). The stereotypical morphologies and molecular markers associated with the different stages of OL development are outstanding tools for researching OL biology both in vivo and in vitro.

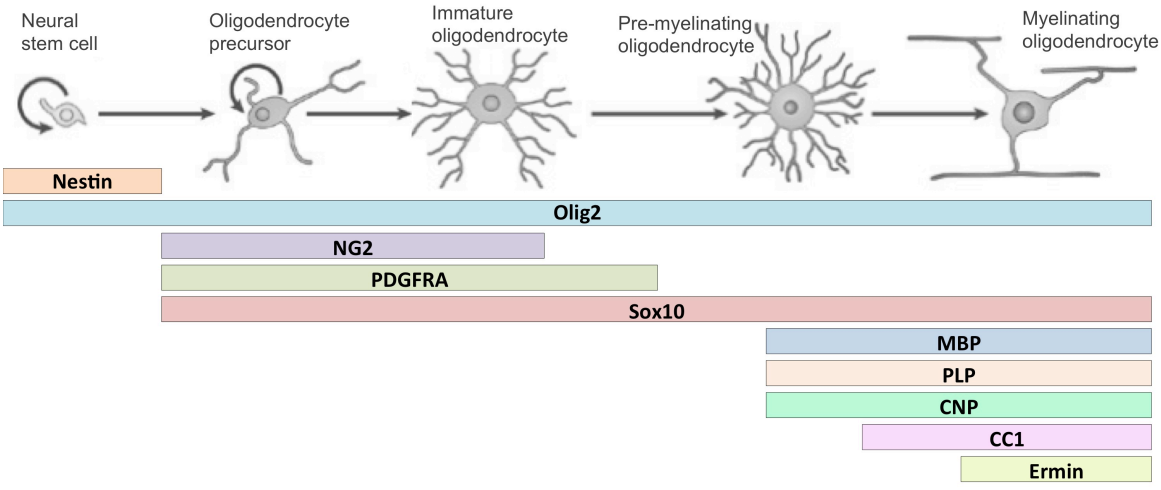

(Image adapted from *Nishiyama et al., 2009*)

Figure 2. Multi-stage oligodendrocyte development and lineage marker expression. OLPs derive from neural stem cells in the ventricular zone of the developing CNS. Differentiation of OLPs to mature and myelinating OLs involves stepwise transition through several intermediate stages. Different progenitor cell-types are associated with stereotypical morphologies and expression of stage-specific protein markers.

Origins of OLPs

The prevailing view among glial biologists was, until at least the early 1990s, that OLs arose from all parts of the embryonic ventricular zone. It has been clearly demonstrated since, however, that while mature OLs are widely and evenly distributed throughout the adult CNS, fate-restricted OLPs are in fact born from discrete areas of the ventricular zone during development (Richardson et al., 2006). Newly specified OLPs migrate away from the specific germinal zones, eventually colonizing the entire CNS, before differentiating to become mature and myelinating OLs.

Embryonic spinal cord

The ventricular zone of the mammalian embryonic spinal cord is divided into distinct progenitor domains along its dorsal-ventral axis (Figure 3) (Jessell, 2000). Neuroepithelial stem cells resident in the different regions express domain-specific combinations of transcription factors (TFs) and generate characteristic subtypes of specialized neurons and glia. Along the caudal neural tube, the antecedent structure to the spinal cord, the protein morphogen Sonic hedgehog (Shh) is secreted from the ventral notochord and floorplate (Dessaud et al., 2008). The concentration and length of exposure to Shh, which diminishes with distance from the ventral midline, differentially regulates transcription of various, frequently cross-repressive TFs. Collectively, specific TF expression profiles define five distinct progenitor domains across the ventral spinal cord – ventral-most p3 - pMN - p2 - p1 - p0 (Figure 3).

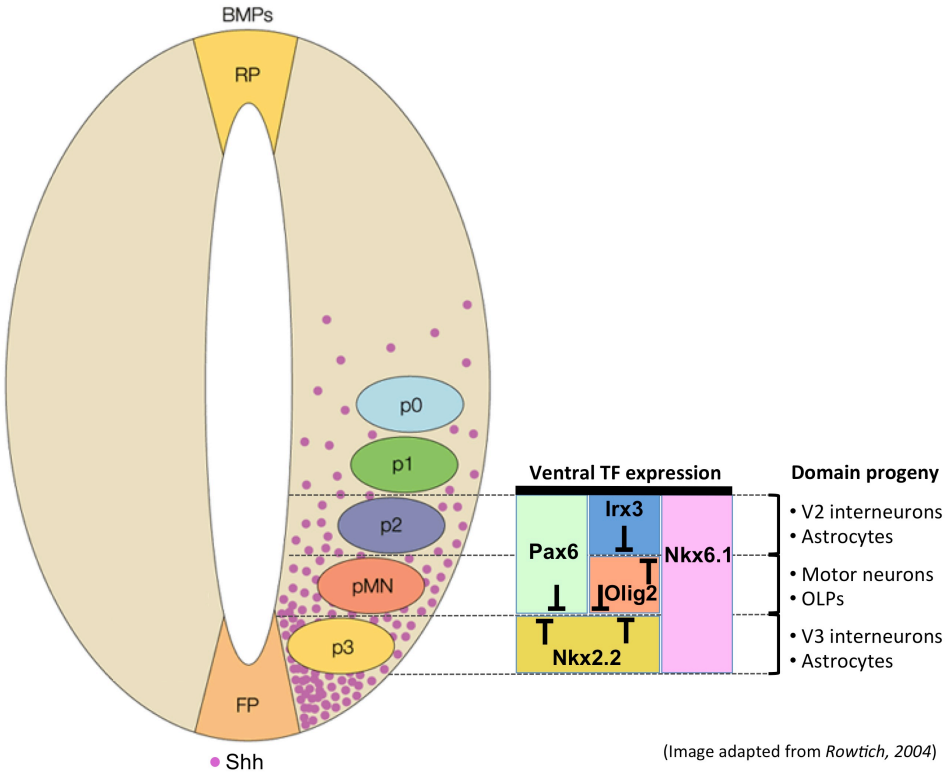

Figure 3. Ventral patterning of the embryonic spinal cord. The ventricular zone of the embryonic spinal cord is patterned along its dorsal-ventral axis into distinct progenitor domains. In the ventral portion, graded sonic hedgehog (Shh) signaling induces segmental expression of different combinations of transcription factors (TFs). Specific combinations initiate unique developmental programmes and generate particular neuronal and glial subtypes within the discrete progenitor domains. (BMPs, bone morphogenetic proteins; FP, floorplate; RP, roofplate.)

Stem cells of the pMN (progenitor of motor neuron) neuroepithelial domain specifically express the basic helix-loop-helix TF Olig2, along with more broadly induced TFs Pax6 and Nkx6.1 (Ericson et al., 1997; Briscoe et al., 2000; Vallstedt et al., 2001; Zhou & Anderson, 2002). This Olig2-positive progenitor pool contributes approximately 80% of the OLs in the adult spinal cord. The restricted source of most OLs was, however, first identified in rats before the discovery of the *Olig* genes (Warf et al., 1991; Pringle & Richardson, 1993; Noll & Miller, 1993; Yu et al., 1994; Timsit et al., 1995). Early in vitro experiments showed OL development in explant cultures derived from ventral but not dorsal rat spinal cord, suggesting that the capacity of spinal cord progenitors to generate OLPs varies with position along the dorsal-ventral axis (Warf et al. 1991). RNA in situ hybridization (ISH) experiments

then established transient, focal expression of OL lineage markers (*platelet-derived growth factor receptor alpha* [*PDGFRA*] and *2',3'-cyclic-nucleotide 3'-phosphodiesterase* [*CNP*]) in the ventral spinal cord at embryonic day 14 (E14), consistent with the notion of spatially restricted OLP generation (Pringle & Richardson, 1993; Yu et al., 1994). The discovery in 2000 and subsequent characterization of OL lineage genes *Olig1* & *Olig2* specifically delineated the pMN domain and confirmed the restricted, ventral origin of OLPs (Lu et al., 2000; Zhou et al., 2000; Lu et al., 2002; Zhou et al., 2002).

The contribution of a small fraction – now understood to be ~20% – of OL lineage cells from dorsal neuroepithelium after the emergence at E12.5 in mouse of pMN OLPs continued to be a controversial idea until 2005 (Richardson et al., 2000; Spassky et al., 2000; reviewed by Richardson et al., 2006). Analysis of OL marker activation in *Shh*-null and *Nkx6.1/Nkx6.2* compound-null mouse lines, both lacking pMN-derived OLs, revealed Shh-independent production of OLPs from dorsal progenitor cell populations (Cai et al., 2005; Vallstedt et al., 2005). These observations were independently supported by *Cre-lox* fate mapping experiments in *Dbx-Cre^{ERT2}:Reporter* transgenic mice; OLPs (Sox10+; Olig2+) derived from Dbx-positive neuroepithelium (spanning the dorsoventral midline) were identified at late embryonic (E16.5 & E18.5) stages (Fogarty et al., 2005).

In brief, OLPs primarily arise in the ventral pMN domain of the developing spinal cord, first appearing around E14 in rat and E12.5 in mouse. At approximately E15 in mouse, a subsequent Shh-independent wave of OLP generation begins from more dorsal regions of the ventricular zone. Oligodendrogenesis continues until late gestation, with newly born OLPs migrating away from the ventricular germinal zone and populating the entire spinal cord.

Forebrain

Aside from the embryonic spinal cord, research into the origins of OLPs has focused on the developing forebrain. The first indication that OLPs derive from specific regions of the rostral neural tube came from the RNA ISH experiments described above (Pringle & Richardson, 1993). Labeling coronal sections of E15 rat forebrain, Pringle & Richardson observed intense *PDGFRA* signal in the ventral forebrain pre-optic area (beneath the Foramen of Monro). Additional experiments from the Richardson Lab followed the distribution of OLPs through the developing rat telencephalon from E14.5-E20.5 and elucidated a major role for ventral Shh signaling in forebrain oligodendrogenesis (Tekki-Kessari et al., 2001). Considering what was known by 2001 about OLP specification in the rodent spinal cord, this data appeared consistent with a restricted origin of OLPs in the ventral forebrain. The data did not, however, exclude the possibility of OLP production from additional sources within or outside the telencephalon.

Research from a number of labs pointed to oligodendrogenesis from outside the MGE. In vitro clonal analysis and *Dlx2* lineage tracing in vivo showed widespread subpallial OLP production from the lateral and caudal ganglionic eminences (LGE and CGE), as well as the medial ganglionic eminence (MGE) (He et al., 2001; Marshall et al., 2002). Examination of *Emx1-Cre:Reporter* transgenic mice also revealed local OLP generation in the developing cerebral cortex (Gorski et al., 2002). These observations, along with the results from early retroviral fate mapping experiments that appeared to demonstrate postnatal OL specification in the forebrain subventricular zone, fuelled skepticism over the ventral origins of OLs in the forebrain (Levison et al., 1993). In 2006, Kessaris et al. resolved the issue using three *Cre-Reporter* mouse lines to label and trace distinct forebrain stem cell populations in the MGE (*Nkx2.1*-expressing), the LGE/CGE (*Gsh2*-expressing) and in the cortex (*Emx1*-expressing) (Kessaris et al., 2006). The analysis revealed precise spatio-temporal control of OLP

production from multiple sites. MGE-derived OLPs first emerged around E11.5, with subsequent specification from the LGE/CGE at ~E15 and from the cortex after birth. Experimentally observed as three distinct oligodendrogenic phases, forebrain OLP production probably proceeds as a continuous wave, moving from ventral to dorsal over time.

OL development in the forebrain mimics the spinal cord. The first OLPs arise from ventral progenitors through a Shh signaling-dependent process. Specification from more dorsal progenitors occurs later and independently of Shh. Surprisingly, MGE-derived OLs (the earliest-born) are eliminated after birth and are largely absent from the adult forebrain, though the mechanism(s) and explanation for their removal have not been discovered (Kessaris et al., 2006).

Behaviour of ventrally versus dorsally derived OLPs

After the early morphological classification of different OL subtypes by Del Rio Hortega in the 1920s, identification of different OL populations originating from different VZ territories reinforced suggestions of functional heterogeneity among OLs. In the forebrain, Kessaris et al. (2006) adapted their Cre-Reporter strategy to eliminate OLPs derived from specific progenitor populations. This demonstrated that targeted ablation of any population of OLPs (for example the LGE/CGE-derived pool) was effectively compensated for by expansion of neighbouring populations of OLPs, indicating functional redundancy among OLs, regardless of origin. More recently, research in the spinal cord has examined whether ventrally versus dorsally derived OLPs possess different electrophysiological properties (Tripathi et al., 2011). Tripathi et al. generated a transgenic dual reporter mouse line that differentially labels OL lineage cells according to place of birth. All OLPs were morphologically indistinguishable, and although two electrophysiological subtypes were identified – spiking and non-spiking – neither subtype was linked to a particular developmental origin. This study, however, did

identify population-specific patterns of migration and myelination. Compared to ventrally derived OLPs, dorsal progenitors migrate less widely from their sources, predominantly settling and myelinating axons in the dorsal tract. Furthermore, the proportion of ventrally derived OLs in the dorsal spinal cord decreases from roughly 45% at P13 to less than 20% at P67, indicating that the dorsally derived cells possess some selective advantage and are capable of displacing ventrally derived OLs from regions of shared occupancy.

A motor neuron-oligodendrocyte connection

In the developing CNS, neuroepithelial stem cells resident in different regions of the ventricular zone generate particular subtypes of neurons and glia (Briscoe et al., 2000; Jessell, 2000). While the periods of neurogenesis and gliogenesis vary substantially among different germinal zones, neuronal specification always precedes glial specification; stem cells in a given region produce neurons before switching to produce glia. In the embryonic spinal cord, ventrally derived OLPs arise from the same progenitor domain – the pMN domain – that previously gives rise to all adult motor neurons (MNs) (Kessaris et al., 2001). In the mouse, MNs are born from ~E9.5 - ~E12.5 with pMN-derived OLPs first emerging immediately after the end of neurogenesis (Figure 4).

The production of different neuronal subtypes at specific dorsal-ventral positions across the spinal cord, including a ventral origin of MN precursors, was described in chick embryos as early as 1970 (Langman & Haden, 1970). By 1991, tissue-grafting experiments demonstrated the role of polarizing floor plate and notochord activity in controlling the pattern of motor neuron specification, though the mechanisms and diffusible signal(s) remained unclear (Yamada et al., 1991). Echelard et al. (1993) identified three mammalian relatives of the Drosophila polarity gene *hedgehog*: *Desert hedgehog*, *Indian hedgehog* and *Sonic hedgehog*

(*Shh*) (Echelard et al., 1993). Examining the pattern of endogenous Shh signaling and the effect of ectopic Shh expression (under control of the *Wnt-1* regulatory element; *Wnt1:Shh*) revealed a role in floor plate induction and CNS polarity. Research from several different groups subsequently confirmed the restricted ventral origin of motor neuron development and its sensitivity to graded Shh from the notochord and floor plate (Marti et al., 1995; Roelink et al., 1995; Tanabe et al., 1995; Chiang et al., 1996; Ericson et al., 1996).

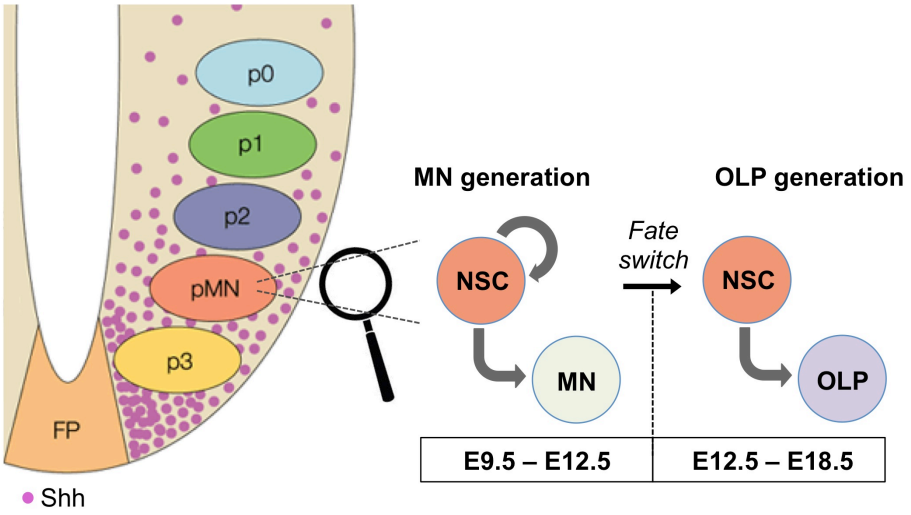

(Image adapted from *Rowitch, 2004*)

Figure 4. Sequential generation of motor neurons and oligodendrocyte precursors. From E9.5 – E12.5 in mouse, neural stem cells (NSCs) resident in the ventral pMN domain of the developing spinal cord divide and differentiate to produce motor neurons (MNs). At ~E12.5, the fate of pMN NSCs changes and a programme of OLP specification replaces the early programme of MN production.

The pattern of PDGFRA-positive OLP development and the demonstration of its dependence on Shh signaling raised the possibility that MNs and OLPs are descended from a common population of neuroepithelial precursors (Pringle & Richardson, 1993; Pringle et al., 1996; Richardson et al., 1997; Richardson et al., 2000). Initial recombinant retroviral examination of MN genealogy in the chick spinal cord pointed to lineal relationships of MNs with both astrocytes and putative OLs (Leber et al., 1990). Analysis in mouse spinal cord by Sun et al. (1998) found that OLPs and Islet2-positive/Lim3-positive MNs originate from the most

ventral Pax6-expressing cells, and that the generation of both cell types is similarly altered in mice lacking functional Pax6 (Sun et al., 1998). Identification of the OL-lineage transcription factor Olig2 provided firm evidence for common MN and OL origins (Lu et al., 2000; Zhou et al., 2000; Takebayashi et al., 2000; Lu et al., 2002; Takebayashi et al., 2002). The pMN-specific expression of Olig2 over the course of both MN and OLP specification, and the discovery of its fundamental role in both developmental phases, clearly demonstrated that MN and ventral OL generation occurs sequentially from the same Olig2-positive neuroepithelium.

The precise NSC lineage relationship between MNs and OLPs is not yet fully understood. As opposed to MNs and OLPs deriving in sequence from a uniform population of multipotent Olig2+ NSCs, the restricted ventral origin of both cell types and their common developmental requirement for transcription factor Olig2 might in fact disguise distinct pre-MN and pre-OLP progenitor populations within the pMN domain (Rowitch et al., 2004). In this model, neuronal lineage-restricted Olig2+ precursors (or neuroblasts) generate MNs before Olig2+ glioblasts – dormant throughout MN generation – generate OLPs. In support of this hypothesis, lineage tracing analysis in the caudal forebrain using *Plp-Cre^{ERT2}:Reporter* transgenic mice identified the progeny of E9.5 or E13.5 progenitors and indicates neurons and glia are sequentially generated from two unique subpopulations of progenitor (Delauney et al., 2008). In contrast to this segregative model of MN and OLP development, however, retroviral lineage tracing experiments performed in the embryonic chick, along with in vitro clonal analysis of cultured NSCs derived from embryonic rat spinal cord, suggest a shared MN/OL lineage (Leber et al., 1995; Kalyani et al., 1997). Moreover, Park et al. (2004) performed in vivo clonal analysis of Olig2+ pMN NSCs in zebrafish that demonstrated the MN and OL lineages have not diverged at the onset of neurogenesis, favouring a 'switching' (as opposed to a 'segregating') model of development (Rowitch et al., 2004).

1.3 ANGIOGENESIS & THE MOTOR NEURON-OLIGODENDROCYTE PRECURSOR FATE SWITCH

The precise sequential generation of MNs and OLPs from the ventral population of Oig2+ NSCs in the developing spinal cord indicates stringent regulation of the switch from motor neurogenesis to oligodendrogenesis (referred to hereafter as the MN-OLP fate switch). In pMN domain-resident NSCs, however, the trigger(s) of the MN-OLP fate switch have not been established and there remain a number of legitimate hypotheses. For example, the timing of the spinal MN-OLP fate switch might be cell autonomous, with pMN domain NSCs 'hardwired' to switch at a specific developmental time point (near E12.5 in mice) from generating MNs to generating OLPs. Alternatively, instructive cues might induce the MN-OLP fate switch in a non-cell autonomous manner. In this case, overlying developmental changes would signal – directly or indirectly – to pMN NSCs and alter the programme of fate specification. In the embryonic CNS, tissue angiogenesis occurs around the time of the MN-OLP fate switch and is a promising candidate developmental cue that might crucially regulate NSC fate in the pMN domain. In the following section, I focus on the potential role of angiogenesis in governing the timing of spinal OLP formation and highlight the potential mechanisms of an angiogenesis-dependent MN-OLP fate switch.

Development of the vascular pattern within the spinal cord has been visualized in a range of animal models, including sheep, pig and chick embryos, by India ink injection (Sterzi, 1904; Hoskins, 1914; Watterson & Feeney, 1946). These classic experiments revealed a consistent spatio-temporal pattern of invasion from somatic tissue outside the CNS: blood vessels approach the cord at the ventro-lateral border and sequentially invade the ventral, lateral and finally dorsal surfaces. We now understand vascular endothelial cells (ECs) invade from the perineural vascular plexus (PNVP) and follow vascular endothelial growth factor (VEGF)

gradients, growing toward the ventricular neuroepithelium where these signaling factors are produced (reviewed by Eichmann & Thomas, 2013). At the leading edge of a developing vessel, “tip” cells extend filopodia toward hypoxic regions producing VEGF. Binding of VEGF to VEGF receptor 2 (VEGFR2) expressed on tip cell filopodia triggers Notch-signaling to adjacent ECs. In these neighbouring ECs, Notch signal activation induces differentiation into follower “stalk” cells. Stalk cells, insensitive to VEGF, proliferate to form the capillary lumen, enabling blood flow and tissue oxygenation.

A possible role for MNs in regulating vascular sprouting from the PNVP has been described by Nagase et al. (2005). Islet-1/2-positive MN columns in the ventral and lateral neural tube express VEGF immediately before vascular invasion. Moreover, in whole mouse embryo cultures, blockade of Shh signaling by cyclopamine administration from E8.5 both eliminated MN induction and impaired vascular sprouting, suggesting that MNs might directly regulate spinal cord angiogenesis via expression of VEGF. An extension of this idea is therefore that MNs, by inducing spinal cord angiogenesis, indirectly regulate the timing of OLP production from pMN NSCs. It should be noted, however, that the vascular phenotype observed in these experiments might not be the result of MN deficiency but of an additional, independent effect of cyclopamine treatment and blocking Shh signaling.

Angiogenic regulation of NSC fate choice in the developing spinal cord could occur through one or a combination of three principal mechanisms: 1. Changing tissue oxygen (O2) tension; 2. Endocrine signaling; 3. EC-NSC signaling (either contact-dependent or paracrine signaling).

1. Changing tissue oxygen tension

Oxygen is an important regulator of progenitor cell behaviour throughout embryonic and postnatal development (Mohyeldin et al., 2010). The limited diffusion distance of oxygen (estimated at approximately 150 μm in various mammalian tissues) means that before the establishment of the circulatory system, early mammalian development predominantly occurs in an oxygen-poor environment (Krogh, 1919). Hypoxia-inducible factor 1 (HIF1), a heterodimeric bHLH TF containing an O2-sensitive alpha subunit (HIF1A) and the constitutively expressed beta subunit (HIF1B), is the primary intracellular mediator of the hypoxic response (Wang & Semenza, 1993; Wang & Semenza, 1995). In normoxic cells, oxygen-dependent prolyl hydroxylation of HIF1A induces interaction with von Hippel-Lindau tumour suppressor (VHL) protein, the recognition component of an E3 ubiquitin ligase complex, which rapidly targets the alpha subunit for proteasomal degradation (Weidemann & Johnson, 2008). Under low oxygen conditions, stable HIF1A accumulates in the nuclei of hypoxic cells, forming the functional HIF1A:HIF1B dimers that bind and regulate expression of hypoxia-responsive target genes. Homozygous knockout of either *HIF1A* or *HIF1B* subunit is embryonic lethal by E11 in mice and clearly demonstrates the importance of the HIF pathway during development (Iyer et al., 1998; Ramirez-Bergeron et al., 2006). Indeed, neural cell-specific knockout of *HIF1A* with a *Nestin* promoter-driven Cre results in major, though non-lethal, CNS defects (Tomita et al., 2003).

In culture, spontaneous differentiation of human embryonic stem cells (hESCs) is reduced in low (3-5% v/v) [O2] (Ezashi et al., 2005). There is also considerable in vitro evidence of hypoxia regulating NSC differentiation, along glial and neuronal lineages. Studer et al. (2000) found rodent embryonic CNS precursor cells showed enhanced survival and proliferation under low [O2] compared to atmospheric (~20%) levels. Differentiation of rat precursors into

tyrosine hydroxylase-positive dopaminergic neurons is also selectively promoted in lowered [O2]. In addition, research using Nestin-positive human subventricular zone precursors demonstrated a similar effect on proliferation of near-physiological (5%) [O2] versus atmospheric [O2] (Erecinska & Silver, 2001; Pistollato et al., 2007). Expansion in 5% [O2] yields greater cell numbers and a higher proportion with CD133-/CD24-positive stem cell-like character, while high [O2] triggers mitotic arrest and stimulated astrocyte and OL differentiation. Comparable results were obtained using mouse cortical precursor cultures (Chen et al., 2007). Overall, the data from these in vitro culture experiments support the idea that [O2] can regulate NSC development.

At the molecular level, O2 availability and HIF modulate Wnt/β-catenin and Notch signaling, important pathways for both neural stem cell and OL development. In mouse embryonic and neural stem cells, hypoxic exposure stimulates HIF1-dependent activation of Wnt/β-catenin signaling and upregulation of Wnt target genes (Mazumdar et al., 2010). In vivo, regions of active Wnt/β-catenin signaling correlate strongly with low O2 tension in both the embryonic and adult mouse brain. In addition, in the dentate gyrus of the adult hippocampus, a primary neurogenic stem cell niche, inducible deletion of *HIF1A* reduces Wnt signaling and suppresses neurogenesis. These findings indicate that under low oxygen conditions, HIF1 influences NSC function through direct regulation of Wnt/β-catenin signaling. In embryonic OL development, Wnt signaling has been shown to negatively regulate specification of OLPs in both the telencephalon and spinal cord (Langseth et al., 2010; Dai et al., 2014). In the embryonic telencephalon, inhibition of Wnt signaling, by electroporation of either a soluble Wnt antagonist or a dominant-negative transcriptional regulator, prompts precocious and excessive OLP production (Langseth et al., 2010). In addition, transgenic β-catenin activation in the pMN domain of mutant embryonic spinal cords results in generation of significantly fewer Sox10-/PDGFRA-positive OLPs (Langseth et al., 2010). Therefore, oxygen delivery via

the nascent vasculature might, through HIF1 degradation, relieve pMN domain-resident NSCs from Wnt-mediated suppression of OL specification, and trigger the MN-OLP fate switch.

The Notch pathway is a direct cell-cell signaling system with crucial roles in controlling stem cell self-renewal and fate choice in the vertebrate CNS (Louvi & Artavanis-Tsakonas, 2006). Notch receptors interact with ligands – including Delta and Jagged – expressed on the surface of adjacent cells. Ligand binding induces a series of internal proteolytic cleavages, liberating the Notch intracellular domain (Notch ICD), which translocates to the nucleus and activates Notch downstream genes, such as the *Hes* and *Hey* TFs. Gustafsson et al. (2005) elucidated an important role for Notch in underpinning the link between hypoxia and maintenance of the undifferentiated cell state. In vitro, blocking the Notch pathway in cultured rat cortical precursors revealed hypoxia-induced inhibition of differentiation requires functional Notch signaling. Exploring the mechanism of the Notch-mediated effect of hypoxia, Gustafsson et al. (2005) found that under low [O2], HIF1A physically interacts with the Notch1 ICD. The Notch1-ICD:HIF1A transcriptional complex stabilizes the Notch1 ICD and activates expression of Notch target genes. Subsequent research has provided additional insight into the importance and precise nature of crosstalk between the Notch and hypoxia signaling pathways (Wang et al., 2006; Zheng et al., 2008; Sahlgren et al., 2008; Chen et al., 2010; Mukherjee et al., 2011).

In differentiating NSCs, expression of proneuronal bHLH TFs Mash1 and the Neurogenins induce expression of Notch ligands, which activate Notch signaling in neighbouring cells (Kageyama et al., 2005). The Notch-induced *Hes* genes – homologues of Drosophila *Hairy* and *Enhancer of split* – encode repressor bHLH TFs that directly antagonize proneuronal TF activity through repression of transcription and inhibition at the protein level. In restricting the commitment of NSCs to neuronal fates, Notch signaling and Hes TFs serve critical

functions in maintaining neural stem cell populations for successive developmental phases such as oligodendrogenesis. In the optic nerve, Notch1 signaling in OLPs – activated by Jagged1 expressed on the axons of retinal ganglion cells – inhibits OL differentiation (Wang et al., 1998). In line with this observation, Notch1 deficiency in vivo causes premature differentiation of OLPs into myelinating OLs (Givogri et al., 2002). In chick and mouse embryos, the Notch ligand Jagged2 (JAG2) is transiently expressed in pMN domain cells under the control of Shh signaling. JAG2-mediated activation of Notch signaling inhibits OL gene expression, and forced up- or down-regulation of JAG2 suggests that JAG2-Notch signaling is both necessary and sufficient to block the MN-OLP fate switch. Similar to the oxygen-mediated attenuation of Wnt signaling and the potential effect on oligodendrogenesis described above, spinal cord angiogenesis and the consequent increase in pMN oxygen tension might inhibit hypoxia-induced Notch pathway activation and thereby permit OLP formation.

2. Endocrine signaling

Endocrine signaling molecules (protein and steroid hormones), secreted directly into the blood, travel through the circulatory system and trigger specific responses in hormone receptor-expressing target cells. Endocrine signaling plays a major role in the development and function of a wide variety of tissues, including the CNS. Indeed, a number of endocrine factors are known regulators of OL differentiation. Vascularization of the embryonic spinal cord might, therefore, permit delivery of hormone(s) that trigger the MN-OLP fate switch.

Thyroid hormone T3 signaling has profound effects on OL development. Hypothyroid humans and rodents display reduced myelin phenotypes, while increasing thryoid hormone levels both in vitro and in vivo enhances OL differentiation and myelin synthesis (Walters & Morell,

1981; Leung et al., 1992; Rodriguez-Pena et al., 1993; Barres et al., 1994; Jagannathan et al., 1998; Marta et al., 1998; Pombo et al., 1998). In addition to thyroid hormone, steroid hormone signals – notably glucocorticoids and progesterone – and the peptide hormone insulin-like growth factor (IGF)-1 promote OL maturation and myelin formation. In the adult mouse brain, glucocorticoid receptor (GR), along with its cofactor steroid receptor co-activator 1 (SRC-1), are expressed in >95% NG2-positive OLPs (Matsusue et al., 2014). After early post-natal adrenalectomy (surgical removal of the corticosteroid-producing adrenal glands) rats develop a hypomyelinated CNS phenotype, while corticosteroid treatment induces expression of differentiation markers MBP and PLP in OLP cultures and inhibits OLP proliferation in vivo (Preston & McMorris, 1984; Alonso, 2000; Clarner et al., 2011). Myelinogenic effects have also been described for progesterone, a steroid hormone classically known for its role in reproduction. In rat cerebellar slice cultures, progesterone significantly stimulates OLP proliferation and increases the rate of myelination (Ghoumari et al., 2003; Ghoumari et al., 2005). Finally, similar to the action of progesterone, IGF1 promotes proliferation and OL differentiation in rat OLPs in vitro, as well as myelination in rat brain aggregate cultures (McMorris & Dubois-Dalcq, 1988; Mozell & McMorris, 1991).

In contrast to the extensive data regarding OL differentiation and myelination, very little is known about the role(s) of endocrine signaling in OLP specification. It remains an interesting idea that hormones released from either maternal or embryonic sources and delivered through the developing vasculature might transform NSC behaviour and trigger the MN-OLP fate switch.

3. Endothelial cell-neural stem cell signaling

Besides the delivery of a fate switch-inducing agent carried in the blood (whether oxygen or endocrine), spinal cord angiogenesis might enable direct signaling from vascular ECs to pMN domain NSCs. In this case, EC-NSC contact or secretion of EC-derived paracrine factor(s) might direct NSC fate choice, with expansion of the vascular network into the ventral ventricular zone thereby timing the MN-OLP fate switch.

EC-NSC contact-dependent signaling. Contact-dependent – or juxtacrine – signaling between ECs of the developing spinal cord vasculature and pMN-resident NSCs could potentially induce the MN-OLP fate switch. In the mouse embryonic cortex, radial glial neural progenitors are in contact with and interact with nascent blood vessels (Ma et al., 2013). In the adult subventricular zone, NSCs are closely apposed to vascular ECs, and disruption of the NSC-EC contact in co-culture assays affects NSC proliferation and differentiation (Shen et al., 2008; Tavazoie et al., 2008). One highly conserved juxtacrine cell-cell signaling pathway with established roles in neural development is the Notch pathway. As described above, Notch receptor activation by JAG1 and JAG2 ligands has been reported to inhibit OLP differentiation and specification, respectively (Wang et al., 1998; Rabadan et al., 2012). Indeed, in the pMN domain of the developing spinal cord, JAG2-Notch signaling during neurogenesis maintains a reservoir of multipotent progenitors, and JAG2 deficiency induces premature OLP formation in the pMN domain. There are, however, a number of studies suggesting Notch signaling actually induces OLP formation. In mutant zebrafish embryos lacking both DeltaA and DeltaD Notch ligands, excess MNs develop from the pMN domain at the expense of OLPs, which are entirely absent (Park et al., 2003). Conversely, expression of a constitutively active form of Notch results in reduced MN formation and increased OLP numbers (Park et al., 2003). Notch-induced OL specification has also been described for Olig2+ radial glia in adult

zebrafish spinal cord (Kim et al., 2008). Vascular endothelial cells prominently express Notch ligands JAG1 and Dll4, and might in principle trigger OLP formation through Notch pathway activation in pMN NSCs (Hellstrom et al., 2007; High et al., 2008). The observation of JAG2-dependent inhibition of OLP generation in the mouse pMN domain appears difficult to reconcile with this hypothesis and with the zebrafish data (Wang et al., 1998; Rabadan et al., 2012). One possibility is that different Notch ligands induce specific developmental responses; for instance, while JAG2-Notch signaling between neighbouring pMN cells blocks premature OLP formation, Dll4-Notch signaling from ECs to NSCs might initiate OL gene activation.

Endothelial paracrine factors. As part of the neurovascular niche, ECs are understood to be a rich source of molecular trophic signals with important roles in regulating adult neural stem cell homeostasis and function (Leventhal et al., 1999; Shen et al., 2004; Lok et al., 2007). In addition to the well-documented involvement in neurogenic progenitor cell behaviour, recent research has elucidated analogous communication between the vascular endothelium and OL lineage cells. Brain-derived neurotrophic factor (BDNF), related to the canonical nerve growth factor (NGF), is secreted from cortical ECs and is known to regulate NSC and OL development. BDNF promotes OLP proliferation and differentiation in vivo and in vitro, and these effects are mediated through Trkb and the MAP kinase pathway (Van't Veer et al., 2009; Vondran et al., 2010; Xiao et al., 2010). Furthermore, in cultured NSCs derived from the cortices of newborn mice, BDNF enhances commitment to the OL lineage (Chen et al., 2013).

Similar to BDNF, FGF-2 is expressed by ECs and has potent effects on OL differentiation (Issa et al., 2005). In the ventral embryonic forebrain, loss-of-function experiments revealed that FGF signaling through FGFR1 and FGFR2 is necessary for OLP generation, while exogenous FGF administration in vitro and in vivo suggests that FGF signaling is sufficient to induce OLP

production (Kessaris et al., 2004; Furusho et al., 2011; Chandran et al., 2003; Naruse et al., 2006; Azim et al., 2012). Treating neural progenitor cell cultures derived from spinal cord with FGF2 triggers Olig2 expression and OLP generation, and microinjection of FGF-2 into the ventricles of the mouse fetal forebrain results in ectopic induction of OLPs in vivo (Chandran et al., 2003; Naruse et al., 2006).

Whether BDNF and/or FGF are *a)* synthesized and released from the embryonic spinal cord vasculature, and *b)* affect OLP specification from pMN-resident NSCs, is yet to be properly investigated. In more rostral brain structures, however, the expression of these soluble signals from vascular ECs and their important roles in OL development exemplify how spinal cord angiogenesis might influence NSC fate choice through short-range action of paracrine signaling molecules.

Summary

The mechanism(s) governing the timing of the MN-OLP fate switch are yet to be established. The timing of spinal angiogenesis and the significant involvement of a number of vascular-related signals – including both long- and short-range signaling factors – in controlling neural stem cell proliferation and differentiation, as well as OL development more specifically, hints at a possible regulatory role in the MN-OLP fate switch.

1.3 TRANSCRIPTION FACTOR OLIG2

At a molecular level, several transcriptional regulators of OL development and function have been identified. Olig1 and Olig2 are members of the basic helix-loop-helix (bHLH) family of transcription factors. These proteins are characterized by a common structural motif (the bHLH domain) and are key regulators of cell-type specification and tissue development in vertebrates and invertebrates. The proneuronal functions of several Drosophila bHLH gene homologs, including Mash1 (Mouse Achaete-scute homolog 1) and the Neurogenin family of Atonal-related transcription factors, were established before identification of the *Olig* genes (Johnson et al., 1990; Sommer et al., 1996). In the human and mouse genomes, *Olig1* and *Olig2* both lie in the same 50 kb region of the genome, indicating duplication of a single ancestral *Olig* gene. The absence of *Olig1* homologues in more primitive non-mammalian vertebrates suggests *Olig2* is the primal variant. Olig2 is expressed throughout oligodendrocyte development and is considered a master regulator of OL lineage commitment and progression. Alongside its oligodendrogenic function, Olig2 is expressed in a variety of distinct neuroepithelial stem cell populations and plays a key role in regulating neuronal as well as glial development. Indeed, closer examination of *Olig* gene function in *Olig1-/Olig2*-single and -compound knockout mouse lines distinguished the critical function of Olig2 for neural tube patterning and MN specification, as well as in OL development (Lu et al., 2002; Park et al., 2002; Takebayashi et al., 2002; Zhou et al., 2002). A third member of the Olig family, Olig3, has been identified. Its transient and isolated expression in distinct regions of the CNS, however, indicates non-overlapping functions with Olig1 and Olig2 (Takebayashi et al., 2000; Takebayashi et al., 2002).

Role in spinal cord patterning

Olig2 expression in the ventral embryonic spinal cord is essential for the establishment of the pMN domain. In *Olig2* knockout (*Olig2*-KO) mice, the Irx3-positive p2 and Nkx2.2-positive p3 domains, spatially separated by the intermediate pMN domain in wild-type embryos, are immediately apposed (Lu et al., 2002). The absence of the pMN in Olig2-deficient mutants is a consequence of ventral expansion of the p2 domain, which subsumes territory normally occupied by Olig2-positive MN progenitor cells. In normal spinal cord development, the induction of Olig2 in the ventral ventricular zone is mediated by Shh signaling from the notochord and floorplate (Lu et al., 2000; Zhou et al., 2000). Global deletion of *Shh* eliminates ventral Olig2 expression, while transgenic Shh production in the dorsal spinal cord in *Wnt-1:Shh* mice is accompanied by ectopic expression of Olig2 (Rowitch et al., 1999; Lu et al., 2000). However, Cre-recombinase labeling indicates that the range of Shh-dependent induction of Olig2 initially includes the putatively Olig2-negative p2 and p3 domains (Dessaud et al., 2007; Dessaud et al., 2010). Concerted down-regulation of Olig2 in the neuroepithelium surrounding the pMN then refines the early, broad pattern of Olig2 expression exclusively to the pMN domain by the onset of neurogenesis at ~E9.5.

Sonic hedgehog-dependent induction and subsequent refinement of Olig2 expression delineates the ventral pMN domain in the nascent spinal cord. After establishment of the pMN domain, resident Olig2-positive neuroepithelial stem cells divide and differentiate to generate MNs followed by OLs. Olig2 is absolutely necessary for formation of the pMN and remains critically important for regulating commitment to both the MN and OL lineages in the spinal cord.

Role in motor neuron specification

Before the discovery of the *Olig* genes, mapping the spatiotemporal pattern of MN and OLP development strongly indicated the two cell types arise in sequence from a single region of the developing spinal cord, the pMN domain (reviewed in Richardson et al., 1997 & 2000). Despite the evidence, however, no pMN-specific factor distinguishing the common progenitors and linking both MN and OLP specification had been identified. Preliminary characterization of Olig2 confirmed restricted expression in ventral neuroepithelium before the emergence of Olig2/PDGFRA double-positive OLPs during the period of MN generation, indicating a possible involvement of Olig2 in MN production.

Olig1 and *Olig2* single-knockout and double-knockout (dKO) mouse lines resolved the developmental requirements for both genes and validated the particular importance of *Olig2* for MN specification (Lu et al., 2002; Zhou et al., 2002). *Olig1/2*-dKO mice fail completely to generate MNs and OL lineage cells throughout the CNS. Comparison with an *Olig2* single-knockout (*Olig2*-KO), in which PDGFRA/Sox10 double-positive OLPs were identified in limited numbers in regions of the rostral CNS, indicates that *Olig1* can partially compensate for the absence of *Olig2* outside the spinal cord. In the spinal cords of *Olig2*-KO mice, however, MN development is entirely replaced by additional V2 interneuron generation from the enlarged p2 domain. In contrast to *Olig2*, *Olig1* was found to be expendable for spinal MN and OL specification (Paes de Faria et al., 2014).

Despite the requirement for Olig2 in MN formation, research in 2005 revealed that Olig2, after initially priming pMN progenitors for neuronal lineage commitment, inhibits differentiation of post-mitotic MNs (Lee et al., 2005). The observations helped to explain both the limited capacity of ectopic Olig2 to trigger MN generation and the abrupt down-

regulation of Olig2 in newly born MNs (Mizuguchi et al., 2001; Novitch et al., 2001; Du et al., 2006). The data suggest that the transition of individual MN progenitors to post-mitotic MNs in the pMN domain is determined by the relative abundance of nuclear Olig2 and pro-neuronal bHLH transcription factor Neurogenin 2 (Ngn2). $Olig2^{high}Ngn2^{low}$ promotes maintenance of the progenitor state over commitment to the MN lineage, and vice versa. Lee et al. (2005) propose that Olig2 performs essential dual functions in MN development. Early on, Olig2 is required for the establishment of the pMN domain and for early neurogenic instruction. Thereafter, Olig2 blocks commitment to the MN lineage in a selection of pMN progenitors by opposing the activity of pro-neuronal factors such as Ngn2.

Role in oligodendrocyte specification

Since its identification in the year 2000, in vivo and in vitro characterization has clearly demonstrated that Olig2 is absolutely critical for embryonic OL specification (Lu et al., 2002; Park et al., 2002; Zhou et al., 2002). ISH mapping experiments confirmed focal *Olig2* expression in the ventral oligodendrogenic neuroepithelium before the emergence of OLPs (Lu et al., 2000). At later embryonic stages, Olig2 is faithfully co-expressed with OLP markers Sox10 and PDGFRA. In the spinal cords of *Olig2*-KO mice, both ventral and dorsal OLP populations fail to develop. Interestingly, discrete clusters of Sox10/PDGFRA double-positive cells do emerge in more rostral structures in the *Olig2*-KO that are entirely absent in *Olig1/2*-dKO mice, indicating that Olig1 can partially compensate for Olig2 deficiency in specific regions of the CNS (Lu et al., 2002). Consistent with this observation, targeted ablation of the *Olig2* gene in dorsal multipotent progenitors in the telencephalon does not entirely prohibit formation of OLPs (Yue et al., 2006). In the embryonic spinal cord, however, *Olig2* is absolutely essential for OL lineage specification – a feature that appears highly conserved among different species (Lu et al., 2002). In the zebrafish spinal cord, for example, MN and

OL development follows an almost identical spatiotemporal structure, and is similarly abolished upon loss of Olig2 (Park et al., 2002).

Beyond the requirement for OL specification, the sufficiency of Olig2 to induce OL lineage commitment proved a more contentious question. In both mouse and human fetal stem cell cultures, Olig2 over-expression triggers differentiation to myelination-competent OLPs in vitro and after engraftment into the dysmyelinated brains of *shiverer* mice (Copray et al., 2006; Maire et al., 2009). In vivo studies performed in chick have, however, yielded conflicting results. Early *Olig2* electroporation experiments clearly indicated that ectopic OLP formation required misexpression of Olig2 in combination with Nkx2.2, and that neither factor alone was adequate (Sun et al., 2001; Zhou et al., 2001). In direct contrast to these results, research published in 2007, adopting a very similar electroporation strategy, identified ectopic and precocious Sox10-positive OLPs four days after introduction of an *Olig2*-only expression construct, suggesting Olig2 on its own is sufficient for OL fate selection (Liu et al., 2007). The authors suggest that the different observations might be a consequence of variation in the intensity and duration of exogenous Olig2 expression.

Role in oligodendrocyte differentiation

The sustained expression of Olig2 along the OL lineage gave an early indication that Olig2 might function in OL differentiation. More recent research has validated the importance of Olig2 in regulating maturation, as well as uncovering the dynamic nature of its involvement – Olig2 performs specific roles depending on the stage from OLP to myelinating OL (Yue et al., 2006; Mei et al., 2013). In cell culture experiments, antisense knockdown of *Olig2* in cultures derived from rodent spinal cord significantly delays induction of late-stage OL lineage markers GalC and proteolipid protein (PLP) (Fu et al., 2002). Co-suppression of transcription

factor (TF) Nkx2.2 and Olig2 in these cultures also has an additive inhibitory effect, suggesting both transcription factors synergistically and positively regulate OL differentiation. In vivo, conditional deletion in early cortical progenitors in mice indicates progression of OLPs to myelinating OLs requires Olig2 (Yue et al., 2006). Olig2-deficiency does not prevent generation of cortical OLPs but does result in a marked reduction in the expression of myelin genes and severe hypomyelination. In support of a central and positive regulatory role in driving OL differentiation, prolonged misexpression of Olig2 (for five days) in the chick spinal cord induces mature OL markers myelin basic protein (MBP) and PLP (Liu et al., 2007).

This straightforward view of Olig2 promoting differentiation was called into question by the results of comprehensive immunostaining for OL lineage TFs Olig1, Olig2, Sox10 and Nkx2.2 (Kitada & Rowitch, 2006). Analysis of Olig2 expression alongside established OL lineage markers in the adult mouse spinal cord found terminal differentiation of mature OLs coincides with down-regulation of Olig2. The functional significance of the observation, however, was unclear. Mei et al. (2013) directly addressed the question of diversity of Olig2 function in early postnatal OLPs versus OLs, and characterized a complex and dynamic influence on differentiation. Stage-specific deletion under either *CNP* promoter (OLP-specific) or *PLP* promoter (immature OL-specific) Cre drivers revealed divergent functions of Olig2 at different points along the lineage. In the early phase of OLP development, Olig2 positively regulates differentiation, stimulating progression towards becoming a mature OL. In contrast, Olig2 appears to inhibit myelination, arresting pre-myelinating OLs immediately before the final stage of maturation.

The existing data indicate that Olig2 is initially a necessary positive regulator of commitment to and early progression along the OL lineage. At later stages of OL differentiation, the role of Olig2 appears to transform from pro- to anti-maturation, with development of myelinating

OLs requiring a reduction in the level of Olig2. Despite down-regulation of Olig2 in mature OLs in the adult CNS, however, Olig2 continues to be expressed and localized to the nucleus throughout the OL lineage. This observation is difficult to reconcile with the reported anti-maturation role of Olig2 in immature OLs, and suggests there are important facets of Olig2-mediated regulation of OL differentiation that are still to be discovered. Indeed, the precise function of Olig2 in mature and myelinating OLs is yet to be addressed in vivo.

Additional roles of Olig2: forebrain neurogenesis and astrogliogenesis

Forebrain neurogenesis

Analysis of the localisation and distribution of Olig2-positive cells at different embryonic stages established a dynamic spatiotemporal pattern of Olig2 expression in the developing mouse forebrain (Takebayashi et al., 2000; Furusho et al., 2006; Kessaris et al., 2006; Ono et al., 2008). In the telencephalon, Olig2 expression begins at E10.5 in the ventral ventricular zone, localizing to the medial ganglionic eminence (MGE), septum and anterior entopeduncular area (AEP) until E12.5. By E17.5, Olig2-positive cells are distributed throughout the parenchyma of the telencephalon but remain clustered in the ventral ventricular zone [including the lateral ganglionic eminence (LGE)]. The progeny of Olig2-expressing stem cells in the forebrain have been characterized by short- and long-term lineage tracing experiments using an inducible *Olig2-Cre-Reporter* system (Furosho et al., 2006; Miyoshi et al., 2007; Ono et al., 2008).

In the basal forebrain, Olig2 lineage cells generate excitatory cholinergic (choline acetyl-transferase- (ChAT-) positive) neurons (Furosho et al., 2006). In the MGE, labeling Olig2-expressing cells at different time points revealed that different inhibitory cortical interneuron subtypes are generated in strict temporal sequence (Miyoshi et al., 2007). In addition, a

considerable number of excitatory glutamatergic neurons derive from Olig2 progenitors and are found in the adult hypothalamus (Ono et al., 2008). These fate-mapping studies clearly show that Olig2-positive cells in the embryonic forebrain contribute to a number of distinct neuronal populations – both excitatory and inhibitory – and that subtype generation is spatially and temporally determined.

The nature of Olig2 function in different forebrain progenitor populations at different embryonic time points has not been fully elucidated. In *Olig2*-null mice, the effect of Olig2 deficiency on neuronal specification varies according to neuronal subtype. For cholinergic neuron development in the basal forebrain, *Olig2* knockout leads to an approximately 40% reduction at E18.5 in mice (Furosho et al., 2006). In contrast, the number and distribution of GABAergic interneurons appears unchanged in E18.5 *Olig2*-null mutant embryos (Ono et al., 2008). A recent study using *Olig1*-null mice, however, indicates that Olig1 is a repressor of *Dlx1/2* and a negative regulator of interneuron production in the mammalian brain (Silbereis et al., 2014). Nonetheless, while the details of Olig2 function in forebrain neurogenesis are unclear, the existing data indicate Olig2 serves specific functions in different neurogenic niches.

Astrogliogenesis

Lineage tracing experiments performed in transgenic mice demonstrated that Olig2-expressing pMN domain stem cells in the embryonic spinal cord contribute a subset of astrocytes that localize to the ventral pial surface (Masahira et al., 2006). Olig2 has been detected in astrogenic populations of both embryonic and postnatal progenitor cells but is absent from mature astrocytes (Lu et al., 2000; Zhou et al., 2000; Marshall et al., 2005; Masahira et al., 2006; Cai et al., 2007; Chen et al., 2008; Ono et al., 2008; Zhu et al., 2011). Indeed, development of fully mature astrocytes from neural progenitors in vitro is inhibited

by forced expression of Olig2 (Fukuda et al., 2004; Setoguchi & Kondo, 2004). In contrast however, retroviral introduction of either normal or dominant-negative forms of Olig2 in mice demonstrated wild-type Olig2 promotes astrocytic over neuronal development in progenitor cells in the neonatal subventricular zone (Marshall et al., 2005). Taken together, the results suggest that Olig2 might initially promote formation of immature astrocytes while removal of Olig2 is necessary for the later steps of astrocyte differentiation. More recent research in vivo has described transient Olig2 expression in immature astrocytes and subsequent down-regulation over later stages of differentiation (Cai et al., 2007). In addition to the temporal variation along the astrocyte lineage, targeted *Olig2* knockout in mice has revealed spatial differences in Olig2 function (Cai et al., 2007; Zhu et al., 2012). Conditional *Olig2* deletion using a human *GFAP* promoter-driven Cre has been reported to generate an astrocyte deficit in the cortical and spinal white matter (Zhuo et al., 2001; Cai et al., 2007). In contrast, conditional *Olig2* deletion in neocortical NG2 cells using an *NG2-Cre* line triggered protoplasmic astrocyte formation at the expense of OLs, suggesting that Olig2 inhibits astrocyte specification in NG2 cells (Zhu et al., 2012). It therefore appears that, similar to its roles in forebrain and spinal cord neurogenesis, the involvement of Olig2 in astrocyte development differs according to cell maturity and region-specific subtype.

1.4 REGULATION OF OLIG2 EXPRESSION IN THE EMBRYONIC SPINAL CORD

The first two *Olig* genes (*Olig1/2*) were first isolated in the year 2000, screening for transcription factor determinants of OL fate. Research since has examined the central role of the ancestral variant Olig2 in CNS development. Olig2 is critical for proper neural tube patterning and for regulating both motor neuron and oligodendrocyte development, as well as anterior neurogenesis. In the following section, I describe the mechanisms underlying regulation of expression of Olig2 in the establishment of the pMN domain, the generation of MNs and the development of both ventral and dorsal OL populations in the embryonic spinal cord (see *Origins of OLPs* above).

Regulation of Olig2 expression in establishment of the pMN domain

Induction of Olig2 expression. Before the onset of neurogenesis in the neural tube, protein morphogen Shh emanating from the ventral notochord and floorplate induces expression of progenitor domain-specific combinations of transcription factors (Briscoe et al., 2000). Shh signaling directly represses class I homeodomain transcription factor genes *Pax6*, *Pax7*, *Irx3*, *Dbx1* and *Dbx2*, and activates class II homeodomain factor genes *Nkx6.1* and *Nkx2.2*. The duration and intensity of exposure of an individual cell to Shh diminishes with distance from the floorplate. As a result, the precise combinatorial expression of homeodomain proteins is determined by a cell's position along the dorsal-ventral axis of the spinal ventricular zone. Strong Nkx6.1 (class II) and weak Pax6 (class I) expression initially characterize presumptive pMN domain cells (Ericson et al., 1997; Qiu et al., 1998; Mizuguchi et al., 2001; Novitch et al., 2001; Balaskas et al., 2012). Transcription of *Olig2* is indirectly regulated by Shh via Nkx6.1 (Novitch et al., 2001; Vallstedt et al., 2001; Liu et al., 2003). Olig2 expression in the ventral ventricular zone is significantly reduced in *Nkx6.1*-null mice and completely absent (a

phenocopy of *Shh*-null mutants) from *Nkx6.1/Nkx6.2* (*Nkx6*-) double-knockout spinal cord at E10.5 and E12.5. In addition, gain-of-function experiments in embryonic chick demonstrated that ectopic Nkx6.1 induces misexpression of Olig2 (Novitch et al., 2001; Liu et al., 2003). After broad Nkx6.1-mediated induction of Olig2 across the ventral third of the spinal ventricular zone (including in the presumptive p2 and p3 domains), transcriptional and post-transcriptional repression in p2 and p3 progenitor cells refines the dorsal and ventral limits of Olig2 expression to the pMN domain.

Refinement of Olig2 expression. In the ventral p3 domain, sustained exposure of progenitor cells to Shh initiates expression of class II homeodomain TF Nkx2.2, which silences *Olig2* gene transcription (Briscoe et al., 1999; Briscoe et al., 2000). *Nkx2.2*-null mice lack the p3 domain and do not generate V3 interneurons, instead producing additional MNs from an expanded Olig2-positive pMN domain (Novitch et al., 2001; Qi et al., 2001). In normal development, mutually repressive interaction between Nkx2.2 and Pax6 at the transcriptional level, potentially combined with a cross-inhibitory physical interaction of Olig2 and Nkx2.2 proteins, restricts dorsal expansion of the p3 domain and defines the p3/pMN boundary (Ericson et al., 1997; Briscoe et al., 2000; Sun et al., 2003). The dorsal extent of Olig2 expression is refined through the cross-repressive transcriptional relationship between the p2 domain-specific class I TF Irx3 and Olig2 itself (Mizuguchi et al., 2001; Novitch et al., 2001). Analogous to the neurogenic phenotype of animals lacking *Nkx2.2*, in *Olig1/2* double-knockout (*Olig1/2*-dKO) mice, ventral expansion of the Irx3-positive p2 domain abolishes the pMN (Zhou et al., 2002). Conversely, in the chick neural tube, electroporation of an Olig2 expression construct silences *Irx3* and triggers ectopic MN production (likewise, *Irx3* electroporation effectively represses *Olig2* and promotes V2 interneuron generation) (Mizuguchi et al., 2001; Novitch et al., 2001).

On top of transcription factor-mediated regulation, more recent research has shown involvement of the RNA interference (RNAi) pathway in fine-tuning the pattern of Olig2 (Chen et al., 2011). In E9.5 mice, microRNA cluster *mir-17~92* is upregulated in the p2 domain. As part of the RNA-induced silencing complex, mature *mir-17* specifically hybridizes with the 3' untranslated region (UTR) of *Olig2* messenger RNA, targeting the transcript for degradation and precluding Olig2 protein synthesis. *Mir-17~92*-null mutants exhibit errant Olig2 expression in the p2 domain, a phenotype also observed in *Dicer* mutants incapable of generating functional miRNAs from primary immature transcripts.

Regulation of Olig2 expression in motor neuron specification

Adult MNs derive exclusively from multipotent Olig2-expressing stem cells of the pMN domain (Lu et al., 2002; Takebayashi et al., 2002; Zhou et al., 2002). During development, post-mitotic immature MNs migrate away from the ventricular zone, settling in the ventral and lateral horns of the spinal cord, before undergoing the final stages of differentiation. The transition from uncommitted progenitor to post-mitotic immature MN is associated with the rapid down-regulation of *Olig2* (Lu et al., 2000; Zhou et al., 2000; Mizuguchi et al., 2001; Novitch et al., 2001). The transcription factor(s) responsible for negatively regulating *Olig2* gene expression are not known. Expression of Olig2 with the motor neuron determinant Homeobox 9 (Hb9) is temporally non-overlapping, indicating that upregulation of Hb9 might directly or indirectly silence Olig2 gene transcription (Lee et al., 2005). The swift removal of Olig2 protein from differentiating MNs also suggests that additional, cooperative mechanisms might be involved, perhaps including *mir-17~92* microRNAs.

Regulation of Olig2 expression in dorsal oligodendrocyte specification

Approximately 20% of OLs in the spinal cord derive from stem cells resident in the dorsal ventricular zone (Richardson et al., 2006; Tripathi et al., 2011). Production of dorsal Olig2-positive cells begins around E14.5, approximately 2 days after the emergence of the first pMN-derived OLPs. In contrast to Shh- and Nkx6.1-mediated ventral induction of Olig2, specification of OLPs from dorsal dp3, dp4 and dp5 progenitor domains persists in both *Shh*-null and *Nkx6*-null mutant mice (Cai et al., 2005; Vallstedt et al., 2005; Fogarty et al., 2005). The demonstration in 2005 of Shh- and Nkx6-independent induction of Olig2 in dorsal oligodendrogenesis posed the question of how Olig2 expression is initiated in these precursors.

In the dorsal aspects of the developing spinal cord, specification of neural identity is predominantly determined by graded bone morphogenetic protein (BMP) signaling from the roofplate, analogous to the ventral Shh countergradient (reviewed by Ulloa & Briscoe, 2007; Chizhikov & Millen, 2004). In vitro and in vivo, BMPs inhibit OLP formation while exposure of dorsal progenitors to BMP antagonists Noggin and Chordin triggers precocious OLP formation (Mekki-Dauriac et al., 2002; Miller et al., 2004; Vallstedt et al., 2005). A progressive reduction in BMP concentration during development is therefore thought to relieve repression of OLP genetic programmes, including Olig2 expression.

In cultures of dorsal cord neural progenitors, treatment with fibroblast growth factor (FGF) activates Olig2 expression and stimulates OL production, an observation that remains unaffected by co-administration of cyclopamine, a potent inhibitor of Hh signaling (Chandran et al., 2003; Kessaris et al., 2004). In addition, a small molecule antagonist of FGF receptor signaling blocks induction of Olig2 and OL development in dorsal Pax7-expressing progenitors

(Chandran et al., 2003). In vivo evidence for FGF-mediated regulation of *Olig2* gene expression came in 2010 from research into the control of neural cell diversity in the zebrafish hindbrain (Esain et al., 2010). The data confirm that dynamic BMP activity and FGF signaling combine to regulate dorsal Olig2 expression.

In vitro research has explored the molecular mechanism underlying regulation of Olig2 by BMP and FGF (Bilican et al., 2008). The experiments – also performed using isolated rat dorsal spinal cord progenitors – revealed that the intracellular BMP signaling intermediate SMAD4 associates with the *Olig2* promoter and its dissociation from this genomic binding site correlates with *Olig2* transcription. Induction of *Olig2* after FGF2 addition also requires mitogen activated protein kinase (MAPK) pathway-dependent sequestration of BMP-activated SMAD1 in the cytoplasm (Bilican et al., 2008). In vivo, regulation of sub-cellular localisation of BMP signaling factors by downstream effectors of FGF might critically modulate BMP signaling and thereby permit *Olig2* gene expression and OLP specification in the dorsal spinal cord.

Regulation of Olig2 expression in oligodendrocyte differentiation

Nuclear Olig2, expressed in multipotent pMN NSCs and upregulated in dorsal progenitors upon OL fate specification, is continuously expressed over OL lineage development (Lu et al., 2000; Zhou et al., 2000). Variation in the level of Olig2 expression has, however, been observed in vivo and down-regulation is proposed to regulate critical final steps in OL maturation (see *Introduction to TF Olig2: OL differentiation*) (Kitada & Rowitch, 2006; Mei et al., 2013). The pathways underlying this in vivo adjustment in Olig2 synthesis have not yet been identified. In vitro, cultured OLPs purified from adult spinal cord express BMP receptor subunits Ia, Ib and II, and treatment with BMP2 and 4 results in reduced Olig2 expression and

blocks OL differentiation (Cheng et al., 2007). Inhibition of OL differentiation is rescued by forced Olig2 expression, indicating BMP-induced down-regulation of Olig2 might regulate OL development in vivo, preserving a pool of responsive and proliferative $Olig2^{low}$ OLPs in the adult.

Olig2 sub-cellular localization and astrocyte development

Long-term fate-mapping experiments using an inducible *Olig2-Cre-Reporter* mouse line demonstrated that Olig2+ pMN NSCs generate a discrete population of astrocytes (Masahira et al., 2006). Olig2 is absent from mature astrocytes and its role in regulating pMN astrogliogenesis is not clear. One possibility is that repression of *Olig2* in pMN NSCs initiates a phase of pMN astrocyte production. In the ventral embryonic forebrain, astrocyte specification from Olig2-expressing progenitors requires down-regulation of Olig2 for activation of astrocyte lineage genes such as *glial fibrillary acidic protein* (*GFAP*) (Fukuda et al., 2004). Moreover, conditional deletion of *Olig2* in postnatal NG2 cells is sufficient to trigger a developmental fate switch from OL to astrocyte production in some regions of the CNS (Zhu et al., 2012). The pathways underlying regulation of this Olig2-dependent fate switch have not been identified.

An additional mechanism for modulating TF activity is regulation of nuclear versus cytosolic distribution within the cell. In astrocytes born from Olig2-positive stem cells in the subventricular zone of adult mice, Olig2 is localized exclusively to the cytoplasm, suggesting that nuclear-cytoplasmic translocation might attenuate Olig2 function and thereby permit astrocyte development (Setoguchi & Kondo, 2004). In cell culture, redistribution of Olig2 requires nuclear export signal receptor CRM1 and is necessary for ciliary neurotrophic factor-(CNTF-) induced astrocyte differentiation (Setoguchi & Kondo, 2004). The reported

mechanism involves CNTF-mediated activation of phosphoinositide 3-kinase and Akt intracellular signaling pathways; Akt-dependent phosphorylation of Olig2 at serine 30 induces nuclear-cytoplasmic translocation of Olig2 via nuclear export receptor CRM1 recognition of an Olig2 nuclear export signal peptide.

1.5 MOLECULAR MECHANISMS OF OLIG2 FUNCTION

The uninterrupted expression of Olig2 from early multipotent stem cells, through neurogenic and oligodendrogenic phases of pMN development, to widely distributed, mature and myelinating OLs suggests that Olig2 is performing particular roles in different developmental contexts. Basic HLH transcription factors typically function through cofactor dimerization and regulation of expression of specific target genes, primarily binding E-box consensus sequences in DNA. Here I describe what is understood of the molecular functions of Olig2 during spinal MN specification and OL development.

Olig2 regulation of motor neuron formation

Novitch et al. (2001) and Mizugutchi et al. (2001) explored the pre-oligodendrogenic role of Olig2 in MN induction. Gain-of-function experiments demonstrated Olig2 upregulates pan-neuronal bHLH gene *Neurogenin2* (*Ngn2*), and motor neuron-specific homeodomain genes *MNR2* and *Lim3*. Interestingly, introduction of either an Olig2 'Activator' construct – Olig2 bHLH domain fused to the herpes simplex virus protein 16 transactivation domain – or an Olig2 'Repressor' construct – Olig2 bHLH fused to the repressor domain of *Drosophila* Engrailed protein – indicated that Olig2-mediated gene activation relies on transcriptional repressor activity. Expression of the Olig2 Activator within the pMN domain resulted in loss of Isl1-/Isl2-positive MNs, while the Olig2 Repressor mimicked wild-type Olig2 activity, presumably via indirect de-repression of pan-neuronal (*Ngn2*) and motor neuron-specific (*MNR2* and *Lim3*) determinants (Mizugutchi et al., 2001; Novitch et al., 2001).

Further work has revealed additional complexities in the role of Olig2 in MN development. Besides indirectly activating transcriptional programmes associated with MN specification,

Olig2 also inhibits differentiation of post-mitotic MNs (Lee et al., 2005). DNA binding studies showed that the Ngn2:E47 activator complex and Olig2 target the same E-box elements of pro-MN differentiation genes such as Homeobox gene *Hb9*, activating and suppressing *Hb9* expression, respectively. Dimerization is necessary for bHLH transcription factor activity (Massari et al., 2000; Jones, 2004). Yeast-two-hybrid and co-immunoprecipitation assays detected preferential formation of Olig2:Olig2 homodimers, along with both Olig2:Ngn2 and Olig2:E47 heterodimers (Lee et al., 2005). Repressive Olig2 homodimers competitively bind pro-MN gene regulatory elements, while Olig2 hetero-interactions with Ngn2 and E47 'squelches' the cofactors away from one another and inhibits formation of the functional Ngn2:E47 activator complex (Figure 5). These observations helped to explain the limited capacity of ectopic Olig2 to trigger MN differentiation and the abrupt extinction of Olig2 in newborn MNs (Mizuguchi et al., 2001; Novitch et al., 2001). On the basis of the gene regulation and protein-protein interaction data, Lee et al. (2005) propose a revised model of Olig2 function in the pMN domain (Figure 5). During the neurogenic phase, Olig2 primes pMN-resident stem cells for neuronal differentiation by de-repressing genes such as *Ngn2* and *Lim3*. In Ngn2/Olig2 double-positive cells, Olig2 antagonizes Ngn2 through occupancy of common gene regulatory elements and co-activator sequestration, thereby preventing further MN differentiation. The transition of individual pMN cells from MN progenitors to post-mitotic MNs depends on the relative abundance of nuclear Olig2 and Ngn2; $Olig2^{high}/Ngn2^{low}$ promotes maintenance of the progenitor state over neuronal commitment, and vice versa (Figure 5).

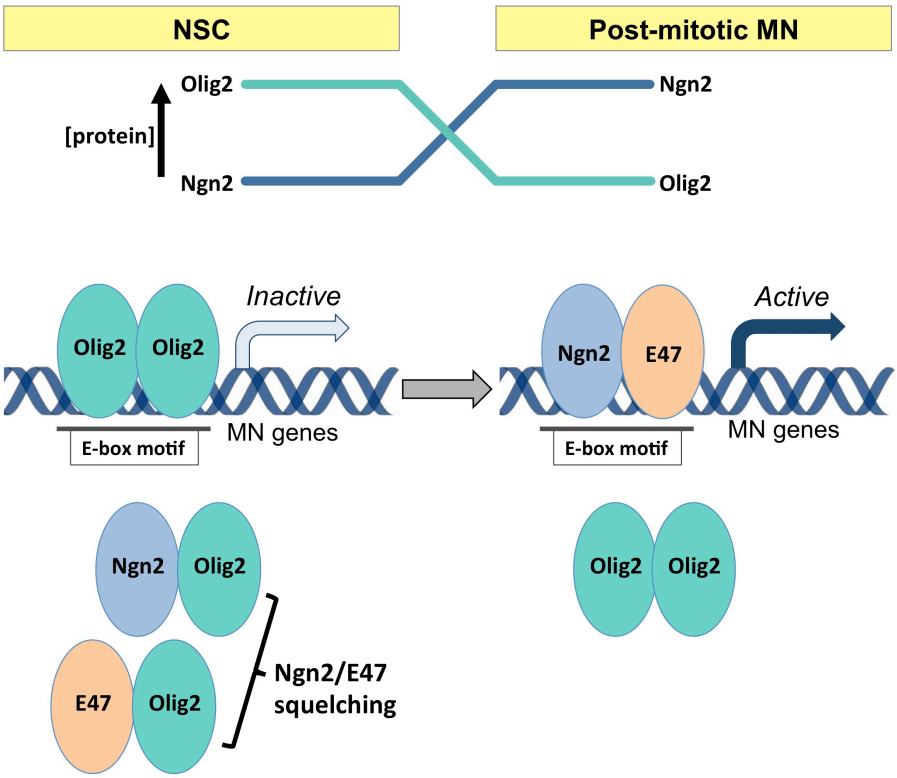

Figure 5. Lee et al. (2005) model for Olig2 and Ngn2 function in MN specification. Olig2 and Ngn2 suppress and activate MN gene expression, respectively. The relative abundance of Olig2 and Ngn2 determines NSC commitment to become post-mitotic MNs. In $Olig2^{high}/Ngn2^{low}$ NSCs (left): 1. Olig2 homodimers bind E-box motifs at MN genes and repress gene transcription; 2. Olig2 squelches Ngn2 and E47 thereby preventing pro-MN Ngn2:E47 complex formation. In $Olig2^{low}/Ngn2^{high}$ post-mitotic MN progenitors (right): 1. Ngn2:E47 heterodimers displace Olig2 from E-box motifs at MN genes and activate gene transcription.

Ligon et al. (2007) characterized an additional Olig2-dependent mechanism for preserving the replication-competent progenitor pool. In neurosphere cultures derived from wild-type or *Olig2*-null embryonic rats, the absence of Olig2 is associated with a significant reduction in proliferation rate, suggesting that Olig2 promotes cell cycle progression. Computational analysis predicted that the p53-inducible inhibitor of cell cycle progression $p21^{WAF/CIP1}$ (*p21*) is a direct target of Olig2. Chromatin immunoprecipitation (ChIP) of Olig2 bound genomic fragments confirmed Olig2 occupancy of the *p21* promoter in neural progenitor cell cultures. Finally, in a human glioma cell line, forced expression of Olig2 suppresses activation of a *p21/luciferase* reporter construct, suggesting that Olig2 opposes post-mitotic MN

differentiation by direct transcriptional repression of the *p21* gene and inhibition of cell cycle exit.

Examining the gene regulatory network regulating NSC development, Mateo et al. (2015) reported the results of high-throughput Olig2 ChIP-seq from primary cultures of NSCs. The genome-wide location analysis revealed that Olig2 occupies the *cis*-regulatory elements of genes required for neuronal differentiation and quiescence. Integrating the ChIP-seq results with data from parallel DNA microarray analysis of *Olig2*-expressing and *Olig2*-null NSC cultures established a dual role for Olig2 in transcriptional regulation. Olig2 deficiency induced upregulation and down-regulation of distinct Olig2 target genes, indicating that Olig2 acts as both a transcriptional activator and repressor. Moreover, gene ontology (GO) analysis revealed enrichment of several GO terms relating to neuronal differentiation (including "neurogenesis") among Olig2-repressed genes. Conversely, the GO analysis found Olig2-activated genes are significantly associated with biological processes including "cell cycle" and "DNA replication", consistent with a role for Olig2 in promoting NSC proliferation. Overall, the data highlight the dual functionality of Olig2 as a transcriptional activator and repressor in promoting NSC self-renewal and inhibiting neuronal differentiation.

Olig2 is essential for MN development, though its role in regulating MN generation is more complex than was first appreciated. Olig2 appears to act as an early positive regulator of neuronal differentiation, activating genes such as Ngn2, before switching to anatagonize neuronal differentiation, acting instead to preserve the undifferentiated stem cell state and maintain a reservoir of non-restricted pMN progenitors for the gliogenic phase of development.

Olig2 regulation of oligodendrogenesis

Electroporation of *Olig2* into the chick spinal cord is sufficient to trigger ectopic and precocious OL differentiation (Liu et al., 2007). Genetic evidence from these experiments indicates that High Mobility Group (HMG) box TF Sox10 acts downstream of Olig2 and directly mediates Olig2 function. Introduction of Sox10 alone mimics the effects of ectopic Olig2 expression – inducing OL markers MBP and PLP – but on an accelerated timeline. Kuspert et al. (2011) identified the conserved upstream *U2 enhancer* of *Sox10* gene as an Olig2 target and important regulatory element in OL development. The expression pattern of a *U2-lacZ* transgene that specifically labels *U2*-active cells revealed that the *U2 enhancer* drives *Sox10* expression in OLPs after the initial induction of *Sox10* expression. The *U2 enhancer* is also silenced during terminal differentiation and remains inactive in mature OLs, suggesting that additional regulatory regions drive both early and late stage *Sox10* transcription in OLs in vivo. Although the *U2 enhancer* is not active immediately post-specification and in mature OLs, both of which are Sox10+ stages of the OL lineage, the *U2 enhancer* is necessary for *Sox10* gene expression in committed OLPs. In vitro, electromobility shift (EMS) and luciferase reporter assays confirmed that Olig2:E47 dimer binding at the *U2 enhancer* site triggers enhancer activation. In vivo, analysis of a transgenic mutant *U2mut-lacZ* reporter mouse line, lacking the principal Olig2 target sequence within the *U2 enhancer*, revealed diminished *U2* activation in E16.5 spinal cords and the importance of the site for Olig2-binding and *U2* activity in vivo.

In addition to transcriptional regulation of Sox10, yeast two-hybrid screens for mouse Sox10 binding partners identified Olig2, suggesting the two TFs might physically interact in Sox10-positive OLPs in vivo (Wissmuller et al., 2006). Interestingly, in zebrafish, Olig1 alone specifically associates with Sox10 and enhances Sox10-mediated activation of MBP

expression in vivo (Li et al., 2007). It is possible that Olig2 and Sox10 engage in a similar manner to regulate MBP transcription and promote OL differentiation in mice, though this has not as yet been described in vivo.

Since the introduction of next generation DNA sequencing technologies, results from independent genome-wide Olig2 target-mapping experiments have been published (Weng et al., 2012; Yu et al., 2013; Mateo et al., 2015). Weng et al. (2012) performed Olig1 and Olig2 ChIP-seq using purified rat OLs. The data identified 5439 distinct candidate Olig2 binding sites. Comparison with the Olig1 dataset revealed *Smad-interacting protein 1* (*Sip1*) is a common gene target of both Olig TFs, with multiple Olig2 binding sites within the *Sip1* gene. The effects on Sip1 expression of either Olig2 deficiency in vivo or of forced Olig2 over-expression in cultured neural progenitors clearly suggest Olig2 directly activates Sip1 transcription. In OLPs, Sip1 – a member of the zinc finger homeobox family of TFs – indirectly blocks BMP-induced expression of Inhibitor of Differentiation TFs ID2 and ID4. This process, mediated largely through Sip1-mediated transcriptional activation of the BMP signaling inhibitor *Smad7*, is critical for OL maturation and myelinogenesis, but not for formation of PDGFRA-positive OLPs.

Olig2 is itself a key target of BMP/ID pathway-mediated inhibition of OL differentiation. The BMP signaling effectors ID2 and ID4 directly interact with Olig2, sequestering Olig2 away from its genomic targets and disrupting its pro-OL function (Samanta & Kessler, 2004). Olig2/Sip1-dependent silencing of ID2 and ID4 expression, therefore, upregulates Olig2 activity, forming a positive feedback loop driving OL lineage progression, while BMP-induced IDs sensitize individual cells to BMP signaling by repressing Olig2 function and thereby prevent OLP differentiation. As both a regulator and target in BMP signaling, Olig2 thereby facilitates crosstalk between the pro- and anti-OL differentiation pathways.

Yu et al. (2013) carried out Olig2 ChIP-seq experiments in OLPs, immature OLs (iOLs) and mature OLs (mOLs), characterized according to stage-specific combinatorial expression of OL lineage genes CNP, Mag, PLP and MBP. The three datasets consist of 21901, 25787 and 2759 Olig2 binding sites in OLPs, iOLs, and mOLs respectively, confirming the dynamic nature of Olig2 target choice over the course of OL differentiation. Parallel genome-wide mapping of Brg1 – the central ATPase subunit of the SWI/SNF chromatin remodeler complex – revealed Brg1 is predominantly associated with genomic sites pre-occupied by Olig2 in immature OLs, including at the established *U2 enhancer* of *Sox10* (Kuspert et al., 2011). Brg1 and Olig2 co-occupancy correlates strongly with histone modifications marking active transcription (such as histone 3 lysine 27 (H3K27) acetylation), and RNAi knockdown of Brg1 in culture reduces OL lineage gene expression. Furthermore, Olig2 and Brg1 co-immunoprecipitate in iOLs, suggesting that Olig2 physically recruits Brg1 to its OL gene E-box binding sites to activate gene expression and promote the OLP to iOL transition. In mature OLs, Brg1 and Olig2 do not co-localize at common sites and instead regulate distinct target genes. The mechanisms underlying the transient nature of Olig2/Brg1 cooperation have not been investigated.

Opposing roles for Olig2 at different points along the OL lineage – promoting OLP-iOL but inhibiting iOL-mOL transitions – were described in 2013 based on the results of stage-specific *Olig2* deletion in mice in vivo (Mei et al., 2013). Mei et al. reported that the pro- and anti-OL functions of Olig2 correlate with contrasting effects on Olig1 expression. *Olig2* ablation in OLPs results in a reduction in Olig1 expression, while similar ablation in iOLs is reported to trigger excessive Olig1 expression. In combination, the observations suggest that Olig2 encourages OLP differentiation via activation of expression of Olig1, before repressing Olig1 in iOLs to restrict late-stage lineage progression. The observation in vitro that forced up- or down-regulation of Olig1 is sufficient to rescue the effect of *Olig2* ablation in OLPs and iOLs,

respectively, suggests Olig2-mediated regulation of Olig1 expression might be an important component of Olig2 function. For both the OLP-specific activation and iOL-specific repression of Olig1 expression, however, the mechanism underlying the proposed regulatory role of Olig2 (transcriptional or post-transcriptional; direct or indirect) is not known. In addition, it should be noted that analysis of *Olig1*-null mice has confirmed Olig1 is expendable for OL development, indicating Olig1 is non-essential for Olig2-mediated regulation of OL lineage progression (Mei et al., 2013; Paes de Faria et al., 2014).

Additional Olig2 cofactors have been identified in vitro. Co-immunoprecipitation assays performed in transfected Cos7 cells have shown Olig2 physically interacts with both Nkx2.2, a homeodomain TF necessary for OL differentiation, and the transcriptional activator p300, a histone acetyltransferase (Sun et al., 2003; Fukuda et al., 2004). The functional significance of these interactions in OL lineage cells in vivo has not been established.

While our understanding is far from complete, research to date has revealed Olig2 performs a number of functions in different cell types at different developmental stages. This variety in function is underscored by a diverse and dynamic range of molecular operations, including direct activation and suppression of target gene transcription, hetero-complex formation and regulation of cofactor function at the protein level.

1.6 OLIG2 PHOSPHORYLATION

Discovery of the different developmental and molecular functions of Olig2 has been accompanied by research into the mechanisms directing its stage- and cell type-specific activity. Post-translational modifications (PTMs) at specific amino acid residues – including serine/threonine phosphorylation – coordinate, often in combination, the precise functions of transcription factors, altering secondary and tertiary structure and modulating sub-cellular localization, DNA binding, stability and association with coregulator proteins (Benayoun & Veitia, 2009; Filtz et al., 2014). Mouse Olig2 contains more than 60 serine/threonine residues (of 323 total), suggesting that post-translational addition and removal of phosphate groups might be critical for modulating the different functions of Olig2 (Li et al., 2011; Sun et al., 2011). Two-dimensional PAGE and western blot (WB) analysis of Olig2 before and after treatment with calf intestinal phosphatase has confirmed phosphorylation at multiple sites in vivo (Li et al., 2011). Summarized below, research from several labs has begun to characterize the regulation and functional significance of particular phospho-modifications of Olig2 (Figure 6).

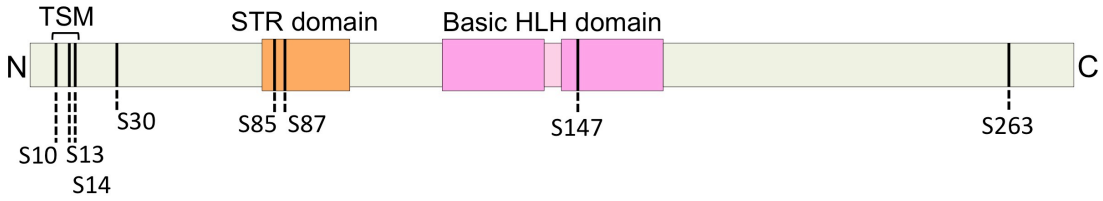

Figure 6. Serine phosphorylation sites conserved in human and mouse Olig2. Olig2 contains a number of established phospho-acceptor serine residues, including the N-terminal triple-serine motif (TSM), S85 and S87 within the serine-threonine-rich (STR) domain and S147 within the bHLH domain. The TSM and S147 are also entirely conserved in chicken, *Xenopus laevis* and zebrafish.

Serine-threonine-rich domain phosphorylation

The amino-terminal half of mammalian Olig2 contains a string of 12 contiguous serine/threonine residues, known as the serine-threonine-rich (STR) domain. Huillard et al. (2010), examining the role of the prolific serine/threonine kinase casein kinase 2 (CK2) in NSC proliferation and OLP specification, identified Olig2 as a CK2 substrate. In vitro, radioactive ^{32}P incorporation demonstrated CK2-dependent phosphorylation of an N-terminal Olig2 fragment (amino acids 1-177), while subsequent Edman degradation isolated the STR domain as the target within the phosphorylated Olig2(1-177) peptide. Of the 12 constituent amino acids that form the STR domain, S85 and S87 were identified as the major phospho-acceptors, along with minor sites S84, T86 and S88. Experiments conducted with neurosphere cultures suggest that the STR domain is required for the pro-OL activity of Olig2. However, Huillard et al. (2010) did not characterize the impact of STR domain phosphorylation on Olig2 function either in vitro or in vivo.

Serine 30 phosphorylation

Setoguchi and Kondo revealed phosphorylation-dependent regulation of Olig2 intracellular localization (Setoguchi & Kondo, 2004). CNTF-stimulated Akt activation induces Olig2 translocation from the nucleus to the cytoplasm – an essential process for NSC astrocyte differentiation in vitro – via nuclear export signal (NES) receptor CRM1. In an in vitro kinase assay, Akt phosphorylates wild-type Olig2, while a phospho-null mutant form of Olig2 in which serine 30 is mutated to an alanine (Olig2-S30A) remains unmodified, indicating that Akt directly targets Olig2 S30. In transfected cultures of COS cells and primary NSCs, Olig2-S30A is predominantly nuclear, in contrast to largely cytoplasmic wild-type Olig2, and mutant expression is associated with a reduced capacity for generating GFAP+ astrocytes in the

presence of CNTF. Taken together the results indicate Akt-mediated phosphorylation of Olig2 at serine 30 triggers Olig2 expulsion from the nucleus and regulates astrocyte differentiation from NSCs in the adult subventricular zone (Setoguchi & Kondo, 2004).

Amino terminal triple-serine phosphorylation

Sun et al. (2011) mapped bona fide phosphorylation sites in endogenous Olig2 purified from primary human glioma xenografts and neurosphere cultures by mass spectrometry (MS). High-confidence phosphorylation sites were identified in both mouse and human Olig2 at S10, S13 and S14, constituting a highly conserved triple-serine motif within the amino terminal domain. Phosphorylation of the Olig2 S10/13/14 motif is developmentally regulated and an important positive regulator of neural progenitor cell proliferation. Using an antibody that specifically recognizes the phosphorylated Olig2 triple-serine motif, Sun et al. (2011) observed a decrease in Olig2 S10/13/14 phosphorylation at postnatal versus earlier embryonic stages of development. In secondary neurosphere assays measuring the proliferative capacity of NSCs, the population growth of *Olig2*-null cells complemented with a triple phospho-null Olig2 expression construct (S10/13/14 all mutated to either valine or glycine) was markedly limited. In contrast, S10/13/14 substitution with the negatively charged amino acid glutamate in a triple phospho-mimetic Olig2 mutant rescued the pro-mitogenic function of Olig2, suggesting S10/13/14 phosphorylation is crucial for Olig2-mediated regulation of NSC proliferation. Consistent with these results, the oncogenic potential – after inoculation into the mouse brain – of triple phospho-null Olig2-expressing tumour neurospheres is significantly lower than wild-type Olig2-expressing neurospheres. The findings of Sun et al. (2011) indicate phosphorylation of Olig2 at its amino terminal triple-serine motif regulates proliferation and potentially entry into post-mitotic phases of differentiation of neural progenitors over the course of development.

Research published more recently from the same group investigated precisely how phosphorylation of the triple-serine motif influences Olig2 activity (Meijer et al., 2014). In the DNA-binding mutant Olig2-N114H – in which mutation of bHLH asparagine 114 to histidine abolishes the DNA-binding capability of Olig2 – S10/13/14 triple-serine mutation does not affect neural progenitor cell proliferation in vitro, indicating that the pro-mitogenic effects of S10/13/14 phosphorylation require Olig2:DNA interaction. RNA-seq analysis uncovered important, growth-/proliferation-related differences in the gene expression profiles of *Olig2*-null NSCs transduced with either triple phospho-null or phospho-mimetic Olig2 variants. ChIP analyses performed on the same cells, however, found no difference in genomic binding site occupancy between the Olig2 mutants, indicating that Olig2 S10/13/14 phosphorylation regulates gene transcription but not E-box target recognition. Exploring the phosphorylation state-specific regulation of a constant set of gene targets, Meijer et al. (2014) describe differential intranuclear compartmentalization (open versus condensed chromatin) of endogenous S10/13/14 phosphorylated and dephosphorylated Olig2 in wild-type NSC cultures. Phospho-Olig2 is enriched in open chromatin, while Olig2 isolated from condensed chromatin structures is typically dephosphorylated. This uneven distribution of different Olig2 isoforms is accompanied by differential access to coregulator proteins. Tandem antibody purification and MS of Olig2 binding partners identified open chromatin fraction-specific cofactors, including HDAC1, and condensed chromatin-specific cofactors, including NF1A, both of which were confirmed by co-immunoprecipitation from different nuclear fractions.

The successive studies by Sun et al. (2011) and Meijer et al. (2014) characterize a developmentally regulated phosphorylation of Olig2 at a highly conserved amino terminal triple-serine motif. In the nuclei of neural progenitors, phosphorylated Olig2 is concentrated

in regions of transcriptionally active open chromatin, where interaction with compartment-specific protein partners regulates gene expression, promoting cell cycle progression and progenitor cell proliferation. Dephosphorylation triggers intranuclear relocalization of Olig2 to condensed chromatin, and interaction with different cofactors. The precise function of these interactions in transcriptionally inert chromatin structures is not fully understood.

Basic helix-loop-helix domain serine 147 phosphorylation

Post-translational modification of the bHLH domain regulates cofactor dimerization and DNA binding in a number of different TFs (for example, Ngn2 [Hindley et al., 2012] and Twist [reviewed by Xue & Hemmings, 2012]). Phosphorylation of Olig2 at serine 147 (S147) has been identified by Li et al. (2011) as a key determinant of pMN domain-resident NSC fate in the embryonic spinal cord, regulating the developmental switch from MN to OLP production (see *Oligodendrocyte Specification* above). Alignment of the Olig2 protein sequences from different species and in silico motif analysis identified an evolutionarily conserved and predicted protein kinase A (PKA) target site within the bHLH domain, S147. In vitro analysis comparing wild-type Olig2 and an Olig2 phospho-null (Olig2-S147A) mutant confirmed that Olig2 can be phosphorylated at S147. Visualizing the phosphorylation state of S147 in E9.5, E11.5 and E13.5 mice spinal cord by western blot, using an antibody that specifically recognizes the phospho-S147 form of Olig2, revealed that endogenous Olig2 is initially phosphorylated at S147 during the MN specification phase and dephosphorylated over the MN-OLP fate switch.

In order to study the role of Olig2 phosphorylation at S147 in vivo, Li et al. generated a transgenic mouse line expressing the phospho-null Olig2-S147A mutant protein on an *Olig2*-null background (Olig2-S147A). These Olig2-S147A mice display a similar patterning defect to

Olig2-null mutants, in which ventral expansion of the Olig2-negative, Irx3-positive p2 domain completely supplants the pMN domain (Lu et al., 2002). As a consequence, Olig2-S147A mutant mice die at birth having failed to generate MNs. This evidence suggests S147 phosphorylation is necessary for Olig2 to perform its early patterning and neurogenic functions in the developing spinal cord. Unlike in Olig2 deficient embryos, however, which also entirely lack spinal cord Sox10-/PDGFRA-positive OLPs, sparse OLP formation is observed in Olig2-S147A mutant spinal cords by E18.5, suggesting that Olig2 S147 phosphorylation is not required for OL development. In fact, forced expression of Olig2-S147A in both the dorsal chick neural tube and cultured P19 cells induces OLP formation at greater efficiency than wild-type Olig2. In differentiating P19 cell cultures transfected with wild-type Olig2 Hb9-positive MNs also arise in significant numbers, and these are virtually absent under the same conditions when expressing the Olig2-S147A mutant form of Olig2. In pMN-resident NSCs, phospho-S147 Olig2 therefore appears to establish the pMN domain and potentially regulate MN generation. Dephosphorylation of Olig2 S147 at ~E12.5 in mice then arrests the programme of MN specification and initiates the successor programme of OLP formation.

As well as elucidating the developmental impact of Olig2 (de)phosphorylation at S147, Li et al. (2011) performed preliminary in vitro experiments to identify the underlying molecular mechanisms. Computational analysis of the Olig2 primary structure revealed that S147 in its primary structure context conforms to the PKA target consensus motif. To assay the effect of PKA activity on Olig2 S147 phosphorylation, Olig2-S147A and wild-type Olig2 expression constructes were transfected either alone or in combination with a dominant-negative form of PKA (dnPKA) into Cos 7 cells, and the phosphorylation patterns compared by two-dimensional PAGE and WB. The dnPKA altered the wild-type phospho-Olig2 signal to resemble that of Olig2-S147A, indicating that PKA can phosphorylate Olig2 S147 in vitro.

The position of S147 within the bHLH domain implied that S147 phosphorylation might affect TF dimerization and/or DNA-binding. Differences in the co-immunoprecipitation of wild-type or phospho-null mutant Olig2 with the established Olig2 cofactors Ngn2, Sox10, Olig1 and Olig2 itself indicated that S147 phosphorylation alters the dimerization properties of Olig2. Wild-type Olig2 forms homodimers and Olig2:Olig1 heterodimers, while Olig2-S147A preferentially binds Ngn2. These phospho-dependent changes in co-factor choice were confirmed in a mammalian two-hybrid system. An electro-mobility shift assay (EMSA) using the known Olig2 target E-box within the *Hb9* promoter also revealed a diminished DNA binding activity of the mutant Olig2-S147A. Interestingly, however, in a luciferase assay measuring the activity of the *Hb9* promoter, phospho-null mutant Olig2 acted as a more potent repressor of Ngn2-mediated transcription than wild-type Olig2, suggesting that Olig2-S147A:Ngn2 dimer formation is sufficient to silence *Hb9* transcription independent of Olig2 occupancy of the *Hb9* promoter. It should be noted, however, that the Olig2-S147A mutant might not accurately model the dephosphorylated form of wild-type Olig2. In other words, the S147A mutation might alter the molecular properties of Olig2 independent of phosphorylation. Li et al. (2011) propose that the stability, nuclear localisation and capacity of the mutant protein to bind known transcriptional partners and drive spinal OLP formation indicates that Olig2-S147A does not represent a loss-of-function mutant. Nonetheless, in the absence of a comparative analysis of the protein- and DNA-binding properties of dephosphorylated wild-type Olig2 and the Olig2-S147A mutant, the veracity of the phosphonull mutant model remains to be fully established. This could, for example, be addressed in vitro using the Cos7 cell system, co-transfecting wild-type or phosphonull mutant Olig2 with a dnPKA – shown by Li et al. (2011) to dephosphorylate Olig2 at S147 – and examining the activity of the dephosphorylated wild-type and mutant Olig2 proteins.

Unifying the in vivo and in vitro data, Li et al. (2011) propose a model of how reversible phosphorylation of Olig2 S147 might sequentially regulate MN and OLP fates in the embryonic spinal cord (Figure 7). During the initial patterning and neurogenic phases of development, Olig2 is phosphorylated at S147, preferentially forming Olig2 homodimers. In this state, pro-neuronal TFs, such as Ngn2, activate a programme of MN gene expression, while phospho-S147 Olig2 homodimers bind and repress OL lineage genes. At the time of the MN-OLP fate switch, Olig2 S147 dephosphorylation – catalyzed by an as yet unidentified phosphatase enzyme – induces a change in Olig2 cofactor choice from homo- to heterodimer formation. Dephosphorylated Olig2 complexes with Ngn2 and presumably additional co-regulator proteins and – through a combination of DNA-independent (pro-MN TF sequestration) and DNA-dependent (OL gene activation) mechanisms – replaces the programme of neurogenesis with a programme of oligodendrogenesis.

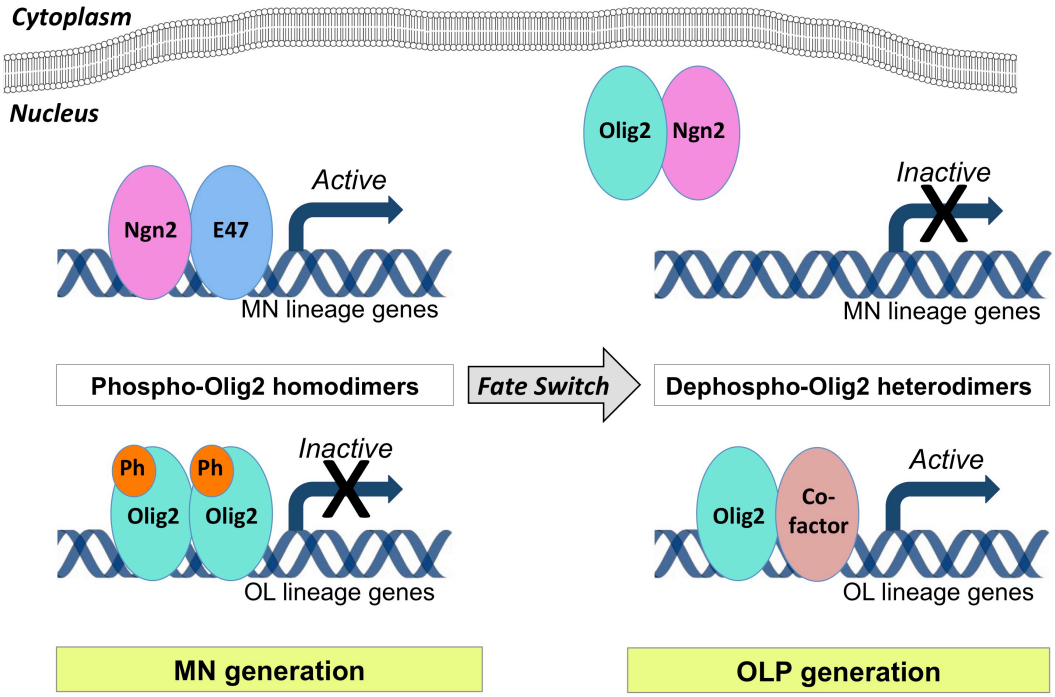

Figure 7. Li et al. (2011) model of Olig2-mediated NSC fate specification. *MN generation:* Olig2 – expressed in pMN domain-resident NSCs – is phosphorylated at S147. Phospho-Olig2 forms homodimers, repressing OL lineage gene expression and enabling activation of MN lineage genes by pro-neuronal TFs such as Ngn2. *OLP generation:* Over the MN-OLP fate switch, Olig2 is dephosphorylated at S147. Dephospho-Olig2 forms heterodimers, sequestering pro-neuronal TFs such as Ngn2 to inactivate MN lineage genes and activating OL lineage genes in complex with additional co-regulator proteins.

1.7 SUMMARY

Our understanding of the importance of myelinating OLs for proper CNS function, and the profound consequences of OL loss in neurodevelopmental disease, has nurtured a longstanding interest in OL biology. Over the last twenty years, advancements in the genetic tools available to researchers have yielded major improvements in our understanding of OL development. OLPs arise in specific regions and at specific developmental stages in the embryonic brain and spinal cord, before migrating and settling in all parts of the CNS. Cycling OLPs, a reservoir of which is maintained throughout life, transition through a series of well-characterized progenitor phases on their way to becoming mature, myelinating OLs. Basic HLH TF Olig2 is continuously expressed along the OL lineage, performing a variety of different functions to regulate OL lineage progression. Besides dynamic expression of co-regulator proteins, post-translational modification of Olig2 – notably serine phosphorylation – determines its activity at different stages of development. In the embryonic spinal cord, for example, Olig2 is expressed early in multipotent NSCs resident in a discrete ventral progenitor domain, the pMN domain, responsible for generating all the MNs and ~80% of the OLs in the adult spinal cord. Initially, Olig2 is reversibly phosphorylated at S147 within the bHLH domain and Olig2-expressing NSCs exclusively form MNs. Dephosphorylation of S147 then alters the DNA-binding and dimerization properties of Olig2 and induces a switch in NSC fate in the pMN domain from MN to OL lineages.

1.8 PROJECT AIMS

Upstream regulation of Olig2 and the MN-OLP fate switch

In light of recent advances in our understanding of the intimate lineal relationship of ventral spinal OLPs with MNs and the integral role of Olig2 in regulating NSC fate and OL lineage progression, a number of key questions have emerged. Olig2 S147 dephosphorylation is a critical mediator of the MN-OLP fate switch. At a molecular level, however, the intracellular signaling pathway(s) and phosphatase enzyme(s) that mediate removal of the S147 phosphate group have not been established. Furthermore, the broad developmental changes that induce S147 dephosphorylation and trigger the MN-OLP fate switch remain entirely unknown. Whether, for example, the timing of the fate switch is intrinsic to cells of the pMN domain or regulated via external changes that influence pMN NSC behaviour is unclear. I therefore intended to examine the molecular and developmental regulation of Olig2 and the MN-OLP fate switch. The aims of my project in this regard were as follows:

1. Explore the role of spinal cord angiogenesis and changing tissue oxygen tension in triggering the MN-OLP fate switch.

2. Identify the phosphatase enzyme catalyzing Olig2 S147 dephosphorylation over the fate switch.

Olig2-mediated regulation of OL specification and differentiation

The molecular mechanisms underlying Olig2-mediated regulation of NSC fate and OL development are only partially understood. While S147 dephosphorylation has been shown to alter the cofactor binding properties of Olig2, the effects on Olig2 gene target specificity

have yet to be examined in detail (Li et al., 2011). Establishing precisely how Olig2 S147 dephosphorylation induces the profound change in NSC behaviour observed over the MN-OLP fate switch will be fundamental to improving our understanding of MN and OL formation. On top of the known phospho-modifications of Olig2, additional Olig2 post-translational modifications and their impacts on Olig2 function and cell development also have yet to be explored. Overall, further research into Olig2 phosphorylation will provide valuable detail regarding the molecular regulation of neural development. I therefore aimed to:

1. Identify genomic binding sites of Olig2 and establish if S147 phosphorylation state affects gene target specificity.

2. Analyse Olig2 phosphorylation in silico and characterize the role of Olig2 carboxyl terminus (S263) phosphorylation (Figure 6), detected at high confidence in previous MS analysis and a putative target of P38 mitogen-activated protein kinase (MAPK) (Sun et al., 2011; Bulavin et al., 2001).

These four aims form the structure of the following Results section, with the background specific to each aim introduced at the beginning of the respective chapter.

All together this research will significantly improve our understanding of oligodendrocyte development in the embryonic spinal cord, and will provide important insights into the mechanisms of stem cell fate choice.

CHAPTER 2

MATERIALS & METHODS

2.1 GENERAL

Chemicals and reagents were purchased from Sigma-Aldrich Co Ltd, unless otherwise stated. Falcon sterile plastic-ware was purchased from Marathon Ltd. RNase/Dnase-free microcentrifuge tubes were purchased from Starlab. All water used was purified using the MilliQ system (Millipore). Sterilization of solutions was performed by autoclaving at 15 lb/sq.in for 20 mins.

2.2 BACTERIAL BIOLOGY

For standard cloning, plasmids were maintained in *Escherichia coli* (*E.coli*) strain XL1-Blue. For Phage artificial chromosome (PAC) cloning *E.coli* strain EL250 was used. The EL250 strain (available via MTA from Neal G. Copeland) is a modified DH10B strain (Gibco) containing a replication defective λ prophage (Yu et al., 2000), containing genes with temperature-sensitive homologous recombination functions and the arabinose-inducible Flp-recombinase gene (Lee et al., 2001).

Bacteria were grown in Luria-Bertani (LB) broth in a shaking incubator (250 rotations per minute [rpm]) or on LB agar plates, at 37 ^{o}C when XL1-Blue strains were used and at 32 ^{o}C when EL250 strains were used. When appropriate, LB broth or LB-agar was supplemented with antibiotics: Ampicillin (final concentration of 100 μg/ml for plasmid transformed

bacteria and 20 μg/ml for PAC transformed bacteria), Kanamycin (final concentration of 15 μg/ml for plasmid transformed bacteria and 12.5 μg/ml for PAC transformed bacteria) or Chloramphenicol (final concentration of 30 μg/ml for plasmid transformed bacteria and 15 μg/ml for PAC transformed bacteria).

For long-term storage, glycerol stocks of bacterial cultures were made by adding 15% v/v of glycerol and 1.5ml aliquots were stored at -80^{o}C.

Preparation of electrocompetent bacteria

400 ml or 50 ml of LB broth was inoculated with 5 ml or 1 ml of overnight culture of XL1-Blue and EL250 strain, respectively. When optical density at 600 nm (OD_{600}) reached 0.5-0.8, the cultures were cooled down in ice water for 5 min, transferred into several falcon tubes and centrifuged at 2200 rpm for 8 min at 4 ^{o}C. Each pellet was re-suspended in 1 ml of sterile water and transferred to 1.5 ml microcentrifuge tubes. The suspension was centrifuged at 13000 rpm for 20 seconds at 4 ^{o}C and the pellet gently re-suspended in 1 ml of water. This wash was repeated three times. If being used immediately, the final pellet was re-suspended in 50 μl of sterile water. For long term storage the pellet was re-suspended in 50 μl of water containing 10% v/v glycerol, transferred into pre-cooled cryo-tubes, snap-frozen in liquid nitrogen and stored at -80 ^{o}C.

Transformation of electrocompetent bacteria

50 μl of electrocompetent bacteria was thawed on ice and mixed with 1 μl of DNA (either ligation reaction or mini/maxi prep DNA). The mixture was transferred to a chilled 0.1 cm electroporation cuvette (Bio-Rad). Electroporation was performed with a Gene Pulser electroporator equipped with Pulse Controller (Bio-Rad Laboratories Ltd) set to 1.8 kV (for

EL250) or 2.5 kV (for XL1-Blue), 200 Ω, 25 µF. Electroporated bacteria were resuspended in 250 µl LB broth and incubated at correct temperature (37 ^{o}C for 1 hr for XL1-Blue or 32 ^{o}C for 2 hr for EL250) before plating on antibiotic-supplemented LB agar plates. When using blue-white selection to screen for recombinant plasmids, 20 µl of X-gal (50 mg/ml) and 10 µl of IPTG (0.1 M) were added to LB agar plates and white colonies were selected.

2.3 DNA & RNA PREPARATION

Small-scale plasmid preparation (mini prep)

For preparation of small quantities (<2 mg) of plasmid DNA, the following mini prep protocol was used. 2 ml LB broth containing the appropriate antibiotic was inoculated with a single colony of transformed bacteria and incubated in a shaking incubator (250 rpm) at 37 ^{o}C. After overnight (o/n) incubation, 1.5 ml of bacteria was transferred to a microcentrifuge tube and centrifuged at 13000 rpm for 2 min. The pellet was re-suspended in 100 µl of Solution I (50 mM glucose, 25 mM Tris-HCl, pH 8.0, 10 mM EDTA, pH 8.0). 200 µl of Solution II (0.2 N NaOH, 1% w/v SDS) was added and the solution mixed by inversion to lyse the cells. 150 µl of Solution III (3 M potassium acetate, 11.5% v/v glacial acetic acid) was added and the samples mixed then centrifuged at 13000 rpm for 10 min at RT. The supernatant was transferred to a new microcentrifuge tube and 900 µl of 100% ethanol (EtOH; stored at -20^{o}C) added. The samples were centrifuged at 13000 rpm for 10 min. The DNA pellet was washed with 200 µl of 70% EtOH then centrifuged for 1 min at 13000 rpm. The DNA precipitate was re-suspended in 50 µl of H_2O and stored at -20 ^{o}C.

Large-scale plasmid preparation (maxi prep)

For preparation of large quantities (>1 mg) of plasmid DNA, the following maxi prep protocol was used. 50 ml LB was inoculated with 200 µl of overnight culture and grown in a shaking incubator (250 rpm) at 37 ^{o}C. After o/n incubation, the culture was transferred to a 50 ml falcon tube and centrifuged at 4000 rpm for 10 min at 4 ^{o}C. The pellet was re-suspended in 4 ml Solution I and held on ice for 5 min. 8ml of Solution II was added, mixed by inversion and incubated at RT for 5 min. 6ml of Solution III was added, mixed by inversion and incubated on ice for 10 min. The solution was centrifuged at 4000 rpm for 15 min at 4 ^{o}C. The supernatant was filtered through a double sheet of autoclaved muslin into a fresh 50 ml Falcon tube. 17 ml isopropanol was added to the supernatant and the solution incubated on ice for 15 min before centrifugation at 4000 rpm for 15 min at 4 ^{o}C. The DNA pellet was re-suspended in 2 ml of TE buffer and 2.5 ml of 4.4 M LiCl added. The mixture was incubated on ice for 1 hour then centrifuged at 4000 rpm for 15 min at 4 ^{o}C. The supernatant was transferred to a new falcon and 9 ml of 100% EtOH added. The DNA was precipitated by incubating at RT for 10-15 min and collected by centrifugation at 4000 rpm for 15 min at 4 ^{o}C. The DNA pellet was washed with 70% EtOH then re-suspended in 400 µl TE buffer. The DNA suspension was transferred to a new microcentrifuge tube and treated with 5µl of 4 mg/ml DNase-free RNase A for 15 min at 37 ^{o}C. 10 µl of 20% Sodium Dodecyl Sulphate (SDS) were then added and the mixture incubated at 70 ^{o}C for exactly 10min. This was followed by phenol-chloroform extraction (see below).

Large-scale PAC preparation (PAC maxi prep)

NB: To avoid PAC DNA shearing, large pipette tips were used and the solutions mixed by gentle inversion.

400 ml LB broth supplemented with antibiotic was inoculated with 500 µl of a 5 ml starter culture (EL250 *E. coli* transformed with PAC DNA and grown o/n at 32 ^{o}C). The maxi culture was grown at 32 ^{o}C in a shaking incubator (250 rpm). After o/n incubation, the culture was transferred to 50 ml falcon tubes and centrifuged at 3750 rpm for 10 min at 4 ^{o}C. Each pellet was re-suspended in 8 ml of PAC Solution I (PI) (50 mM Tris-HCl pH 8.0, 10 mM EDTA pH 8.0, 100 µg/ml RNase A). An equal volume (8 ml) of PAC Solution II (PII) (0.2 N NaOH, 1% SDS) was added and mixed. The mixture was incubated at RT for 5 min. 8 ml of PAC Solution III (PIII) (3 M potassium acetate, 11.5% w/v glacial acetic acid) was added and mixed. The mixture was incubated on ice for 1 hr. The suspensions were centrifuged at 3750 rpm for 15 min at 4 ^{o}C and the supernatants filtered into fresh falcon tubes through a double sheet of autoclaved muslin. 24 ml ice-cold isopropanol was added, mixed and the solutions incubated for 5 min at RT. DNA was pelleted by centrifugation at 3750 rpm for 15 min at 4 ^{o}C. Each DNA pellet was re-suspended in 2 ml TE buffer. 2.5 ml of 4.4 M LiCl was added followed by incubation on ice. After 30-60 min, the mixture was centrifuged at 3750 rpm for 15 min at 4 ^{o}C and the supernatants from an individual 400 ml PAC maxi culture collected and pooled into a single falcon tube. 18 ml of 100% EtOH were added to each “pooled” falcon tube, mixed and centrifuged at 3750 rpm for 15 min at 4 ^{o}C. PAC DNA pellets were washed with 5 ml RT 70% EtOH and re-suspended in 0.5 ml TE buffer. 12.5 µl of 20% SDS was added to each tube and the solutions incubated at 70 ^{o}C for precisely 10 min. Phenol/chloroform extraction of DNA followed by EtOH precipitation was performed as described below. The pellets were air-dried until the edge of the DNA pellets turned translucent then re-suspended in 200 µl water and stored at 4 ^{o}C.

Phenol-chloroform extraction

An equal volume of phenol:chloroform:isoamylalcohol (IAA) (25:24:1) was added to the DNA-containing solution and mixed by gentle inversion. The mixture was centrifuged at 13000 rpm for 2-5 min at room temperature (RT). The aqueous phase was transferred to a clean microcentrifuge tube. An equal volume of chloroform:IAA (24:1) was added and the mixture centrifuged at 13000 rpm for 1-2 min at RT. For PAC DNA the phenol:chloroform step was performed twice. The aqueous phase was transferred to a fresh microcentrifuge tube and 3 M sodium acetate (pH 5.3) was added to a final concentration of 0.3 M. A double volume of 100% EtOH was added and the mixture centrifuged at 13000 rpm for 15-30 min at 4 ^{o}C. The DNA pellet was washed with 70% EtOH then re-suspended in an appropriate buffer. With the exception of PAC DNA – stored at 4^{o}C to avoid shearing – DNA was stored at -20^{o}C.

Agarose gel DNA purification

The QIAquick Gel Extraction Kit was used according to the manufacturer's instructions. DNA fragments were initially separated and visualized by agarose gel electrophoresis (see DNA analysis).

Genomic DNA extraction from mouse tissue

Mouse ear (postnatal) and tail (embryonic) biopsy samples were digested at 55 ^{o}C in 250 µl of extraction buffer (100 mM Tris-HCl, pH 8.5, 5 mM EDTA, pH 8.0, 200 mM NaCl, 0.2% w/v SDS) containing 0.48 mg/ml Proteinase K. After o/n incubation, 100 µl of 6 M ammonium acetate was added and the samples mixed by vortexing then incubated for 15 min on ice. The solutions were then centrifuged at 13000 rpm for 15 min at 4 ^{o}C and the supernatant

transferred to a clean microcentrifuge tube. 250 µl of isopropanol was added and the DNA precipitated by centrifuging at 13000 rpm for 3 min at RT. The DNA pellet was washed with 70% EtOH then re-suspended in 50 µl of water. Purified genomic DNA samples were stored at 4 ^{o}C.

RNA preparation

RNA was extracted from cultured NSCs using Trizol (Invitrogen) following the manufacturer's instructions. Purified RNA was stored at -80 ^{o}C.

Complementary DNA synthesis

Complementary DNA (cDNA) synthesis was performed with random hexamer primers and using SuperScript II reverse transcriptase (Invitrogen) following the manufacturer's instructions.

2.4 DNA ANALYSIS

Genotyping PCR

PCR was used to genotype animals. Each PCR reaction contained: 1 X PCR buffer (500 mM KCl, 100 mM Tris-HCl pH 9.0, 1% (v/v) Triton X-100), 1.5 mM MgCl2, 0.2 mM dNTPs (Amersham Pharmacia Biotech), 20 pmole of each primer (Table 1), 1 µl of Taq DNA Polymerase (purified by Matthew Grist) and 2 µl of genomic DNA made up to a final volume of 25 µl with water. The PCR conditions were as follows: 94 ^{o}C, 4 min; 40 cycles of [94 ^{o}C, 30 s; the primer pair-specific annealing temperature (typically 60 ^{o}C), 45 s; 72 ^{o}C, 1 min]; 72 ^{o}C,

10 min. After the last step, PCR reactions were held at 4 ^{o}C. PCR products were visualized by agarose gel electrophoresis (see below).

Quantitative PCR

ChIP DNA and cDNA (qRT-PCR) samples were analysed by qPCR using gene-specific primer sets (Table 1) and the SYBR Green PCR Master Mix (Invitrogen) in 25 µl reactions according to the manufacturer's instructions. The samples were amplified using a Mastercycler Ep Realplex system (Eppendorf). For ChIP analysis, Input DNA was serially diluted 1:8, 1:64 and 1:256 in water. For each primer set, ChIP and diluted Input DNA samples were amplified by qPCR in triplicate. ChIP enrichment was calculated using the Percentage Input method (Invitrogen – ChIP Analysis). Briefly, the Input DNA Ct values were adjusted for dilution. The ChIP and adjusted Input Ct values were then used to calculate the percentage of Input for each ChIP sample. For quantitative RT-PCR, cDNA samples were amplified using gene-specific primer sets in triplicate. Enrichment was calculated by normalization to the reference gene GAPDH (Invitrogen – qPCR Education).

Agarose gel electrophoresis

Agarose gels were made by dissolving 1% w/v agarose in TAE buffer (0.04 M Tris, 1 mM EDTA, 0.35% v/v glacial acetic acid) then adding 0.5 µg/ml ethidium bromide. DNA samples were supplemented with loading buffer (50% glycerol, 1 mM EDTA pH 8.0, 0.125% bromophenole blue, 0.125% xylene cyanol). 15 µl of samples and 5 µl of Hyperladder I (Bioline) were loaded and run in a Peqlab Biotechnologie GmbH gel tank at 100-150 V. Gels were visualized under UV illumination and the DNA properties evaluated relative to the Hyperladder I standards.

Pulse-field gel electrophoresis

To separate PAC DNA fragments of >15 kb, pulse field gel electrophoresis (PFGE) was performed using contour-clamped homogenous electric field electrophoresis cell powered by a CHEF DR II control module and CHEF DR II drive module (Bio-Rad). Agarose gels were made by dissolving 1% w/v agarose in 0.5 X TBE buffer (45 mM Tris-borate, 1 mM EDTA pH 8.0). DNA samples were mixed with 10% loading buffer and loaded into the gel along with 2 mm of Pulse Marker™ (0.1-200 kb). DNA was run for 12 hours in a 6 V/cm field with initial switch time of 2.1 s and a final switch time of 10 s at 4 ^{o}C in 2 L of 0.5 x TBE. After completion of PFGE the gel was stained with ethidium bromide and visualized on a UV transilluminator.

DNA quantification

The concentration of DNA was determined using either NanoDrop 1000 V3.6.0 or Qubit (Invitrogen) spectrophotometers or the Agilent 2100 Biolanalyzer, following the manufacturer's instructions for each system.

DNA Sequencing

DNA Sequencing was performed by the Wolfson Institute for Biomedical Research (WIBR) Scientific Support Services team on a Beckman Coulter CEQ 8000 Genetic Analysis System. DNA samples were prepared by maxi or mini prep (see above) and submitted with necessary primers according to instructions provided by the service.

Restriction digestion and DNA ligation

Restriction enzymes and buffers were purchased from New England Biolabs (NEB) and used according to the manufacturer's instructions.

Ligation reactions were performed with T4 DNA Ligase (NEB) using gel purified backbone and insert DNA fragments according to the manufacturer's instructions.

DNA mutagenesis

Olig2 S263 mutagenesis was performed using the QuikChange Site-Directed Mutagenesis Kit (Agilent) according to the manufacturer's instructions. Briefly, the Olig2 ORF in pcDNA4.1 (pcDNA4.1-Olig2^{WT}) was mutated at S263 using mutagenic oligonucleotide primers (Table 1) and the high fidelity PfuTurbo DNA polymerase. Thermal cycling (16 X [94 °C for 30 s, 58 °C for 1 min and 68 °C for 10 min]) and incorporation of the primers generated a mutated plasmid containing staggered nicks. The product was treated with DpnI (37 °C for 1 hr) to selectively digest the parental pcDNA4.1-Olig2 template. The DpnI-treated nicked DNA containing the desired mutation (pcDNA4.1-Olig2^{S263A}) was then transformed into XL1-Blue supercompetent cells for plasmid preparation and sequencing, as describe above.

2.5 CELL CULTURE AND TRANSFECTION

Primary NSC culture

Primary adherent NSC cultures were derived from the dissociated cortices of E13.5 mice, as previously described in Pollard et al., 2006. Isolated cortices were dissected using Leica

Dissection Microscope (Fisher Scientific) and mechanically dissociated in 1 ml NSC medium (DMEM/F-12 (Invitrogen) supplemented with: 1 X PenStrep (Invitrogen), 1 X non-essential amino acids (NEAA) (Invitrogen), 0.12 mg/ml bovine serum albumin (BSA), 0.1% 2-mercaptoethanol, 0.5 X B27 (Invitrogen), 0.5 X N2 (Invitrogen), 10 ng/ml FGF-2 (Invitrogen), 10 ng/ml EGF (Invitrogen), 1 μg/ml Laminin). The cell suspensions were passed through a sterile 100 μm nylon cell strainer and plated on poly-D-lysine coated culture dishes (1 X 6 cm plate / embryo). Cells were cultured in NSC medium at 37 ^{o}C with 20% (v/v) O2 and passaged at 80% confluency.

For primary NSC culture differentiation, NSC medium was replaced with Differentiation medium (DMEM/F-12 (Invitrogen) supplemented with: 1 X PenStrep (Invitrogen), 1 X non-essential amino acids (NEAA) (Invitrogen), 0.12 mg/ml bovine serum albumin (BSA), 0.1% 2-mercaptoethanol, 0.5 X B27 (Invitrogen), 0.5 X N2 (Invitrogen), 20 ng/ml FGF-2 (Invitrogen), 10 ng/ml PDGF-AA (Invitrogen), 1 μg/ml Laminin).

For hypoxic culture, NSC cultures in NS or Differentiation medium were cultured in a specialized hypoxic chamber at 37 ^{o}C with 2-4% (v/v) O2 and 83.5% (v/v) N2.

For anisomycin treatment, NSCs were cultured in Differentiation medium supplemented with 2 μg/ml anisomycin.

P19 and C6 cell culture

C6 cells were cultured at 37 ^{o}C in DMEM (Invitrogen) supplemented with: 1 X PenStrep (Invitrogen), 1 X non-essential amino acids (NEAA) (Invitrogen), 10% (v/v) fetal bovine serum (FBS) (Invitrogen).

P19 cells were cultured at 37^{o}C in MEM (Invitrogen) supplemented with: 1 X PenStrep (Invitrogen), 1 X non-essential amino acids (NEAA) (Invitrogen), 5% (v/v) fetal bovine serum (FBS) (Invitrogen).

Plasmid transfection

Transfection of plasmid DNA was performed with FuGENE® HD Transfection Reagent (Promega) according to the manufacturer's instructions.

2.6 IN SILICO ANALYSIS

Phosphorylation predictions

Human Olig2 protein sequence (Q13516) was processed by online services NetPhos (http://cbs.dtu.dk/services/NetPhos) and NetPhosK (http://cbs.dtu.dk/services/NetPhosK) for identification of putative phosphorylation sites and the predicted kinases, respectively.

Sequence alignment

Olig2 protein sequences from human [Q13516], mouse [Q9EQW6], chick [Q90XB3] and zebrafish [Q6P0J2]) were aligned using ClustalOmega (ebi.ac.uk/Tools/msa/clustalo/).

2.7 CHROMATIN IMMUNOPRECIPITATION

For ChIP-qPCR, the input NSC cultures each comprised ~1-2 X 10^7 cells. For ChIP-seq, the input NSC cultures each comprised ~1 X 10^8 cells.

Crosslinking: Adherent NSC cultures (see above) were treated with DMEM/F-12 supplemented with 1% formaldehyde (5 ml / 10 cm plate) and incubated at RT. After precisely 10 min, the crosslinking reaction was stopped by addition of 1.25 M glycine to a final concentration of 0.125 M. Crosslinked NSC cultures were then rinsed once with DMEM/F-12 (5 ml / 10 cm plate) and treated with 0.25% Trypsin (Invitrogen) in DMEM/F-12 (5 ml / 10 cm plate) and incubated at 37 ^{o}C. After 20 min, crosslinked NSCs were collected using a P1000 Gilson pipette and transferred to a 15 ml falcon. The cell suspension was centrifuged at 300 g for 10 min at 4 ^{o}C. The cell pellet was re-suspended in 1 ml ice-cold PBS and transferred to a 1 ml microcentrifuge tube. The cell suspension was centrifuged at 300 g for 10 min at 4 ^{o}C and the supernatant discarded.

Cell lysis and sonication: Formaldehyde-crosslinked NSC pellets were re-suspended in 1 ml Lysis buffer 1 (50 mM Hepes KOH pH 7.5, 140 mM NaCl, 1 mM EDTA, 10% glycerol, 0.5% NP-40, 0.25% Triton X-100) supplemented with Complete protease inhibitor cocktail (Roche) and incubated for 10 min at 4 ^{o}C. Nuclei were pelleted by centrifugation at 3000 rpm for 10 min at 4 ^{o}C. The isolated nuclei were rinsed with 1 ml Lysis buffer 2 (10 mM Tris-HCl pH 8.0, 200 mM NaCl, 1 mM EDTA, 0.5 mM EGTA) supplemented with Complete protease inhibitor cocktail (Roche) and re-pelleted by centrifugation at 3000 rpm for 10 min at 4 ^{o}C. Nuclei were re-suspended in 1 ml Lysis buffer 3 (10 mM Tris-HCl pH 8.0; 100 mM NaCl; 1 mM EDTA; 0.5 mM EGTA; 0.1% sodium deoxycholate; 0.5% N-lauryl sarcosine) supplemented with Complete protease inhibitor cocktail (Roche). The nuclei suspension was sonicated over 10, 20, 30, 40

or 50 rounds of 30 s on, 30 s off at 4 ^{o}C in a Bioruptor (Diagenode) to generate DNA fragments in the 200-1000 bp range. Genome fragmentation was assessed by de-crosslinking (see below) and agarose gel electrophoresis (see above). Insoluble debris was pelleted by centrifugation at 13000 rpm for 15 min at 4 ^{o}C and the supernatant transferred to a fresh microcentrifuge tube.

Clearing: 50 µl Protein A Agarose beads (Roche) per ChIP were rinsed with Lysis buffer 3 then added to the nuclear lysate and incubated at 4 ^{o}C on a rotator set at 8 rpm. After 1 hr, clearing beads were pelleted by centrifugation at 10000 rpm for 30 s at 4 ^{o}C and the 1 ml supernatant transferred to a fresh microcentrifuge tube. At this stage, a 5% (50 µl) Input sample was taken from each nuclear lysate and stored on ice until de-crosslinking (see below). 50 µl of Lysis buffer 3 was added to the remaining 950 µl of nuclear lysate to restore the volume to 1 ml.

ChIP-qPCR Immunoprecipitation: To each 1 ml cleared nuclear lysate sample, 2 µl rabbit anti-Olig2 antibody (Millipore; AB9610) was added and the mixture incubated at 4 ^{o}C on a rotator set at 8 rpm. After 3 hr, 50 µl pre-rinsed Protein A Agarose beads were added and the mixture incubated o/n at 4 ^{o}C on a rotator set at 8 rpm.

ChIP-seq Immunoprecipitation: To each 1 ml cleared nuclear lysate sample, 10 µl rabbit anti-Olig2 antibody (Millipore; AB9610) plus 1 µl rabbit anti-Olig2 (Stiles lab; Ligon et al., 2004) was added and the mixture incubated at 4 ^{o}C on a rotator set at 8 rpm. After 3 hr, 50 µl pre-rinsed Protein A Agarose beads were added and the mixture incubated o/n at 4 ^{o}C on a rotator set at 8 rpm.

Washes, elution and de-crosslinking: After o/n immunoprecipitation, Protein A agarose beads were pelleted by centrifugation at 10000 rpm for 30 s at 4 ^{o}C. The beads were washed twice at 4 ^{o}C for 10 min each in 1 ml of each of the following buffers: Wash buffer 1 (0.1% SDS, 1% Triton X-100, 2 mM EDTA, 20 mM Tris-HCl pH 8.0, 150 mM NaCl), Wash buffer 2 (0.1% SDS, 1% Triton X-100, 2 mM EDTA, 20 mM Tris-HCl pH 8.0, 500 mM NaCl) and LiCl Wash Buffer (0.25 M LiCl, 1% NP-40, 0.7 % sodium deoxycholate, 1 mM EDTA, 10 mM Tris pH 8.0). After each wash, beads were pelleted by centrifugation at 10000 rpm for 30 s at 4 ^{o}C. After the final wash, the bead pellet was rinsed once in 1 ml TE buffer (10 mM Tris-HCl pH 8.0, 1 mM EDTA) then pelleted by centrifugation. The immunoprecipitated materials were eluted from the beads by adding 200 µl Elution buffer (10 mM Tris-HCl pH 8.0; 1 mM EDTA; 1 % SDS) to each ChIP reaction and incubating at 65 ^{o}C for 20 min with vortexing every 2 min. The beads were pelleted by centrifugation at RT and the 200 µl eluate transferred to a fresh microcentrifuge tube. 150 µl of Elution buffer was also added to each saved Input material (50 µl) and these 200 µl samples were processed together with the ChIP samples. One volume (200 µl) of TE buffer was added to each sample. For protein and RNA digestion and de-crosslinking, proteinase K and RNase A were added to final concentrations of 0.2 mg/ml and 0.2 mg/ml, respectively, and the mixtures incubated at 65 ^{o}C for 4 hr.

ChIP DNA Purification: The Input/ChIP DNA in each ~400 µl sample was purified using the ChIP DNA Purification Kit (Active Motif) and eluted in 20 µl water. Purified DNA samples were then analysed by qPCR (see above) or quantified and submitted to Source Bioscience for library generation and Illumina Sequencing according to the instructions provided by Source Bioscience.

ChIP optimization with Olig2-expressing P19 cells

For each ChIP optimization IP, 1 X 10^7 Olig2-expressing P19 cells were lysed, sonicated and cleared as described above for NSCs. Immunoprecipitation was performed with 2, 5 or 10 µl of Millipore rabbit anti-Olig2 antibody (AB9610) and 0.25, 0.5 or 1.0 µl of Stiles lab rabbit anti-Olig2 antibody (Ligon et al., 2004). The antibody binding solution was initially incubated for 3 hr at 4 ^{o}C or o/n at 4 ^{o}C. After antibody incubation, 25, 50 or 100 µl Protein A Agarose beads were added. Depending on the initial incubation time, the antibody and bead mixture was incubated o/n (after 3 hr antibody incubation) or for 3 hr (after o/n antibody incubation). The Protein A Agarose beads were pelleted and washed as described above for NSC ChIP. Immunoprecipitated proteins were eluted and denatured using NuPAGE Sample Reducing Agent (Invitrogen) and NuPAGE LDS Sample Buffer (Invitrogen), according to the manufacturer's instructions. The beads were pelleted by centrifugation and the supernatant extracted and stored at -20 ^{o}C for PAGE/WB analysis (see below).

2.8 PROTEIN ANALYSIS

Immunoprecipitation

For transfected C6 cells (see above), IP was performed at 48 hr post-transfection with 1 X 6 cm plate at 80% confluency per IP.

For primary NSC cultures (see above), IP was performed using 1 X 10 cm plate at 80% confluency per IP.

Immunoprecipitation was performed according to instructions provided with Protein A Agarose beads (Roche). For protein phosphorylation-dependent analysis, Complete protease inhibitor cocktail (Roche) was supplemented with PhosSTOP phosphatase inhibitor cocktail (Roche) according the manufacturer's instructions.

Protein samples were eluted and denatured using NuPAGE Sample Reducing Agent (Invitrogen) and NuPAGE LDS Sample Buffer (Invitrogen), according to the manufacturer's instructions. After elution, IP beads were pelleted by centrifugation and the supernatant extracted and stored at -20 ^{o}C for PAGE/WB analysis (see below).

Polyacrylamide gel electrophoresis (PAGE)

Resolving (12% bis/acrylamide, 0.375 Tris-HCl pH 8.8, 0.1% SDS) and stacking (5% bis/acrylamide, 0.125 M Tris-HCl pH 6.8, 0.1% SDS) gels were polymerized using fresh 10% ammonium persulfate (final concentration 0.1%) and TEMED (final concentration 0.1%) and cast using the BioRad Hand Casting system, according to the manufacturer's instructions. Gels were loaded into the Mini-PROTEAN Tetra cell (Biorad).

Protein samples eluted in NuPAGE Sample Reducing Agent (Invitrogen) and NuPAGE LDS Sample Buffer (Invitrogen) were incubated at 85 ^{o}C for 10 min then centrifuged at 10000 rpm for 30 s. 12-20 µl of each sample and 10 µl Precision Plus Protein ladder (Biorad) were loaded into the gels in separate wells and electrophoresed in Running buffer (2.5 mM Tris pH 8.3; 19.2 mM glycine; 0.1% SDS) at ~150 V for ~2 hr.

Western blotting

After PAGE, gel proteins were blotted onto PVDF using the Mini Trans-Blot Electrophoretic Transfer Cell (Biorad), according to the manufacturer's instructions. PVDF was initially washed in 100% MeOH at RT then rinsed twice for 5 min each in 1 X Transfer buffer (25 mM Tris pH 8.3; 192 mM glycine; 20% MeOH) at 4 ^{o}C. Blotting was performed in pre-cooled 1 X Transfer buffer for 1-2 hr at 100 V at 4 ^{o}C.

After blotting, the PVDF membrane was washed three times for 10 min each in 0.1% Tween-20 in phosphate buffered saline (0.1% PBTw). PVDF was then blocked in WB Block solution (3% Marvel Dried Milk (w/v) in 0.1% PBTw) for 1 hr at RT. Blocked PVDF was incubated with primary antibody (Table 2) diluted in WB Block o/n at 4 ^{o}C. After primary antibody incubation, PVDF was washed three times for 10 min each in 0.1% PBTw then incubated with Protein A-HRP (Invitrogen) diluted 1:10000 in WB Block for 1 hr at RT. After Protein A-HRP incubation, PVDF was washed three times for 10 min each in 0.1% PBTw. Western blot (HRP) signal was detected using Amersham ECL Plus (GE Healthcare) according to the manufacturer's instructions and developed on Amersham Hyperfilm ECL (GE Healthcare) in an SRX-101A (Konica Minolta) radiograph processor under darkroom conditions.

2.9 ZEBRAFISH HANDLING

Zebrafish were grown and maintained as previously described and according to protocols approved by the Yale University Animal Care (Westerfield et al., 1995). The Tg(sox10:mCherry) and Tg(VEGFR2:GFP)^{la116} lines were used (Kirby et al., 2006; Anderson et al., 2008). Embryos were raised and staged as previously described and when appropriate

embryo medium was supplemented with 0.003% phenylthiourea (PTU) from 24 hpf to inhibit melanin formation (Kimmel et al., 1995; Westerfield et al., 1995).

For SU5416 treatment, SU5416 was prepared at 10 mM in DMSO and added to fish water to a final concentration of 5 μM from 20 SS. For control treatment, fish water was supplemented with a matching volume of DMSO.

For live imaging, zebrafish were anaesthetized using 0.03% w/v tricaine methanesulfonate (MS222) in fish water.

2.10 MOUSE HANDLING

All mice were maintained on a ~12 hour light-dark cycle (6pm-7am, twilight for the first and the last hours). The day of embryonic conception was designated as embryonic day (E) 0. For histological experiments the embryonic age of the animals is precisely stated.

Transgenic lines

$Olig2^{+/-}$ mice were originally obtained from Charles Stiles (Dana Farber Cancer Institute, Harvard Medical School) and David Rowitch (University of California, San Francisco) and were maintained in the WIBR Animal Facility (Lu et al., 2002).

$Olig2^{+/-}$;$Olig2^{S147A}$ mice were generated from crossing progeny of $Olig2^{S147A}$ PAC-transgenic founders with $Olig2^{+/-}$ mice and maintained in the WIBR Animal Facility (Li et al., 2011).

Cdh5-Cre^{ERT2} mice were originally obtained from Ralf H. Adams (CRUK London research Institute) and were maintained in the Yale CVRC Animal Facility (Wang et al., 2010).

Notch1$^{fl/fl}$ mice were originally obtained Freddy Radtke (Ludwig Institute for Cancer Research, University of Lausanne) and were maintained in the Yale CVRC Animal Facility (Wolfer et al., 2001).

VEGFR3$^{fl/fl}$ mice were originally obtained from Kari Alitalo (Haartman Institute, University of Helsinki) and were maintained in the Yale CVRC Animal Facility (Haiko et al., 2008).

Tamoxifen administration

To induce Cre^{ERT2} recombinase activity, 4-OHT was prepared at 25 mg/ml in sunflower seed oil. 4-OHT was administered via intra-peritoneal injection into pregnant female mice at 120 mg/kg at E9.5 and E10.5.

Hypoxic incubation

Pregnant female mice were exposed to hypoxia (FiO2 8-10%) for 1 or 2 d in a rodent hypoxia chamber with a calibrated oxygen controller and sensor (BioSepherix).

Mouse embryo collection and fixation

Pregnant female mice were sacrificed by cervical dislocation at E9.5, E10.5, E11.5, E12.5 or E13.5. Embryos were dissected out in ice-cold EBSS using a Leica Dissection Microscope (Fisher Scientific) and immediately transferred to fixation solution (4% w/v

paraformaldehyde in phosphate buffered saline [PBS]) and incubated at 4 ^{o}C for either 30 min (short fix) or o/n (long fix). For cryoprotection, fixation solution was then replaced with diethylpyrocarbonate (DEPC)-treated 20% w/v sucrose in PBS. After o/n incubation at 4 ^{o}C, the embryos were embedded in Optimal Cutting Temperature (OCT) medium (Tissue Tek) and frozen in isopentane on dry ice and stored at -80^{o}C.

2.11 TISSUE HISTOLOGY AND IMMUNOCYTOCHEMISTRY

In situ hybridization

All solutions used for preparation of the probe and the hybridization step of the protocol were DEPC-treated, when required, to ensure that they are RNase free and subsequently autoclaved to removed traces of DEPC.

Probe synthesis: To prepare the probes for in situ hybridisation either plasmid DNA or DNA clones from the IMAGE consortium were used as a template. 10 µg of template DNA was linearized at an appropriate point by restriction enzyme digestion at 37 ^{o}C for 4 hours in a total volume of 100µl. Linearized template DNA was visualized by agarose gel electrophoresis and purified using the QIAquick Gel Extraction Kit (see above). The RNA probe transcription reaction was carried out using 20 units of promoter-specific T3, T7 or SP6 RNA polymerase, 1 µg template DNA, 1 X transcription buffer (Promega), 30 mM dithiothreitol (DTT), 1 X RNA labeling mixture (DIG labeling; Roche), 1 X RNase inhibitor (Promega) in a total volume of 25 µl. The reaction mixture was incubated at 37 ^{o}C for 2.5 hr. Probe synthesis was evaluated by agarose gel electrophoresis using 1 µl of transcription reaction mix. The remaining 24 µl of RNA probe was diluted with 76 µl of hybridization buffer (50% deionized formamide, 10% w/v dextran sulphate (Fluka), 0.1 mg/ml yeast tRNA (Roche),

1 X Denhardt's solution (Sigma), and 1 X salt solution (10 X salt stock: 2 M NaCl, 50 mM EDTA, 100 mM Tris-HCl pH 7.5, 50 mM $NaH_2PO_4.2H_2O$, 50 mM Na_2HPO_4, DEPC-treated) and stored as 5 µl aliquots at -80 ^oC.

RNA probe hybridization: From OCT-embedded and frozen mouse embryonic tissue, spinal cord cross-sections of 15-20 µm were cut on a Bright OTF5000 Leica cryostat and collected on SuperFrost® Plus slides (VWR International) then dried for 2 hr at RT. RNA probe was diluted 1:1000 in hybridisation buffer. The diluted probe was denatured at 70 ^oC for 5-10 min, mixed by vortexing and immediately applied to the tissue sections. The sections were then incubated in a sealed and hybridization buffer-humidified chamber at 65 ^oC. After o/n hybridization, slides were washed 3 times in pre-warmed (65 ^oC) Wash solution (50% formamide, 1 X SSC, 0.1% Tween-20) for 30 min each at 65 ^oC. After 65 ^oC washes, sections were washed twice in 1 X MABT (5 X stock: 0.5 M maleic acid, 0.75 M NaCl, 1 M NaOH pH 7.5, 0.5% v/v Tween-20) for 30 min each at RT. The sections were then blocked in ISH Block solution (2% blocking reagent (Roche) 1 X MABT, 20% heat-incativated sheep serum) for 1 hr at RT. Anti-digoxigenin (DIG) alkaline phosphatase (AP)-conjugated antibody (Roche) was diluted 1:1500 in ISH Block solution and applied to the sections in a humidified chamber at 4 ^oC. After o/n incubation, the sections were washed 5 times in 1 X MABT for 20 min each at RT, then twice in staining buffer (0.1 M NaCl, 0.05 M $MgCl_2$, 0.1 M Tris pH 9.5, 0.1% Tween-20) for 10 min each at RT.

NBT/BCIP chromogenic detection: The staining was developed in 20 ml staining buffer, 1 ml 1 M $MgCl_2$, 87 µl NBT (1 g 4-nitroblue-tetrazolium chloride crystals in 7 ml dimethyl-formamide and 3 ml distilled water), 67 µl BCIP (1 g in 20ml dimethyl-formamide) and 20 ml of a 10% polyvinylalcohol (PVA) solution (10% w/v PVA in 0.1 M NaCl, 0.1 M Tris pH 9.5 and 0.1% Tween-20). Reactions were protected from light and incubated at 37 ^oC. Signal development

was assessed under a Leica dissection microscope. After development of sufficient signal, the development reaction was stopped by rinsing the slides with water. Stained sections were dehydrated by sequential washing in 30%, 60%, 80%, 95% and 100% ETOH for 30 s each at RT then rinsing twice with xylene. Finally, sections were mounted under a coverslip using DPX mountant (Fluka).

Immunohistochemistry

From OCT-embedded and frozen mouse embryonic tissue, spinal cord cross-sections of 15-20 µm were cut on a Bright OTF5000 Leica cryostat and collected on SuperFrost® Plus slides (VWR International) then dried for 2 hr at RT. Sections were washed 3 times in PBS for 5 min each at RT then permeabilized with 0.1% v/v Triton X-100 in PBS (0.1% PBX) for 15 min at RT. Sections were blocked using Antibody Block (10% v/v sheep or cow serum in 0.1% PBX) for 1 hour at RT. Primary antibodies and Isolectin B4 were diluted in Antibody Block (Table 2) and the primary antibody solution applied to the sections. After o/n incubation at 4 ^{o}C, sections were washed 3 times in PBS for 10 min each at RT. Secondary antibodies and DAPI (Sigma) were diluted in Antibody Block and applied for 1 hr at RT. After secondary antibody incubation, sections were washed 3 times in PBS for 10 min each at RT. Finally, sections were mounted using fluorescent mounting medium (Dako), coverslipped and stored in the dark at 4 °C.

Immunocytochemistry

For immunocytochemistry, NSCs were cultured on poly-D-lysine-coated 10 mm diameter glass coverslips (BDH) in 24-well Multiwell plates (Falcon).

NSC medium was aspirated and the adherent NSCs washed once with ice-cold PBS for 20 s then fixed with 4% PFA in PBS for 10 min at RT. After fixation, the NSCs were washed 3 times in PBS for 5 min and blocked, stained then mounted as described above for immunohistochemistry.

Zebrafish whole-mount immunohistochemistry

Dechorionated zebrafish embryos were collected at 48 hours post fertilization (48 hpf) and fixed in 4% PFA in PBS o/n at 4 ^{o}C. After fixation, embryos were washed once in PBS for 5 min at RT then incubated in 100% MeOH o/n at -20 ^{o}C. Embryos were rehydrated through 75%, 50% and 25% MeOH in 0.5% PBX for 5 min each at RT then washed twice in 0.5% PBX for 5 min each at RT. Embryos were permeabilized using 10 µg/ml proteinase K in 0.5% PBX for 15 min at RT then washed 5 times in 0.5% PBX for 5 min each at RT. Blocking was performed by incubation in Wholemount Block (5% sheep serum in 0.5% PBX) for 2 hr at RT. Primary antibody was diluted in Wholemount Block and primary antibody solution applied to the embryos. After o/n primary antibody incubation at 4 ^{o}C, the embryos were washed 5 times in 0.5% PBX for 30 min each at RT. Secondary antibody was diluted in Wholemount Block and applied o/n at 4 ^{o}C. After secondary incubation, the embryos were washed 5 times in 0.5% PBX for 30 min each at RT. Finally, embryos were mounted in 1% low melting point agarose in PBS.

2.12 MICROSCOPY AND IMAGE ANALYSIS

Imaging was performed using either a Zeis Axioplan light microscope and Hamamatsu digital camera, Leica LED Fluorescent microscope or Leica TCS SPE confocal laser scanning microscope. For confocal microscopy, standard excitation and emission filters for visualizing

DAPI, Alexa Fluor 488, CY3, Alexa Fluor 568, CY5 and Alexa Fluor 647 were used. Confocal z stacks were captured at a maximum of 2 µm increments.

Images were assembled using ImageJ. All manipulations were performed solely to enhance clarity and were applied equally across the whole image.

Primer name	Procedure	Sequence (5' - 3')
MutGTR	Genotyping	ACGCATCTCTCCATCGCTTC
New1	Genotyping	AGCGGTGTCCAGCGCCTCTCTAC
Nkx2.1 #3	Genotyping	TCGCCTTCTATCGCCTTCTTGACGAG
Olig2 3'	Genotyping	GCATGCCGCCCCAGTGCTGGAAGCCACCGC
Olig2-WT1	Genotyping	CTCGTAGCTCGGAGCTCAGCTCTGGCGGGC
Olig2-WT2	Genotyping	TAGAAGGCCAGACTGCCGCGGCGTAGATGC
GAPDH-Fw	Quant. RT-PCR	ACAACTTTGGCATTGTGGAA
GAPDH-Rev	Quant. RT-PCR	GATGCAGGGATGATGTTCTG
Olig1-Fw	Quant. RT-PCR	ACCAACGTTTGAGCTTGCTT
Olig1-Rev	Quant. RT-PCR	GGTTAAGGACCAGCCTGTGA
Olig2-Fw	Quant. RT-PCR	CTGGTGTCTAGTCGCCCATC
Olig2-Rev	Quant. RT-PCR	GAGGTGCTGGAGGAAGATGA
PDGFRA-Fw	Quant. RT-PCR	CTGCAGACAACTGCAGCATT
PDGFRA-Rev	Quant. RT-PCR	GTACCGGATTCCAAGAAGGA
Sox10-Fw	Quant. RT-PCR	TAGCCGACCAGTACCCTCAC
Sox10-Rev	Quant. RT-PCR	TGTAGTCCGGATGGTCCTTT
Hb9-ChIP-Fw	ChIP qpCR	GCAACACTTCCAGGCTCAGCCAG
Hb9-ChIP-Rev	ChIP qpCR	CTGTTCTTGCAGACTAGCAGG
Olig1-ChIP-Fw	ChIP qpCR	CCACCCGGAACTCTCTTCT
Olig1-ChIP-Rev	ChIP qpCR	ACTTCATCAGCCCCTTCTTG
PDGFRA-ChIP-Fw	ChIP qpCR	GATAGGTACCGCAAGGCCAAGCTGGA
PDGFRA-ChIP-Rev	ChIP qpCR	GCCGGACTAGTGTGTCAATACAAGCAAC
Sox10-ChIP-Fw	ChIP qpCR	CGACAGCCCCTACAGCTGC
Sox10-ChIP-Rev	ChIP qpCR	GTGACTGAGAGTCTGAGAGC
Olig2-S263A-Fw	Mutagenesis	ACGGCCTGCTCAAGGCACCGTCGGCAG
Olig2-S263A-Rev	Mutagenesis	CTGCCGACGGTGCCTTGAGCAGGCCGT
FLAG-Tag-Fw	FLAG Tag synthesis	CTAGAGGTGACTACAAAGACCATGACGGTGA TTATAAAGATCATGATATCGATTACAAGGATG ACGATGACAAGTGAGCTAGCA
FLAG-Tag-Rev	FLAG Tag synthesis	CCGGTGCTAGCTCACTTGTCATCGTCATCCTTG TAATCGATATCATGATCTTTATAATCACCGTCAT GGTCTTTGTAGTCACCT

Table 1. Primer sequences. (Quant. RT-PCR, quantitative reverse transcription PCR; ChIP-qPCR, chromatin immunoprecipitation quantitative PCR)

Primary Antibody	Species	Dilution	Conjugation	Manufacturer
B-Tubulin E3	Mouse	WB 1:10	N/A	Richardson Lab, UCL
Cleaved Caspase 3	Rabbit	IHC 1:1000	N/A	Cell Signal
GFAP	Rabbit	IHC 1:400	N/A	Dako
GFP Tag	Rabbit	IHC 1:100	Alexa 488	Invitrogen
Hb9	Mouse	IHC 1:10	N/A	Developmental studies hybridoma bank
HIF1A	Mouse	WB 1:100	N/A	Novus Biologicals
ICAM2	Rat	IHC 1:500	N/A	BD Biosciences
Isolectin B4	N/A	IHC 1:800	Alexa 488	Invitrogen
Nestin	Mouse	IHC 1:250	N/A	Santa Cruz
Olig1	Rabbit	IHC 1:600	N/A	Stiles Lab, Harvard U.
Olig2	Goat	WB 1:2000	N/A	R&D Systems
Olig2	Rabbit	IHC 1:800 / WB:4000	N/A	Millipore
Olig2	Rabbit	IHC 1:4000 / WB 1:10000	N/A	Stiles Lab, Harvard U.
PDGFRA	Rat	IHC 1:400	N/A	BD Biosciences
Phospho-histone H3	Rabbit	IHC 1:400	N/A	Cell Signal
PhosphoS147-Olig2	Rabbit	WB 1:100	N/A	Richardson Lab, UCL
Ppp1r14a	Rabbit	IHC 1:400	N/A	Abcam
Sox10	Guineau pig	IHC 1:2000	N/A	Wegner Lab, U. of Hamburg
TujI	Mouse	IHC 1:500	N/A	Sigma
Zebrafish HuC	Mouse	IHC 1:20	N/A	Invitrogen
Secondary antibody	**Species**	**Dilution**	**Conjugation**	**Manufacturer**
Guineau pig IgG	Goat	IHC 1:1000	Cy3	Invtirogen
Mouse IgG H+L	Goat	IHC 1:800	Alexa 488	Invitrogen
Mouse IgG H+L	Goat	IHC 1:800	Alexa 568	Invitrogen
Mouse IgG H+L	Goat	IHC 1:800	Alexa 647	Invitrogen
Protein A	N/A	WB 1:10000	HRP	Invitrogen
Rabbit IgG	Goat	IHC 1:800	Alexa 488	Invitrogen
Rabbit IgG	Goat	IHC 1:800	Alexa 568	Invitrogen
Rabbit IgG	Goat	IHC 1:800	Alexa 647	Invitrogen
Rat IgG	Goat	IHC 1:800	Alexa 488	Invitrogen
Rat IgG	Goat	IHC 1:800	Alexa 568	Invitrogen
Rat IgG	Goat	IHC 1:800	Alexa 647	Invitrogen

Table 2. Primary and secondary antibodies. (IHC, immunohistochemistry; WB. Western blot)

CHAPTER 3

SPINAL CORD ANGIOGENESIS AND THE MN-OLP FATE SWITCH

3.1 INTRODUCTION

In the pMN domain of the developing spinal cord, Olig2-expressing NSCs initially generate MNs before switching to produce OLPs (reviewed by Rowitch, 2004 and Richardson et al., 2006). In mice, the period of MN generation runs from ~E9.5-E12.5, with OLP specification beginning immediately after neurogenesis. Basic helix-loop-helix (HLH) transcription factor (TF) Olig2 is expressed through both developmental phases and dephosphorylation of Olig2 at serine 147 (S147) is known to be a key regulator of the MN to OLP fate switch (Lu et al., 2000; Takebayashi et al., 2000; Zhou et al., 2000; Li et al., 2011). However, it is not known what triggers dephosphorylation at S147. I aimed to examine whether neural tube angiogenesis – a developmental landmark with major physiological consequences for the surrounding CNS tissue, including the ventricular zone stem cell niche – might provide crucial instructive signals that induce the MN-OLP fate switch.

In this chapter I present the results of experiments designed to examine the role of spinal cord angiogenesis in OLP formation from pMN NSCs. The majority of this work was conducted at the Yale Cardiovascular Research Centre, Yale University, Ct. USA, under the supervision of Prof. Anne Eichmann and Prof. Jean-Leon Thomas.

3.2 RESULTS

Timeline of spinal cord angiogenesis in mouse

If blood vessel formation induces OLP specification in the embryonic pMN domain, angiogenic developments must occur in the immediate run up to the MN-OLP fate switch (approximately E12.5 in mouse). In order to characterize development of the vasculature over this critical period, I used a FITC-conjugated Isolectin B4 (IB4) that specifically labels endothelial cell α-D-galactosyl residues to visualize the mouse spinal cord vasculature at E9.5, E10.5, E11.5, E12.5 and E13.5 (Figure 1). At E9.5, the absence of IB4 signal indicates the spinal cord is devoid of blood vessels. At E10.5, I observed scattered IB4-positive structures within the spinal cord. The primitive vascular structures continued to develop until E13.5, with increasing IB4 signal coverage and network formation. This sequence indicates that the nascent spinal cord vasculature first emerges between E9.5 and E10.5, with angiogenesis continuing over the period of the MN-OLP fate switch (approximately E12.5) until at least E13.5, well into the period of oligodendrogenesis. The development of the ventral spinal cord vasculature over the MN-OLP fate switch period is consistent with the “vascular trigger” hypothesis.

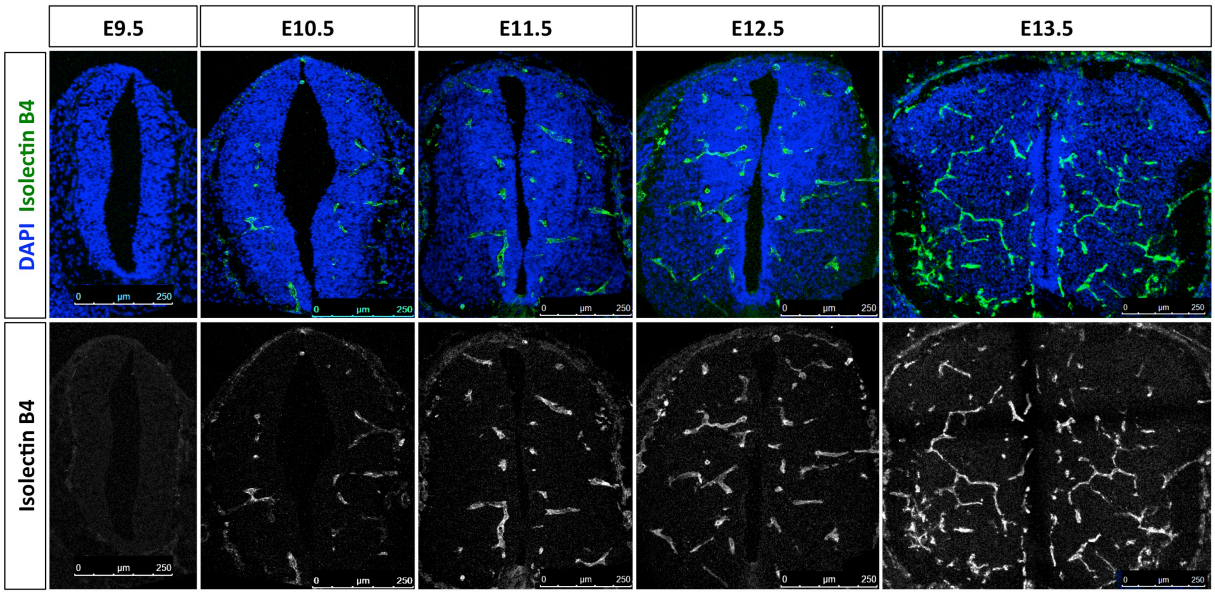

Figure 1. Time-course of angiogenesis in the embryonic mouse spinal cord. Isolectin B4 (IB4, green) labeling of vascular endothelium in thoracic spinal cord cross-sections at E9.5, E10.5, E11.5, E12.5 and E13.5.

Effect of oxygen concentration on OLP specification in vitro and in vivo

Oxygen and the HIF signaling pathway are major regulators of CNS development and NSC function (Mohyeldin et al., 2010). Spinal cord angiogenesis might, therefore, induce the MN-OLP fate switch through changing tissue oxygen tension and disruption of the HIF pathway. To explore the role of oxygen in OLP specification, I began by analysing OLP formation under normal and hypoxic conditions using an in vitro cell culture model of Olig2-expressing NSCs.

Primary adherent Olig2-expressing NSC cultures were derived from the dissociated cortices of E13.5 mice and expanded in a 'NSC medium' containing EGF and FGF, as described by Pollard et al. (2006). These cultures have been shown to retain neuronal and glial – both astrocyte and OL – differentiation potential after multiple passages, and are widely considered to represent bona fide NSCs (Conti et al., 2005; Pollard et al., 2006; Glaser et al., 2007). I initially examined the character of these in vitro NSC populations after 4 days under either normoxic (~20% [O2]) or hypoxic (2-4% [O2]) conditions. In both normal and oxygen-depleted environments, cultured NSCs uniformly expressed Olig2 and the neurofilamentous

stem cell marker Nestin (Figure 2A). Limited expression (<1% cells) of neuron (Tuj1), OL (Sox10) and astrocyte (GFAP) lineage markers was observed in either condition (data not shown). To assess the effect of hypoxic incubation on HIF1A stability and HIF pathway activitation, I prepared total cell lysates from normoxic and hypoxic cultures, and visualized HIF1A expression by western blot using a HIF1A-specific antibody (Figure 2B). As expected, HIF1A protein was significantly more abundant in cells cultured in low [O2], indicating activation of the HIF1-mediated hypoxic response.

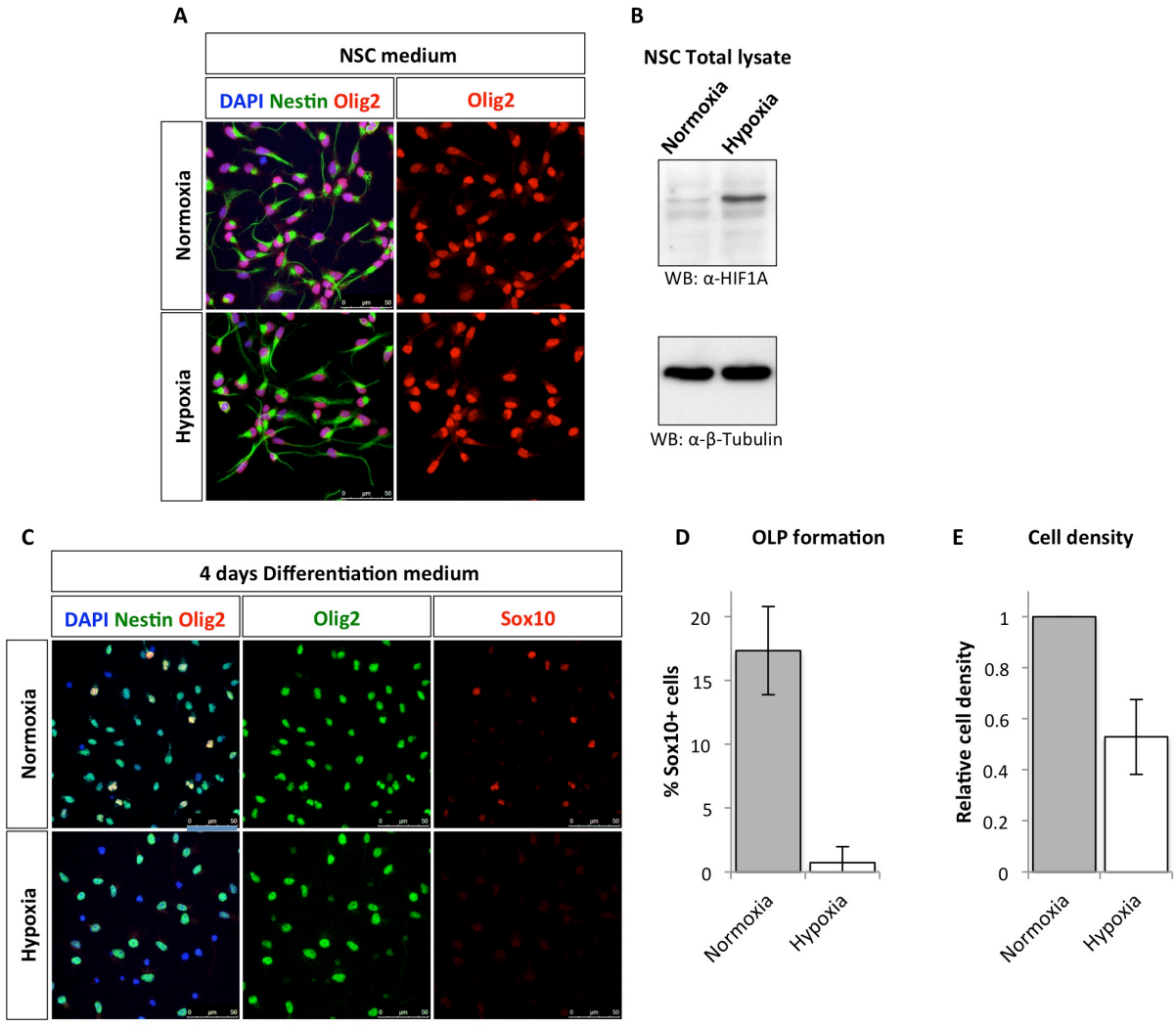

Figure 2. Hypoxia and OLP formation from cultured NSCs. A. Antibody labeling of TF Olig2 (red) and the filamentous neural stem cell marker Nestin (green) in NSCs cultured in NSC medium under normal and hypoxic conditions. **B.** Western blot analysis of HIF1A levels in NSCs cultured under normal and hypoxic conditions. **C.** Antibody labeling of Olig2 (green) and OL lineage marker Sox10 (red) in NSCs after 4 days in Differentiation medium under normal and hypoxic conditions. **D-E.** Quantification of OLP formation and relative cell density after 4 d in Differentiation medium under normal and hypoxic conditions.

To analyse NSC differentiation, NSC medium was substituted with 'Differentiation medium' containing PDGF-AA and increased FGF, a growth factor combination known to enhance specification (FGF) and proliferation (PDGF-AA) of OLPs. After 4 days in Differentiation medium under either normoxic or hypoxic conditions, OLP formation was observed by immunolabeling with Olig2- and Sox10-specific antibodies and quantified (Figure 2C-D). In atmospheric conditions, 4 day exposure to Differentiation medium yielded significant numbers (~15-20% total cells) of Olig2-/Sox10-double positive OLPs. Under hypoxic conditions, however, OLPs made up only ~1% total cell number. Significant differences were also detected in the total cell numbers, with ~50% fewer cells in hypoxic cultures (Fig. 2E), though there was no evidence of substantially increased cell death based on observations of pyknotic cell nuclei. This preliminary data indicates hypoxia inhibits the generation of OLPs in vitro.

In order to understand if hypoxia inhibits OLP generation in vivo, I analysed the effect of maternal hypoxia during gestation on embryonic OLP development. The experimental strategy is shown in Figure 3A. From conception (E0) until E11.5 (pre-fate switch), pregnant female mice were housed under normoxic (20% [O2]) conditions. At E11.5, pregnant female mice either remained under normoxic conditions (control) or were transferred to a low-oxygen chamber (8-10% [O2]; exposure of neonatal mice to 10% [O2] is known to result in reduced OL numbers in vivo [Yuen et al., 2014]). The pregnant female mice were sacrificed and the embryos analysed at E12.5 or E13.5 – after 1 or 2 days hypoxic/normoxic incubation over the MN-OLP fate switch. At the whole-embryo level, one-day (E11.5-E12.5) and two-day (E11.5-E13.5) hypoxia did not result in a global developmental delay, assessed by the appearance of stage-specific limb structures (data not shown). Spinal cord angiogenesis and OLP development was visualized in cross-section by labeling with IB4, anti-Sox10 and anti-

Olig2 antibodies (Figure 3B-C). It should be noted that the absence of littermate controls in these experiments prevented quantitative analysis.

In normal E12.5 and E13.5 embryos (Figure 3B I-I' & 3C I-I'), I observed multiple Sox10+ OLPs within the ventral pMN domain, itself delineated by focal Olig2 expression. Individual, early migratory Olig2-/Sox10-double positive OLPs were also observed outside the ventricular zone. As expected, from E12.5 to E13.5, the number of Sox10+ OLPs increased and the distribution of migratory OLPs expanded. After one-day and two-day hypoxic incubations (Figure 3B II-II' & 3C II-II'), OLP formation at E12.5 and E13.5, respectively, closely resembled the age-matched controls, with grossly similar patterns of Sox10 and Olig2 expression. These results suggest that maternal exposure to 8-10% O2 for one or two days over the period of the MN-OLP fate switch (E11.5 – E12.5/E13.5) did not seriously influence embryonic pMN development or OLP formation. Time constraints precluded the collection and analysis of embryos from multiple litters that would have enabled the robust statistical analysis of embryonic OLP formation in each of the control and hypoxic conditions. In the absence of sufficient replicate litters, I did not quantify OLP generation or migration.

I performed additional experiments to determine the effect of maternal hypoxia on cell division, MN formation and cell death (Figure 3D-E). Spinal cords of control and hypoxic E12.5 mice were immunostained in cross-section with antibodies labeling phosphorylated Histone H3 (ph-HH3) (a mitosis-specific marker), and Hb9 (a post-mitotic MN-specific marker) and Activated Caspase 3 (Casp3) (an apoptosis-specific marker). As a result of antibody-specific fixation requirements, the Hb9 and Casp3 staining experiments were performed using independent embryonic litters, distinct from the litters of control and hypoxic embryos stained for ph-HH3, Olig2 and Sox10.

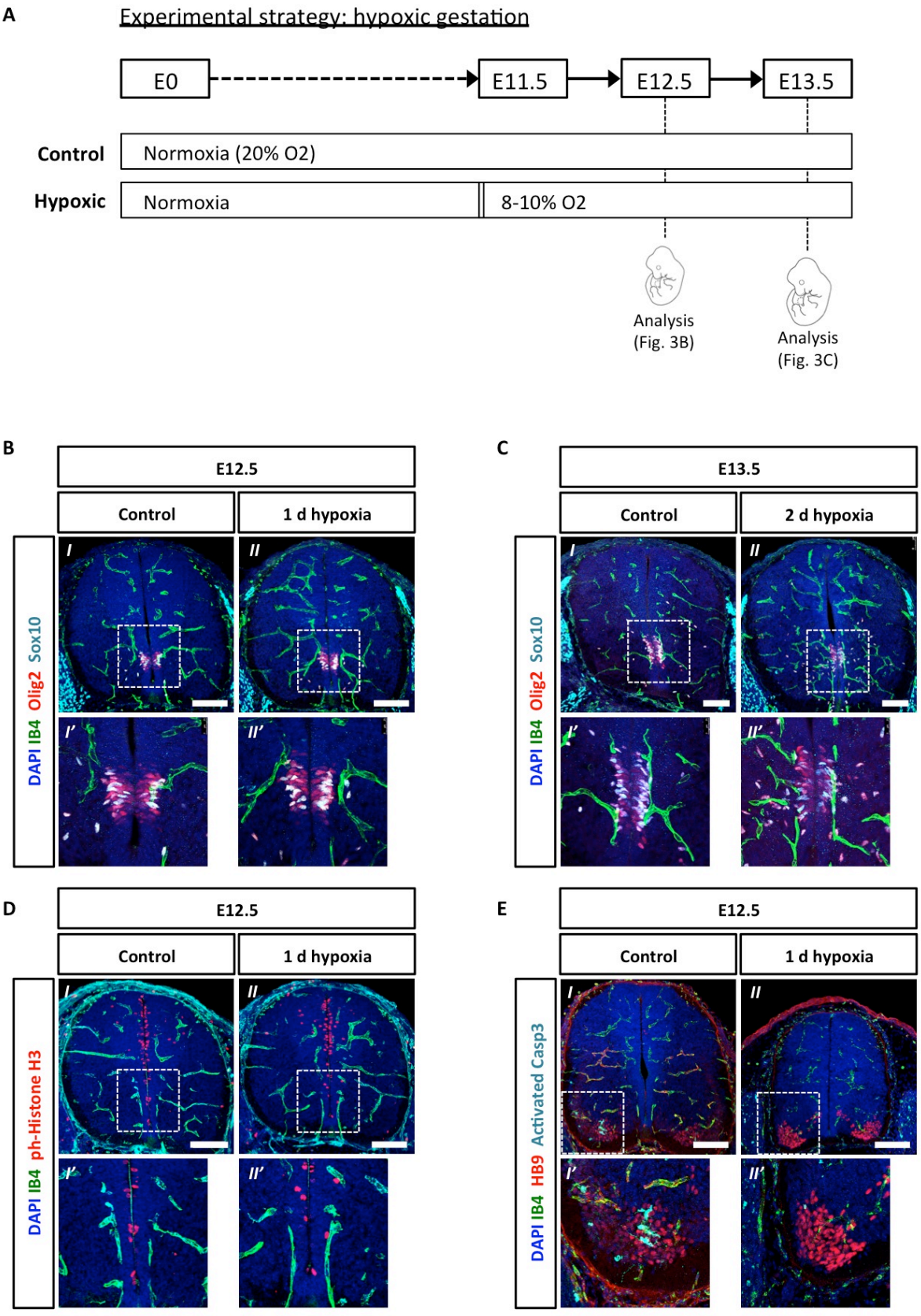

Figure 3. Maternal hypoxia and embryonic OLP development. A. Plan of the experimental strategy. From E11.5, pregnant wild-type female mice were housed under either normal (control) or oxygen-depleted (hypoxic) conditions. Pregnant females were sacrificed after 1 or 2 days (E12.5 or E13.5, respectively) and embryonic spinal cord development examined. **B-C.** Isolectin B4 (IB4, green), Olig2 (red) and Sox10 (cyan)

labeling of spinal cord vascular endothelium and OLP formation at E12.5 and E13.5 after 1 or 2 d under hypoxic conditions. **D.** IB4 (green) and phospho-histone H3 (red) labeling of spinal cord vascular endothelium and cell mitosis at E12.5 after 1 d under hypoxic conditions. **E.** IB4 (green), Hb9 (red) and activated Caspase 3 (cyan) labeling of spinal cord vascular endothelium, post-mitotic MNs and cell apoptosis at E12.5 after 1 d under hypoxic conditions.

In control E12.5 embryos, ph-HH3+ dividing cells appeared tightly clustered along the lumenal walls of the dorsal spinal cord (Figure 3D I). In the ventral spinal cord, ph-HH3+ cells were also found in the ventricular zone, though at a significantly reduced density compared to the dorsal region. This spatial pattern of cell division was also observed in the spinal cords of hypoxic E12.5 embryos, indicating that gestation at 8-10% [O2] from E11.5 to E12.5 did not significantly affect regulation of cell division in the embryonic spinal cord.

In both control and hypoxic E12.5 embryos, Hb9-expressing post-mitotic MNs were primarily observed in the ventral horns of the developing cord, with small numbers of migratory Hb9+ cells found between the pMN and ventral horn regions (Figure 3E). Robust Casp3 signal – an indicator of cell apoptosis – was observed in ventral horn cell populations of control E12.5 embryos, probably marking the early stages of developmental cell death of excess MNs (Sendtner et al., 2000). In contrast, only relatively sparse Casp3 labeling was detected in the same region of hypoxic embryos, indicating reduced cell death. The data indicate that incubation from E11.5 – E12.5 in 8-10% [O2] did not markedly impact formation and migration of Hb9+ post-mitotic MN precursors, but might affect physiological MN cell death. Considering the smaller cross-sectional area of the hypoxic spinal cord relative to the control, however, the observed difference in Casp3 labeling is likely to be an artefact of an age gap and not a consequence of maternal exposure to an oxygen-depleted environment.

In summary, the experiments performed on normoxic and hypoxic differentiating NSC cultures suggested that oxygen concentration regulated OLP generation in vitro. In vivo analysis of embryos harvested from control or hypoxic pregnant females (housed at

atmospheric (20%) or 8-10% [O2] over the period of the MN-OLP switch), however, did not support the in vitro findings. Gestation under low [O2] from E11.5 to E12.5 or E13.5 had no discernible qualitative effect on MN or OLP development.

Transgenic manipulation of angiogenesis and OLP formation

In the absence of in vivo evidence for oxygen-dependent OLP production, I aimed to use vascular mutant mouse lines to establish the effect of premature (hypervascular) and delayed (hypovascular) angiogenesis on OLP development. The transgenic mouse lines selected were as follows:

Hypovascular:

1. *Cdh5-Cre^{ERT2}:Nrp1$^{fl/fl}$*
2. *Cdh5-Cre^{ERT2}:VEGFR2$^{fl/fl}$*

Hypervascular:

1. *Cdh5-Cre^{ERT2}:Notch1$^{fl/fl}$*
2. *Cdh5-Cre^{ERT2}:VEGFR3$^{fl/fl}$*

The *Cdh5-Cre^{ERT2}* transgene consists of the *Cre^{ERT2}* coding sequence inserted into the *VE-Cadherin* (*Cdh5*) P1 artificial chromosome (PAC) (Feil et al., 1996; Benedito et al., 2009; Sorensen et al., 2009). The construct provides tamoxifen-inducible, endothelial cell-specific Cre recombinase activity.

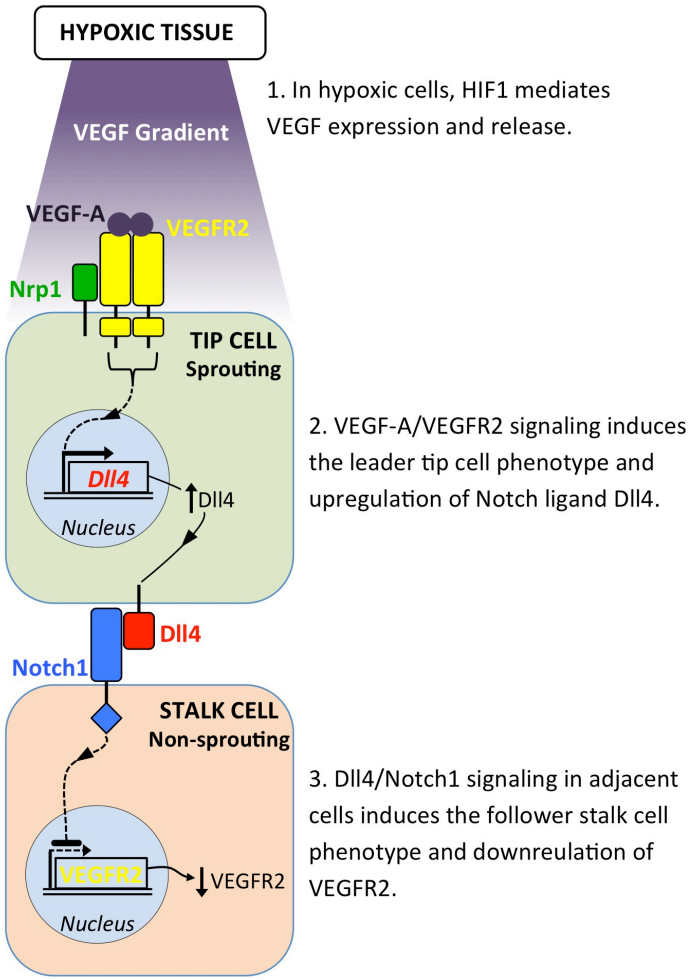

Figure 4. VEGF & Notch signaling in tip/stalk endothelial cell specification.

Hypovascular transgenic mutants

In sprouting angiogenesis, endothelial cells adopt two distinct cellular phenotypes: leader "tip" cells and follower "stalk" cells (Gerhardt et al., 2003). Tip cells extend chemoresponsive filopodia and guide the nascent vessel towards hypoxic regions of the surrounding tissue. Proangiogenic VEGF-A – expressed and secreted from hypoxic cells in a HIF1/2-dependent manner – interacts with the endothelial tip cell surface receptor VEGFR2 (Figure 4) (reviewed by Blanco & Gerhardt, 2013). VEGF ligand-receptor binding triggers VEGFR2 dimerization and successive activation of downstream signaling pathways that regulate the angiogenic program. The cell surface glycoprotein Neuropilin1 (Nrp1) acts as a critical non-kinase VEGF co-receptor that enhances the VEGF/VEGFR interaction and modulates VEGF signaling output. In *Cdh5-Cre^{ERT2}:VEGFR2$^{fl/fl}$* and *Cdh5-Cre^{ERT2}:Nrp1$^{fl/fl}$* mice, endothelial cell-specific

deletion of *Nrp1* and *VEGFR2* therefore disrupts transduction of extracellular proangiogenic VEGF signals and results in severely reduced vascular development in the embryonic mouse brain (Fantin et al., 2013).

Hypervascular transgenic mutants

The cell contact-dependent Notch signaling pathway has been implicated in the angiogenic regulation of endothelial cell specification and differentiation (Blanco & Gerhardt, 2013). In developing vessels, VEGF/VEGFR2 signaling triggers upregulation of the Notch1 ligand Dll4 in tip cells. Dll4-expressing tip cells activate the Notch1 signaling pathway in adjacent ECs and induce the stalk cell phenotype (Figure 4) (Hellstrom et al., 2007; Lobov et al., 2007; Siekmann et al., 2007; Suchting et al., 2007; Tammela et al., 2008). Selection of the stalk cell phenotype involves down-regulation of tip cell-dominant VEGFR2 and thereby prevents excess sprout formation. In *Cdh5-Cre^{ERT2}:Notch1$^{fl/fl}$* mice, endothelial cell-specific deletion of *Notch1* therefore results in excessive tip cell numbers and vessel hyperplasia (Tammela et al., 2011). In contrast to Notch1, VEGFR3 is highly expressed on endothelial tip cells and blocking VEGFR3 with antibodies inhibits postnatal angiogenesis (Tammela et al., 2008). Genetic deletion of *VEGFR3* in *Cdh5-Cre^{ERT2}:VEGFR3$^{fl/fl}$* mice, however, triggers excessive vessel sprouting and branching and generates a hypervascular phenotype closely resembling the *Notch1* mutant mice described above (Tammela et al., 2011).

Over the course of my project, I was unable to analyse either of the selected hypovascular mutant mouse lines. In this section, I present the results of analysis of both the Notch1 and VEGFR3 conditional knockout mice.

1. *Cdh5-Cre^{ERT2}:Notch1$^{fl/fl}$*

I crossed *Cdh5-Cre^{ERT2}:Notch1$^{fl/+}$* males with *Notch1$^{fl/fl}$* females. Cre recombinase activity was induced in embryos by intraperitoneal (IP) administration of 4-hydroxytamoxifen (4-OHT) to pregnant females at E9.5 and E10.5. Biological replicate litters were collected at E12.5 and individual embryos genotyped by PCR from genomic DNA preparations. I compared spinal cord angiogenesis and OLP development in *Cdh5-Cre^{ERT2}:Notch1$^{fl/fl}$* (Cre+) and *Notch1$^{fl/fl}$* (Cre- control) littermates by labeling cross-sections of cervical spinal cord with IB4, anti-Olig2 and anti-Sox10 antibodies.

In both litters #1 and #2, the pattern of spinal cord IB4 staining appeared similar in Cre+ and control littermate embryos (Figure 5A & 5C), and this was confirmed by ImageJ quantification of IB4 signal (Figure 5B & 5D), indicating the vascular phenotype in Cre+ embryos was no different to Cre- controls. This might be the result of low recombination efficiency or the inefficacy of endothelial cell-specific *Notch1* deletion for stimulating spinal cord angiogenesis. As expected, given the lack of vascular defects in Cre+ mutant mice, Sox10+/Olig2+ OLPs and Sox10-/Olig2+ NSCs were observed in both Cre+ and control littermate embryos with qualitatively similar distributions (Figure 5A III-IV' & 5B III-IV'). In the absence of a vascular phenotype, I did not quantify OLP generation.

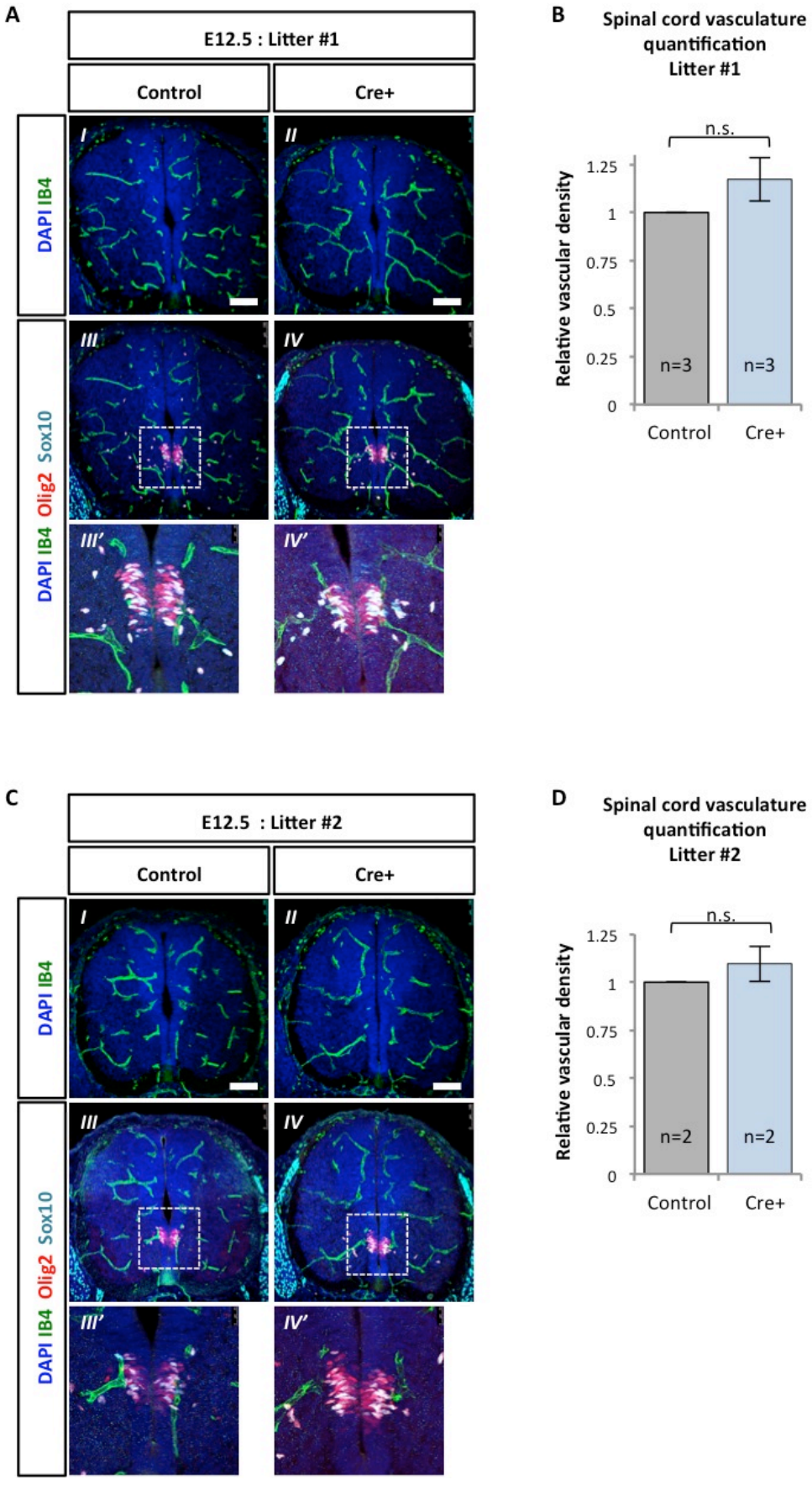

Figure 5. Spinal cord angiogenesis and OLP development in *Cdh5-Cre^{ERT2}:Notch1$^{fl/fl}$* E12.5 mice. A & C. Isolectin B4 (IB4, green), Olig2 (red) and Sox10 (cyan) labeling of spinal cord vascular endothelium and OLP formation in E12.5 control and Cre+ littermate embryos. **B & D.** ImageJ quantification of the relative vascular density in spinal cords of control and Cre+ littermate embryos.

2. *Cdh5-Cre^{ERT2}:VEGFR3$^{fl/fl}$*

I crossed *Cdh5-Cre^{ERT2}:VEGFR3$^{fl/fl}$* males with *VEGFR3$^{fl/fl}$* females. 4-OHT was administered by IP injection into pregnant females at E9.5 and E10.5. Two replicate litters were collected at E12.5 and one at E11.5 spinal cord angiogenesis and OLP development was analysed using IB4 and anti-Olig2 and anti-Sox10 antibodies.

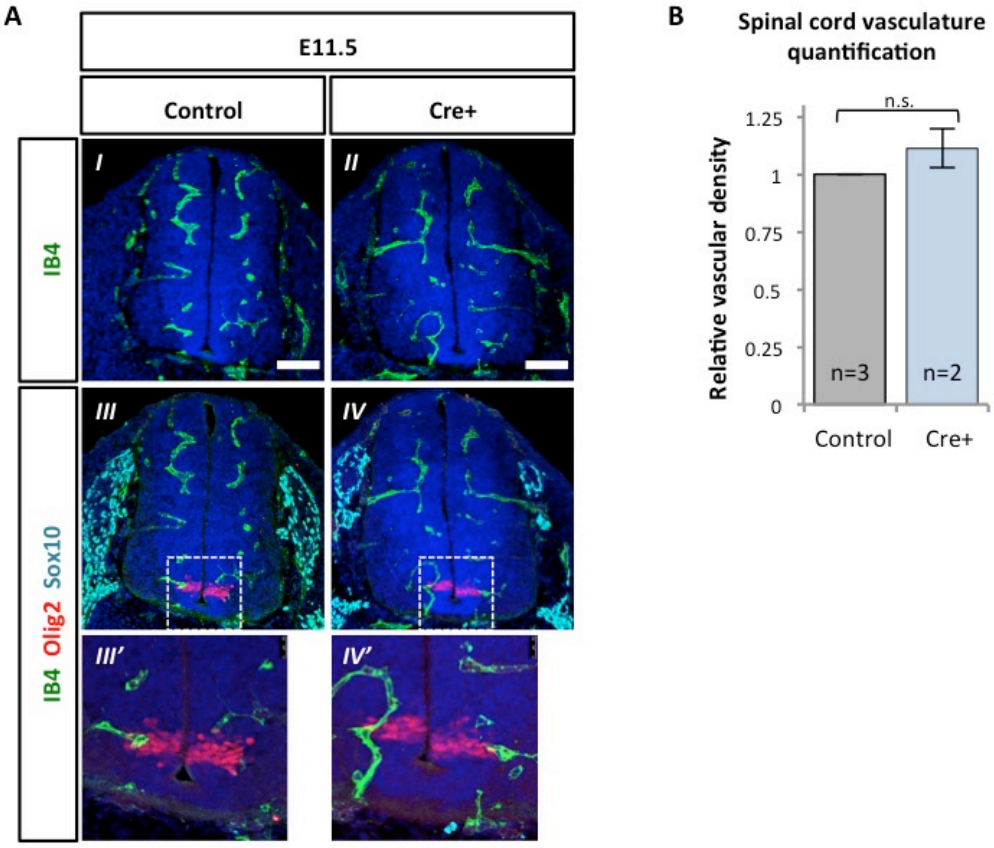

Figure 6. Spinal cord angiogenesis and OLP development in *Cdh5-Cre^{ERT2}:VEGFR3$^{fl/fl}$* E11.5 mice. A. Isolectin B4 (IB4, green), Olig2 (red) and Sox10 (cyan) labeling of spinal cord vascular endothelium and OLP formation in E11.5 control and Cre+ littermate embryos. **B.** ImageJ quantification of the relative vascular density in spinal cords of control and Cre+ littermate embryos.

If angiogenesis triggers the MN-OLP fate switch, a hypervascular phenotype would be expected to induce premature OLP formation. I therefore initially examined blood vessel and OLP development in E11.5 mutant embryos (Figure 6). In control and Cre+ embryos, the pattern of IB4 signal within the spinal cord appeared similar. ImageJ quantification of IB4 signal confirmed Cre+ embryos did not exhibit a vascular phenotype. In both Cre+ and

control E11.5 embryos, clustered Olig2 labeling delineated the ventral pMN domain, while negligible anti-Sox10 signal within the spinal cord indicated OLPs were absent and oligodendrogenesis had not begun.

At E12.5, IB4 signal coverage within the embryonic spinal cord was visibly greater – tracing larger and more abundant vessel-like structures – in Cre+ embryos compared to control littermates (Figure 7A & 7E). ImageJ quantification confirmed a 25-30% increase in spinal cord IB4 signal in *VEGFR3*-deficient Cre+ embryos in both Litters #1 and #2 (Figure 7B & 7F). The difference in IB4 staining indicates the induction of Cre recombinase activity at E9.5-E10.5 and resultant *VEGFR3* deletion in vascular endothelial cells stimulated excessive spinal cord angiogenesis and generated a hypervascular phenotype by E12.5.

In view of the clear and consistent vascular phenotype, I examined OLP formation in Cre+ and control embryos. Preliminary qualitative analysis did not reveal any obvious OLP phenotype. I quantified both OLP specification and migration. OLP specification was calculated as the percentage of Olig2-/Sox10-double positive OLPs relative to the total number of Olig2-expressing cells (both OLPs and pMN domain NSCs). The average fold-change in the percentage of OLPs in Cre+ versus Cre- control embryos is shown in Figure 7C & 7G for Litter #1 and Litter #2, respectively. The data indicated there was no significant impact on OLP formation in the hypervascular Cre+ embryos.

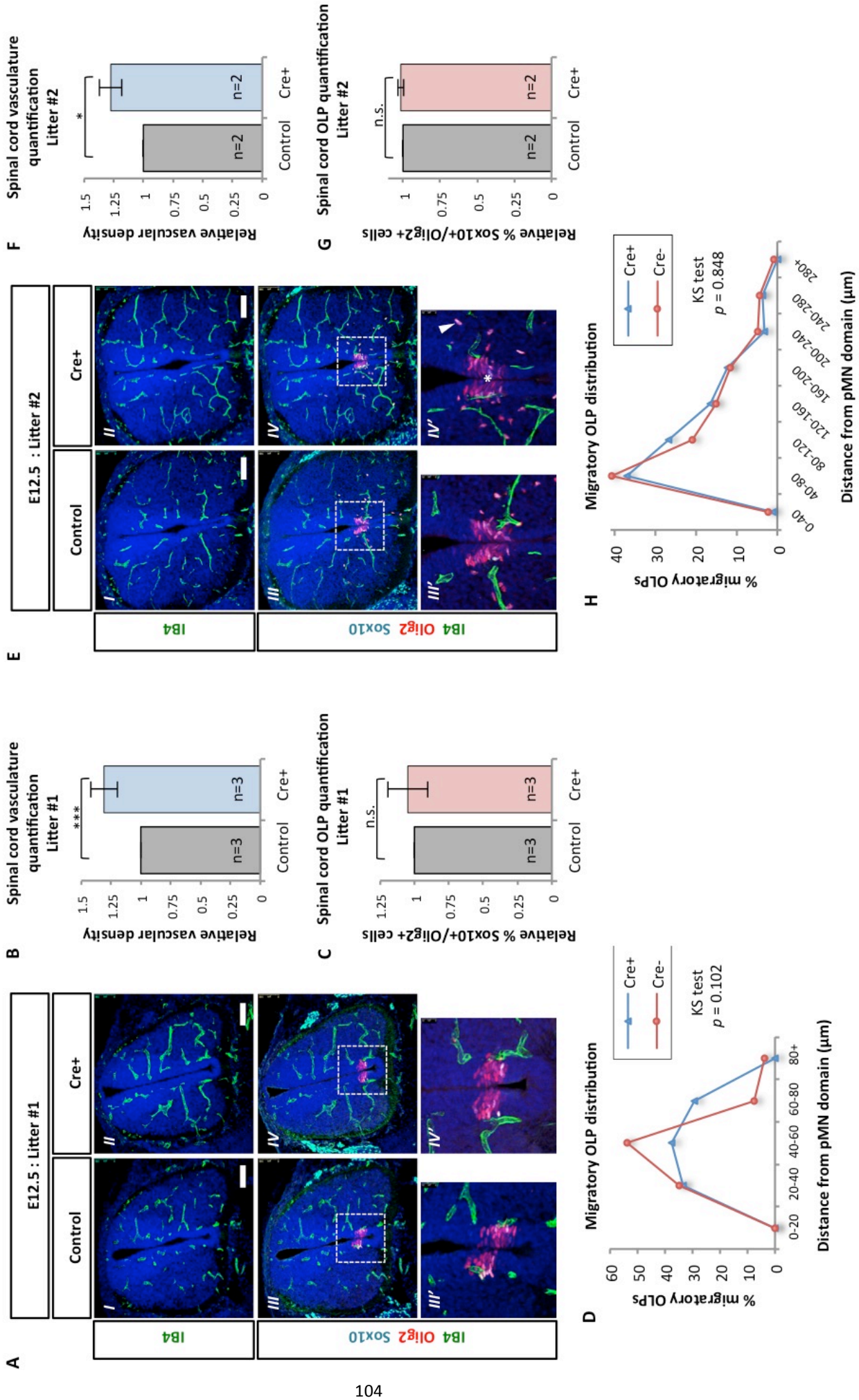
A
E12.5 : Litter #1
Control
Cre+
IB4
IB4 Olig2 Sox10
B
Spinal cord vasculature quantification Litter #1
Relative vascular density
***
n=3
n=3
Control
Cre+
C
Spinal cord OLP quantification Litter #1
Relative % Sox10+/Olig2+ cells
n.s.
n=3
n=3
Control
Cre+
D
Migratory OLP distribution
% migratory OLPs
Cre+
Cre-
KS test
p = 0.102
0-20
20-40
40-60
60-80
80+
Distance from pMN domain (µm)
E
E12.5 : Litter #2
Control
Cre+
IB4
IB4 Olig2 Sox10
F
Spinal cord vasculature quantification Litter #2
Relative vascular density
*
n=2
n=2
Control
Cre+
G
Spinal cord OLP quantification Litter #2
Relative % Sox10+/Olig2+ cells
n.s.
n=2
n=2
Control
Cre+
H
Migratory OLP distribution
% migratory OLPs
Cre+
Cre-
KS test
p = 0.848
0-40
40-80
80-120
120-160
160-200
200-240
240-280
280+
Distance from pMN domain (µm)

Figure 7. Spinal cord angiogenesis and OLP development in hypervascular *Cdh5-Cre^{ERT2}:VEGFR3$^{fl/fl}$* E12.5 mice. A & E. Isolectin B4 (IB4, green), Olig2 (red) and Sox10 (cyan) labeling of spinal cord vascular endothelium and OLP formation in E12.5 control and Cre+ littermate embryos. **B & F.** ImageJ quantification of the relative vascular density in spinal cords of control and Cre+ littermate embryos. **C & G.** Quantification of the relative OLP formation in spinal cords of control and Cre+ littermate embryos. **D & H.** Histogram plots of the percentages of OLPs at different distances from the pMN domain. The asterisk and arrowhead in E *IV'* mark the centre of the pMN domain (origin) and a migratory OLP, respectively.

OLP migration was measured by straight-line distance of parenchymal OLPs from the centre of the pMN domain (asterisk Figure 7E IV'). For each litter, the distribution of migratory OLPs is presented as a percentage frequency distribution. For Litter #1 (Figure 7D), 33.3% and 34.6% of migratory OLPs were observed in the 20-40 µm range in Cre+ and control embryos, respectively. Outside the 40 µm boundary, over 50% of OLPs in control embryonic spinal cords resided in the 40-60 µm range, with ~12% beyond 60 µm. In contrast, in the Cre+ littermates, 37.5% were 40-60 µm from the pMN domain, with ~30% beyond 60 µm. For Litter #2, no substantial differences (>10%) were observed in the proportion of migratory OLPs within a given distance from the pMN domain. In both Cre+ and control embryos, roughly 40% were observed in the 40-80 µm range, with steadily decreasing percentages over successive ranges and >99% migratory OLPs within 280 µm of the pMN domain centre. To determine whether the distributions of migratory OLPs in Cre+ and control embryos were different to a statistically significant degree, I independently analysed the distribution data for both litters using the Kolmogorov-Smirnov (KS) non-parametric test. The *p* values generated were 0.102 (Litter #1) and 0.848 (Litter #2), indicating the distribution of migratory OLPs in Cre+ embryos was not significantly different from Cre- littermates. Combined, the data suggests that the hypervascular spinal cord phenotype observed in Cre+ *VEGFR3*-deficient embryos does not affect either OLP specification or migration.

IB4 labeling and quantification confirmed that Cre+ spinal cords are hypervascular. IB4 staining, however, does not reveal vessel patency and therefore might not represent

functionality. In order to establish if vessel patency differed in *VEGFR3*-deficient and control E12.5 spinal cords, I co-labeled spinal cord cross-sections of Litter #1 and Litter #2 with IB4 and an antibody specific to intracellular adhesion molecule 2 (ICAM2), a marker of lumenized vessels (Figure 8). With very few exceptions (arrowheads Figure 8A), spinal IB4+ endothelial structures were co-labeled for ICAM2 in the Cre+ and control embryos of both E12.5 litters. This indicated that the vessels in hypervascular spinal cords were lumenized, and suggested that the vascular phenotype will generate differences in tissue perfusion. In light of these data and the analysis of OLP specification and migration performed in the same specimens (Figure 7), it appeared that the additional patent vasculature in Cre+ spinal cords did not affect OLP development.

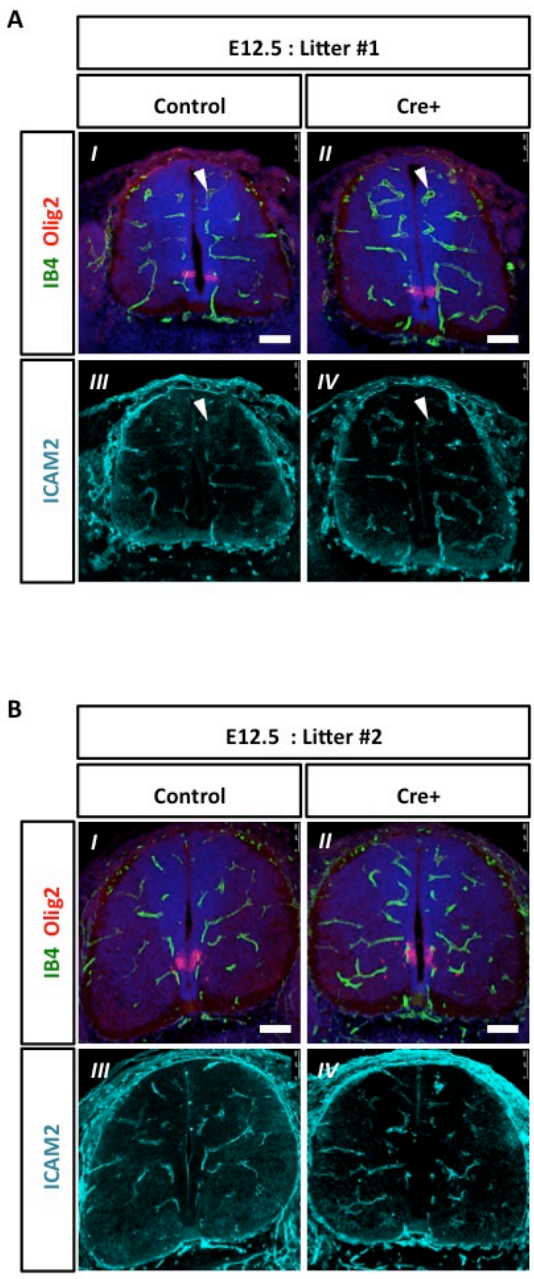

Figure 8. Spinal cord angiogenesis and vessel lumenization in hypervascular *Cdh5-Cre^{ERT2}:VEGFR3$^{fl/fl}$* E12.5 mice. A & B. Isolectin B4 (IB4, green) and lumenized vessel marker ICAM2 (cyan) labeling of spinal cord vascular endothelium in E12.5 control and Cre+ littermate embryos. Arrowheads in A mark ICAM2-negative, IB4-positive vascular endothelium.

Summary

I have described a series of experiments designed to establish whether spinal cord angiogenesis influences development in the embryonic spinal cord, in particular the MN-OLP fate switch of PMN domain-resident NSCs. In culture, differentiation of multipotent NSCs to Sox10+ OLPs was inhibited by hypoxia, indicating that oxygen delivery by the nascent vasculature might in principle be able to trigger OLP formation in the embryonic spinal cord. In vivo, however, hypoxic incubation over the period of the fate switch (mid gestation) did not grossly affect OLP development. Moreover, transgenic manipulation of angiogenesis in *Cdh5-Cre^{ERT2}:VEGFR3$^{fl/fl}$* mice generated a hypervascular spinal cord phenotype but this did not alter OLP formation or migration. Unfortunately, analysis of a hypovascular mutant mouse line was not possible during my project.

3.3 DISCUSSION

In the developing spinal cord, OLP formation is tightly regulated, both spatially and temporally. The vast majority of OL lineage cells arise from a discrete region in the ventral ventricular zone, the pMN domain, also the birthplace of all spinal cord MNs. Neural stem cells resident in the pMN domain generate MN progenitors before switching abruptly – around E12.5 in mice – to generate OLPs. The underlying developmental changes that trigger the fate switch are not known. One interesting possibility is that angiogenesis in the spinal cord could alter NSC/OLP development through one or a combination of oxygen delivery, systemic hormone signaling and short-range EC-NSC signaling mechanisms. In this chapter, I explored how manipulating oxygen tension and angiogenesis affected generation of OLPs. My results suggested that hypoxia inhibited OLP differentiation from NSCs in vitro; however, incubation of pregnant wild type mice in low oxygen conditions did not disrupt OLP development in the embryonic spinal cord in vivo. In addition, hypervascular development in transgenic mice did not detectably influence OLP formation. The results therefore failed to establish a regulatory role for blood vessel development in spinal OLP specification in vivo.

Spinal cord angiogenesis

Labeling thoracic spinal cord cross-sections of E9.5, E10.5, E11.5, E12.5 and E13.5 wild-type spinal cords with EC marker IB4 revealed the time-course of vascular development. Primitive vascular structures first emerge between E9.5 and E10.5. From E10.5-E13.5, the vascular network continues to develop, with increasing vessel size, coverage and complexity. OLPs arise around E12.5, during a period of significant vascular growth. The dynamic state of the blood vessel network in the run up to the MN-OLP fate switch is consistent with an instructive role for angiogenesis in regulating pMN NSC fate. The vascular development prior

to the pMN fate switch might, for example, facilitate delivery of a fate switch-inducing agent such as oxygen.

Oxygen and MN/OLP development

To address the potential role of oxygen in OLP specification, I analyzed OLP formation under normal and oxygen-depleted conditions both in vitro and in vivo. In differentiating NSCs in culture, hypoxia inhibited OLP development and cell proliferation without inducing widespread apoptosis. The scarcity of OLPs in hypoxic cultures could, therefore, be the consequence of decreased OLP proliferation and not OLP specification. However, in a study examining the effect of oxygen tension on human OLP progenitors, low O2 has actually been shown to enhance PDGFRA+ cell proliferation (Pistollato et al., 2007). Regardless of whether due to its effect on specification or proliferation or a combination of the two, hypoxia effectively inhibits OLP generation in my differentiating NSC cultures. This is in direct opposition to recent research into the effect of oxidative stress on oligodendrogenesis in primary rat neural progenitor cell cultures (Perez-Estrada et al., 2014). In these experiments, exposure to the reactive oxygen species hydrogen peroxide (normally produced in cells under hypoxic stress) significantly increased the OL yield in differentiating neural progenitor cell cultures. The disparity in the observations reported here and by Perez-Estrada et al. (2014) might be explained by differences in cell culture – adult rat neural progenitors versus embryonic mouse neural progenitors – or more likely the contrasting effects of hydrogen peroxide treatment and hypoxic incubation.

In line with the anti-OLP effects of hypoxia I describe, pro-OL differentiation roles for oxygen have previously been reported in several studies. In vitro, when OLPs were differentiated at 20% O2 as opposed to 5% O2, oligodendrocyte maturation was significantly enhanced

(Pistollato et al., 2007). More recently, it has been reported that oxygen tension, mediated via effects in OLP-intrinsic HIF, is an essential regulator of postnatal myelination (Yuen et al., 2014). HIF pathway activation inhibits OLP maturation, and HIF degradation – induced by oxygen delivery – is required for OL differentiation and myelination in the early post-natal mouse brain. Finally, oxidative stress – induced chemically using cobalt chloride in OLP culture and by hypo-perfusion in mice – similarly results in a reduction in mature OLs and myelination (Miyamoto et al., 2013). My results suggest that oxygen tension might, in addition to regulating OLP differentiation into myelinating OLs, also regulate the initial specification of NSCs to OLPs. This could time the MN-OLP fate switch in embryonic spinal cord, and might be necessary to accommodate the increased metabolic requirements of OLPs.

I did not examine specification of other neural cell types – neurons and astrocytes – under normal and hypoxic conditions. It would be interesting to know if the observed effect on OLP formation is cell type-specific or the result of an all-round differentiation block. In the mouse retina, for example, tissue hypoxia is accompanied by an increase in the proliferation of immature astrocytes and delayed astrocyte differentiation (West et al., 2005). As regards neuronal development, if oxygen delivery to the ventral ventricular zone by the newly formed vasculature halts MN generation and initiates OLP development in vivo, one might expect to observe enhanced neuron formation under hypoxic conditions. While this is yet to be examined with the NSC culture system described here, there are published reports of oxygen concentration differentially affecting the generation of specific neuronal lineages in vitro (reviewed by Panchision, 2009). For example, low oxygen tension promotes formation of tyrosine hydroxylase-positive dopaminergic neurons (Studer et al., 2000). Conversely, low [O2] has also been shown to repress differentiation of Tuj1+ neurons (Gustaffson et al., 2005). Taken together, the evidence suggests that oxygen tension can regulate neural cell

development in a lineage-specific manner (Panchision, 2009). Prior to spinal cord angiogenesis, low oxygen tension in the pMN domain of the embryonic spinal cord might promote MN production before blood vessel-mediated oxygen delivery induces the MN-OLP fate switch.

To explore the effect of hypoxia on embryonic OLP formation in the spinal cord, I incubated pregnant wild-type female mice in a hypoxic chamber (8-10% O2) at E11.5 and characterized the effect on spinal OLP development at E12.5 (1 d hypoxia) and E13.5 (2 d hypoxia). After 1 or 2 d hypoxia, no substantial differences were observed in the patterns of angiogenesis (revealed by labeling for IB4), NSC/OLP development (Olig2 & Sox10), cell proliferation (phospho-histone H3), MN production (Hb9) or cell death (cleaved Casp3) compared to control embryos. Hypoxic incubation did not, therefore, grossly affect any examined aspect of spinal cord development. It should be noted that the experimental design required comparison between embryos of different litters as opposed to within the same litter, introducing potential variation in, for example, the precise age of the embryos being compared. Nevertheless, my data suggest that maternal hypoxia does not have a major effect on cell fate determination in the pMN domain of the embryonic spinal cord.

An additional consideration is the physiological effect of the maternal hypoxic incubation in utero. Over the course of my research, I did not demonstrate that gestation under low [O2] (8-10%) altered tissue oxygen tension in the spinal cords of the developing embryos. As such, the lack of an observable phenotype might be due to the insufficiency of this strategy for inducing hypoxia in the embryonic spinal cord. A number of viable methods have previously been described to detect tissue hypoxia, including HIF1A immunohistochemistry, VEGF-A RNA in situ hybridization and/or nitroimidazole markers of hypoxia such as pimonidazole and EF5, which generate adducts with thiol containing proteins specifically in hypoxic cells (Lord

et al., 1993; Arteel et al., 1995; Varia et al., 1998; Ozaki et al., 1999; Schoch et al., 2002). However, I found both HIF1A immunolabeling and nitroimidazole markers EF5/pimonidazole labeling methods intractable, failing to detect hypoxia in the spinal cord at E9.5, prior to angiogenesis (data not shown).

Spinal angiogenesis in E12.5 *Cdh5-Cre^{ERT2}:Notch1$^{fl/fl}$* mice

Over and above examining the specific role of oxygen, I intended to establish whether spinal angiogenesis regulates OLP development by analysis of hypervascular transgenic mice. I initially examined spinal cord angiogenesis in E12.5 *Cdh5-Cre^{ERT2}:Notch1$^{fl/fl}$* mice after 4-OHT-inducible deletion of *Notch1* specifically in Cdh5+ endothelial cells. IB4 staining and ImageJ quantification indicated the vasculature in Cre+ embryos was not significantly over-developed compared to controls. There are several possible explanations for the lack of a spinal vascular phenotype. The transgenic mice did not contain a transgenic reporter of Cre-recombination, such as *ROSA26-YFP*. In the absence of such a reporter, I could not estimate the recombination efficiency and, although the *Cdh5-Cre^{ERT2}* is a well-established and validated transgenic tool, it is possible that the IP administration of 4-OHT failed to induce efficient *Notch* deletion in endothelial cells. Indeed, low efficiency of Cre recombination has been previously reported for the same transgenic embryos after injection at E11.5 (Cristofaro et al., 2013).

An alternative possibility is that endothelial-specific genetic deletion of Notch does not trigger vascular overgrowth in the developing spinal cord. The existing model of Notch1 regulation of angiogenesis involves VEGFR2-induced upregulation of Notch ligand Delta-like 4 (Dll4) in endothelial cells (Tung et al., 2012). Membrane bound Dll4 interacts with and activates Notch 1 receptors expressed on neighboring endothelial cells, ultimately inducing down-regulation of VEGFR2 expression in Notch-activated cells. This signaling cascade

generates VEGFR2-/Dll4-expressing tip cells and adjacent stalk cells. The research that revealed this tip versus stalk cell fate selection mechanisms was performed using the same transgenic approach (*Cdh5-Cre*^{ERT2} x *Notch1*$^{fl/fl}$) and examining retinal angiogenesis post-natally, where endothelial *Notch1* ablation generates a profound hypervascular phenotype (Hellstrom et al., 2007). In a subsequent study of arteriolar network formation, endothelial cell-specific *Notch1* deletion also generated a clear vascular phenotype in the mouse brain at E13.5 (Cristofaro et al., 2013). To date, however, there has been no published analysis of Notch signaling in embryonic spinal cord angiogenesis and it remains possible that an alternative tip/stalk fate selection mechanism is active there. Tammela et al. (2011) have shown, for example, VEGFR3-mediated control of tip-stalk conversion via induction of Notch target genes in endothelial cells independent of canonical Notch signaling. VEGF-C/VEGFR3 signaling induces Notch target gene expression through phosphatidylinositol-3-kinase (PI(3)K) signaling – a positive regulator and effector of the Notch pathway – and loss of VEGFR3 leads to a decrease in Notch target gene activation, thereby triggering tip cell dominance and excessive angiogenic sprouting and branching (Takeshita et al., 2007). This mechanism for driving differentiation towards the stalk cell phenotype might therefore dominate over Dll4-Notch1 signaling in the spinal cord and explain the lack of a *Cdh5-Cre*^{ERT2}*:Notch1*$^{fl/fl}$ phenotype.

Unfortunately, over the course of my research, I did not have the opportunity to analyse the retinal or brain vascular phenotype in the Cre+ and control embryos. This analysis would have provided a useful confirmation of effective recombination. For example, architectural differences in the vasculature of these tissues in Cre+ versus control embryos would suggest effective *Notch1* deletion and imply regional variation in the requirement for Notch1 signaling for normal angiogenesis.

Spinal angiogenesis & OLP development in *Cdh5-Cre^{ERT2}:VEGFR3$^{fl/fl}$* mice

In parallel with the *Cdh5-Cre^{ERT2}:Notch1$^{fl/fl}$* embryonic analysis, I examined spinal vascular development and OLP formation in *Cdh5-Cre^{ERT2}:VEGFR3$^{fl/fl}$* embryonic mice at E12.5 and E11.5, after 4-OHT administration to pregnant females at E9.5 and E10.5. During embryonic development, VEGFR3 is expressed in the tip cells of angiogenic sprouts (Tammela et al., 2008). Similar to inactivation of Notch1 signaling in endothelial cells, deletion of *VEGFR3* increases tip cell numbers and induces vessel hyperplasia (Tammela et al., 2011).

At E12.5, IB4 staining and ImageJ quantification revealed a consistent hypervascular phenotype across the spinal cords of *Cdh5-Cre^{ERT2}:VEGFR3$^{fl/fl}$* embryos of two litters compared to the littermate controls. At E11.5, no hypervascular phenotype was observed in the Cre+ embryos of the single litter analysed. The development of an observable difference by E12.5 indicated effective 4-OHT-induced Cre-mediated recombination in Cdh5+ endothelium. The lack of any vascular difference at E11.5 is therefore likely due to insufficient time between 4-OHT administration and analysis.

If angiogenesis were both necessary and sufficient for timing the MN-OLP fate switch, vascular hyperplasia might be expected, through premature delivery of a diffusible or endothelial cell surface signal, to induce precocious OLP formation. I analysed spinal pMN/OLP development by immunolabeling with anti-Olig2 and -Sox10 antibodies. Antibody labeling did not reveal any gross qualitative effect on pMN NSC (Olig2+/Sox10-) or OLP (Olig2+/Sox10+) phenotypes and quantification confirmed similar OLP formation in hypervascular *Cdh5-Cre^{ERT2}:VEGFR3$^{fl/fl}$* and control embryos. For further analysis, I also examined OLP migration. Quantification of the distribution of OLPs across the transverse

plane of the spinal cord revealed no significant differences between Cre+ and control embryos.

Together these data indicated that the vascular hyperplasia observed in Cre+ embryos at E12.5 was not associated with an effect on OLP development, potentially reflecting the lack of any important role for angiogenesis in regulating OLP specification and migration in the embryonic spinal cord. There are, however, a number of qualifications. For example, development of the blood vessel network might be necessary but not sufficient to induce OLP formation. If additional cell intrinsic or extrinsic pathways were required to regulate pMN NSC differentiation, then in the absence of coordinated activation of all those pathways, OLPs would not emerge or develop prematurely.

To resolve the requirement for angiogenesis in OL development in the embryonic mouse spinal cord, I plan to perform similar immunolabeling experiments using hypovascular transgenic mutants. Genetic deletion of endothelial *VEGFR2* or *Neuropilin 1* (*Nrp1*) results in severely restricted blood vessel growth (Shalaby et al., 1995; Fantin et al., 2013). These experiments will provide a critical test of the role of the vasculature in regulating OLP specification; if vascular development were a necessary regulator of OL development, disrupting angiogenesis would alter OLP development.

Conclusions

Elucidating the mechanism(s) that time the MN-OLP fate switch – and potentially regulate OLP formation and migration thereafter – will be fundamental to a proper understanding of OL development. Discovering the conditions under which OLPs develop in vivo will also inform approaches to treating OL diseases such as multiple sclerosis, for example for

optimizing ex vivo production methods for efficient cell replacement therapies. In addition, the data might provide valuable insight into the general mechanisms regulating NSC fate choice in the developing CNS. Here, I have explored the role of angiogenesis and oxygen on OLP development both in vitro and using mouse models in vivo. Ultimately, the data I have presented here do not conclusively support or oppose an involvement for spinal angiogenesis in triggering the MN-OLP fate switch. Additional experiments are therefore required to determine the role of vascularization in regulating pMN NSC development.

CHAPTER 4

OLIG2 S147 DEPHOSPHORYLATION: IDENTIFYING THE PHOSPHATASE

4.1 INTRODUCTION

Phosphorylation of bHLH TF Olig2 at S147 critically regulates NSC fate in the developing spinal cord (Li et al., 2011). In embryonic development, Olig2 – expressed in pMN domain-resident NSCs – is initially phosphorylated, forming homodimers and inducing MN generation. At approximately E12.5 in mouse, Olig2 S147 dephosphorylation alters the binding preference of Olig2 from homodimerisation to heterodimerisation, abruptly halting MN production and initiating a programme of OLP specification.

The extracellular stimuli and intracellular signaling pathways that induce Olig2 S147 dephosphorylation and the MN-OLP fate switch are not known. Establishing the kinase and phosphatase enzymes that catalyze addition/removal of a phosphate group at S147 will provide important insight into how Olig2 S147 phosphorylation is regulated and the molecular mechanisms governing spinal NSC fate. Bioinformatic analysis of Olig2 revealed that S147 is a predicted protein kinase A (PKA) substrate and the site (R[R/K]X[S/T]) (X, any amino acid) is conserved during evolution (Li et al., 2011). In addition, Olig2 S147 can be phosphorylated by PKA in cultured Cos-7 cells and a dominant negative form of PKA inhibits phosphorylation (Li et al., 2011). A role for PKA in Olig2 S147 phosphorylation in vivo, however, has not been confirmed, and it remains possible that Olig2 S147 is phosphorylated by a different protein kinase.

In addition to the kinase pathway(s) responsible for phosphorylating Olig2, the identity of the phosphatase that dephosphorylates Olig2 S147 and thereby triggers the MN-OLP fate switch is yet to be determined. In contrast to kinase prediction, reliable computational tools for prediction of phosphatase targets are not yet available. In this short chapter I report the results of work aimed at identifying the Olig2 S147-targeting phosphatase, activation or expression of which might initiate OLP production.

4.2 RESULTS

To identify candidate phosphatases that might dephosphorylate S147, Huiliang Li (a post-doctoral member of the Richardson Lab) examined the microarray data of Nielsen et al (2006), Cahoy et al. (2008) and Hu et al. (2004) for evidence of altered expression of specific phospho-kinase/phosphatase pathway proteins in neural progenitors and OLPs (Table 1). The analysis identified Dual specificity phosphatase 9 (Dusp9) along with a number of catalytic and regulatory (inhibitory) subunits of protein phosphatase 1 (PP1) and PP2 (Table 1). In the case of PP1/PP2 regulatory subunits, down-regulation could in principle relieve inhibition and allow PP1/PP2-mediated dephosphorylation of Olig2 S147. Of the candidate phosphorylation pathway proteins, Dusp9 and Ppp1r14a, a regulatory subunit of PP1, exhibited the most substantial changes (+14.1 and -13.7 fold, respectively) between neural progenitors and OLPs and were selected for further analysis.

Gene symbol	Gene name	OLP versus NSC expression (fold change)
Dusp9	Dual specificity phosphatase 9	14.1
Ppp1r14a	Protein phosphatase 1 regulatory subunit 14A	-13.7
Ppm2c	Protein phosphatase 2 magnesium dependent catalytic subunit	-8.7
Ppp2r3a	Protein phosphatase 2 regulatory subunit B alpha isoform	7.9
Ppp1r1a	Protein phosphatase 1 regulatory subunit 1A	-7.3
Ppp1r1b	Protein phosphatase 1 regulatory subunit 1B	-6.3
Ppp2r3a	Protein phosphatase 2 regulatory subunit B gamma isoform	-6

Table 1. Candidate phosphatases/phosphatase-components with significantly altered expression OLPs and NSCs. Positive/negative values indicate increases/decreases respectively. (H. Li, pers comm.)

If dynamic expression of Dusp9 or Ppp1r14a directly mediates dephosphorylation of Olig2 and induces the MN-OLP fate switch, the expression level might be expected to change in

pMN-resident NSCs over the period of the fate switch. I therefore used RNA in situ hybridization (ISH) to examine the pattern of *Ppp1r14a* and *Dusp9* messenger RNA expression in embryonic mouse spinal cord at E11.5 (pre-fate switch), E12.5 and E13.5 (post-fate switch) (Figures 1 & 2). As a positive control and in order to delineate the pMN domain, I mapped *Olig2* expression by RNA ISH in parallel. *Dusp9*, *Ppp1r14a* and *Olig2* RNA antisense probes were synthesized by reverse strand transcription from cDNA clones in vitro (see *Materials & methods*; data not shown).

1. ***Olig2*** (Figure 1). At E11.5, E12.5 and E13.5, focal signal at the ventral midline identified the clustered *Olig2*+ cells of the pMN domain. At E13.5, isolated *Olig2*+ cells were clearly distinguished outside the ventral pMN domain, consistent with post-fate switch migration of Olig2+ OLPs.

2. ***Ppp1r14a*** (Figure 1). Dynamic expression of *Ppp1r14a* was observed in the spinal cord over the period of the fate switch. At E11.5, elevated *Ppp1r14a* signal was observed in the ventral ventricular zone, including but not restricted to the pMN domain. *Ppp1r14a* expression was also evident at the lateral edges of the dorsal ventricular zone but not in the ventricular zone itself. At E12.5, a similar spatial pattern of *Ppp1r14a* expression was observed, though less pronounced. Finally, at E13.5, elevated *Ppp1r14a* expression was not observed in any region of the spinal cord, including the pMN domain.

3. ***Dusp9*** (Figure 2). In contrast to *Ppp1r14a*, no discernible spatiotemporal pattern of Dusp9 expression was visible within the spinal cord over the period of the fate switch.

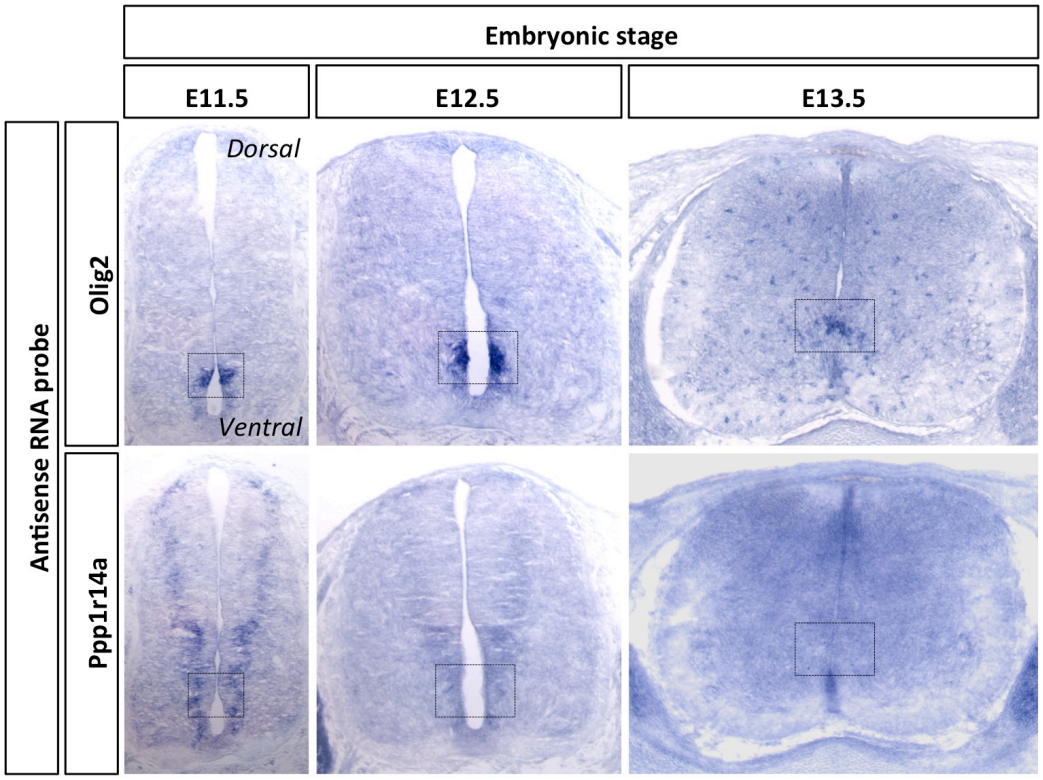

Figure 1. RNA in situ hybridization mapping of *Olig2* and *Ppp1r14a* RNA expression in E11.5, E12.5 and E13.5 spinal cord. Focal *Olig2* signal marks the pMN domain (dashed boxes). At E13.5 scattered *Olig2* signal is consistent with the migratory spread of Olig2+ OLPs.

In order to confirm the specificity of dynamic *Ppp1r14a* expression, I performed additional RNA ISH experiments for PP1 subunits *Ppp1r3g* (regulatory) and *Ppp1ca* (catalytic) (Figure 2). Over E11.5, E12.5 and E13.5, no spatiotemporal pattern of expression was observed for these subunits.

The early expression and subsequent down-regulation of *Ppp1r14a* in the ventral ventricular zone is consistent with a role in the MN-OLP fate switch. To confirm this result and to relate it to the expression of Ppp1r14a protein, I performed immunolabeling on pre- and post-fate switch spinal cords (E10.5 and E13.5 respectively) with anti-Ppp1r14a and anti-Olig2 antibodies (Figure 3). Anti-Olig2 antibody labeled the pMN domain at E10.5 and E13.5 and early migratory OLPs at E13.5. At E10.5, Ppp1r14a protein was expressed in the nuclei of cells

of the ventral ventricular zone, including the Olig2+ cells of the pMN domain. Strikingly, by E13.5, Ppp1r14a was entirely absent from ventricular zone.

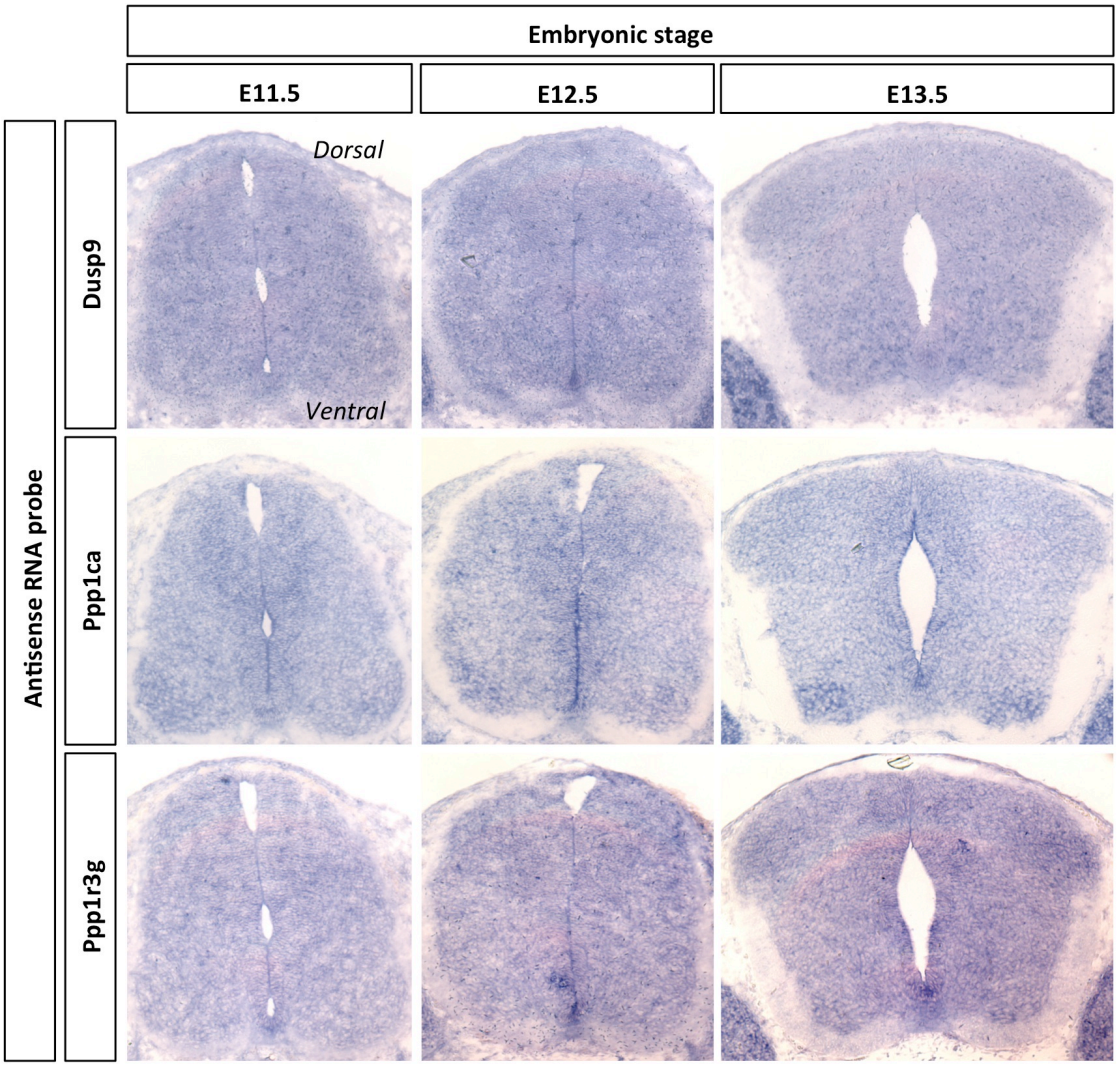

Figure 2. RNA in situ hybridization mapping of Dusp9, Ppp1ca and Ppp1r3g transcript expression in E11.5, E12.5 and E13.5 spinal cord.

These data indicate that down-regulation of nuclear Ppp1r14a might de-repress PP1 and induce Olig2 S147 dephosphorylation and the MN-OLP fate switch. Due to time constraints, I have been unable to follow up these provocative data during my PhD. However, exploring the functional relationship between Ppp1r14a expression and Olig2 S147 phosphorylation is an important task for the future.

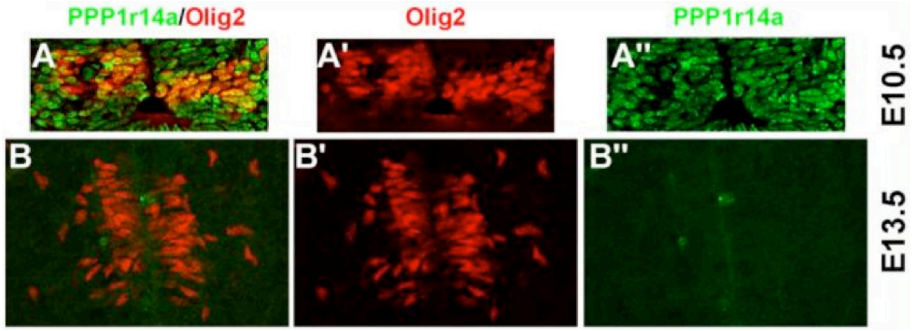

Figure 3. Immunolabeling for Olig2 (red) and Ppp1r14a (green) in the ventral ventricular zone of E10.5 and E13.5 spinal cord.

4.3 DISCUSSION

In pMN domain NSCs, dephosphorylation of Olig2 at S147 triggers the MN-OLP fate switch (Li et al., 2011). At the molecular level, precisely how S147 dephosphorylation modifies Olig2 function and thereby regulates NSC fate choice is only partially understood. Moreover, the extra- and intracellular signaling pathways that mediate phosphorylation and dephosphorylation of Olig2 have not been established. While computational and in vitro analysis suggests that PKA is the kinase responsible for phosphate addition at S147, there is no evidence implicating a specific phosphatase in S147 dephosphorylation.

From a list of phosphatase components displaying significantly altered expression in OLPs versus NSCs, I have identified the Ppp1r14a regulatory subunit of PP1 as a potential regulator of Olig2 S147 dephosphorylation over the period of the MN-OLP fate switch. The initial bioinformatic screen, however, did not exemplify the ideal strategy for constructing the list of candidate phosphatase and phosphatase-related proteins. The approach examined published transcriptome databases from independent microarray analyses and revealed phosphatase components exhibiting differential expression in OLPs and NSCs. In contrast to the stable expression observed by microarray in purified NSC and OLP populations, dephosphorylation of Oig2 at S147 at the onset of oligodendrogenesis might require only the transient expression or repression of the specific phosphatase component; after effective dephosphorylation of Olig2, the expression might return to the pre-OLP level. In this scenario, the Olig2 phospho-regulator would not exhibit the differential expression in NSCs and OLPs required for identification in the computational screen described here. I cannot therefore exclude the possibility that the key regulator of Olig2 S147 dephosphorylation is not among the candidate phosphatase proteins reported here.

I have demonstrated dynamic expression – at both the RNA and protein levels – of Ppp1r14a in pMN domain NSCs over the period of the MN-OLP fate switch. Ppp1r14a was originally identified as an inhibitory subunit of PP1 in smooth muscle (Eto et al., 1997). PP1 is a serine/threonine (S/T) phosphatase and a member of the phosphoprotein phosphatase super-family (Peti et al., 2013). In contrast to protein kinases, the catalytic domains of S/T phosphatases, including PP1, have limited intrinsic specificity. The mammalian genome, for example, encodes only ~40 S/T phosphatases to offset the activity of ~400 S/T kinases (Bollen et al., 2010). The phosphatase activity of the ubiquitously expressed PP1 catalytic core is instead regulated and directed toward specific target substrates via interaction with additional protein subunits – so called PP1 interacting proteins – of which there are more than 200 (Peti et al., 2013). Ppp1r14a is a validated PP1 interacting protein and Ppp1r14a expression has previously been reported in the human and mouse CNS (Li et al., 2001). A detailed understanding of exactly how Ppp1r14a affects PP1 activity in specific cell types has not been fully worked out. In P19 embryonic carcinoma cells, Ppp1r14a was found to be a transcriptional target of Ngn2, a proneural basic HLH TF that is fundamental in MN formation and that can directly interact with Olig2 (Lee et al., 2005; Li et al., 2011). This is consistent with a role for Ppp1r14a in maintaining phosphorylation of Olig2 during the period of motor neuron production.

Here, I show Ppp1r14a protein expression at E11.5 – during MN production – in the nuclei of pMN domain NSCs (Li et al., 2001). After E11.5, Ppp1r14a expression diminished and disappeared completely by E13.5. The systematic down-regulation of nuclear Ppp1r14a in pMN NSCs over the period of the MN-OLP fate switch suggests Ppp1r14a might regulate dephosphorylation of Olig2 S147. In this case, Ppp1r14a/PP1 complex formation would alter PP1 activity and preserve Olig2 S147 phosphorylation. The observed decrease in Ppp1r14a

expression would de-repress PP1, triggering PP1-mediated removal of the phosphate from Olig2 S147 and initiating the MN-OLP fate switch.

Despite the broadly concordant in situ hybridization and immunolabeling results, there is a marked discrepancy in the *Ppp1r14a* RNA and Ppp1r14a protein signals at E11.5 and E10.5, respectively. The robust co-localisation of Ppp1r14a and Olig2 protein in the nuclei of Olig2+ NSCs in the ventricular zone of the E10.5 spinal cord contrasts with the partially non-overlapping RNA expression patterns. The Ppp1r14a protein expression in *Ppp1r14a* RNA-negative territory might represent non-specificity in the anti-Ppp1r14a antibody. In order to validate the specificity of the primary antibody, it will be important to repeat the immunolabeling experiments and conduct the appropriate absorption controls. Western blot analysis of E10.5 and E11.5 spinal cord lysates will also enable confirmation of the antibody specificity for an antigen migrating at the predicted molecular weight of Ppp1r14a. In addition to issues of antibody non-specificity, the differing *Ppp1r14a* RNA and Ppp1r14a protein expression patterns might reflect local translation – and therefore sequestration – of the *Ppp1r14a* messenger RNA in a discrete intracellular region away from the Ppp1r14a+ nucleus. Ultimately, however, the lack of age-matched specimens in these in situ hybridization (performed at E11.5) and the immunolabeling (performed at E10.5) experiments, confounds the integration of the different results.

In ordr to confirm an in vivo role for the Ppp1r14a subunit of PP1, it is necessary to examine the effect of conditionally deleting this subunit in Olig2-expressing NSCs. I have submitted a request to the European Mammalian Mutant Cell Repository (www.eummcr.org/) for generation of the *Ppp1r14a* conditional knockout stem cell line (*Ppp1r14a*$^{fl/fl}$). *Ppp1r14a*$^{fl/fl}$ stem cells will enable generation of *Ppp1r14a*$^{fl/fl}$ mice. Using the Olig2-Cre mouse line, analysis of *Olig2-Cre;Ppp1r14a*$^{fl/fl}$ double-transgenic mice will determine the requirement of

Ppp1r14a for Olig2 S147 phosphorylation and MN production from pMN NSCs (Schuller et al., 2008). In these animals, Cre recombinase expression driven from the Olig2 promoter would selectively eliminate *Ppp1r14a* in pMN NSCs in the spinal cord. The phosphorylation state of Olig2 S147 could be determined by spinal Olig2 IP and WB using our phospho-S147-specific antibody, and the timing of the MN-OLP fate switch by immunolabeling for MN and OL lineage markers (Li et al., 2011). If down-regulation of Ppp1r14a activates PP1 and thereby triggers S147 dephosphorylation in wild-type mice, genetic deletion of *Ppp1r14a* would be expected to induce premature dephosphorylation of Olig2 and hence premature OLP formation.

Summary

Research into the upstream pathways and intracellular components mediating Olig2 dephosphorylation at the time of the MN-OLP fate switch will provide valuable insight into the regulation of spinal MN and OLP development. On the basis of its dynamic nuclear expression in pMN cells over the period of the MN-OLP fate switch, I have identified the inhibitory Ppp1r14a subunit of PP1 as a potential regulator of Olig2 S147 phosphorylation. Further work is required to test the involvement of Ppp1r14a in regulating Olig2 phosphorylation in vivo. In addition to identifying the phosphatase, it will be fundamental to explore the signals and molecular mechanisms governing phosphatase expression/activation. Gaining a detailed understanding of OLP specification will contribute to the design of OLP production methods for efficient cell replacement therapies and in vitro drug screens aimed at identifying modulators of OL development.

CHAPTER 5

OLIG2 S147 PHOSPHORYLATION & GENE TARGET CHOICE

5.1 INTRODUCTION

Basic HLH transcription factor Olig2 is expressed throughout the development of the OL lineage and has been described as a master regulator of OLP specification and differentiation (Rowitch, 2004; Li & Richardson, 2008; Meijer et al., 2012). In the pMN domain of the embryonic spinal cord, Olig2 is also expressed in multipotent NSCs over the periods of motor neuron specification and subsequent OLP specification. *Olig2* knockout results in complete failure to generate spinal cord MNs and OL lineage cells and highlights the critical importance of Olig2 for production of pMN-derived MNs and OLs (Lu et al., 2002; Park et al., 2002; Zhou et al., 2002). Research exploring the role of Olig2 in the generation of both neuronal and glial cell types revealed that dynamic Olig2 phosphorylation is a critical regulator of stem cell fate (Li et al., 2011). During MN specification, Olig2 is phosphorylated at serine 147 within the HLH domain, while S147 dephosphorylation – modeled by phospho-null Olig2 S147A mutation – abolishes MN production without preventing OLP production. Li et al. (2011) conclude that dephosphorylation of Olig2 at S147 triggers the MN-OLP fate switch.

Examining the molecular mechanisms underlying Olig2 S147 phosphorylation-dependent control of stem cell fate, Li et al. (2011) identified significant differences in the cofactor binding properties of wild-type and S147A mutant Olig2. Compared to wild-type Olig2, the Olig2-S147A mutant shows: 1. a severely reduced ability to form Olig2:Olig2 homodimers; 2. an increased affinity for the pan-neuronal bHLH TF Ngn2. The results demonstrated that

S147A mutation seriously influences Olig2 cofactor choice without grossly affecting protein structure or stability. Taken together, the data indicate that during the initial neurogenic phase, phospho-S147 Olig2 homodimers regulate expression of MN lineage genes and repression of OL lineage genes. Dephosphorylation of Olig2 at S147 induces homodimer dissociation and formation of heterodimers, abruptly silencing the genetic programme of MN specification and activating an OL genetic programme.

In addition to Olig2 cofactor preference, the position of S147 within the DNA-binding basic HLH domain suggests that Olig2 S147 dephosphorylation might affect gene target specificity, although this has not been investigated as yet. In this case, phosphorylation-specific association with MN/OL lineage gene regulatory sequences would, in concert with dynamic protein-complex formation, coordinate different developmental programmes of gene expression. In support of this hypothesis, genome-wide mapping of Olig2 gene targets in OLPs and mature OLs revealed occupancy of stage-specific binding sites at later stages of OL differentiation (Yu et al., 2013). Alternatively, Olig2 S147 dephosphorylation might regulate recruitment of specific co-factors to the same set of Olig2 gene targets. Analysis of the amino-terminal S10/13/14 phosphorylation of Olig2 using triple phospho-null or phospho-mimetic Olig2 variants indicated that S10/13/14 phosphorylation regulates gene transcription and neural progenitor proliferation but has no major impact on target E-box recognition (Meijer et al., 2014). In order to better understand how Olig2 S147 phosphorylation regulates neuronal versus glial cell fate decisions in the pMN domain of the developing spinal cord, I planned to identify the genomic binding sites of Olig2 in NSCs by chromatin immunoprecipitation-sequencing (ChIP-seq) and to determine if S147 phosphorylation affects gene target specificity.

5.2 RESULTS

Derivation and characterization of NSC cultures

A diagram illustrating the ChIP-seq workflow is shown in Figure 1.

To obtain DNA for Illumina sequencing, I used primary adherent NSC cultures derived from the dissociated cortices of E13.5 mice (Figure 2A) (Pollard et al., 2006). For identification of phospho-S147 Olig2 gene targets, NSCs were isolated from *Olig2*$^{+/-}$ (Olig2-WT) embryos. In parallel, to identify the gene targets of dephosphorylated Olig2, NSCs were isolated from *Olig2*$^{-/-}$;*Olig2*^{S147A} (Olig2-S147A) phospho-null mutant embryos (Li et al., 2011). As a control for background ChIP enrichment, NSC cultures were also derived from *Olig2*$^{-/-}$ (Olig2-null mutant) embryos (Li et al., 2011). NSCs were cultured over multiple passages in a chemically defined medium containing FGF-2 and EGF (NSC medium).

I initially characterized my primary NSC cultures by immunolabeling for expression of a range of protein markers (Figure 2). Olig2-WT, Olig2-S147A and Olig2-null cells all expressed the filamentous stem cell marker Nestin. Olig2-WT and Olig2-S147A phospho-null cells uniformly expressed Olig2, which was as expected entirely absent from Olig2-null cultures. Finally, to observe spontaneous neural differentiation along OL, astrocyte or neuronal lineages, I labeled my NSC cultures with antibodies against Sox10, GFAP and Tuj1, respectively. No Sox10+ cells were identified in any of the Olig2-WT, Olig2-S147A and Olig2-null cultures, while Tuj1+ and GFAP+ cells were observed in extremely limited numbers (<1%), indicating negligible NSC differentiation in NSC medium.

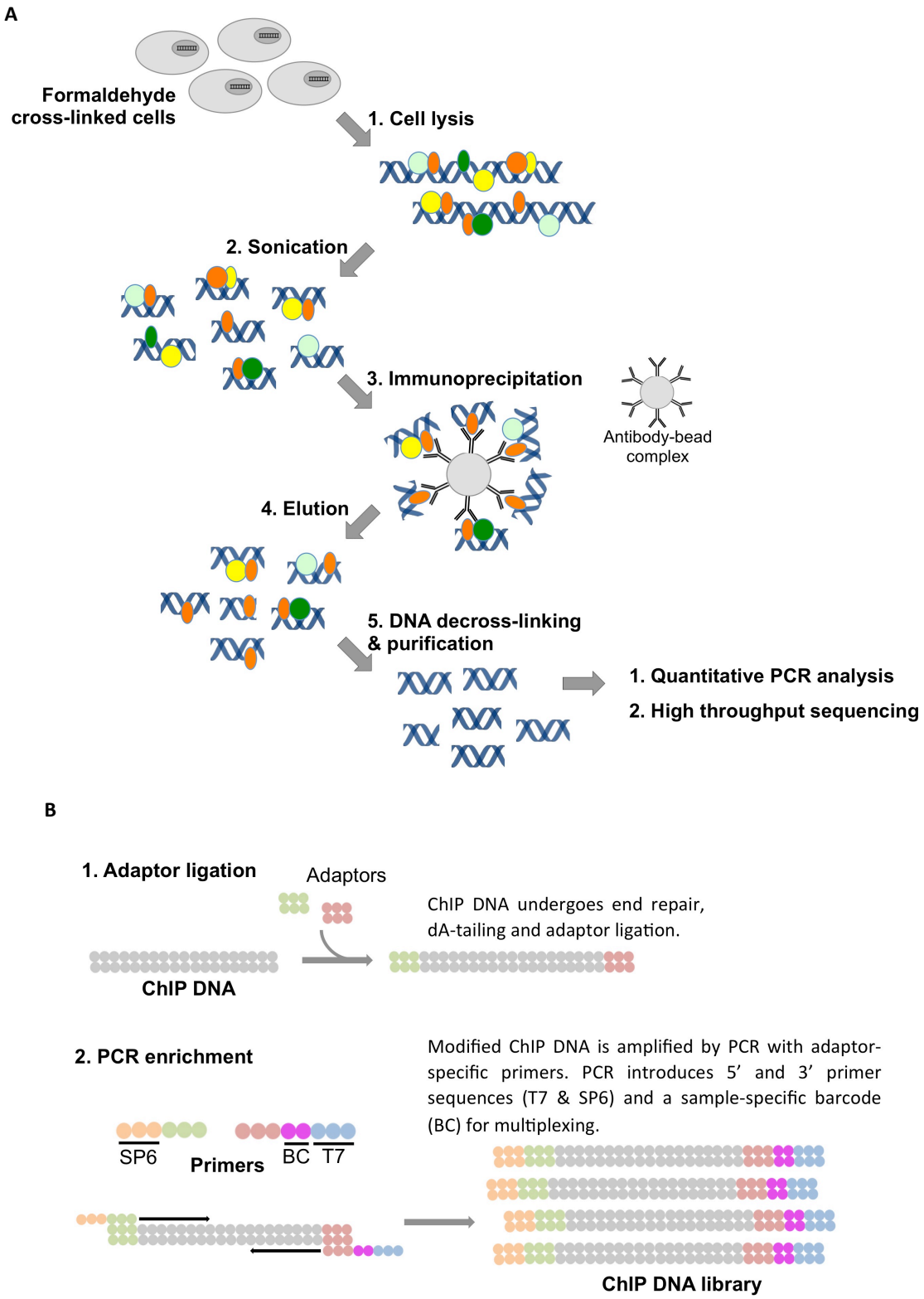

Figure 1. ChIP-seq workflow. A. Chromatin immunoprecipitation. 1. Formaldeyde-treated cells are lysed. 2. Crosslinked chromatin is sheared by sonication to generate 200-1000 bp fragments. 3. Target protein-bound DNA fragments are immunoprecipitated using a protein-specific antibody. 4-5. Immunoprecipitated DNA is eluted and purified for subsequent PCR and/or sequencing analysis. **B-D.** Sequencing workflow for ChIP purified DNA fragments. **B.** Library generation. 5' and 3' adaptors are ligated to DNA fragments. A ChIP DNA library is synthesized by PCR amplification using adaptor-specific primers, incorporating terminal SP6 and T7 promoter sequences and a unique barcode (BC) sequence for multiplexing. *(Continued overleaf.)*

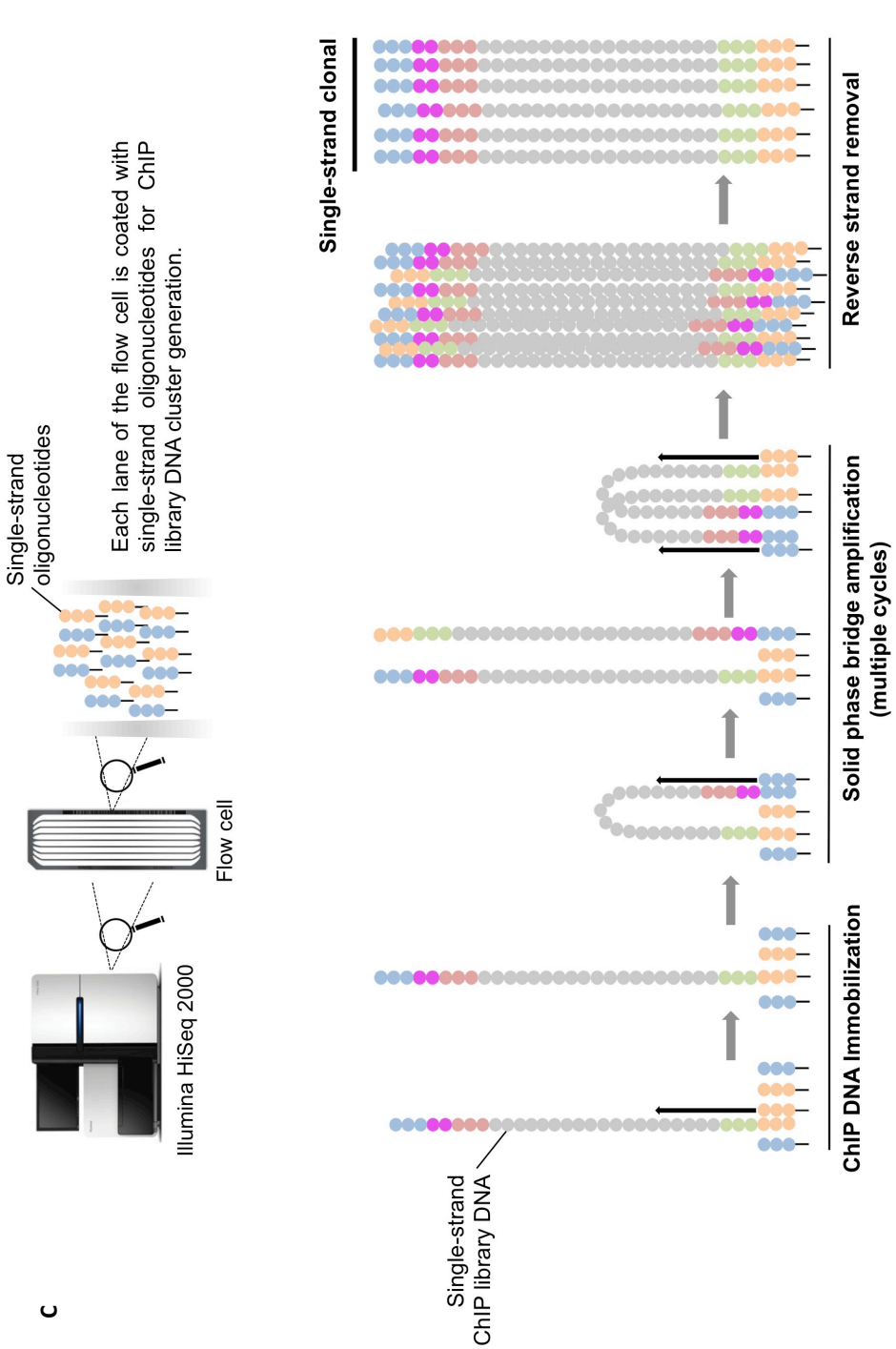

Figure 1 cont'd. C. Single-strand clonal cluster generation. Single-stranded library DNA is hybridized to the surface of the flow cell via a complementary oligonucleotide. An immobilized complement of the annealed fragment is generated by PCR. The original template is cleared and the remaining immobilized strands clonally amplified by bridge amplification. Reverse strands are cleaved and removed, generating clonal clusters of forward strand DNA tethered to the surface of the flow cell. *(Continued overleaf)*

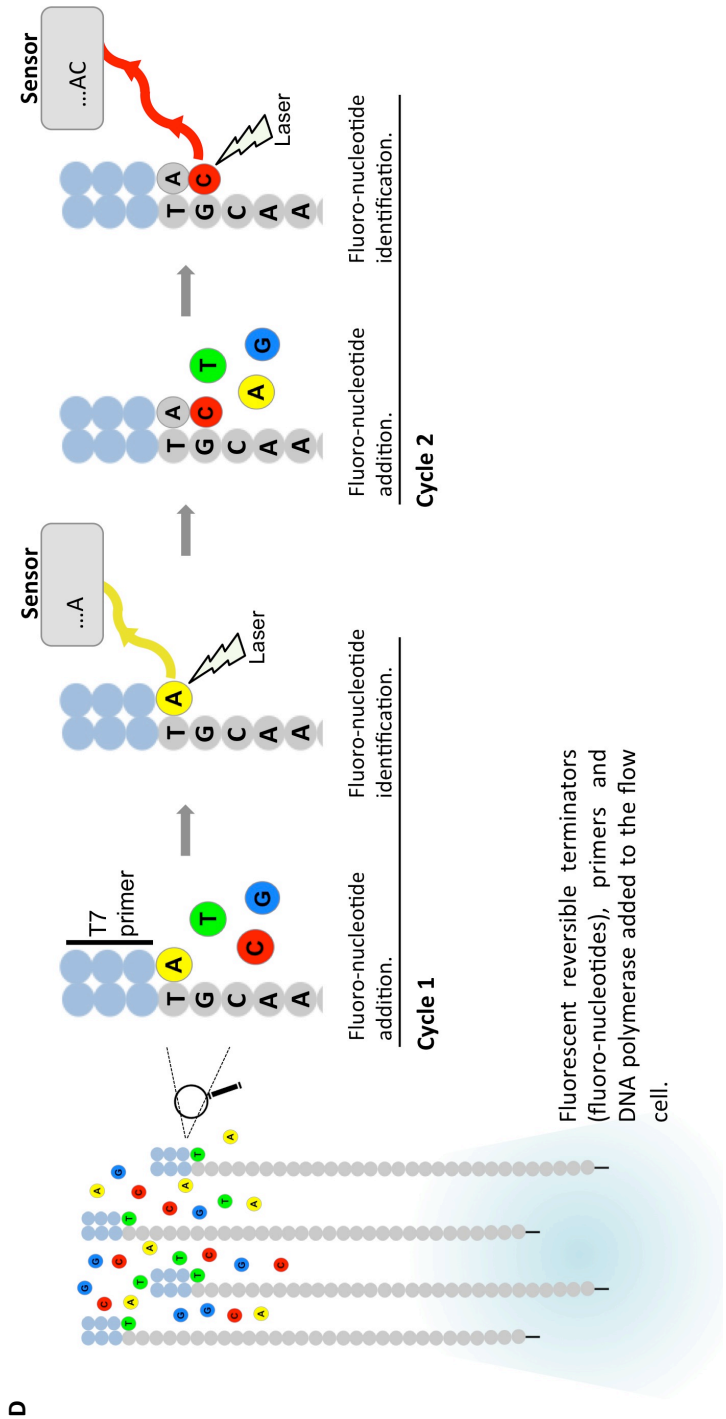

Figure 1 cont'd. D. Illumina sequencing. The T7 sequencing primer anneals to single-strand clonal cluster DNA. Primer extension occurs with differently fluorescently tagged nucleotides. Cycle by cycle the DNA fragment sequence is determined by incorporation, excitation and detection of the nucleotide-specific fluorophore at each clonal cluster. After each cycle, the fluorophore is cleaved and removed to enable clear identification of the subsequent nucleotide.

Olig2 expression in Olig2-WT and Olig2-S147A mutant NSC cultures was further examined at the RNA level by quantitative reverse transcription-PCR (qRT-PCR) and at the protein level by whole-lysate SDS-PAGE and western blot (WB) analysis (Figure 3A-B). Quantitative RT-PCR revealed that the abundance of *Olig2* mRNA – relative to housekeeping gene *GAPDH* mRNA – in Olig2-WT and Olig2-S147A NSCs is comparable. SDS-PAGE and WB analysis using a rabbit anti-Olig2 antibody showed similar levels of expression of WT and mutant Olig2 protein – relative to the loading control B-Tubulin-E7 – in the Olig2-WT and Olig2-S147A cultures. Together the results confirmed that WT Olig2-expressing, phospho-null mutant Olig2-S147A-expressing and Olig2-null NSC cultures were suitable for Olig2 ChIP.

It was clearly important to establish that Olig2 was phosphorylated at S147 in Olig2-WT NSC cultures. In order to observe phosphorylation of WT Olig2 at S147 I immunoprecipitated Olig2 from the total lysates of Olig2-WT and Olig2-S147A cultures, and visualized the immunoprecipitates by PAGE and WB using both a rabbit anti-Olig2 antibody and a custom-made rabbit antibody that specifically recognizes the S147-phosphorylated form of Olig2 (anti-ph-S147 Olig2). Quantitative ELISA analysis, first published by Li et al. (2011), demonstrated the specificity of the anti-ph-S147 Olig2 antibody for Olig2 phosphorylated at S147 (Figure 3C). Olig2 was clearly visible in both Olig2-WT and Olig2-S147A NSC immunoprecipitates (Figure 3D). WT Olig2 was observed as two distinct bands, a major upper band and a weaker lower band. The major band overlapped precisely with the phospho-S147-Olig2 signal observed with the anti-ph-S147 Olig2 antibody, and migrated with an apparently higher molecular weight compared to the single Olig2-S147A band, consistent with the presence of a negatively charged phosphate group on S147 (Winkler et al., 1993). The lower WT band aligned with Olig2-S147A, indicating that it comprises dephospho-S147 Olig2 and suggesting that dephosphorylated Olig2 was present at low levels in Olig2-WT NSC cultures. Overall, the data indicated that WT Olig2 was typically phosphorylated at S147 in

Olig2-WT NSCs, and that ChIP from Olig2-WT and Olig2-S147A mutant NSC cultures would therefore provide suitable material for comparison of the gene targets of phosphorylated and dephosphorylated Olig2.

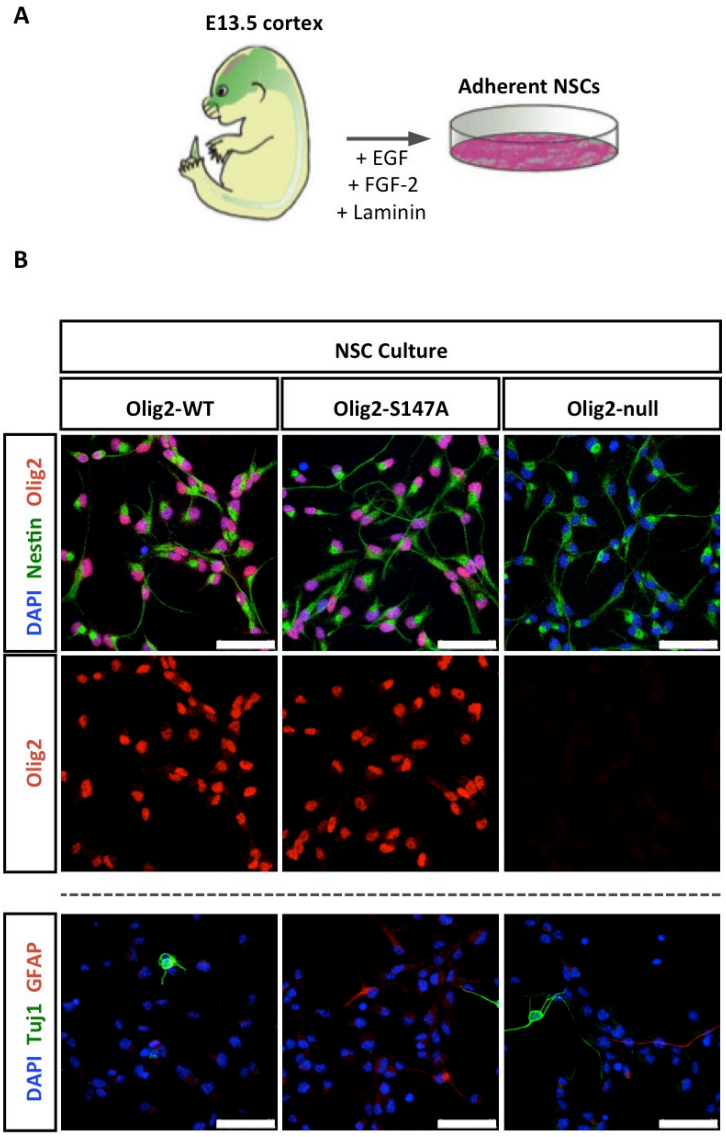

Figure 2. Primary adherent embryonic NSC cultures. A. NSCs were derived from the dissociated cortices of E13.5 mice and cultured in medium containing EGF, FGF-2 and Laminin. **B.** Immunostaining of Olig2-WT, Olig2-S147A and Olig2-null NSC cultures using antibodies labeling Olig2, Nestin, Tuj1 and GFAP.

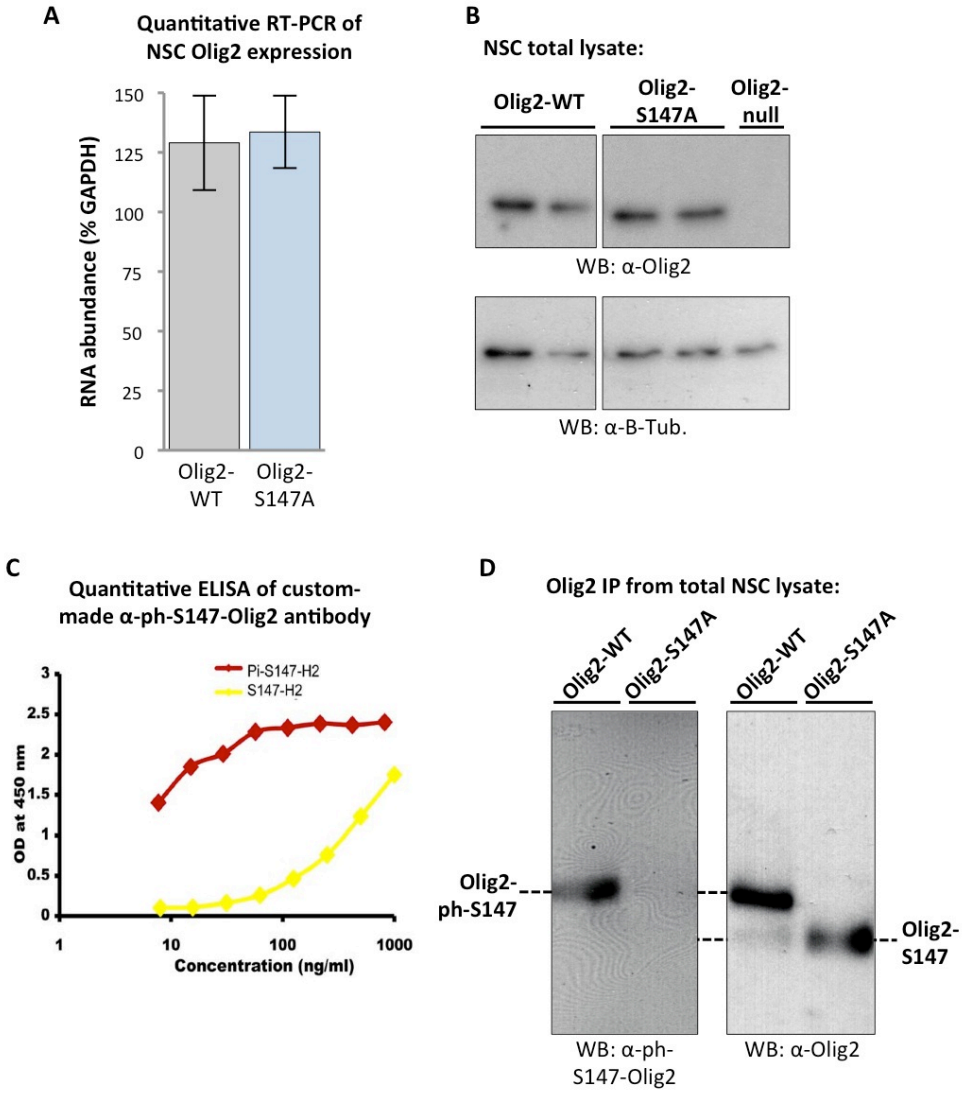

Figure 3. Olig2 expression and S147 phosphorylation in NSC cultures. A. Quantitative RT-PCR analysis of Olig2 mRNA expression in Olig2-WT and Olig2-S147A NSC cultures. **B.** Western blot analysis of Olig2 protein abundance in Olig2-WT, Olig2-S147A and Olig2-null NSC culture total lysates using anti-Olig2 and anti-B-Tubulin E7 antibodies. **C.** Quantitative ELISA analysis of phosphorylated and dephosphorylated Olig2 S147 peptide recognition by the custom-made anti-ph-S147-Olig2 antibody (Li et al., 2011). **D.** Olig2 immunoprecipitation from Olig2-WT and Olig2-S147A NSC cultures and WB analysis using anti-ph-S147-Olig2 and anti-Olig2 antibodies.

Sonication and preliminary ChIP analysis

Chromatin IP extraction of specific protein-bound DNA fragments initially requires formaldehyde-mediated DNA-protein crosslinking and the sonication of crosslinked genomic DNA into 200-1000 bp fragments (Figure 1A). The sonication conditions required to generate ChIP-suitable samples vary depending on the cell type and the formaldehyde crosslinking conditions. Under-sonication will compromise specificity and effective immunoprecipitation, while over-sonication can lead to protein denaturation and degradation. To establish the optimum parameters, I sonicated formaldehyde-treated Olig2-WT cells over 10, 20, 30, 40 or 50 sonication cycles and analysed the degree of genomic fragmentation by de-crosslinking and agarose gel electrophoresis (Figure 5A). In the absence of sonication, crosslinked genomic DNA displayed negligible gel mobility (data not shown). Sonication over 10 cycles primarily produced fragments in the 200-600 bp range, with additional cycles generating shorter fragments tending to an observed lower limit of 100-200 bp. The predicted minimum fragment size is 147 bp, the length of one nucleosome DNA wrap. These results indicated a 10-cycle sonication strategy is suitable for ChIP from NSCs.

I performed preliminary Olig2 ChIP followed by quantitative PCR (ChIP-qPCR) analysis from Olig2-WT, Olig2-S147A and Olig2-null NSC cultures (Figure 4A). Recovery of candidate Olig2 target DNA sequences was quantified as a percentage of input material by qPCR using target-specific primer pairs. Olig2 occupancy was determined by enrichment versus the Olig2-null negative control. Enrichment of a known Olig2 E-box target site – within the conserved *U2 enhancer* in the distal 5' flank of the OL lineage gene *Sox10* – from the Olig2-WT ChIP confirmed phospho-S147 Olig2 binding at the *Sox10* regulatory sequence and validated my ChIP protocol (Kuspert et al., 2011). In addition, I analysed Olig2 occupancy of E-box sites in the *PDGFRA*, *Olig1* and *Hb9* genes (Figure 4A) (Lee et al., 2005). The results demonstrated

Olig2-WT occupancy at the *PDGFRA* and *Olig1* binding sites, but not at the *Hb9* gene, which showed no significant enrichment relative to the Olig2-null control. The *PDGFRA* and *Olig1* gene E-boxes were therefore identified as novel and bona-fide phospho-S147 Olig2 binding sites. In contrast to the phospho-S147 Olig2-WT, Olig2-S147A ChIP-qPCR revealed that the phospho-null Olig2-S147A mutant does not target any of the *Sox10*, *PDGFRA*, *Olig1* or *Hb9* regulatory regions examined, suggesting that the *Sox10*, *PDGFRA* and *Olig1* (all known OL lineage genes) are phospho-S147-specific Olig2 binding sites.

To determine whether occupancy of Olig2 at the *Sox10*, *PDGFRA* and *Olig1* binding sites is associated with altered gene expression, I analysed target gene transcription by quantitative RT-PCR from Olig2-WT and Olig2-S147A phospho-null total RNA extracts. Relative to housekeeping gene *GAPDH*, *Sox10*, *PDGFRA* and *Olig1* mRNA levels were insignificant (≤5% GAPDH mRNA abundance) in both Olig2-WT and Olig2-S147A mutant NSC cultures (Figure 4B). These observations were supported by the results of immunolabeling for Olig2 target gene protein expression. Sox10, PDGFRA or Olig1 proteins were not detected in either Olig2-WT or Olig2-S147A NSCs, indicating that changes in Olig2 binding at these OL lineage gene targets is not sufficient to activate transcription (Figure 4C).

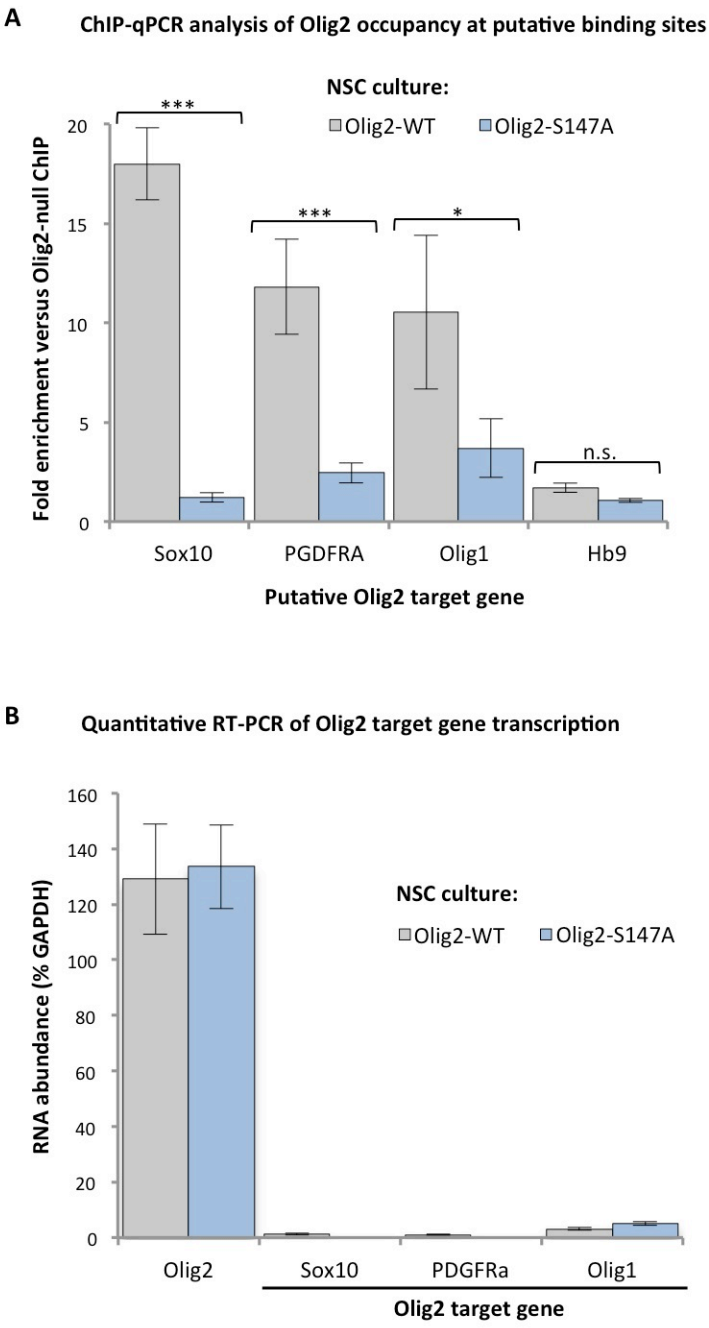

Figure 4. Preliminary Olig2 ChIP qPCR analysis. A. ChIP qPCR analysis of Olig2 occupancy at putative binding sites. Olig2 occupancy of specific putative binding sites in the *Sox10*, *PDGFRA*, *Olig1* and *Hb9* genes was determined by fragment enrichment in Olig2-WT/-S147A ChIP samples relative to the Olig2-null control. Fragment enrichment was quantified by qPCR using putative binding site-specific primer pairs. **B.** Olig2 and Olig2 target gene expression in Olig2-WT and Olig2-S147A NSC cultures analysed at the RNA level by quantitative RT-PCR. *(Continued overleaf)*

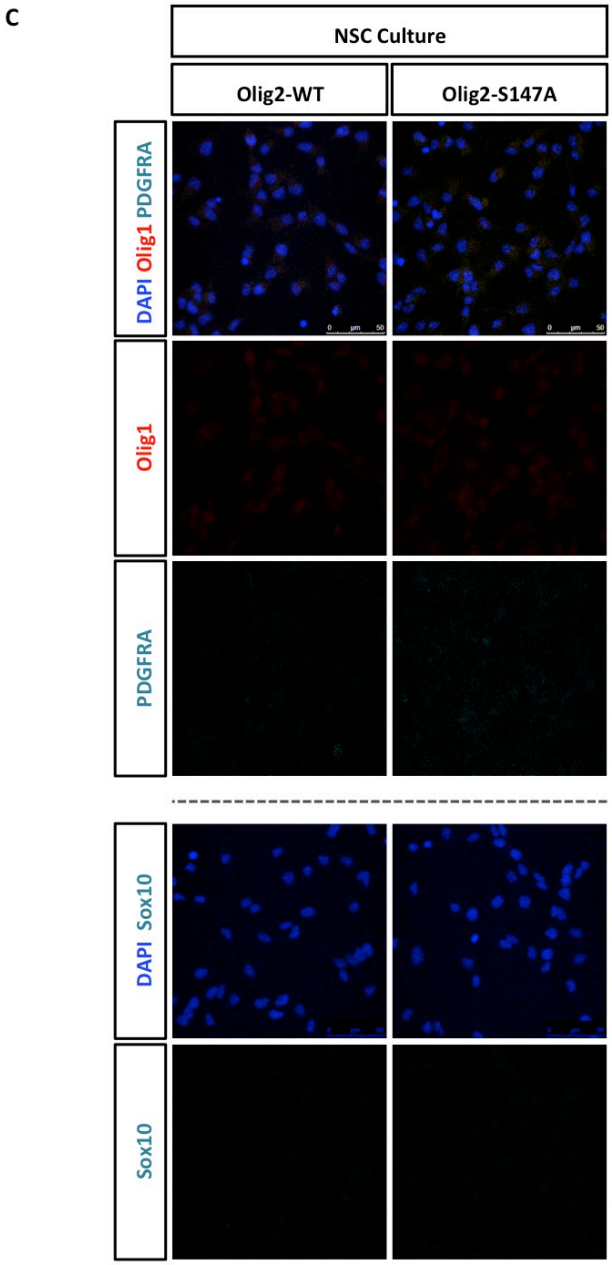

Figure 4 cont'd. C. Olig2 target gene expression in Olig2-WT and Olig2-S147A NSC cultures analysed at the protein level by immunostaining with target-specific antibodies.

ChIP optimization

In order to identify the full repertoire of phospho-S147 Olig2 and Olig2-S147A gene targets, I planned to submit Olig2 ChIP DNA samples purified from Olig2-WT, Olig2-S147A mutant and Olig2-null cultures for high-throughput Illumina sequencing (Figure 1). Illumina sequencing requires library preparation from 25 ng of purified ChIP DNA at a minimum concentration of 1 ng/µl (Source Bioscience, pers comm). The preliminary ChIP extractions did not recover sufficient DNA for library preparation (data not shown). To optimize the protocol for Olig2 immunoprecipitation (IP) – a key stage in the Olig2 ChIP protocol – I conducted parallel Olig2 IPs from cultured Olig2-expressing P19 cells with varying concentrations of two rabbit anti-Olig2 antibodies and protein A-conjugated agarose beads (Figure 5C). In these optimization experiments, an increase in the recovery of Olig2 protein – assessed by WB with a goat anti-Olig2 antibody – demonstrates an improvement in the Olig2 IP; a direct measure of ChIP DNA purification by parallel ChIP-qPCR from Olig2-expressing P19 cells was not obtained. The anti-Olig2 antibodies used were: 1. a commercially available Millipore polyclonal antibody; 2. a custom-made polyclonal antibody developed and generously provided by Charles D. Stiles (Ligon et al., 2004). The use of multiple primary antibodies in tandem is an uncommon strategy for improving the IP recovery of a target protein. In this case, however, the published Millipore and Stiles anti-Olig2 antibodies were raised against different epitopes within Olig2 and might, I reasoned, synergistically improve the recovery of Olig2. It should be noted that in the absence of parallel IPs performed using the Olig2 antibodies individually as well as in combination, the effectiveness of this strategy remains to be validated.

The comparable recovery of Olig2 from IPs 1, 3 and 6 (Figure 5C) – in which antibody concentration remained unchanged but protein A bead concentration was altered – indicated that increasing the concentration of protein A-conjugated agarose beads did not

substantially affect the recovery of Olig2 protein. In contrast, however, comparison of IPs 3, 4 and 5 (Figure 5C) – increasing antibody concentration with constant bead volume – indicated that Olig2 extraction improved significantly with increasing antibody concentration. The WB indicated that maximal recovery of Olig2 was achieved using 10 µg/ml Millipore plus 1 µl/ml Stiles anti-Olig2 antibodies and 50 µl/ml protein-A beads. It should be noted that although further improvements in Olig2 recovery might have been possible with additional increases in antibody concentration, considerations of cost and reagent supply made this impractical.

In addition to the optimization described above, I analysed the effect on immunoprecipitation of Olig2 of two alternative incubation protocols. Protocol 1 (Figure 5C, IP 2) included 3 hours of antibody-only incubation followed by overnight antibody-plus-bead incubation. In Protocol 2 (Figure 5C, IP 3), overnight antibody-only incubation was followed by 3 hours of antibody-plus-bead incubation. The modest difference in Olig2 recovery between the different protocols suggested Protocol 1 was more effective.

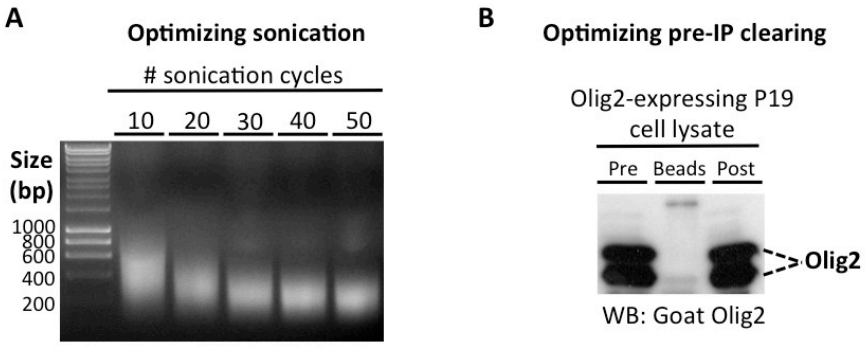

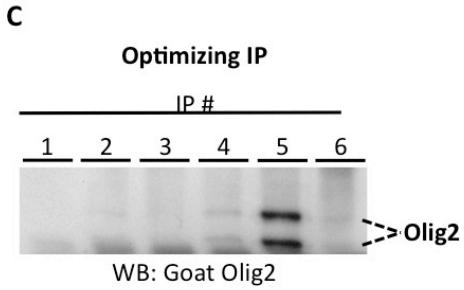

IP conditions

IP #	Ab. 1 (ul)	Ab. 2 (ul)	G-beads (ul)
1	2	0.25	25
* **2**	2	0.25	50
• **3**	2	0.25	50
4	5	0.50	50
5	10	1.00	50
6	2	0.25	100

Ab. 1 = Millipore Ab. 2 = Stiles
* Protocol 1 • Protocol 2

Figure 5. Olig2 ChIP optimization. A. Optimizing sonication. Crosslinked Olig2-WT NSC culture lysate was sonicated over 10, 20, 30, 40 or 50 rounds (30 s on, 30 s off) and chromatin fragmentation assessed by agarose gel electrophoresis. **B.** Optimizing pre-IP clearing. WB analysis of Olig2 protein level in Olig2-expressing P19 cell lysate before (Pre) and after (Post) clearing with protein-A-conjugated agarose beads. **C.** IP optimization. WB analysis of Olig2 protein recovery after Olig2 IP from P19 cells under a range of conditions, including variable antibody and protein-A bead concentrations. Protocol 1: 3 hr antibody-only incubation followed by overnight antibody-plus-bead incubation. Protocol 2: overnight antibody-only incubation followed by 3 hr antibody-plus-bead incubation. (For more details regarding the different protocols, please see *Materials & methods*.)

The preliminary ChIP protocol included a preparatory 'clearing' step for removal of non-specific bead-binding proteins from the input lysate. There remained a possibility, however, that non-specific pull-down of Olig2 during the clearing phase might deplete the input level of Olig2 and result in diminished recovery of Olig2-bound DNA fragments. Finally, I examined the impact of clearing with protein A-conjugated agarose beads on the input level of Olig2 (Figure 5B). Crucially, I did not observe Olig2 in the protein eluate of the clearing beads (Figure 5B, Beads) and I observed similar levels of Olig2 in the input lysate before and after clearing (Figure 5B, Pre/Post). This indicated that Olig2 did not bind protein A-conjugated agarose beads and clearing had no discernible impact on input levels of Olig2. The clearing step was therefore included in subsequent ChIP protocols.

ChIP-seq analysis

Under the optimized sonication and ChIP conditions, Olig2-bound DNA fragments were purified from three Olig2-WT NSC cultures, two Olig2-S147A NSC cultures and a single Olig2-null NSC culture (Figure 6A). The sample concentration of ChIP-purified DNA was quantified using the high sensitivity Qubit Assay (Figure 6B). For all six samples, quantification indicated that sufficient DNA had been isolated for library construction. The six ChIP DNA samples – three Olig2-WT, two phospho-null and one Olig2-null – along with a single pre-ChIP input sample (from wild-type NSCs) were submitted to Source Bioscience for library preparation and multiplexed single-end Illumina HiSeq sequencing.

At Source Bioscience, ChIP DNA libraries were prepared using the standard protocol: end repair and adaptor ligation followed by PCR amplification. Library construction was validated using an Agilent Bioanalyzer. Agilent Bioanalyzer analysis (Figure 6C) indicated successful library generation with an average fragment length of 622 bp. The libraries were pooled and

sequenced in a 100 bp Single End Illumina HiSeq run. Sequencing generated approximately 20 million reads for each of the ChIP DNA samples and 30 million reads for the WT input DNA sample. The raw sequencing data were analyzed at Source Bioscience. The Olig2-WT ChIP sequencing data were analysed in silico as a biological triplicate and the phospho-null Olig2-S147A ChIP samples as a biological duplicate. The bioinformatics analysis included: read mapping to the mouse reference genome (Mm10), peak calling and annotation, differential peak detection for Olig2-WT versus Olig2-S147A sequence enrichment, peak sequence extraction and motif discovery, and gene ontology. For stringency, both the WT Input and Olig2-null ChIP sequencing results were used for background subtraction. As an example, a visualization of the ChIP-seq data mapping to the *Olig1* gene locus is shown in Figure 7A. The pile-up of Olig2-WT ChIP sequence reads mapping to ~3 kb upstream of the *Olig1* open reading frame (ORF), which was absent in both the Olig2-S147A and Olig2-null samples, identified a unique Olig2-WT binding site close to the *Olig1* gene locus.

A

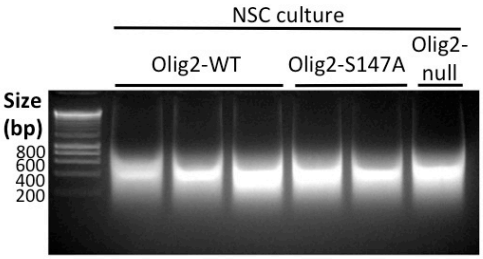

B

ChIP sample	Conc. (µg/ml)
Olig2-WT	4.27
Olig2-WT	3.40
Olig2-WT	4.23
Olig2-S147A	3.83
Olig2-S147A	2.53
Olig2-null	4.16
Input	25.7

C

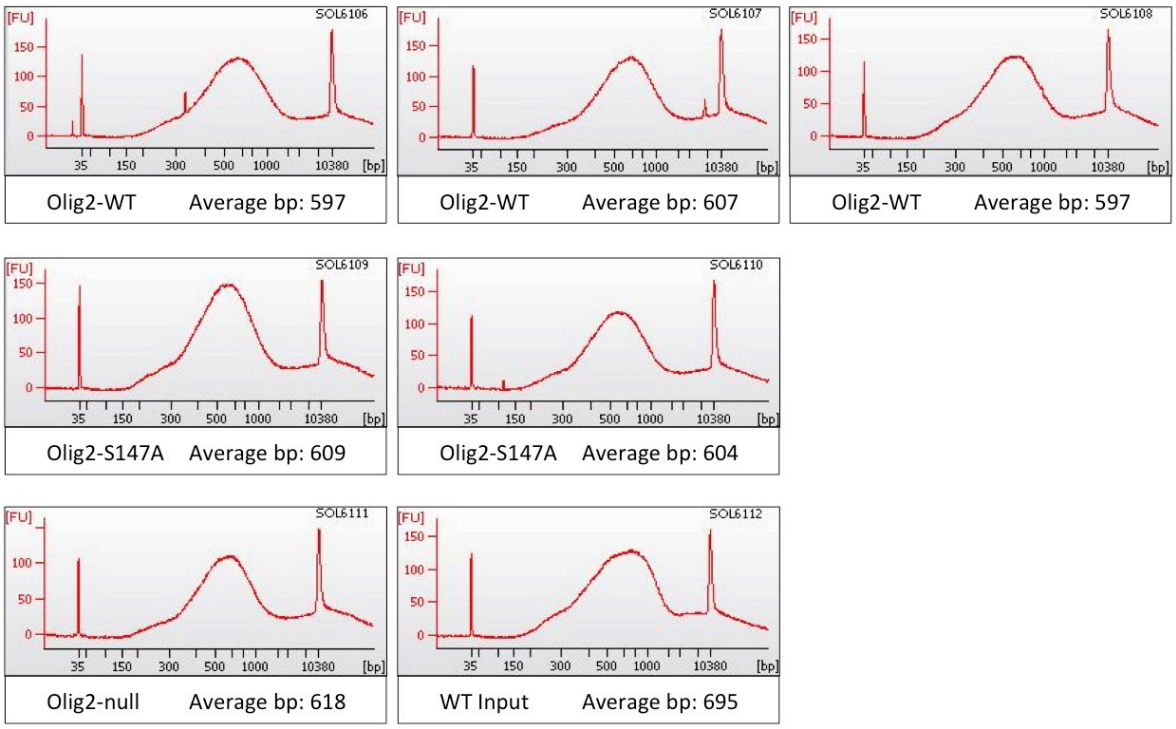

Figure 6. Olig2 ChIP and library construction. A. Chromatin sonication. The cross-linked lysate of three Olig2-WT, two Olig2-S147A and a single Olig2-null NSC cultures underwent sonication to yield 200-600 bp fragments. **B.** ChIP sample concentration. DNA concentration in the six purified ChIP samples and a single input sample was quantified for Library preparation using a high sensitivity Qubit assay. **C.** Agilent Bioanalyzer plots of the seven DNA libraries generated (see Figure 1) from the six ChIP and single input DNA samples.

Bioinformatic analysis of the ChIP-seq data identified 861 discrete WT Olig2 binding sites and 175 mutant Olig2-S147A binding sites (Figure 7B). Of these binding sites, annotation mapped 560 Olig2-WT binding sites and 34 Olig2-S147A binding sites to a nearby or overlapping genetic feature. Interestingly, Olig2-WT and phospho-null Olig2-S147A shared no common binding sites, indicating phospho-S147-Olig2 and Olig2-S147A target completely independent sets of gene targets.

To understand the functional profile of the genes associated with the WT phospho-S147 Olig2-WT and Olig2-S147A binding sites identified in the ChIP-seq analysis, I requested Source Bioscience perform gene ontology (GO) analysis (Figure 7C). The GO project describes genes in terms of the normal biological processes, cellular components and molecular functions with which the gene products are associated. GO analysis therefore identifies the GO terms (for example, 'mitotic cell cycle' or 'histone deacetylase complex') over-represented in a gene set; over-representation is determined based on the probability that a GO term would be observed by chance given the size of the dataset (total number of genes) and the frequency of the GO term within the genome.

In the Olig2-WT dataset, GO analysis displayed a statistically significant ($p < 0.05$) enrichment of genes involved in the following biological processes, cellular components and molecular functions (shown along with the corresponding GO term identifier):

Biological processes:
1. Nervous system development (GO:0007399)
2. Activation of neurological system process (GO:0031646)
3. Activation of nerve impulse transmission (GO:0051971)

Cellular components:
1. Cell projection (GO:0042995)
2. Cell junction (GO:0030054)

Molecular functions:
1. Phospholipid binding (GO:0005543)
2. GTPase regulator activity (GO:0030695)
3. Nucleoside-triphosphatase regulator activity (GO:0060589)
4. Neurotransmitter:sodium symporter activity (GO:0005328)
5. Lipid binding (GO:0008289)

6. Solute:sodium symporter activity (GO:0015370)
7. Actin binding (GO:0003779)
8. Neurotransmitter transporter activity (GO:0005326)
9. Cytoskeletal protein binding (GO:0008092)
10. Organic acid:sodium symporter activity (GO:0005343)
11. Guanyl-nucleotide exchange factor activity (GO:0005085)

The enrichment of nervous system development genes is consistent with the established functions of Olig2. More broadly, the biological processes and cellular components highlighted in the GO analysis are prominent during the later stages of neural differentiation and not in multipotent NSCs.

In conjunction with the GO analysis, basic empirical analysis identified a number of known OL lineage genes in the WT Olig2 ChIP-seq dataset, including *Olig1*. For the *Olig1* gene, two Olig2 binding sites were identified upstream of the open reading frame (ORF), the first at a distance of ~3 kb (Figure 7A) and the second at ~7 kb. Importantly, the more proximal Olig2 binding site identified by ChIP-seq overlapped precisely with the binding site that I initially identified by ChIP-qPCR (see *Sonication and preliminary ChIP analysis* above).

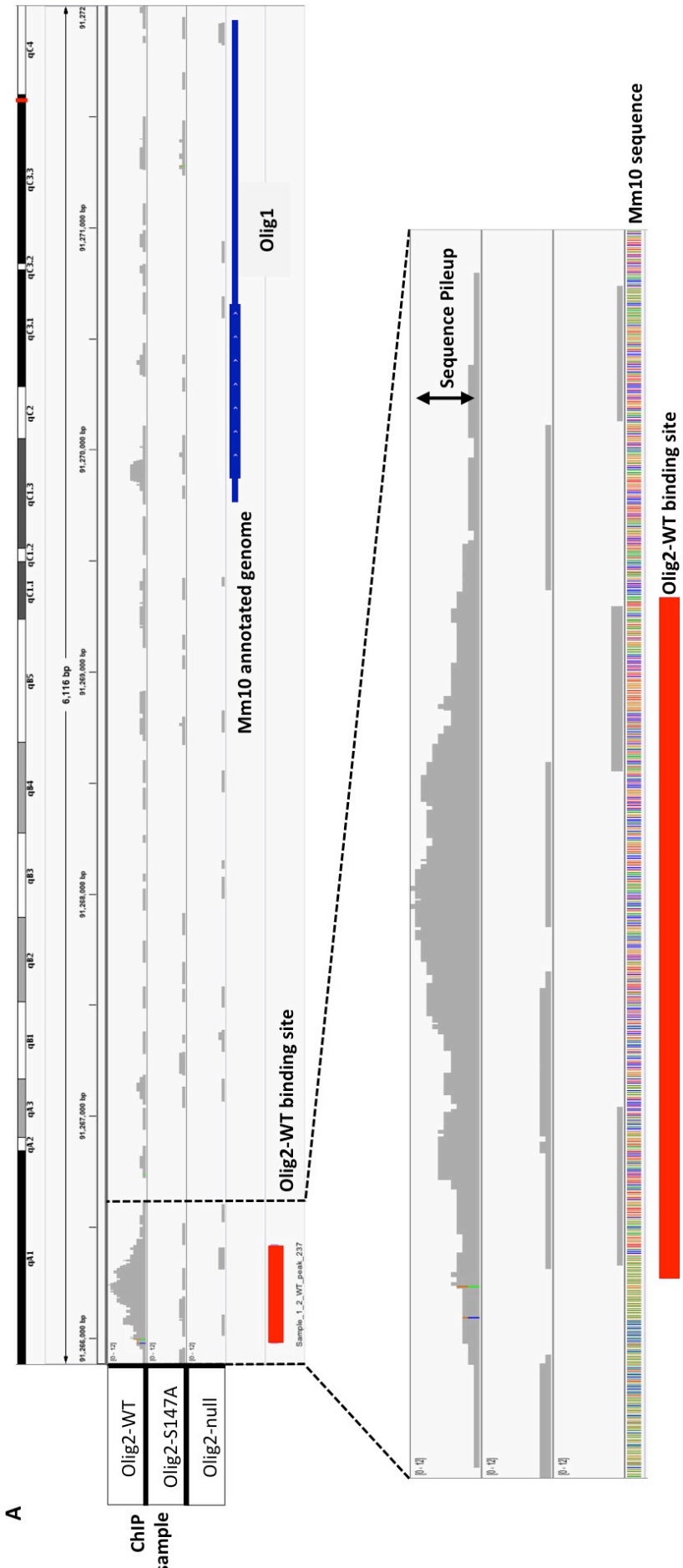

Figure 7. Olig2 ChIP-seq analysis. A. Visualization of the Olig2-WT, Olig2-S147A and Olig2-null ChIP-seq read pile-up at the Olig1 gene locus and identification of an Olig2-WT binding site ~3 kb upstream of the Olig1 open reading frame (ORF). *(Continued overleaf.)*

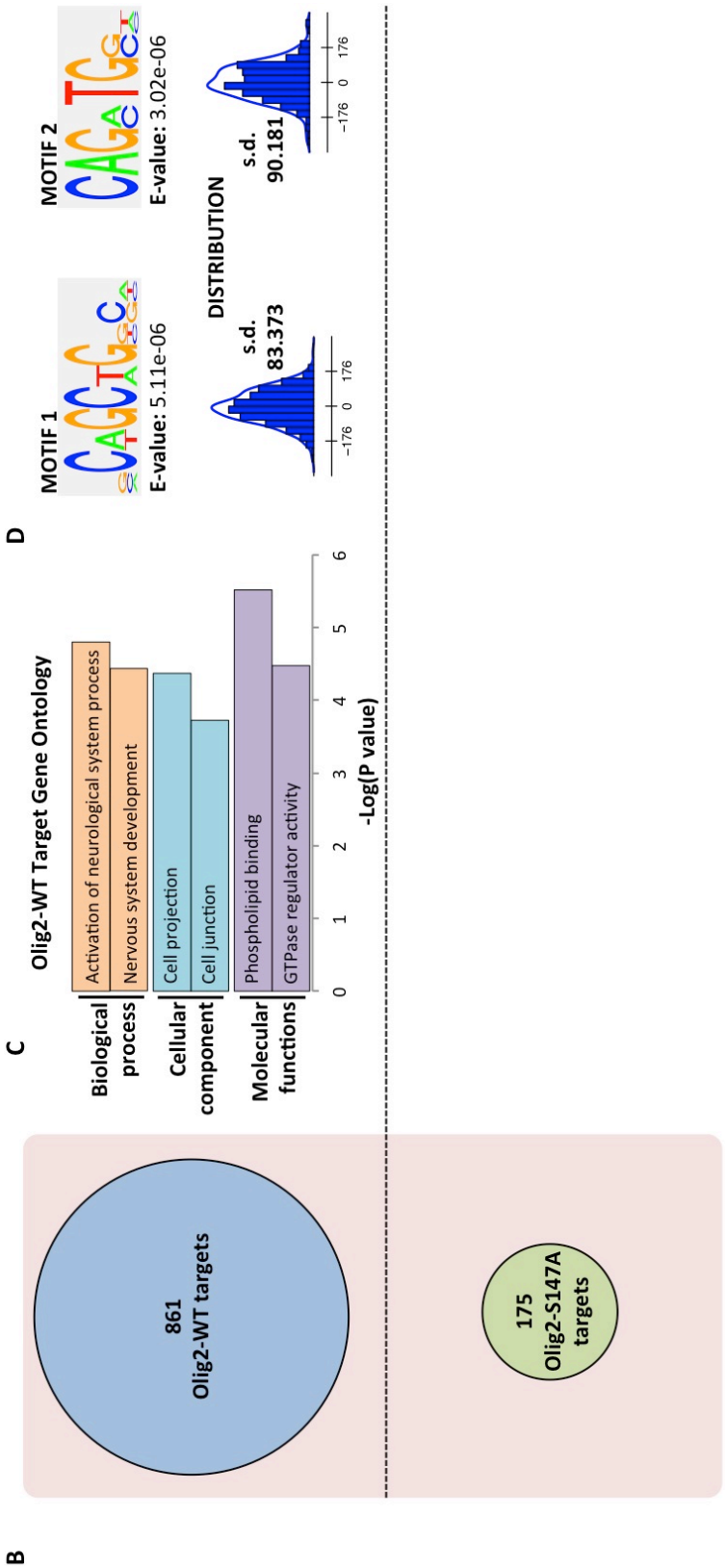

Figure 7 cont'd. B. Venn diagram of the non-overlapping Olig2-WT and Olig2-S147A datasets. **C.** Graphical representation of the Olig2-WT target gene ontology. **D.** Olig2-WT target motifs.

In contrast to the clear results of the GO analysis of phospho-S147 Olig2-WT, GO analysis of the ChIP-seq data for Olig2-S147A identified no statistically significant ($p < 0.05$) over-representation of any GO term. This indicated that the Olig2-S147A target genes are not primarily associated with any specific biological process, cellular component or molecular mechanism, and are in terms of functionality incoherent. In line with this, the GO terms that were represented at the greatest confidence level were not consistent with the known functions of Olig2 in the CNS (data not shown). For example, the biological process and cellular components represented at the highest statistical significance were embryonic digestive tract morphogenesis (GO:0048557) ($p \approx 0.10$) and mitochondrial respiratory chain complex IV (GO:0005751) ($p \approx 0.22$), respectively.

From the raw Olig2-WT ChIP-seq data, a list of candidate motifs was obtained. Of these, two were regarded as real binding motifs on the basis of the calculated *p* value and the Gaussian distribution of the underlying peaks (Source Bioscience, pers comm) (Figure 7D). Basic HLH proteins – such as Olig2 – typically bind to E-box sequences, and the M1 and M2 motifs identified followed the E-box consensus *CANNTG*, where N can be any nucleotide. In direct contrast to the clear and consistent gene target E-box motifs revealed for Olig2-WT, motif analysis of the Olig2-S147A ChIP-seq data failed to identify any Olig2-S147A target motifs and appeared to be weighted towards repetitive or GC-rich DNA sequences.

In conclusion, ChIP-seq analysis of the Olig2 DNA binding sites purified from Olig2-WT NSC cultures indicated that Olig2 phosphorylated at S147 occupied regulatory E-box elements *CAGCTG* and *CAGATG* of genes strongly linked to central nervous system development, structure and function. The limited number of Olig2-S147A binding sites identified by ChIP-seq, combined with the absence of both meaningful gene ontology and motif analysis, indicated that Olig2-S147A – modeling Olig2 dephosphorylated at S147 – does not recognize

specific sequence motifs of a target set of genes and probably does not bind DNA selectively in NSCs.

5.3 DISCUSSION

In the developing spinal cord, transcription factor Olig2 is uniquely expressed in NSCs that reside in a discrete region of the ventral ventricular zone, the pMN domain. Olig2+ NSCs divide and differentiate to produce MNs before switching to produce OLPs, and Olig2 is essential for both the neurogenic and oligodendrogenic phases. Research into precisely how Olig2 regulates the two very different developmental programmes has revealed that reversible phosphorylation of a specific serine residue (S147) within Olig2 is a critical regulator of Olig2 function and NSC fate (Li et al., 2011). S147 is located within the dimerization and DNA-binding basic helix-loop-helix (bHLH) motif and is highly conserved among vertebrates. During the early patterning and MN-producing periods of spinal cord development, Olig2 S147 is phosphorylated. Olig2 S147 is dephosphorylated over the period of the MN-OLP fate switch and analysis in cultured P19 cells and in mouse and chick embryos indicates that S147 dephosphorylation acts as an instructive signal, inducing NSCs to stop becoming MNs and instead generate OLPs (Li et al., 2011).

S147 dephosphorylation alters the protein binding properties of Olig2. Phosphorylated Olig2 preferentially forms homodimers, while dephosphorylated Olig2 – modelled using the phospho-null mutant Olig2-S147A – heterodimerizes with other cofactors such as Ngn2. Olig2 S147 dephosphorylation is proposed to mediate the fate switch through dynamic changes in Olig2 cofactor choice (Li et al., 2011). In concert with the specific protein-protein interactions, basic HLH transcription factors directly regulate the expression of target genes via occupancy of discrete genomic binding sites. Olig2 has been shown to bind to a number of target genes and to regulate target gene expression (Kuspert et al., 2011; Weng et al., 2012; Yu et al., 2013; Mateo et al., 2015). The effect of S147 phosphorylation on Olig2 gene target selection, however, remains to be established. In this chapter, I have explored the DNA

binding activity of Olig2-WT phosphorylated at S147 and the Olig2-S147A phospho-null mutant form of Olig2. Understanding the role of Olig2 gene target choice in regulating the MN-OLP fate switch will provide important insights into the molecular mechanisms underpinning NSC specification in the pMN domain and possibly cell fate specification more broadly.

The primary NSC strategy

My experimental strategy involved derivation of primary adherent NSC cultures expressing either endogenous wild-type Olig2 or the transgenic Olig2-S147A mutant isoform. I confirmed that Olig2-WT was phosphorylated at S147 and analysed Olig2-WT and Olig2-S147A gene target association by ChIP and quantitative PCR/high throughput Illumina sequencing. Here, I discuss the reasoning behind my approach.

In order to obtain sufficient material from the Olig2 ChIP for Illumina sequencing analysis, an expandable in vitro platform was necessary. In theory, Olig2 ChIP could be performed from the dissected and dissociated spinal cords of wild-type E11.5 (pre-fate switch) and E13.5 (post-fate switch) mice. This method should identify the Olig2 targets in bona fide pMN NSCs during neurogenesis and oligodendrogenesis. Realistically, however, the time and effort necessary to collect sufficient numbers of embryonic spinal cords renders this approach unworkable. In addition, the presence of Olig2-expressing OLPs in the spinal cords of E13.5 mice would confound the identification of Olig2 gene targets specifically in NSCs. In contrast, forced expression of Olig2 by transient transfection of a stable cell line would enable simple ChIP purification of sufficient quantities of genetic material for sequencing analysis. The biological relevance of this approach, however, would need to be questioned. The protein milieu and chromatin landscape will vary substantially between pMN NSCs in vivo and the

cells of a stable cell line and might affect occupancy of genomic binding sites. The methodology, therefore, required a trade-off between the experimental viability and the fidelity to the in vivo situation. On that basis, I decided to use primary NSCs derived from the cortices of embryonic mice and expanded in vitro, as previously described by Pollard et al. (2006). These cells express Olig2 naturally, retain neuronal and glial differentiation potential and are widely regarded as a reliable model of endogenous NSCs (Conti et al., 2005; Pollard et al., 2006; Glaser et al., 2007). The cortical source of these primary NSC cultures is clearly distinct to the ventral ventricular zone of the embryonic spinal cord, the in vivo region of interest. The fidelity of the cortical NSC culture strategy to model pre and post MN-OLP fate switch NSCs of the spinal pMN domain might also therefore be called into question. In defense of my approach, I would contest that the ex vivo culture systems often necessary for high-throughput sequencing analysis will invariably alter cell character. In this case, the cortical culture system generates uniform populations of multipotent Olig2-expressing NSCs, with medium supplements FGF2 and EGF acting as potent mitogens to promote NSC proliferation, as well as inducing a ventral molecular phenotype and blocking neuronal/OL lineage commitments, respectively (Guillemot, 2007; Bithell et al., 2008). Overall, given the inevitable limitations of in vitro cell culture systems for modeling in vivo development, my Olig2+ primary NSC cultures balance the methodological requirements for expandability and tractability with a useful degree of biological relevance.

I performed Olig2 ChIP from parallel cultures of NSCs derived from embryonic mice carrying either the Olig2-WT or the Olig2-S147A gene. An alternative strategy using the same NSC cultures would be to compare wild-type NSCs that have either been maintained as stem cells or differentiated into OLPs. This would be an excellent strategy for analysing the activity of Olig2 in NSCs and OLPs. However, I set out to address a different question: how does the activity of phosphorylated versus dephosporylated Olig2 in NSCs regulate commitment to the

neuronal versus glial lineages? Chromatin IP of phosphorylated wild-type Olig2 and the phospho-null mutant Olig2-S147A from NSCs under uniform conditions would, therefore, enable the effect of S147 phosphorylation on Olig2 gene target choice to be analysed in isolation and in a physiologically relevant context.

NSC cultures

NSC cultures were derived from the dissociated cortices of E13.5 mice and characterized by immunolabeling for Nestin, Sox10, GFAP and Tuj1. The ubiquitous expression of the intermediate filament protein and NSC marker Nestin combined with the near absence of the OL, astrocyte and neuron lineage markers Sox10, GFAP and Tuj1, indicated that the cultures retained neural stem cell-like character (Lendahl et al., 1990). These stem-like properties common to both the Olig2-WT and Olig2-S147A cultures indicated that Olig2 dephosphorylation was not by itself sufficient to induce spontaneous OLP formation in my NSC cultures.

ChIP-qPCR analysis

I performed preliminary Olig2 ChIP from Olig2-WT, Olig2-S147A and Olig2-null NSC cultures and examined Olig2-WT and Olig2-S147A DNA binding at specific genomic loci by quantitative PCR. The results revealed that Olig2-WT occupied the regulatory regions of the *Sox10*, *PDGFRA* and *Olig1* genes, identifying two novel Olig2 binding sites in the *PDGFRA* and *Olig1* genes. ChIP-qPCR from Olig2-S147A cultures revealed that the phsopho-null Olig2-S147A did not occupy these binding sites in NSCs, indicating that occupancy of the *Sox10*, *PDGFRA* and *Olig1* gene targets requires Olig2 phosphorylation at S147.

Interestingly, the 5' *U2 enhancer* of gene *Sox10* – identified here as a phospho-S147 Olig2-specific binding site in NSCs – was first established as an Olig2 gene target in committed OLPs (Kuspert et al., 2011). Olig2 binds the *U2 enhancer* in OLPs in vivo, and mutation of the *U2* sequence abolishes Olig2 binding and diminishes enhancer activity. It is therefore perhaps surprising that I did not observe Olig2-S147A occupancy of the *U2 enhancer* of *Sox10* in cultured NSCs. This, however, assumes that the activity of Olig2 is constant in oligodendrogenic NSCs and committed OLPs. In NSCs, dephosphorylation at S147 instead appears to trigger dissociation of Olig2 from the *U2* binding site, before Olig2 reoccupies the same *U2* binding site and drives *Sox10* expression in committed OLPs. Re-association with the *U2* binding site might coincide with re-phosphorylation of S147, although this remains to be established.

In addition to the *U2 enhancer* of *Sox10*, I examined occupancy of another previously reported Olig2 binding site, the upstream *M250 enhancer* of the motor neuron-specific gene *Hb9* (Lee et al., 2004; Lee et al., 2005). The *M250 enhancer* contains two evolutionarily conserved E-boxes – the *M50* E-box and the *M100* E-box – and mediates both *Hb9* gene activation and repression (Lee et al., 2004). Olig2 occupancy of the *M250* enhancer was confirmed in transfected P19 cells by ChIP of Flag-tagged Olig2, and in HEK293 cells Olig2 repressed the activity of an *M250* reporter construct (Lee et al., 2005). In contrast to the results of Lee et al., however, I detected no significant recovery of the *M250* enhancer after Olig2 ChIP from either Olig2-WT or Olig2-S147A NSCs, indicating Olig2 did not occupy either the *M50* or *M100* E-boxes in cultured NSCs. The different observations could relate to differences between the primary NSC and P19 cells used, as well as to the properties of endogenous versus exogenous Flag-tagged Olig2.

ChIP-seq analysis

To identify the full repertoire of phospho-S147 Olig2-WT and Olig2-S147A gene targets, I analysed ChIP-purified DNA samples from Olig2-WT and mutant NSC cultures by high-throughput Illumina sequencing. The ChIP-seq generated more than 25 million 100 bp reads per sample. The Olig2-WT and Olig2-S147A sequencing data were analysed in silico for sequence enrichment relative to input and Olig2-null background controls. The computational analysis identified 871 and 175 discrete binding sites for phospho-S147 Olig2 and Olig2-S147A respectively, with no individual site common to both datasets. The number of Olig2 binding sites identified here is considerably lower than has previously been reported in published high-throughput studies of Olig2 gene target binding: Weng et al. (2012) identified 5439 Olig2 binding sites using purified rat OLs, Yu et al. (2013) identified 21901 Olig2 binding sites in cultured OLPs isolated from neonatal rats, and Mateo et al. (2015) identified 16067 Olig2 gene targets in cultured NSCs. The total number of ChIP-seq peaks, however, is contingent on the thresholds set for peak calling and is therefore difficult to interpret across independent ChIP-seq datasets. Indeed, ChIP-seq performed using mouse neural progenitor cells transduced with wild-type Olig2 identified fewer than 400 Olig2 target genes (Meijer et al., 2014). In the future, it will nonetheless be interesting to explore whether the Olig2 binding sites identified here represent a set of high-affinity targets revealed under more stringent peak calling conditions.

Basic HLH TFs such as Olig2 typically bind to E-box sequences (Murre et al., 1989). Motif analysis performed on the phospho-S147 Olig2-WT ChIP-seq data identified two hexamers conforming to the canonical *CANNTG* E-box motif: *CAGCTG* and *CAGATG*. The *CAGATG* Olig2 target DNA motif has not previously been identified. The *CAGCTG* Olig2 binding motif, however, was previously identified by Yu et al. (2013), indicating that this Olig2 target

sequence is common to NSCs and differentiating OLPs. Furthermore, cross comparison with the Yu et al. (2013) OLP gene target list revealed that 75% of the phospho-S147 Olig2-WT gene targets in NSCs are also Olig2 targets in OLPs. The degree of overlap in NSC and OLP Olig2 gene targets, combined with the discovery of a conserved binding motif mediating target occupancy, suggests Olig2 primarily associates with a stable set of gene targets in both neurogenic NSCs and committed OLPs (Yu et al., 2013).

ChIP-seq identified 175 Olig2-S147A binding sites, none of which was common to the phospho-S147 Olig2-WT dataset. The majority (~80%) of the Olig2-S147A binding sites were not affiliated with any known genomic feature, and motif analysis failed to identify an Olig2-S147A target DNA sequence. In addition, while GO analysis of the phospho-S147 Olig2-WT gene targets revealed significant over-representation of a number of related GO terms, including nervous system development, GO analysis of the Olig2-S147A ChIP-seq data did not establish enrichment of any GO term. In other words, there was no significant over-representation of genes performing any specific molecular function, comprising any specific cellular component or involved in any specific biological process; the dataset as a whole exhibited no discernible functional profile. Finally, a correlation plot and principal component analysis (PCA) demonstrated the two replicate Olig2-S147A mutant peak sets show low concordance (data not shown). In fact, PCA indicated the individual Olig2-S147A datasets show less concordance with one another than they do with the highly concordant phospho-S147 Olig2 datasets, suggesting the replicate Olig2-S147A datasets are essentially unrelated. Overall, the ChIP-seq analysis indicated Olig2-S147A did not bind DNA in a specific manner in NSCs.

On the basis of the ChIP-seq experiments presented here, it appears that phospho-S147 Olig2 homodimers – expressed in pMN domain-resident NSCs during motor neurogenesis –

specifically target *CAGCGT*/*CAGATG* E-box binding sites of neural development genes. Over the NSC fate switch, S147 dephosphorylation triggers Olig2-gene target dissociation, heterodimer formation and induction of the OL-specific genetic programme. Later, in differentiating OLPs, Olig2 re-occupies the phospho-S147-specific binding sites targeted in neurogenic NSCs (Yu et al., 2013). In OLPs, Olig2 occupancy of the upstream *U2 enhancer* of *Sox10* has been shown to upregulate *Sox10* transcription after the initial induction of Sox10 expression and commitment to the OL lineage (Kuspert et al., 2011). This delay between the initial activation of Sox10 expression and Olig2-mediated activation of Sox10 expression might, therefore, reflect the timeline of re-occupancy of specific gene targets by Olig2 in committed OLPs. Moreover, the re-association of Olig2 with its earlier phosphorylation-dependent NSC gene targets might itself be dependent on the re-phosphorylation of S147 in OLPs. The transient dissociation of dephosphorylated Olig2 from its gene targets and phosphorylation dependent re-occupancy of the same gene targets in stable OLPs, however, is yet to be confirmed. Tracking the phosphorylation state of Olig2 S147 along the OL lineage, and examining the ability of Olig2-S147A-expressing NSCs to generate mature OLs will reveal the dynamics of Olig2 phosphorylation and its requirement over the full course of OL development.

The precise molecular activity of dephosphorylated Olig2 in NSCs remains to be fully elucidated. Li et al. (2011) propose that one function of S147 dephosphorylation is to dissociate Olig2 homodimers, allowing monomeric Olig2 to bind and sequester Ngn2 away from the regulatory regions of MN genes, thus halting MN gene expression and facilitating OL lineage gene expression. Consistent with this model, the Olig2-S147A ChIP-seq data reported here suggest entirely DNA-independent roles for dephosphorylated Olig2 in NSCs. There are, however, in addition to DNA-independent functions for Olig2, a number of alternative interpretations of the Olig2-S147A ChIP-seq data. For instance, the lack of a detectable

sequence-specific DNA-binding activity of Olig2-S147A might represent an artefact of the in vitro culture system. The protein complement of pMN domain NSCs in vivo will differ from that of cultured NSCs and might include an additional bHLH protein cofactor that is absent in cultured NSCs and necessary for Olig2-S147A dimerization and DNA binding. In WT NSCs, the capacity of phospho-S147 Olig2 to form homodimers would bypass the requirement for expression of this cofactor. Validatation of the NSC model and the ChIP-seq results that I report here will require comparative transcriptome analysis of genuine post-fate switch pMN domain NSCs and cultured NSCs, along with follow-up DNA binding studies of Olig2-S147A in alternative model systems.

Olig2 regulation of target gene activity

Olig2 has been reported to act as both a transcriptional repressor during neurogenesis and as a transcriptional activator during oligodendrogenesis (Mizugutchi et al., 2001; Novitch et al., 2001; Ligon et al., 2007; Kuspert et al., 2011; Lee et al., 2005; Weng et al., 2012; Yu et al., 2013). Indeed, Mateo et al. (2015) revealed that Olig2 simultaneously activates stem cell/self renewal genes and represses neuronal differentiation and quiescence genes in cultured NSCs. To determine whether phospho-S147 Olig2 acts as either an activator or a repressor at the *Sox10*, *PDGFRA* and *Olig1* gene targets, I analysed gene target expression at the protein and RNA levels in Olig2-WT and phospho-null Olig2-S147A mutant NSC cultures. If Olig2 were acting to repress expression of these genes, dissociation of Olig2 from these DNA binding sites might be expected to de-repress and thereby activate gene expression. For *Sox10*, *PDGFRA* and *Olig1*, I found extremely low RNA abundance (≤5% *GAPDH*) and no observable protein in both Olig2-WT and Olig2-S147A cultures. This suggests that S147 dephosphorylation-dependent dissociation of Olig2 is not sufficient to regulate OL lineage target gene expression. In vivo, OLP formation from pMN NSCs might require Olig2 dissociation-dependent de-repression of OL lineage gene targets combined with expression and/or activation of additional factors that are suppressed under the NSC culture conditions described here. In this case, S147 dephosphorylation-induced changes in Olig2 binding site occupancy would represent a 'priming' step in the NSC-OLP transition.

In the absence of high-throughput gene expression analysis, such as RNAseq or microarray, the genome-wide impact on Olig2 gene target expression of dynamic Olig2 gene target occupancy in phospho-S147 and phospho-null mutant Olig2-expressing NSCs cannot be established. The ChIP-seq data nevertheless imply a repressor function for Olig2. GO analysis revealed that a significant number of Olig2 target genes are involved in late-stage neuronal

processes, such as Activation of nerve impulse transmission (GO:0051971), which are not associated with undifferentiated NSCs. Empirical analysis of the ChIP-seq data also identified a number of established late-stage neuron, OL- and astrocyte-lineage markers, including *Cplx2*, *Nrxn1*, *Nrxn2*, *GFAP*, *Olig1*, *Tenm4* and *Opalin* (Raff et al., 1979; Ushkaryov et al., 1992; Lee et al., 2005; Kippert et al., 2008; Suzuki et al., 2012). In line with this, a number of studies have described gene repressor functions for Olig2 in CNS development (Mizuguchi et al., 2001; Novitch et al., 2001; Zhou et al., 2001; Lee et al., 2005; Ligon et al., 2007; Mateo et al., 2015).

Transcriptional activator functions for Olig2 have also previously been reported in OLPs (Kuspert et al., 2011; Yu et al., 2013). My results indicate that phosphorylated Olig2 binds the *U2 enhancer* of *Sox10* previously identified as an Olig2 gene target in OLPs (Kuspert et al., 2011). In committed OLPs, Olig2 occupancy of the *U2 enhancer* was shown to activate expression of *Sox10*. If Olig2 binding of the *U2 enhancer* inhibits *Sox10* expression in NSCs, Olig2 would repress gene expression in NSCs and activate gene expression in OLPs via occupancy of a single binding site. In this case, the dual functionality might be regulated by NSC-/OLP-specific recruitment of off/on transcriptional machinery.

In NS5 NSC cultures, Olig2 occupancy activates transcription of cell cycle and DNA replication genes, promoting NSC proliferation and self-renewal (Mateo et al., 2015). It remains to be established, however, whether Olig2 displays the same dual functionality and concurrently performs gene activator and repressor functions in the primary NSC cultures analysed here (Pollard et al., 2006). It should be noted that proliferation-/stem cell maintenance-related GO terms such as “Cell cycle” were not statistically over represented in the phospho-S147 Olig2-WT ChIP-seq dataset.

Summary and further work

In this chapter, I have presented the results of ChIP analyses of Olig2 gene target selection in cell culture models of neurogenic (Olig2-WT) and gliogenic (Olig2-S147A) pMN NSCs. I report phospho-S147-specific occupancy of *CAGCGT* and *CAGATG* E-box binding sites at a range of gene targets, including multiple critical regulators of neural development such as *Foxp1*, *Tulp3*, *Notch1*, *Nkx6*.2 and *Sox10* (Kuhlbrodt et al., 1998; Wang et al., 1998; Ikeda et al., 2001; Genoud et al., 2002; Pattyn et al., 2003; Wegner & Stolt, 2005; Vallstedt et al., 2005; Cai et al., 2010; Hisaoka et al., 2010). Quantitative RT-PCR, as well as GO and empirical analysis, suggest that Olig2 gene target occupancy was associated with limited target gene expression and might represent gene target repression. Olig2-S147A ChIP-seq revealed that Olig2-S147A and phospho-S147 Olig2 shared no binding sites and that Olig2-S147A did not bind genomic DNA with any specificity or to perform any discernible function. However, quantitative RT-PCR indicates that the absence of Olig2 from OL-lineage gene targets *Sox10*, *PDGFRA* and *Olig1* was not associated with any significant change in gene expression. This implies that dynamic Olig2 DNA binding was not sufficient to affect transcriptional regulation and might act as a necessary but insufficient prelude to gene activation.

In ChIP-seq experiments performed from cultured OLPs by Yu et al. (2013), the Olig2 gene targets are highly concordant with those reported here for phospho-S147 Olig2 in NSCs. The phospho-S147 Olig2 gene target *CAGCTG* E-box binding motif identified here is also identical to the Olig2 target motif established in OLPs (Yu et al., 2013). I identified an additional related binding motif in NSCs (*CAGATG*) that was not reported in OLPs. The dephosphorylation-induced dissociation of Olig2 from its gene targets therefore appears to be a transient state interposed between the NSC and OLP states. It will be intriguing to

explore the potential mechanisms (S147 re-phosphorylation, for example) inducing Olig2 DNA binding at the same target genes in OLPs.

In future, the phosphorylation state of Olig2 S147 in cultured OL lineage cells at different stages of differentiation can be examined by western blot using the phospho-S147-specific antibody developed by Li et al. (2011). Moreover, the capacity of mutant Olig2-S147A NSCs to generate myelinating OLs could be addressed in vivo by crossing the *Olig2-S147A* and *Sox10-Cre* PAC transgenes onto the $Olig2^{fl/fl}$ background. In these mice, expression of wild-type Olig2 in NSCs during embryonic development would allow normal MN development and postnatal survival of these transgenic mice, while *Sox10*-linked Cre-recombinase expression would ablate the $Olig2^{fl/fl}$ in OL lineage cells leaving only the mutant *Olig2-S147A*. In this system, the ability of the recombined OLPs to become myelinating OLs in vivo would reveal the requirement for Olig2 S147 phosphorylation for OL differentiation.

Exploring how Olig2 affects target gene expression will also be fundamental to understanding the molecular regulation of CNS development. Gene expression profiling of NSCs and OLPs by RNA-seq and/or RNA polymerase II ChIP-seq will enable comparison of Olig2 gene target transcription. For those Olig2 gene targets common to NSCs and OLPs that show significantly different expression levels in NSCs and OLPs, determining precisely how Olig2 contributes to the regulation of transcription will be fascinating. Opposing effects on gene target transcription in NSCs and OLPs would presumably be mediated by recruitment of specific co-regulator proteins, such as histone modifiers and chromatin remodelers. Olig2 has been shown to recruit the SWI-SNF chromatin remodeler Brg1 to E-box enhancer elements in immature OLs, and regulate gene expression and OL differentiation (Yu et al., 2013). A combination of ChIP-seq analysis for enrichment of regulatory histone marks (H3K9 acetylation, for example) at Olig2 target sites and protein-protein interaction assays, such as

yeast-two-hybrid and co-IP experiments, could identify important candidate mechanisms for further analysis.

Overall, I have revealed DNA-binding preferences for wild-type Olig2 phosphorylated at S147 and the constitutively dephosphorylated Olig2-S147A mutant in cultured NSCs. My data suggest a variety of experimental directions for the future that will provide critical information for understanding how Olig2 S147 phosphorylation might regulate stepwise progression along the OL lineage. This research might also provide a paradigm for understanding how phosphorylation of bHLH proteins regulates cell development.

CHAPTER 6

OLIG2 S263 PHOSPHORYLATION

6.1 INTRODUCTION

Basic HLH TF Olig2 has roles in neuron, OLP and astrocyte formation in the developing CNS (Meijer et al., 2012). In the embryonic spinal cord, Olig2 is expressed in multipotent NSCs resident in the ventral pMN domain and is essential for the generation of both spinal MNs and OLs. In addition, Olig2-expressing pMN NSCs produce a subpopulation of astrocytes concentrated at the ventral pial surface of the spinal cord, and postnatal Olig2 function has been reported to be necessary for proper astrocyte differentiation in cerebral white matter (Masahira et al., 2006; Cai et al., 2007). Olig2+ NSCs in the ventricular zone of the embryonic ventral forebrain contribute to excitatory cholinergic and glutamatergic neuron populations, as well as multiple subtypes of inhibitory interneurons, including cortical interneurons (Furosho et al., 2006; Miyoshi et al., 2007; Ono et al., 2008). In OL development, Olig2 is continuously expressed from nascent OLPs to mature and myelinating OLs and is a master regulator of OL differentiation (Li & Richardson, 2008). Recent research indicates that Olig2 initially promotes OL lineage progression before inhibiting the final differentiation of pre-myelinating OLs (Mei et al., 2013). The involvement of Olig2 in the generation of specific astrocyte and neuron sub-types, and its dynamic functions at different stages along the OL lineage, indicates that Olig2 performs a wide range of functions in different cellular contexts.

The activities of Olig2 in these different biological contexts have been explored at a molecular level. During the neurogenic phase of pMN domain development, Olig2 initially

primes NSCs for neuronal differentiation by de-repressing expression of pro-neuronal TFs – including *Ngn2* and *Lim3* – before subsequently antagonizing pro-neuronal TF activity (Lee et al., 2005). In Ngn2/Olig2 double-positive pMN NSCs, Olig2 competitively binds and represses pro-MN gene targets such as *Hb9*, while at the protein level formation of Olig2:Ngn2 and Olig2:E47 heterodimers inhibits formation of the functional pro-neuronal Ngn2:E47 activator complex. High throughput ChIP-seq and RNAseq analyses indicate that Olig2 acts as both a transcriptional activator and a repressor to inhibit neuronal differentiation and maintain the proliferating stem cell state (Mateo et al., 2015). In OLPs, Olig2 directly activates *Sox10* gene expression via the conserved upstream *U2 enhancer* (Liu et al., 2007; Kuspert et al., 2011). The opposing functions of Olig2 in promoting/inhibiting OL lineage progression at early and late stages of differentiation were also observed to coincide with a switch from Olig2-mediated activation of Olig1 gene expression in OLPs to repression of Olig1 in immature OLs (iOLs) (Mei et al., 2013). Moreover, ChIP-seq revealed that Olig2 associates with largely distinct sets of gene targets in OLPs/iOLs and mature OLs (mOLs) (Yu et al., 2013). This dynamic gene target choice is accompanied by stage-specific interaction with protein binding partner Brg1, the central ATPase subunit of the SWI/SNF chromatin remodeler complex. Brg1 and Olig2 have been shown to interact physically and occupy common genomic binding sites in iOLs but not in mOLs. Ultimately, the existing research highlights how the range of different developmental functions of Olig2 is underscored by unique and specific molecular activities.

Protein kinase-mediated phosphorylation at specific serine and threonine residues has been shown to alter key properties of Olig2 and to critically affect Olig2+ cell development. Casein kinase 2B (CK2B) phosphorylates Olig2 at multiple sites in the serine-threonine-rich (STR) domain in vitro and this is proposed to mediate the positive regulatory role of CK2B in OLP specification from embryonic NSCs (Huillard et al., 2010). In adult subventricular zone NSCs,

Akt-mediated phosphorylation of S30 induces nuclear export of Olig2, an essential process for CNTF-induced astrocyte differentiation in vitro (Setoguchi & Kondo, 2004). In the Olig2 amino terminal, S10/13/14 phosphorylation alters Olig2 target gene expression through phosphorylation-dependent compartmentalization of Olig2 to transcriptionally active open chromatin and interaction with specific co-regulator proteins (Sun et al., 2011; Meijer et al., 2014). Finally, Olig2 phosphorylation at S147 in the basic HLH domain determines NSC fate choice in the embryonic pMN domain (Li et al., 2011). Olig2 S147 dephosphorylation alters Olig2 cofactor choice, and potentially gene target selection, to trigger the MN-OLP fate switch, abruptly ending neurogenesis and initiating OL formation.

The diverse range of developmental functions of Olig2 is underscored by specific molecular activities that are in turn modulated through post-translational modification – notably reversible phosphorylation – of specific amino acid residues. Establishing the full repertoire of genuine phosphorylation states of Olig2 and the molecular activity associated with each will be fundamental to understanding CNS development and will require intensive research. In this chapter, I present the results of computational analysis of Olig2 phosphorylation and the early steps in functional characterization of the Olig2 carboxy-terminal S263 phospho-acceptor site.

6.2 RESULTS

In total, mouse Olig2 contains over 60 serine/threonine residues, and a serine content of approximately 15% (50 residues of 323 total). Computational analysis – performed by Professor Cizhong Jiang at Tongji University, China – examining the serine content of 16,403 distinct protein sequences in *Mus musculus* revealed that the 542 TFs identified display a significantly higher serine content than the remaining non-TF proteins (Figure 1). Among this set of 542 serine-rich transcription factors, Olig2 has the 13^{th}-highest serine content (Figure 1). For any protein, each serine residue represents a potential phosphorylation site that might alter its molecular properties and thereby regulate its function. In the case of Olig2, the abundance of potentially phosphorylated serine residues could therefore provide the mechanism for an individual TF to perform a range of functions, with specific multisite phosphorylation states inducing specific activities in different cells.

A

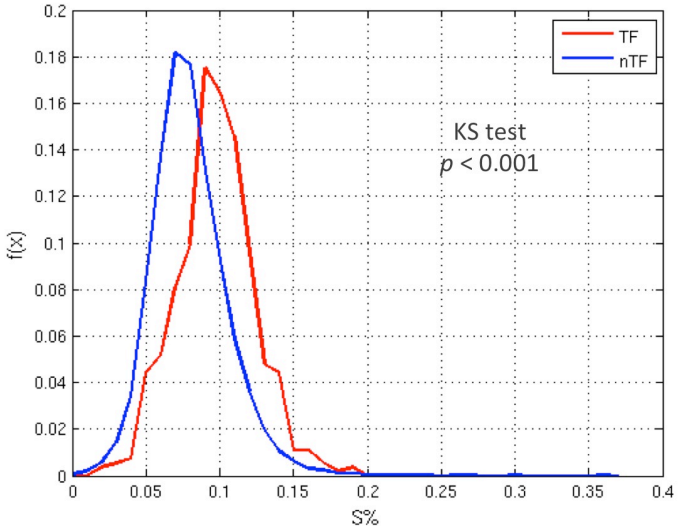

B

Protein	% Serine Content	# serines / # total aa	RANK
Cdkn2aip	19.2	108/563	1
Sox4	18.9	83/440	2
Tcf12	18.1	128/706	3
Zfp36	17.2	55/319	4
Hoxb5	17.1	46/269	5
Egr1	16.9	90/533	6
Otx1	16.3	58/355	7
Nkx6-1	16.2	59/365	8
Elk3	15.9	65/409	9
Klf12	15.7	63/402	10
Twist2	15.6	25/160	11
Tcf3	15.5	101/651	12
Olig2	15.5	50/323	13
Foxf2	15.2	68/446	14
Foxo1	15.2	99/652	15
Pax8	15.1	69/457	16
Twist1	15.0	31/206	17
Otx2	14.9	43/289	18
Mef2c	14.3	68/474	19
Hlx	14.3	68/476	20

Figure 1. Transcription factor serine content. A. Distribution of TF and non-TF percentage serine content. TF proteins carry a significantly higher percentage of serines compared to non-TF (nTF) proteins. **B.** Top 20 serine-rich TFs ranked according to serine content (# serines / # total amino acids). *(Computational analysis provided by Prof. Cizhong Jiang at Tongji University, China.)*

Predicted Olig2 phosphorylation sites

To identify putative phospho-acceptor sites, I analysed the human Olig2 protein sequence using the online tool NetPhos 2.0, which predicts phosphorylation sites using an 'artificial neural network algorithm' (Blom et al., 1999). From among the 60 sites, NetPhos 2.0 predicted 28 are phosphorylated, including the established S10/13/14, S30, STR and S147 sites (Figure 2A) (Setoguchi & Kondo, 2004; Huillard et al., 2010; Sun et al., 2011). In addition to the NetPhos 2.0 analysis, I also used the kinase-specific prediction tool NetPhosK 1.0 to identify the putative kinases targeting different sites (Blom et al., 2004). NetPhosK 1.0 analysis identified 12 protein kinases with predicted substrate residues within the Olig2 protein sequence, 11 of which are predicted to target multiple serine/threonine sites and 8 of which have been previously implicated in OL development and myelination (Figure 2A). Finally, to determine the evolutionary conservation of the predicted phospho-acceptor residues, I used the ClustalO tool to align the protein sequences of human, mouse, zebrafish and chick Olig2. The Olig2 sequences are >95% conserved between human and mouse, while human-to-chick and human-to-zebrafish alignment of Olig2 revealed 85.9% and 70.0% conservation respectively. Of the 28 serine/threonine residues predicted by NetPhos 2.0 to be phosphorylated in human Olig2, 10 – including the validated S10/13/14 and S147 sites but not the S30 and STR sites – are conserved across all species (Setoguchi & Kondo, 2004; Huillard et al., 2010; Li et al., 2011; Sun et al., 2011; Meijer et al., 2014). On the basis of the phosphorylation and kinase predictions, and evolutionary conservation of different putative phosphorylation sites, the computational analysis indicates that Olig2 is phosphorylated at multiple residues besides the known phospho-acceptor serine sites. Identifying the genuine phosphorylation sites within Olig2 and analysing the contribution of each to Olig2 function is an important route to understanding the role of Olig2 in neurodevelopment.

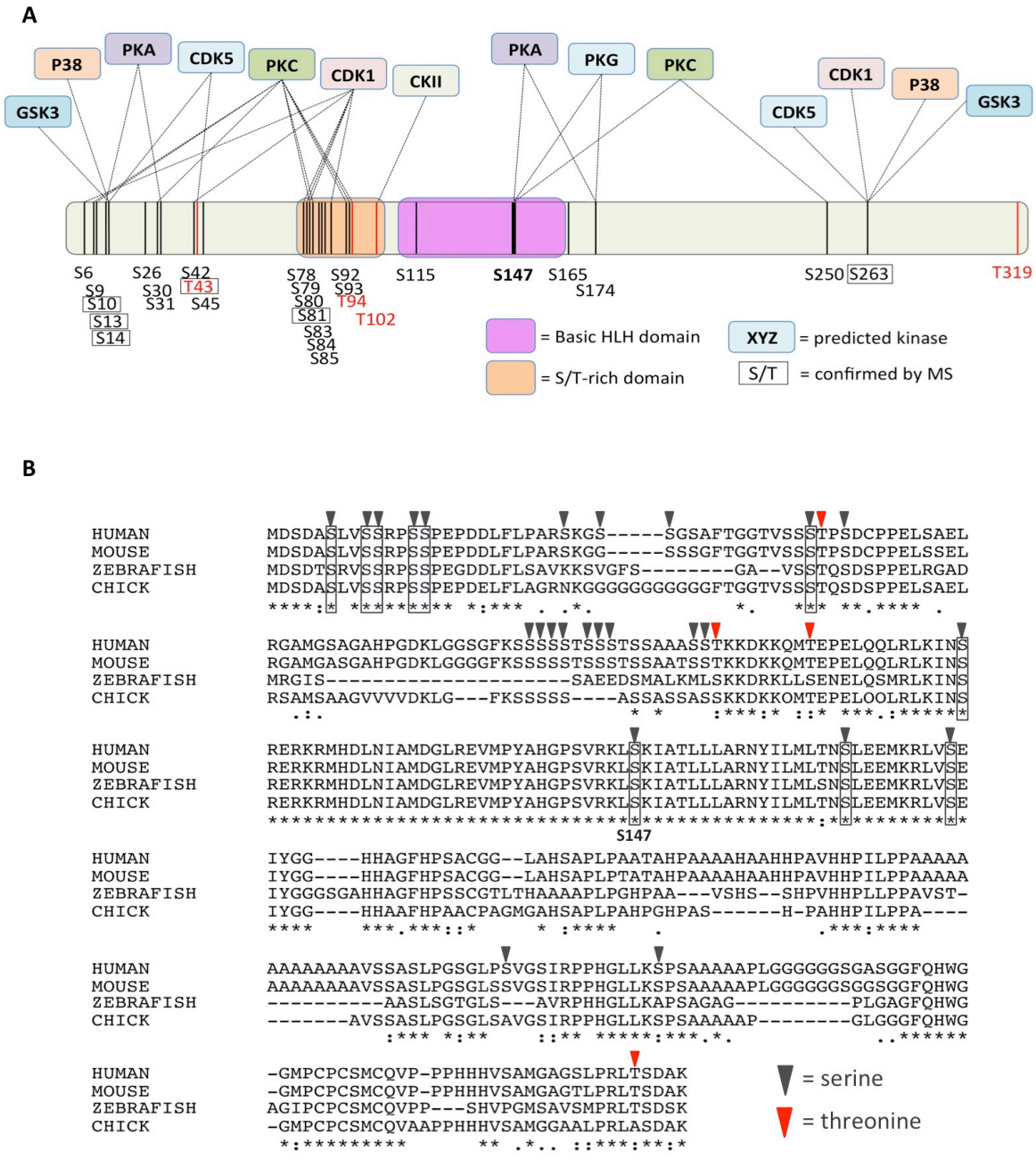

Figure 2. Predicted phosphorylation sites of human Olig2 and their evolutionary conservation. A. Distribution of predicted and confirmed phospho-acceptor sites in human Olig2 and the associated protein kinases. **B.** ClustalO alignment of human, mouse, zebrafish and chick Olig2 protein sequences. Arrowheads mark predicted and confirmed phosphorylation sites from A. Boxes mark the phosphorylation sites conserved across all species analysed.

Carboxy-terminal S263 and P38-MAPK

In addition to the S10/13/14, S30, STR and S147 sites, bona fide phosphorylation of S263 was detected in mass spectrometry analysis of Olig2 purified from transfected COS cells (Sun et al., 2011). The precise function of S263 phosphorylation, however, has not been established. Computational analysis of the Olig2 carboxy terminal amino acid sequence revealed S263 resides immediately upstream of a proline residue and is predicted by NetPhosK 1.0 to be a substrate of several proline-directed protein kinases with known roles in OL development, including P38-MAPK.

Mitogen-activated protein kinases (MAPKs) consist of families of Ser/Thr-specific kinases that mediate the intracellular responses to extracellular stimuli through protein phosphorylation signaling cascades. Four distinct subgroups within the MAPK family have been identified, one of which is the P38-MAPK group. P38-MAPKs are activated by dual phosphorylation at conserved residues, catalyzed by upstream MAP kinase kinases (Zarubin & Han, 2005). Downstream substrates of P38-MAPK include additional kinases as well as transcription factors that directly regulate gene expression in response to P38-MAPK-mediated phosphorylation (Tan et al., 1996). Research published from a number of labs has revealed important roles of P38-MAPK signaling in OLP differentiation and myelination (Baron et al., 2000; Fragoso et al., 2007; Hu et al., 2012; Rafalski et al., 2013).

As a preliminary demonstration of the role of P38-MAPK in OLP development, I analysed the effect of anisomycin-induced P38-MAPK activation on OLP formation from NSCs in vitro. Primary adherent Olig2-expressing NSC cultures were derived from the dissociated cortices of E13.5 wild-type mice and expanded in ‘NSC medium’ (Conti et al., 2005; Pollard et al., 2006). Under these conditions, the cultured NSCs remain Olig2- and Nestin-positive and

Sox10-negative, an indication of pre-OL lineage, stem cell-like character (see *Chapter 3: Spinal cord angiogenesis and the MN-OLP fate switch*). To induce OL lineage commitment, the NSC medium was substituted with 'Differentiation medium', containing 20 ng/ml FGF-2 and 10 ng/ml PDGF-AA, a growth factor combination known to enhance oligodendrogenesis. NSCs were exposed to either unsupplemented Differentiation medium (control) or Differentiation medium supplemented with the P38-MAPK activator anisomycin (+Ani) at 2 µg/ml final concentration. After 24 hrs in control or +Ani Differentiation medium, P38-MAPK activation was assessed by western blot. In +Ani medium, NSCs showed increased P38 phosphorylation (activation) relative to the level of total P38, confirming anisomycin-induced activation of P38-MAPK (Figure 3A). After four days in control or +Ani Differentiation medium, OLP development was analysed by immunolabeling the cultures with anti-Sox10 and anti-Olig2 antibodies, and the emergence of Sox10+/Olig2+ OLPs quantified as a percentage of total cell number. In untreated control cultures approximately 20% of cells were Olig2/Sox10 double-positive, indicating robust OLP generation from NSCs, while in +Ani cultures, Olig2 and Sox10 co-expression was observed in <2% of cells (Figure 3C). In contrast to the reduction in OLP numbers, an increase in the relative cell density was observed in +Ani cultures compared to control (Figure 3D), and based on observations of pyknotic cell nuclei there was no evidence of widespread apoptosis in either condition. The results therefore indicate that the P38-MAPK activator anisomycin potently inhibited OLP production from NSCs in vitro. Whether this effect of anisomycin treatment is mediated via phosphorylation of Olig2 at S263, however, has not been established but remains an intriguing hypothesis.

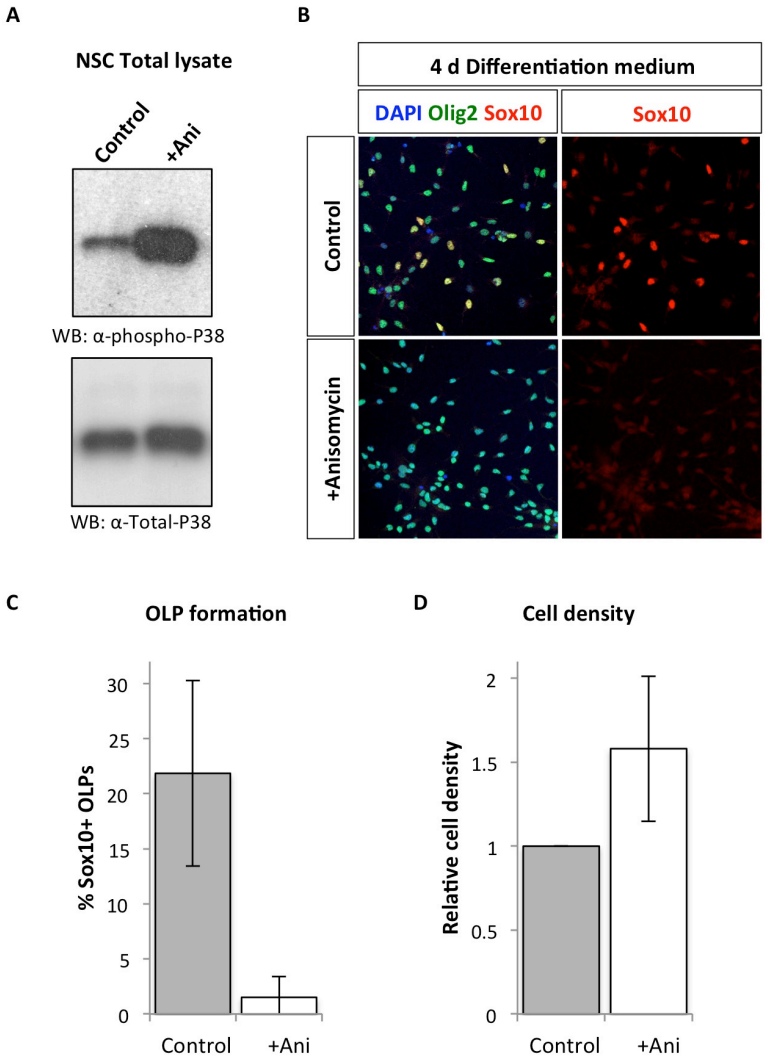

Figure 3. Anisomycin-induced activation of P38-MAPK and its effect on OLP formation in cultured NSCs. A. Western blot analysis of phospho- (activated) P38 and total P38 levels in NSCs cultured for 24 hrs in unsupplemented (control) or anisomycin-supplemented Differentiation medium (+Ani) **B.** Antibody labeling of TF Olig2 (green) and OLP marker Sox10 (red) in NSCs cultured for 4 days in control or +Ani Differentiation medium. **C-D.** Quantification of OLP formation and relative cell density in control and +Ani conditions.

Olig2-S263A expression vector construction

To analyze Olig2 S263 phosphorylation in vitro, I generated expression vector constructs encoding *3xFLAG*-tagged wild-type *Olig2* (*Olig2*^{WT}) and 3xFLAG-tagged phospho-null *Olig2-S263A* (*Olig2*^{S263A}). The mouse *Olig2* cDNA had previously been subcloned into the *pcDNA4.1* expression vector backbone (Figure 4) (obtained from U. Grazini). I used a site-directed mutagenesis strategy to produce the *Olig2*^{S263A}*-pcDNA4.1* from *the Olig2*^{WT}*-pcDNA4.1* parent template (Figure 4). Briefly, oligonucleotide primers containing an intended base-pair mismatch – to produce a serine (TCA) to alanine (GCA) codon change – were used in the mutagenic PCR reaction. The methylated parent vector was destroyed by digestion with DpnI and the *Olig2*^{S263A}*-pcDNA4.1* vector transformed into competent cells for nick repair and plasmid preparation. Sequencing and BLAST alignment with *Mus musculus* Olig2 cDNA sequence confirmed incorporation of the desired mutation and successful generation of *Olig2*^{S263A}*-pcDNA4.1* (Figure 4D).

I replaced the 3' *Myc* tag with a *3xFLAG* tag (Figure 5A). The *3xFLAG* tag fragment was designed to include 5' XbaI and 3' AgeI restriction sites, and was synthesized commercially. The *Myc* tag was excised from the *Olig2*^{WT}- and *Olig2*^{S263A}*-pcDNA4.1* and substituted with the *3xFLAG* tag using XbaI and AgeI restriction enzymes. Successful *3xFLAG* insertion was confirmed by sequencing and ClustalO alignment with *Mus musculus Olig2* cDNA and *3xFLAG* tag sequences.

To confirm functionality of the constructs, I transfected Olig2-negative C6 glioma cells in culture with either the *Olig2*^{WT}- or *Olig2*^{S263A}*-pcDNA4.1* expression vectors and analysed *Olig2*^{WT}/*Olig2*^{S263A} expression by WB with a rabbit anti-Olig2 antibody (Figure 5B). Olig2 was

absent in untransfected C6 cells but present at robust and similar levels in *Olig2*^{WT}- and *Olig2*^{S263A}-transfected cells.

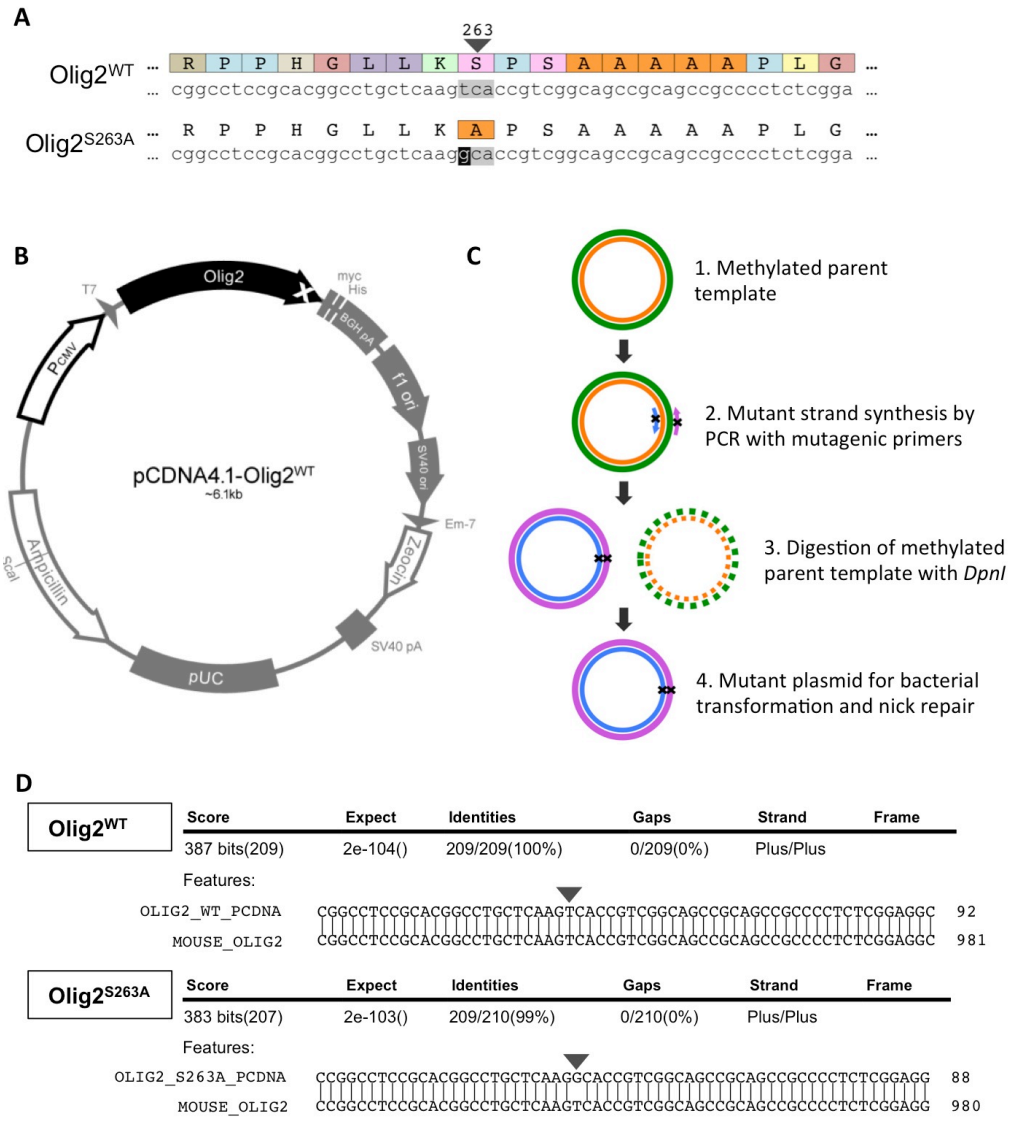

Figure 4. Olig2-S263A mutagenesis. A. Protein and DNA sequences in *Olig2*^{WT} and *Olig2*^{S263A}. **B.** Vector map of *pcDNA4.1-Olig2*^{WT} previously generated in the lab. **C.** Graphical representation of the site-directed mutagenesis strategy. Mutant *Olig2-S263A* is synthesized by PCR with mutagenic primers from the *pcDNA4.1-Olig2*^{WT} template. Methylated *pcDNA4.1-Olig2*^{WT} is removed by digestion with DpnI, leaving only the desired *pcDNA4.1-Olig2*^{S263A} for nick repair and purification. **D.** *Olig2*^{WT} and *Olig2*^{S263A} mutant construct sequences and BLAST alignment with the mouse *Olig2* coding sequence.

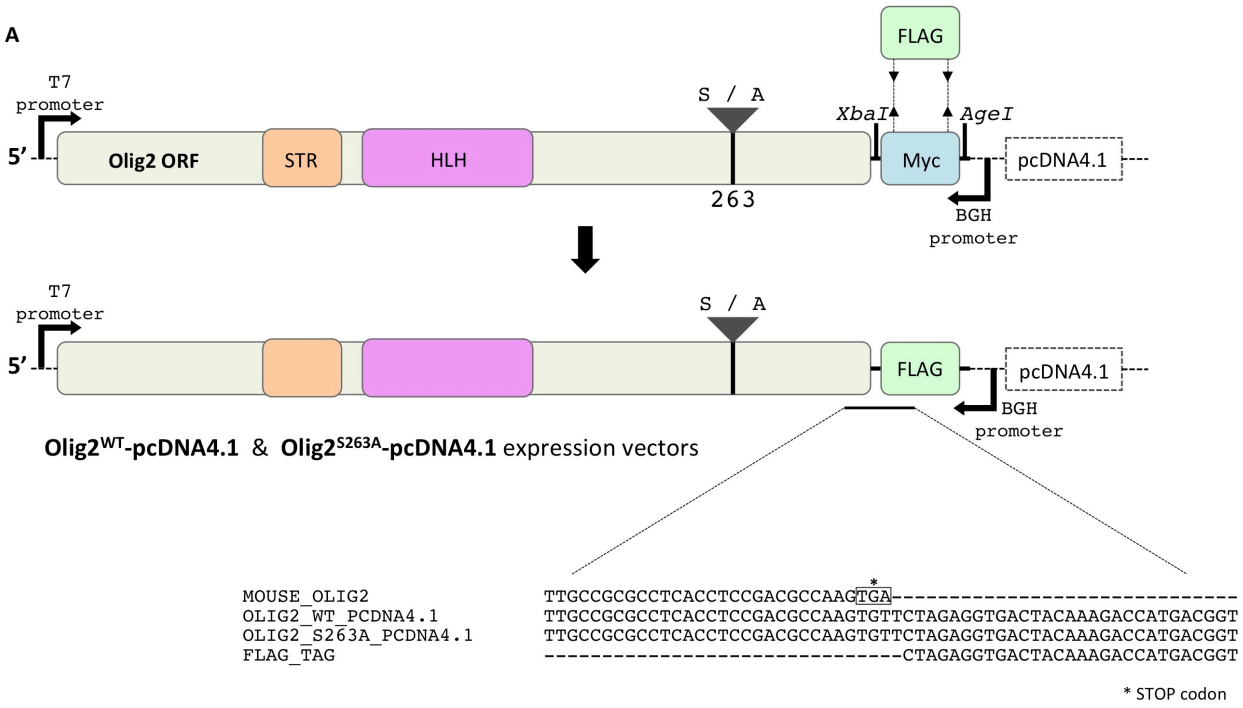

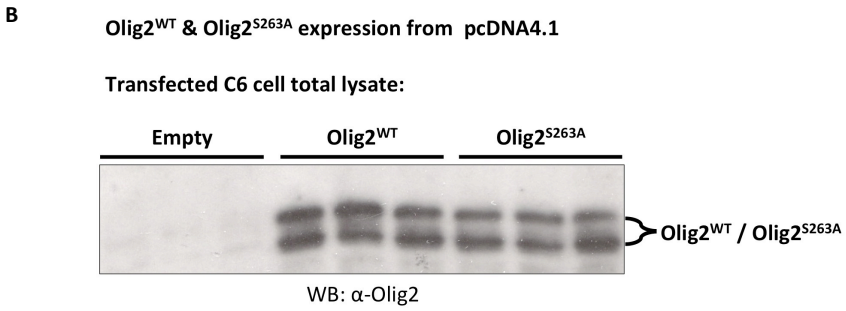

Figure 5. Incorporation of the 3' *3XFLAG* tag into *Olig2*^{WT} - & *Olig2*^{S263A} *-pcDNA4.1*. A. *Olig2*^{WT} - & *Olig2*^{S263A} *-pcDNA4.1* 3' *Myc* tag replaced with *3xFLAG* (FLAG) tag using XbaI and AgeI restriction enzymes. Generation of the complete *Olig2*^{WT} - & *Olig2*^{S263A} *-pcDNA4.1* constructs was confirmed by sequencing and ClustalO alignment with known Mouse *Olig2* and *FLAG* tag sequences. **B.** Olig2^{WT} & Olig2^{S263A} protein expression from *pcDNA4.1* in transfected C6 cells. Empty *pcDNA4.1*, Olig2^{WT} *-pcDNA4.1*, *Olig2*^{S263A} *-pcDNA4.1* were transfected into cultured C6 cells and Olig2 expression analysed by WB with an anti-Olig2 antibody.

Olig2-S263A PAC construction

In order to examine the function of Olig2 S263 phosphorylation in vivo, I aimed to generate a transgenic mouse line carrying a modified version of the original Olig2 P1 artificial chromosome (PAC) encoding the phospho-null mutant Olig2-S263A (Olig2^{S263A}) (Li et al., 2011). Crossing the *Olig2*$^{+/+}$*;Olig2*^{S263A} transgenic mouse line with the viable *Olig2*$^{+/-}$ line

maintained in the lab, it would be possible after two generations to generate *Olig2*$^{-/-}$*;Olig2*^{S263A} mice. Endogenous expression of the phospho-null Olig2-S263A mutant on an Olig2-null background will enable functional analysis of S263 phosphorylation at behavioural, histological and molecular levels. Given Olig2 knockout in mice becomes lethal at birth, the *Olig2*$^{-/-}$*;Olig2*^{S263A} mice would be expected to survive through embryogenesis and therefore provide a useful experimental tool for functional analysis. As a necessary control, I also aimed to generate a transgenic mouse line carrying the corresponding *Olig2*^{WT} PAC.

Using the *Olig2*^{WT}- and *Olig2*^{S263A}*-pcDNA4.1* expression vectors, I initially generated *Olig2*^{WT}*-/Olig2*^{S263A} targeting vectors (Figure 6). I excised and purified the *Olig2*^{WT}*-/Olig2*^{S263A}*-FLAG* cassette using restriction enzymes KpnI and AgeI and agarose gel purification. In parallel, using restriction enzymes KpnI and BglII, I excised the 5' *Olig2 homology-Olig2 ORF-Cre*^{ERT2} cassette from the *pBlueScript-Olig2* targeting vector and purified the *pBlueScript* backbone by agarose gel purification. The *Olig2*^{WT}*/Olig2*^{S263A}*-FLAG* cassette was ligated using T4 DNA ligase into the *pBlueScript-Olig2* targeting vector backbone, and electroporated into XL1-Blue *E. coli* for plasmid preparation. Sequencing and ClustalO alignment confirmed successful generation of *Olig2*^{WT} and *Olig2*^{S263A} targeting vectors.

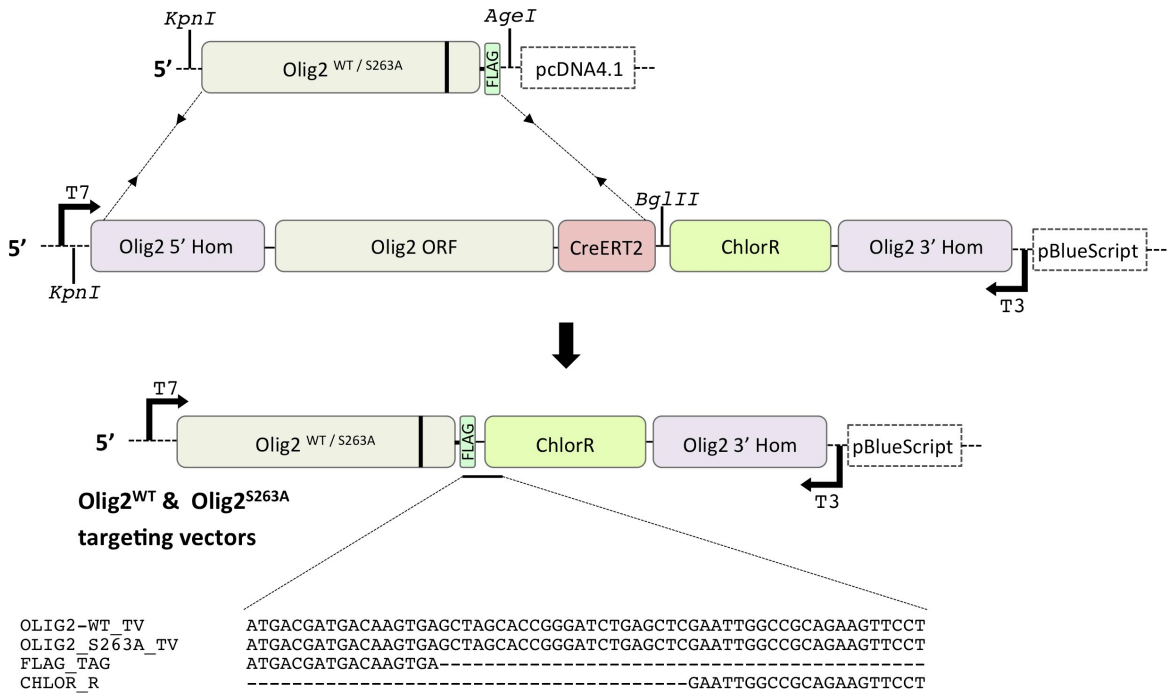

Figure 6. Generation of *Olig2^{WT}* & *Olig2^{S263A}* targeting vectors. The *Olig2^{WT}* & *Olig2^{S263A}* cassettes were excised from *pcDNA4.1* using restriction enzymes KpnI and AgeI, and cloned into the *pBlueScript* targeting vector backbone using KpnI and BglII. Generation of the *Olig2^{WT}* & *Olig2^{S263A}* targeting vectors was confirmed by sequencing and ClustalO sequence alignment with the known *FLAG* tag and chloramphenicol resistance (*ChlorR*) cassette sequences.

Finally, in order to visualize expression of the *Olig2^{WT}-/Olig2^{S263A}-FLAG* transgenes in vivo, I incorporated an *IRES-mCherry* cassette immediately downstream of the *Olig2^{WT}-/Olig2^{S263A}-FLAG* sequence (Figure 7). The *IRES-mCherry* cassette was excised from the commercially available *pmCherry C1* vector using restriction enzymes NheI and XbaI and ligated into the *Olig2^{WT}/Olig2^{S263A}* targeting vector. Sequencing and ClustalO alignment confirmed successful generation of the complete *Olig2^{WT}* and *Olig2^{S263A}* targeting vectors, including a 3' *3xFLAG* tag and *IRES-mCherry* cassette.

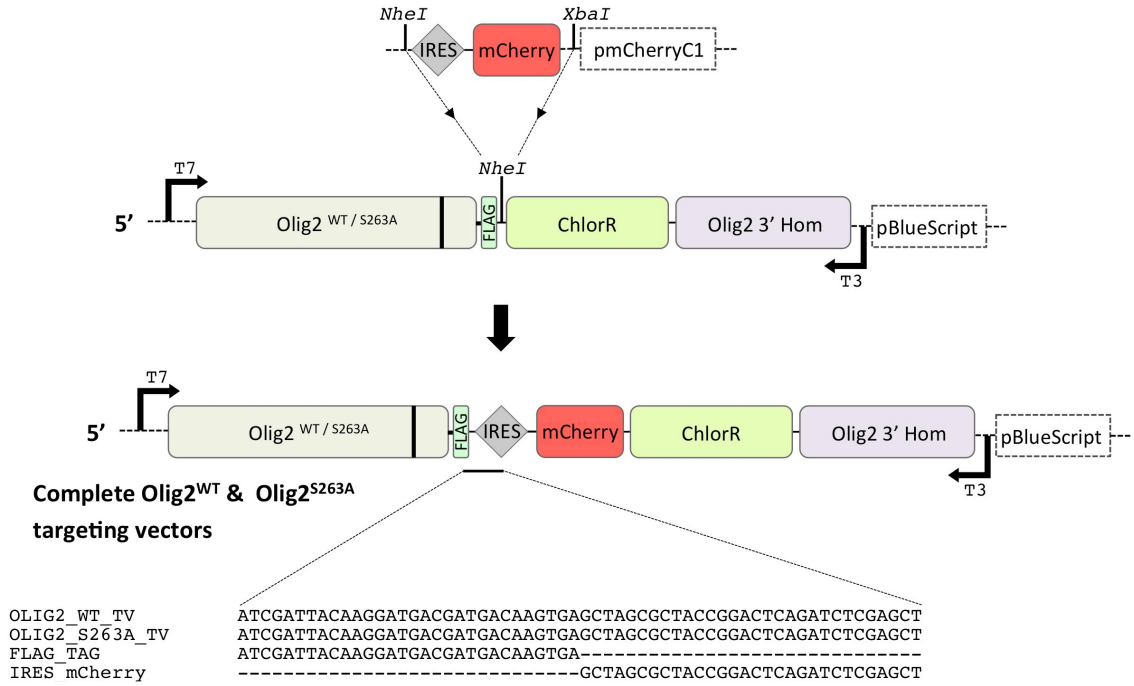

Figure 7. Incorporation of the *IRES-mCherry* cassette into *Olig2*^{WT} & *Olig2*^{S263A} targeting vectors. The *IRES-mCherry* cassette was excised from the *pmCherryC1* parent vector using restriction enzymes NheI and XbaI, and cloned into *Olig2*^{WT} & *Olig2*^{S263A} targeting vectors using NheI. Generation of the complete *Olig2*^{WT} & *Olig2*^{S263A} targeting vectors was confirmed by sequencing and ClustalO sequence alignment with the known *FLAG* tag and *IRES-mCherry* cassette sequences.

The complete and validated targeting vectors were used for homologous recombination-(HR-) mediated modification of the original *Olig2* PAC in *Escherichia coli* (Figure 8). *E. coli* strain EL250 carries a bacteriophage lambda prophage encoding: 1. the double-stranded break repair recombinase proteins Exo and Beta under the control of a temperature-sensitive *cI repressor*; 2. arabinose-inducible Flp recombinase for site-specific recombination between *frt* sites (Lee et al., 2001). In electrocompetent *E. coli* EL250 bacteria, heat-shock at 42^{o}C induced recombinase protein expression. I introduced either the complete *Olig2*^{WT} or *Olig2*^{S263A} linearized targeting vectors by electroporation. Homologous recombination between the 5' *Olig2* ORF and 3' homology region (Olig2 3' Hom) generated the *Olig2*^{WT}- and *Olig2*^{S263A}-PACs. PAC-containing EL250 bacteria were selected using the insert-specific chloramphenicol resistance (*ChlorR*) and *pPAC4* backbone-specific kanamycin resistance (*KanR*) cassettes. The *frt-ChlorR-frt* cassette was removed by arabinose-inducible Flp

expression and *frt* recombination (Figure 9A). At this stage, *Olig2*^{WT}- or *Olig2*^{S263A}-PAC generation and subsequent Flp/*frt*-mediated *ChlorR* excision was assessed by colony PCR using a forward primer that specifically annealed within the *mCherry* sequence and a reverse primer that specifically annealed downstream of the inserted construct, within the original *Olig2* PAC sequence (Figure 9B). Agarose gel analysis of the PCR products indicated successful Exo/Beta and Flp/*frt* recombination. The *Olig2*^{WT}- and *Olig2*^{S263A} PACs were purified then linearized with PvuI. The digests were resolved by pulse field gel electrophoresis (Figure 9C) and the linearized *Olig2*^{WT} and *Olig2*^{S263A} PACs purified for pronuclear injection in mice.

Over the course of the project, the *Olig2*^{WT} and *Olig2*^{S263A} PAC-transgenic lines were not established with time for generation of *Olig2*$^{-/-}$;*Olig2*$^{WT/S263A}$ mice and phenotypic analysis, primarily because of building works that disrupted transgenic production across the board for more than a year. This work is continuing as a high priority in the lab, and will – we expect – produce robust and informative data regarding the function of Olig2 S263 phosphorylation in vivo.

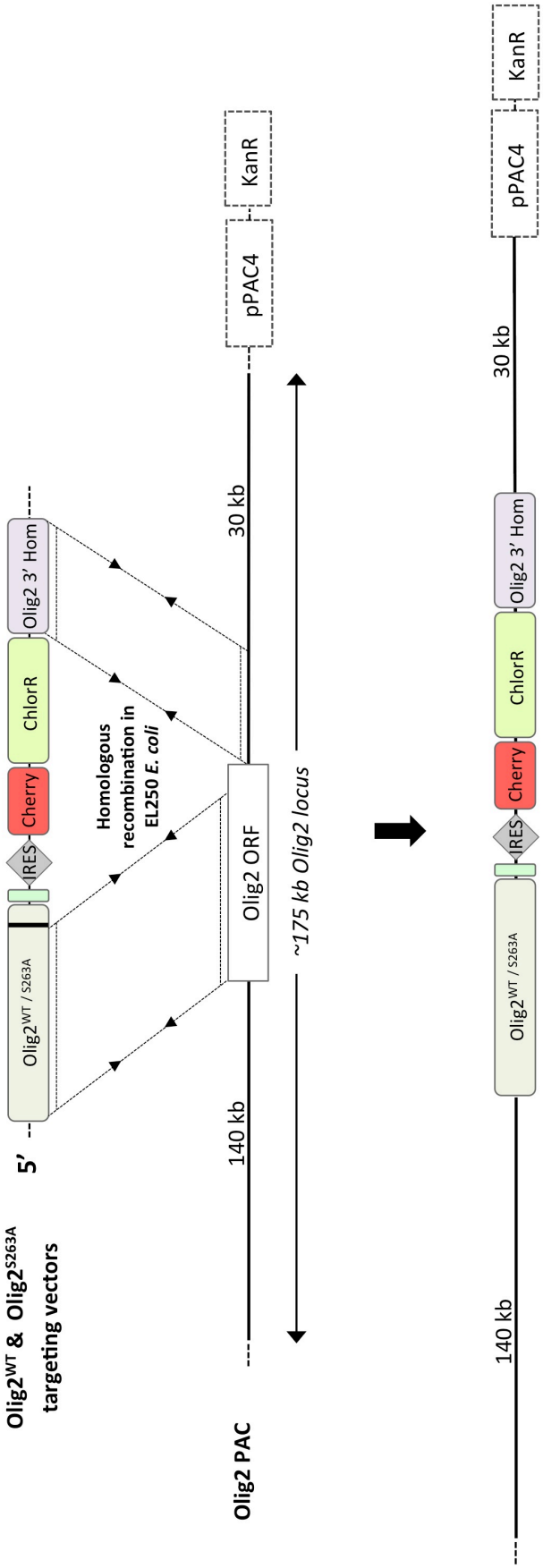

Figure 8. *Olig2* PAC recombination in EL250 *E. coli*. In *E. coli* strain EL250, the original Olig2 PAC was modified by homologous recombination with the $Olig2^{WT}$ & $Olig2^{S263A}$ targeting vectors via the *Olig2* ORF and 3' regions of homology. Kanamycin and chloramphenicol screening selected for the $Olig2^{WT}$ & $Olig2^{S263A}$ PACs.

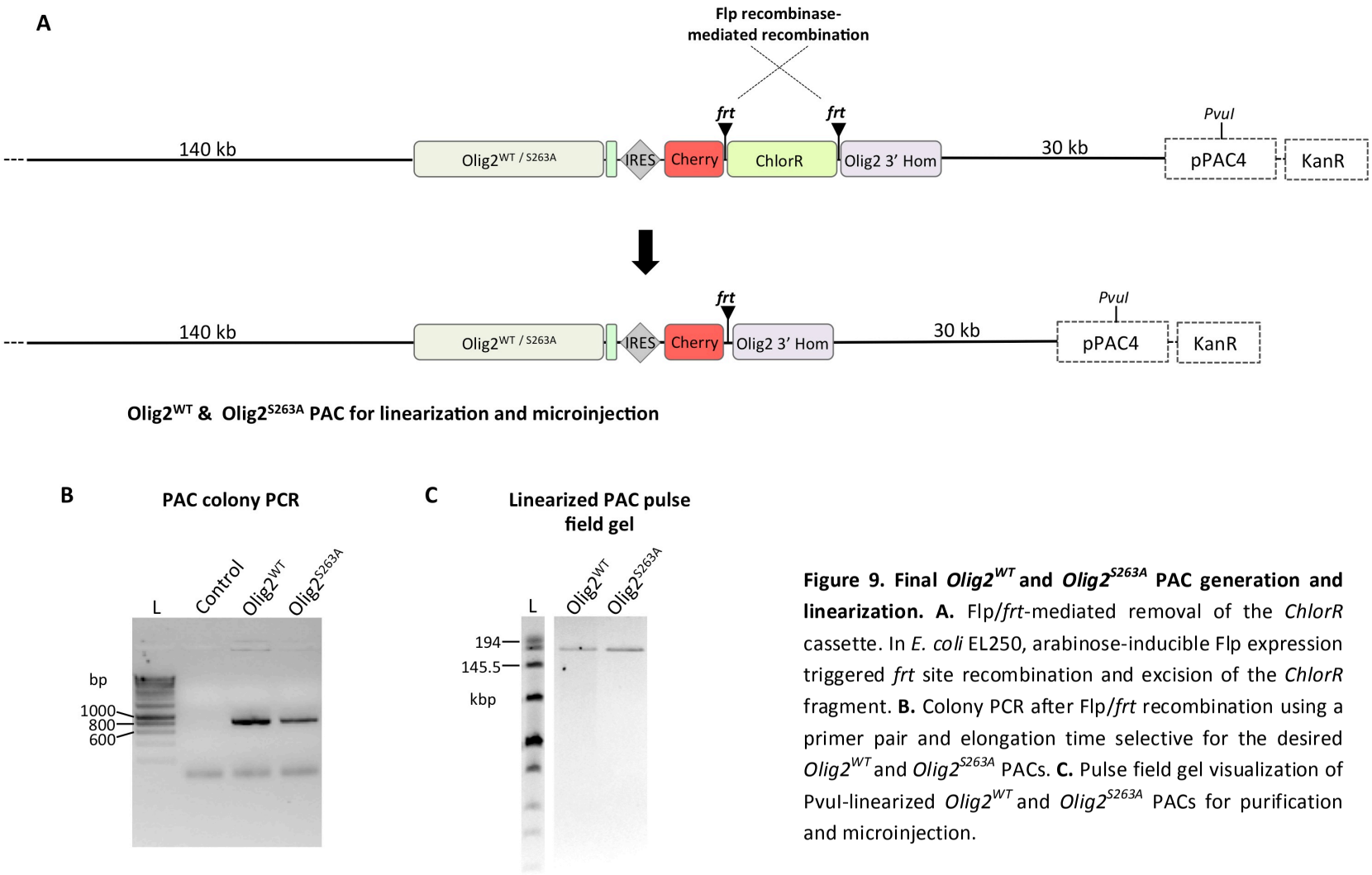

Figure 9. Final *Olig2^{WT}* and *Olig2^{S263A}* PAC generation and linearization. A. Flp/*frt*-mediated removal of the *ChlorR* cassette. In *E. coli* EL250, arabinose-inducible Flp expression triggered *frt* site recombination and excision of the *ChlorR* fragment. **B.** Colony PCR after Flp/*frt* recombination using a primer pair and elongation time selective for the desired *Olig2^{WT}* and *Olig2^{S263A}* PACs. **C.** Pulse field gel visualization of PvuI-linearized *Olig2^{WT}* and *Olig2^{S263A}* PACs for purification and microinjection.

6.3 DISCUSSION

Transcription factor Olig2 is expressed in multiple discrete populations of neurogenic and gliogenic NSCs and in OL lineage cells for the duration of OL development and myelination. In its different cellular environments, Olig2 has been shown to perform a broad range of functions, underscored by an array of specific molecular activities (Meijer et al., 2012). Post-translational modification is a well-known mediator of Olig2 function. Serine phosphorylation, for example, critically regulates NSC proliferation and differentiation by altering Olig2 intracellular localisation and cofactor choice (Setoguchi & Kondo, 2004; Sun et al., 2011; Li et al., 2011; Meijer et al., 2014).

Computational analysis of Olig2 phosphorylation

Of the annotated *Mus musculus* protein sequences, I report known TFs have a significantly higher percentage serine content than non-TFs. Moreover, with 50 serine residues among 323 amino acids (15%), Olig2 reveals itself as an exceptionally serine-rich transcription factor, ranking 13th of 542 TFs in total. Given that serine phosphorylation is a widespread mechanism for regulating protein function, the high serine content of Olig2 suggests an abundance of potential phosphorylation states and complex modulation of activity (Whitmarsh & Davis, 2000). Two-dimensional PAGE has previously revealed a wide range of differently electrically charged isoforms of wild-type Olig2 (Li et al., 2011). Critically, after calf intestinal alkaline phosphatase treatment, the Olig2 signal collapsed to a single isoelectric point, indicating that the charge variants corresponded to different phospho-forms of Olig2 (Li et al., 2011). I used the online tool NetPhos 2.0 to predict phosphorylation sites within the human Olig2 primary sequence. NetPhos 2.0 identified 25 putative phospho-acceptor serines in human Olig2. In addition, ClustalO alignment indicates 96% of these serine residues are

conserved in mouse, 68% in chick and 40% in zebrafish, with the degree of evolutionary conservation providing evidence of potential functionality. Together, the published 2D PAGE and computational analysis suggest that Olig2 can be phosphorylated at multiple sites and that the phospho-acceptor residues are critical to Olig2 function.

Combinatorial (de)phosphorylation would alter the molecular properties of Olig2 and might enable precise modification of Olig2 function under different conditions. Generation of the multiple phospho-forms of Olig2 would be determined by signaling pathway-induced activation of downstream kinase/phosphatase enzymes. Serine-rich TFs such as Olig2 could therefore act as signal integration hubs, with multiple pathways converging on a single TF to mediate the appropriate cellular response. To predict the kinases and upstream signaling pathways that target those sites identified by NetPhos 2.0, I used the online tool NetPhosK 1.0. This indicated that the predicted phospho-acceptor serine residues are substrates for an assortment of different intracellular kinases (Pearce et al., 2010; Varjosalo et al., 2013). Of the predicted kinases, several have been linked to oligodendrocyte development and myelination, with PKA and CK2 previously implicated in direct phosphorylation of Olig2 (Azim & Butt et al., 2011; Tang et al., 1998; Fragoso et al., 2007; Li et al., 2011; Baron et al., 2000; Huillard et al., 2010). It will be interesting to explore whether the reported roles of these kinases in OL lineage cells are mediated through direct phosphorylation of Olig2.

Ultimately, on top of the computational analysis presented here, establishing the bona fide phosphorylation of amino acid residues in Olig2 will be crucial to understanding the role and regulation of Olig2 in different cells and at different stages of development. Mass spectrometry and/or Edman degradation analysis of Olig2 extracted from specific sources (NSCs or OLPs, for example), in conjunction with in vitro phosphorylation assays, will provide robust evidence for the genuine phospho-modification of the as yet unvalidated phospho-

acceptor residues. Furthermore, phospho-null (and potentially phospho-mimetic) mutagenesis studies – both in vivo and in vitro – will elucidate the impact of acquiring different reversible phosphorylation states on the molecular activity and developmental function of Olig2.

Olig2 Serine 263

Of the novel phosphorylation sites predicted by computational analysis, I selected the carboxy terminal S263 for further analysis. Mass spectrometry performed on Olig2 purified from transfected COS cells mapped a high confidence phosphorylation site to S263 (Sun et al., 2011). In contrast to the typical nuclear localization of Olig2, however, ectopic Olig2 expressed in COS cells was primarily cytoplasmic. In addition, S263 phosphorylation was not seen in MS analysis of endogenous Olig2 isolated from mouse neurosphere cultures and grafted human glioma cells. As such, phospho-S263 was initially reported by Sun et al. (2011) as a potentially artefactual by-product of the in vitro COS system. Nonetheless, the observation of S263 phosphorylation by MS confirms S263 is a genuine phospho-acceptor and it remains possible that S263 phosphorylation occurs in vivo, potentially regulating the nuclear/cytoplasmic localisation of Olig2.

Computational analysis revealed that S263 is a predicted P38-MAPK target. Mitogen-activated protein kinases (MAPKs) consist of families of Ser/Thr-specific kinases that mediate the intracellular responses to extracellular stimuli through protein phosphorylation signaling cascades. Four distinct subgroups within the MAPK family have been identified, one of which is the P38-MAPKs. P38-MAPKs are activated by dual phosphorylation at conserved residues, catalyzed by upstream MAP kinase kinases (Zarubin & Han, 2005). Downstream substrates of P38-MAPK include additional kinases, as well as transcription factors that directly regulate

gene expression in response to P38-MAPK-mediated phosphorylation, such as Cyclic AMP response element-binding protein (CREB) and Activating transcription factor 1 (ATF1) (Tan et al., 1996).

Research from a number of labs has revealed important roles of P38-MAPK signaling in OLP differentiation and myelination (Baron et al., 2000; Fragoso et al., 2007; Hu et al., 2012; Rafalski et al., 2013). I analyzed the effect of the potent P38-MAPK agonist anisomycin on OLP specification from NSCs in vitro (Zinck et al., 1995). Using wild-type primary NSC cultures, I confirmed that anisomycin activates P38-MAPK and observed a near-complete ablation of OLP formation in anisomycin-treated cultures. It should be acknowledged, however, that these data do not prove a causal link between P38-MAPK activation and NSC differentiation. Anisomycin is a translational inhibitor of protein synthesis that activates kinase pathways besides P38, including the ribosomal S6 kinases (RSKs) and stress-activated c-Jun N-terminal kinases (JNKs) (Kardalinou et al., 1994; Hazzalin et al., 1998). It remains possible, therefore, that the effect of anisomycin treatment on generation of OLPs from primary NSCs in culture occurs via a non-P38-mediated pathway. Indeed, the anti-OL effects of anisomycin treatment described here contrast with the published data on P38 activity and OL development. Selective P38 inhibition using small molecule antagonists indicates that P38 activity is necessary for myelin formation, and the expansion and differentiation of OLPs (Cui et al., 2014; Hu et al., 2012; Rafalski et al., 2013; Haines et al., 2008; Bhat et al., 2007; Fragoso et al., 2007). Understanding the results shown here will require distinguishing the critical factor(s) mediating the anisomycin-induced inhibition of oligodendrogenesis. If P38 were isolated as a key component of the anti-OLP specification pathway activated in anisomycin-treated NSCs, this would demonstrate opposing functions for P38 in NSCs and OLPs, inhibiting and promoting OL lineage progression, respectively.

Research exploring the mechanisms of P38-mediated regulation of rodent OLP differentiation revealed that P38 regulates the DNA-binding activity of OL lineage TF Sox10 (Chew et al., 2010). Activated P38 is proposed to induce Sox10 occupancy of and thereby transcription from myelin gene promoters, including MBP. It should be noted that Chew et al. (2010) did not confirm direct phosphorylation of Sox10 by P38-MAPK, so the reported impact of P38 activation/inhibition on Sox10 activity might occur via regulation of an additional factor, such as Olig2. In fact, analysis of Sox protein cofactor choice indicated that mouse Sox10 can physically interact with Olig2 (Wissmuller et al., 2006; Li et al., 2007). Moreover, the computational prediction of kinase substrate residues in human Olig2, shown here, identified S263 – conserved in mouse and chick – as a P38-MAPK target. P38-induced phosphorylation of Olig2 S263 might regulate Olig2/Sox10 complex formation and thereby alter the DNA-binding activity of Sox10 in mammalian OLPs. In zebrafish, by contrast, Olig2 and Sox10 do not associate and – on the basis of protein sequence alignment – human Olig2 S263 is not conserved (Li et al., 2007). The correlation between the presence or absence of S263 and the ability of Sox10 and Olig2 to interact in zebrafish versus mouse is consistent with S263 facilitating Olig2/Sox10 complex formation. In any case, P38-MAPK signaling has important consequences for OL development, the roles of Olig2 in which remain to be fully established.

In addition to P38-MAPK, Olig2 S263 is a predicted target of other kinases with important functions in OL development, including CDK5 and GSK3. Below is a brief summary highlighting the various roles of CDK5 and GSK3 in the OL lineage:

Cyclin dependent kinase 5 (CDK5)

The cyclin-dependent kinases (CDKs) are a family of protein kinases predominantly involved in cell cycle regulation. However, CDK5 – related to CDK1 – has not been implicated in control of cell cycle progression. CDK5 is activated exclusively in the nervous system by the CNS-

specific co-activators P35 and P39, and critically regulates certain aspects of neural development including OL migration, differentiation and myelination (Lew et al., 1994; Tsai et al., 1994; Tang et al., 1998; Miyamoto et al., 2007; Miyamoto et al., 2008; He et al., 2011; Yang et al., 2013; Luo et al., 2014). Research from Tang et al. (1998) reported that differentiation of OLs in culture is accompanied by increasing CDK5 activity, suggesting that CDK5 plays a role in OL differentiation (Tang et al., 1998). In vitro, inhibition of CDK5 impaired OL differentiation and reduced OLP migration in response to PDGF (Miyamoto et al., 2007; Miyamoto et al., 2008). In addition, *Emx1-Cre*- and *Olig1-Cre*-mediated *CDK5* knockout in mice impairs OL differentiation in vivo and generates a hypomyelination phenotype (He et al., 2011; Yang et al., 2013). In *CNP-Cre;CDK5*$^{fl/fl}$ conditional knockout mice, myelin repair is also significantly reduced in response to focal demyelinating lesions compared to wild-type animals, despite increased numbers of Olig2-expressing OL lineage cells (Luo et al., 2014). With regard to the mechanisms of CDK5-mediated regulation of OLP migration and differentiation, direct phosphorylation of WAVE2 and Paxillin have been proposed respectively (Miyamoto et al., 2007; Miyamoto et al., 2008). It remains possible, however, that Olig2 is itself a downstream target of CDK5 and is responsible for mediating CDK5 function in OL development.

Glycogen synthase kinase 3 (GSK3)

Initially classified as a kinase exclusively involved in glycogen metabolism, glycogen synthase kinase 3 has since been established as a critical mediator of multiple cell signaling pathways, including proliferation and differentiation signals (Cohen & Frame, 2001). Indeed, GSK3B mediates signaling by insulin-growth factor 1 (IGF-1), fibroblast growth factor 2 (FGF-2), Wnt and Notch, all of which have established and important roles in OL specification and/or development (Wang et al., 1998; Baron et al., 2000; Zeger et al., 2007; Langseth et al., 2010). Exploring the role of GSK3B in OL differentiation in the developing white matter by

intraventricular administration of GSK3B inhibitors revealed that GSK3B is a potent negative regulator of OL differentiation in vivo (Azim & Butt, 2011). In experiments aimed at analysing the role of GSK3 signaling on OLP generation in the postnatal subventricular zone, inhibition of GSK3B robustly stimulated NSC proliferation and oligodendrogenesis (Azim et al., 2014). In addition, CDK5 modulation of OL development and myelination is mediated in part through CDK5-induced inactivation of GSK3B (Luo et al., 2014). The protein substrates of GSK3B that mediate its inhibitory role in OL differentiation have not been established. Olig2 might, therefore, be an important phosphorylation target and downstream effector of GSK3 signaling, with S263 the target phospho-acceptor residue within Olig2.

Olig2-S263A expression vector and PAC analysis

The identification by Sun et al. (2011) of Olig2 S263 phosphorylation by MS, combined with its evolutionary conservation and the computational prediction of S263 as a substrate for several protein kinases with known roles in OL lineage cell development/function justifies further analysis of Olig2-S263 phosphorylation. I have reported successful construction of a phospho-null mutant *Olig2-S263A*-encoding expression vector and PAC for effective examination of S263 phosphorylation in vitro and in vivo. Here I will outline how these tools can be used to yield information about regarding S263 phosphorylation and its involvement in OL development.

The *Olig2*^{WT}- and *Olig2*^{S263A}*-pcDNA 4.1* expression vectors will enable confirmation of Olig2 S263 phosphorylation by P38/CDK5/GSK3 in vitro. In *Olig2*^{WT}-transfected C6 glioma cells in culture, Olig2 IP and WB using Olig2- and phospho-serine-specific antibodies would detect dynamic Olig2 phosphorylation after drug-induced activation or inhibition of the P38/CDK5/GSK3 signaling pathways. In this approach, altered Olig2/phospho-serine WB

signal under different conditions would indicate P38-/CDK5-/GSK3-mediated phosphorylation of wild-type Olig2. Parallel experiments performed with Olig2^{S263A}-transfected C6 cells would indicate whether S263 is a target phospho-acceptor site under these conditions.

Generation of *Olig2*^{WT} and *Olig2*^{S263A} PAC-transgenic mice will enable in vivo analysis of the developmental requirement for Olig2 S263 phosphorylation. Using the *Olig2*$^{+/-}$ mouse line maintained in the lab it will be possible to generate *Olig2*$^{-/-}$*;Olig2*^{WT} and *Olig2*$^{-/-}$*;Olig2*^{S263A} mice. The complement of a single copy of wild-type *Olig2* – expressed from a modified version of the original *Olig2* PAC – is expected to be sufficient for *Olig2*$^{-/-}$*;Olig2*^{WT} PAC-transgenic mice to develop and survive normally (Li et al., 2011). In *Olig2*$^{-/-}$*;Olig2*^{S263A} PAC-transgenic mice, Olig2-S263A expression will model constitutive dephosphorylation of Olig2 at S263. Deficits in CNS development and behaviour in *Olig2*$^{-/-}$*;Olig2*^{S263A} mice versus the *Olig2*$^{-/-}$*;Olig2*^{WT} controls will therefore reveal the biological readouts of S263 phosphorylation. At a cellular level, inclusion of the *IRES-mCherry* reporter construct will enable straightforward analysis of Olig2 expression and Olig2+ cell number, character and distribution at different stages of embryonic and post-natal development. In addition to supporting direct in vivo analysis, the *Olig2*$^{-/-}$*;Olig2*^{S263A} mice might provide a useful source of cellular material for ex vivo molecular analysis of Olig2-S263A, such as protein cofactor or gene target choice (see *Olig2 S147 phosphorylation & gene target choice*).

Summary

Computational examination indicates that Olig2 contains multiple phospho-acceptor residues and that these residues are the targets of a number of different protein kinases. Of the putative phosphorylation sites revealed in silico, S263 – conserved in chick, mouse and human – has previously been validated as a genuine phospho-acceptor by MS analysis (Sun

et al., 2011). Olig2 S263 is a predicted substrate for P38-MAPK, GSK3 and CDK5, kinases with established roles in OL formation and myelination. An attractive hypothesis, therefore, is that S263 phosphorylation modifies Olig2 function and directly mediates the effects of kinase activity in OL lineage cells. A combination of in vitro and in vivo approaches using the Olig2-S263A expression and PAC constructs I have generated will, I anticipate, produce useful information regarding Olig2 S263 phosphorylation. Ultimately, identifying the bona fide Olig2 phosphorylation sites, and determining the regulation of each modification and its impact on Olig2 function, will be fundamental to a detailed understanding of CNS development.

CHAPTER 7

SUMMARY & CONCLUSIONS

In the developing CNS, OLPs arise in discrete regions and at specific stages of development (reviewed by Richardson et al., 2006). In the forebrain, the first OLPs emerge from ventral, MGE-resident NSCs at approximately E11.5 in mouse. Successive waves of oligodendrogenesis then occur from the LGE/CGE at ~E15 and finally from the cortex at early post-natal stages. In the spinal cord, the majority (~80%) of OLPs derive from NSCs resident in the ventral pMN domain, with the first pMN-derived OLPs appearing at ~E12.5. The remaining fraction is born later – from ~E15 – from more dorsal regions of the spinal cord. In terms of function, the different populations of OL lineage cells – defined according to developmental origin – are typically redundant, although specific patterns of migration and myelination have been described for the ventral and dorsal spinal OL populations (Kessaris et al., 2006; Tripathi et al., 2011). The mechanisms underlying the precise spatio-temporal regulation of OLP formation during development, however, remain only partially understood.

In the embryonic spinal cord, graded Shh signaling – emanating from the ventral notochord and floorplate – induces combinatorial expression of specific TFs in ventricular zone NSCs at different distances from the ventral midline (Dessaud et al., 2008). Specific TF expression profiles define distinct progenitor domains, the NSC populations of which sequentially generate characteristic neuronal and glial subtypes (Jessel, 2000). In the case of the pMN domain, the NSCs form MNs before switching to form OLPs. Expression of the bHLH TF Olig2 is specific to pMN NSCs and is essential for both MN and OLP production (Lu et al., 2000; Zhou et al., 2000; Lu et al., 2002; Park et al., 2002; Zhou et al., 2002). Recent research from

the Richardson lab has revealed a crucial role for Olig2 phosphorylation in the MN-OLP fate switch (Li et al., 2011). Initially, during the patterning and neurogenic phases of spinal development, Olig2 is phosphorylated at S147. Dephosphorylation of S147 profoundly alters the molecular properties of Olig2 and induces the switch in NSC fate.

Regulation of Olig2 phosphorylation and NSC fate

At both molecular and cellular levels, the upstream signals that trigger Olig2 S147 dephosphorylation and the fate switch are not known. In research focused on establishing the developmental cues that govern the timing of the MN to OLP fate switch, I examined the role of angiogenesis in pMN NSC development. Constructing a timeline of spinal cord angiogenesis, the observed expansion of the vascular network over the period of the MN-OLP switch is consistent with an instructive role for angiogenesis in regulating pMN NSC fate. The vasculature could, I hypothesized, directly induce the fate switch through one or a combination of three signaling mechanisms: 1. Oxygen signaling; 2. Endocrine signaling; 3. EC-NSC contact signaling. The results reported here indicate oxygen is an important regulator of OLP specification in vitro. Research performed in mice, however, did not clearly establish any regulatory function for oxygen or vascular development in spinal OLP formation in vivo. Further research is required to establish if angiogenesis is necessary for timely OLP production.

In addition, fundamental to understanding the regulation of the fate switch will be elucidating the intracellular signaling pathways that culminate in the dephosphorylation of Olig2 at S147. In order to identify candidate phosphatases responsible for S147 phosphate removal, I analysed published microarray data for phosphatases and phosphatase components with differential expression in NSCs and OLPs. RNA ISH and immunolabeling

experiments confirmed down-regulation of the inhibitory Ppp1r14a subunit of PP1 in Olig2-expressing pMN NSCs over the fate switch. This data suggests in pre-fate switch pMN NSCs, Olig2 S147 phosphorylation might be preserved through Ppp1r14a-mediated regulation of PP1 activity. Repression of Ppp1r14a in pMN NSCs – induced by as yet unknown upstream signals – would activate PP1 and induce Olig2 S147 dephosphorylation. Analysis of a conditional *Ppp1r14a*-null mouse line will reveal the in vivo requirement of dynamic Ppp1r14a expression for normal MN/OLP production. To date, however, attempts to recover Ppp1r14a-null embryonic stem cell clones from the EUCOMM repository have been unsuccessful. I have received the Ppp1r14a targeting vector from EUCOMM but sequencing indicates it does not contain the correct features.

Molecular mechanisms of Olig2 function

Dimerization is critical for bHLH TF activity and phosphorylation of S147 is known to alter the protein binding properties of Olig2 (Li et al., 2011). Moreover, S147 is located within the DNA-binding HLH domain, suggesting the phosphorylation state of S147 could influence Olig2 occupancy of specific genomic binding sites. In addition to the developmental and molecular regulation of Olig2 dephosphorylation and the MN-OLP fate switch, I explored the effect of S147 phosphorylation on Olig2 gene target choice. Performing ChIP-qPCR and ChIP-seq from primary Olig2-expressing NSC cultures, I have identified an array of phospho-S147 Olig2 gene targets. Using the phospho-null Olig2-S147A mutant model, I have revealed a critical effect of S147 dephosphorylation on Olig2 gene target binding activity. Phospho-S147 Olig2 occupied E-box sequences of genes linked to neural development and function. I found the set of phospho-Olig2 gene targets in the NSCs was highly concordant with a published Olig2 ChIP-seq dataset from cultured OLPs, suggesting that Olig2 gene target choice is similar in pre-fate switch NSCs and OLPs (Yu et al., 2013). In contrast, however, Olig2-S147A expressed in NSCs

– modeling post-fate switch NSCs – did not display any specific DNA-binding activity. This suggests that dephosphorylated Olig2 vacates its gene target binding sites in oligodendrogenic NSCs, before reoccupying the majority of sites in committed OLPs. It remains to be established whether the observed transience of Olig2/DNA dissociation coincides with rephosphorylation at S147. Ultimately, this data offers valuable insight into the highly dynamic molecular activity of Olig2 and will provide a useful foundation for a detailed understanding of how Olig2 regulates NSC fate in the developing spinal cord.

Additional phospho-regulation of Olig2

In addition to pMN domain-resident NSCs, Olig2 is expressed throughout the OL lineage, from nascent OLPs to fully mature and myelinating OLs, as well as in a number of distinct neurogenic and gliogenic stem cell populations (reviewed in Meijer et al., 2013). Accompanying the broad expression of Olig2 is a diverse array of cell-type-specific functions. For TFs such as Olig2, post-translational modifications of specific amino acids frequently direct TF function in specific cellular contexts (Benayoun & Veitia, 2009; Filtz et al., 2014). Phosphorylation of Olig2 at specific serine residues – the most common phospho-amino acid – alters intracellular and intranuclear localisation, cofactor choice and gene target recognition, and profoundly regulates neural progenitor proliferation and neural lineage development in vitro and in vivo (Setoguchi & Kondo, 2004; Li et al., 2011; Sun et al., 2008; Meijer et al., 2014). I report that, in mouse, TFs have a significantly higher serine content relative to non-TF proteins, and Olig2 is one of the most serine-rich TFs. The range of expression and developmental functions described for Olig2 could, I propose, be dependent on the modification of multiple phospho-acceptor residues, the status of which would determine Olig2 activity and function.

I have also generated expression vector and PAC constructs for in vitro and in vivo analysis of Olig2 S263 phosphorylation. MS previously identified S263 as a genuine phosphorylation site (Sun et al., 2011). S263 is a putative substrate of P38-MAPK, GSK3 and CDK5, and the genetic tools described here should enable confirmation of kinase-mediated S263 phosphorylation and examination of the physiological requirement of S263 phosphorylation for proper Olig2 function in vivo.

The data presented here provides valuable insight into potentially important phospho-acceptor sites in Olig2 and will be a useful resource for future research. Ultimately, establishing the bona fide phosphorylation sites on Olig2 and the kinases acting on each, as well as the molecular and developmental function of each modification, will be vital for our understanding of Olig2 and its roles in the CNS.

Final remarks

Oligodendrocytes are the myelinating cells of the central nervous system, ensheathing axons and facilitating rapid saltatory conduction of action potentials. In evolution, the emergence of CNS myelin was critical to the formation of larger and more complex neural networks (Hartline & Coleman, 2007). Moreover, myelination has recently been revealed to be necessary for the acquisition of new skills in a mouse model of motor learning, and loss of myelin is a pathophysiology associated with several major neurodegenerative diseases, most significantly multiple sclerosis (Compston & Coles, 2002; McKenzie et al., 2014). The involvement of OLs in fundamental neurological processes and disease has stimulated intense scientific interest in these cells. In animal models of demyelinating diseases and spinal cord injury, proof-of-concept studies have demonstrated robust remyelination with cell replacement strategies, though OL-/myelin-linked cell-based treatments remain

unavailable in the clinic (Yasuda et al., 2011; Huang & Franklin, 2012). At the level of basic research, modern imaging and genetic tools combined with next generation sequencing technologies have brought significant advances in our understanding of OL development and function. In the research reported here, I have applied a range of methods to address important outstanding questions and provide experimental resources for future research. Ultimately, examining OL formation and myelination in vivo and in vitro and integrating the knowledge into robust models of OL development will inform the future generation of clinically viable treatments for demyelinating diseases.

REFERENCES

Alonso, G. (2000). "Prolonged corticosterone treatment of adult rats inhibits the proliferation of oligodendrocyte progenitors present throughout white and gray matter regions of the brain." Glia **31**(3): 219-231.

Anderson, M. J., V. N. Pham, et al. (2008). "Loss of unc45a precipitates arteriovenous shunting in the aortic arches." Dev Biol **318**(2): 258-267.

Arai, K. and E. H. Lo (2009). "An oligovascular niche: cerebral endothelial cells promote the survival and proliferation of oligodendrocyte precursor cells." J Neurosci **29**(14): 4351-4355.

Arteel, G. E., R. G. Thurman, et al. (1995). "Evidence that hypoxia markers detect oxygen gradients in liver: pimonidazole and retrograde perfusion of rat liver." Br J Cancer **72**(4): 889-895.

Azim, K. and A. M. Butt (2011). "GSK3beta negatively regulates oligodendrocyte differentiation and myelination in vivo." Glia **59**(4): 540-553.

Azim, K., O. Raineteau, et al. (2012). "Intraventricular injection of FGF-2 promotes generation of oligodendrocyte-lineage cells in the postnatal and adult forebrain." Glia **60**(12): 1977-1990.

Azim, K., A. Rivera, et al. (2014). "GSK3beta regulates oligodendrogenesis in the dorsal microdomain of the subventricular zone via Wnt-beta-catenin signaling." Glia **62**(5): 778-779.

Balaskas, N., A. Ribeiro, et al. (2012). "Gene regulatory logic for reading the Sonic Hedgehog signaling gradient in the vertebrate neural tube." Cell **148**(1-2): 273-284.

Baron, W., B. Metz, et al. (2000). "PDGF and FGF-2 signaling in oligodendrocyte progenitor cells: regulation of proliferation and differentiation by multiple intracellular signaling pathways." Mol Cell Neurosci **15**(3): 314-329.

Barres, B. A., M. A. Lazar, et al. (1994). "A novel role for thyroid hormone, glucocorticoids and retinoic acid in timing oligodendrocyte development." Development **120**(5): 1097-1108.

Benayoun, B. A. and R. A. Veitia (2009). "A post-translational modification code for transcription factors: sorting through a sea of signals." Trends Cell Biol **19**(5): 189-197.

Benayoun, B. A. and R. A. Veitia (2009). "A post-translational modification code for transcription factors: sorting through a sea of signals." Trends Cell Biol **19**(5): 189-197.

Benedito, R., C. Roca, et al. (2009). "The notch ligands Dll4 and Jagged1 have opposing effects on angiogenesis." Cell **137**(6): 1124-1135.

Bhat, N. R., P. Zhang, et al. (2007). "p38 MAP kinase regulation of oligodendrocyte differentiation with CREB as a potential target." Neurochem Res **32**(2): 293-302.

Bilican, B., C. Fiore-Heriche, et al. (2008). "Induction of Olig2 precursors by FGF involves BMP signalling blockade at the Smad level." PLoS One **3**(8): e2863.

Blanco, R. and H. Gerhardt (2013). "VEGF and Notch in tip and stalk cell selection." Cold Spring Harb Perspect Med **3**(1): a006569.

Blom, N., S. Gammeltoft, et al. (1999). "Sequence and structure-based prediction of eukaryotic protein phosphorylation sites." J Mol Biol **294**(5): 1351-1362.

Bollen, M., W. Peti, et al. (2010). "The extended PP1 toolkit: designed to create specificity." Trends Biochem Sci **35**(8): 450-458.

Briscoe, J., A. Pierani, et al. (2000). "A homeodomain protein code specifies progenitor cell identity and neuronal fate in the ventral neural tube." Cell **101**(4): 435-445.

Briscoe, J., L. Sussel, et al. (1999). "Homeobox gene Nkx2.2 and specification of neuronal identity by graded Sonic hedgehog signalling." Nature **398**(6728): 622-627.

Bullock, T. H., J. K. Moore, et al. (1984). "Evolution of myelin sheaths: both lamprey and hagfish lack myelin." Neurosci Lett **48**(2): 145-148.

Cahoy, J. D., B. Emery, et al. (2008). "A transcriptome database for astrocytes, neurons, and oligodendrocytes: a new resource for understanding brain development and function." J Neurosci **28**(1): 264-278.

Cai, J., Y. Chen, et al. (2007). "A crucial role for Olig2 in white matter astrocyte development." Development **134**(10): 1887-1899.

Cai, J., Y. Qi, et al. (2005). "Generation of oligodendrocyte precursor cells from mouse dorsal spinal cord independent of Nkx6 regulation and Shh signaling." Neuron **45**(1): 41-53.

Cai, J., Q. Zhu, et al. (2010). "Co-localization of Nkx6.2 and Nkx2.2 homeodomain proteins in differentiated myelinating oligodendrocytes." Glia **58**(4): 458-468.

Chandran, S., D. Hunt, et al. (2008). "Myelin repair: the role of stem and precursor cells in multiple sclerosis." Philos Trans R Soc Lond B Biol Sci **363**(1489): 171-183.

Chandran, S., H. Kato, et al. (2003). "FGF-dependent generation of oligodendrocytes by a hedgehog-independent pathway." Development **130**(26): 6599-6609.

Chen, B. Y., X. Wang, et al. (2013). "Brain-derived neurotrophic factor stimulates proliferation and differentiation of neural stem cells, possibly by triggering the Wnt/beta-catenin signaling pathway." J Neurosci Res **91**(1): 30-41.

Chen, E., S. Hermanson, et al. (2004). "Syndecan-2 is essential for angiogenic sprouting during zebrafish development." Blood **103**(5): 1710-1719.

Chen, H. L., F. Pistollato, et al. (2007). "Oxygen tension regulates survival and fate of mouse central nervous system precursors at multiple levels." Stem Cells **25**(9): 2291-2301.

Chen, J., N. Imanaka, et al. (2010). "Hypoxia potentiates Notch signaling in breast cancer leading to decreased E-cadherin expression and increased cell migration and invasion." Br J Cancer **102**(2): 351-360.

Chen, J. A., Y. P. Huang, et al. (2011). "Mir-17-3p controls spinal neural progenitor patterning by regulating Olig2/Irx3 cross-repressive loop." Neuron **69**(4): 721-735.

Chen, L. P., Z. F. Li, et al. (2012). "Regulation of Olig2 during astroglial differentiation in the subventricular zone of a cuprizone-induced demyelination mouse model." Neuroscience **221**: 96-107.

Chen, Y., D. K. Miles, et al. (2008). "The basic helix-loop-helix transcription factor olig2 is critical for reactive astrocyte proliferation after cortical injury." J Neurosci **28**(43): 10983-10989.

Cheng, X., Y. Wang, et al. (2007). "Bone morphogenetic protein signaling and olig1/2 interact to regulate the differentiation and maturation of adult oligodendrocyte precursor cells." Stem Cells **25**(12): 3204-3214.

Chew, L. J., W. Coley, et al. (2010). "Mechanisms of regulation of oligodendrocyte development by p38 mitogen-activated protein kinase." J Neurosci **30**(33): 11011-11027.

Chiang, C., Y. Litingtung, et al. (1996). "Cyclopia and defective axial patterning in mice lacking Sonic hedgehog gene function." Nature **383**(6599): 407-413.

Chizhikov, V. V. and K. J. Millen (2004). "Mechanisms of roof plate formation in the vertebrate CNS." Nat Rev Neurosci **5**(10): 808-812.

Clarner, T., A. Parabucki, et al. (2011). "Corticosteroids impair remyelination in the corpus callosum of cuprizone-treated mice." J Neuroendocrinol **23**(7): 601-611.

Cohen, P. and S. Frame (2001). "The renaissance of GSK3." Nat Rev Mol Cell Biol **2**(10): 769-776.

Compston, A. and A. Coles (2002). "Multiple sclerosis." Lancet **359**(9313): 1221-1231.

Compston, A. and A. Coles (2008). "Multiple sclerosis." Lancet **372**(9648): 1502-1517.

Conti, L., S. M. Pollard, et al. (2005). "Niche-independent symmetrical self-renewal of a mammalian tissue stem cell." PLoS Biol **3**(9): e283.

Copray, S., V. Balasubramaniyan, et al. (2006). "Olig2 overexpression induces the in vitro differentiation of neural stem cells into mature oligodendrocytes." Stem Cells **24**(4): 1001-1010.

Costello, D. J., A. F. Eichler, et al. (2009). "Leukodystrophies: classification, diagnosis, and treatment." Neurologist **15**(6): 319-328.

Cristofaro, B., Y. Shi, et al. (2013). "Dll4-Notch signaling determines the formation of native arterial collateral networks and arterial function in mouse ischemia models." Development **140**(8): 1720-1729.

Cui, Q. L., J. Fang, et al. (2014). "Role of p38MAPK in S1P receptor-mediated differentiation of human oligodendrocyte progenitors." Glia **62**(8): 1361-1375.

Dai, Z. M., S. Sun, et al. (2014). "Stage-specific regulation of oligodendrocyte development by Wnt/beta-catenin signaling." J Neurosci **34**(25): 8467-8473.

De Robertis, E., H. M. Gerschenfeld, et al. (1958). "Cellular mechanism of myelination in the central

nervous system." J Biophys Biochem Cytol **4**(5): 651-656.

Delaunay, D., K. Heydon, et al. (2008). "Early neuronal and glial fate restriction of embryonic neural stem cells." J Neurosci **28**(10): 2551-2562.

Dessaud, E., A. P. McMahon, et al. (2008). "Pattern formation in the vertebrate neural tube: a sonic hedgehog morphogen-regulated transcriptional network." Development **135**(15): 2489-2503.

Dessaud, E., V. Ribes, et al. (2010). "Dynamic assignment and maintenance of positional identity in the ventral neural tube by the morphogen sonic hedgehog." PLoS Biol **8**(6): e1000382.

Dessaud, E., L. L. Yang, et al. (2007). "Interpretation of the sonic hedgehog morphogen gradient by a temporal adaptation mechanism." Nature **450**(7170): 717-720.

Du, Z. W., X. J. Li, et al. (2006). "Induced expression of Olig2 is sufficient for oligodendrocyte specification but not for motoneuron specification and astrocyte repression." Mol Cell Neurosci **33**(4): 371-380.

Echelard, Y., D. J. Epstein, et al. (1993). "Sonic hedgehog, a member of a family of putative signaling molecules, is implicated in the regulation of CNS polarity." Cell **75**(7): 1417-1430.

Eichmann, A. and J. L. Thomas (2013). "Molecular parallels between neural and vascular development." Cold Spring Harb Perspect Med **3**(1): a006551.

Erecinska, M. and I. A. Silver (2001). "Tissue oxygen tension and brain sensitivity to hypoxia." Respir Physiol **128**(3): 263-276.

Ericson, J., S. Morton, et al. (1996). "Two critical periods of Sonic Hedgehog signaling required for the specification of motor neuron identity." Cell **87**(4): 661-673.

Ericson, J., P. Rashbass, et al. (1997). "Pax6 controls progenitor cell identity and neuronal fate in response to graded Shh signaling." Cell **90**(1): 169-180.

Esain, V., J. H. Postlethwait, et al. (2010). "FGF-receptor signalling controls neural cell diversity in the zebrafish hindbrain by regulating olig2 and sox9." Development **137**(1): 33-42.

Eto, M., S. Senba, et al. (1997). "Molecular cloning of a novel phosphorylation-dependent inhibitory protein of protein phosphatase-1 (CPI17) in smooth muscle: its specific localization in smooth muscle."

FEBS Lett **410**(2-3): 356-360.

Ezashi, T., P. Das, et al. (2005). "Low O2 tensions and the prevention of differentiation of hES cells." Proc Natl Acad Sci U S A **102**(13): 4783-4788.

Fantin, A., J. M. Vieira, et al. (2013). "NRP1 acts cell autonomously in endothelium to promote tip cell function during sprouting angiogenesis." Blood **121**(12): 2352-2362.

Feil, R., J. Brocard, et al. (1996). "Ligand-activated site-specific recombination in mice." Proc Natl Acad Sci U S A **93**(20): 10887-10890.

Fields, R. D. (2008). "White matter in learning, cognition and psychiatric disorders." Trends Neurosci **31**(7): 361-370.

Filtz, T. M., W. K. Vogel, et al. (2014). "Regulation of transcription factor activity by interconnected post-translational modifications." Trends Pharmacol Sci **35**(2): 76-85.

Fogarty, M., W. D. Richardson, et al. (2005). "A subset of oligodendrocytes generated from radial glia in the dorsal spinal cord." Development **132**(8): 1951-1959.

Fong, T. A., L. K. Shawver, et al. (1999). "SU5416 is a potent and selective inhibitor of the vascular endothelial growth factor receptor (Flk-1/KDR) that inhibits tyrosine kinase catalysis, tumor vascularization, and growth of multiple tumor types." Cancer Res **59**(1): 99-106.

Fragoso, G., J. D. Haines, et al. (2007). "p38 mitogen-activated protein kinase is required for central nervous system myelination." Glia **55**(15): 1531-1541.

Fu, H., Y. Qi, et al. (2002). "Dual origin of spinal oligodendrocyte progenitors and evidence for the cooperative role of Olig2 and Nkx2.2 in the control of oligodendrocyte differentiation." Development **129**(3): 681-693.

Fukuda, S., T. Kondo, et al. (2004). "Negative regulatory effect of an oligodendrocytic bHLH factor OLIG2 on the astrocytic differentiation pathway." Cell Death Differ **11**(2): 196-202.

Furusho, M., Y. Kaga, et al. (2011). "Fibroblast growth factor signaling is required for the generation of oligodendrocyte progenitors from the embryonic forebrain." J Neurosci **31**(13): 5055-5066.

Furusho, M., K. Ono, et al. (2006). "Involvement of the Olig2 transcription factor in cholinergic neuron

development of the basal forebrain." Dev Biol **293**(2): 348-357.

Genoud, S., C. Lappe-Siefke, et al. (2002). "Notch1 control of oligodendrocyte differentiation in the spinal cord." J Cell Biol **158**(4): 709-718.

Gerhardt, H., M. Golding, et al. (2003). "VEGF guides angiogenic sprouting utilizing endothelial tip cell filopodia." J Cell Biol **161**(6): 1163-1177.

Ghoumari, A. M., E. E. Baulieu, et al. (2005). "Progesterone increases oligodendroglial cell proliferation in rat cerebellar slice cultures." Neuroscience **135**(1): 47-58.

Ghoumari, A. M., C. Ibanez, et al. (2003). "Progesterone and its metabolites increase myelin basic protein expression in organotypic slice cultures of rat cerebellum." J Neurochem **86**(4): 848-859.

Givogri, M. I., R. M. Costa, et al. (2002). "Central nervous system myelination in mice with deficient expression of Notch1 receptor." J Neurosci Res **67**(3): 309-320.

Glaser, T., S. M. Pollard, et al. (2007). "Tripotential differentiation of adherently expandable neural stem (NS) cells." PLoS One **2**(3): e298.

Gorski, J. A., T. Talley, et al. (2002). "Cortical excitatory neurons and glia, but not GABAergic neurons, are produced in the Emx1-expressing lineage." J Neurosci **22**(15): 6309-6314.

Gunther, J. (1976). "Impulse conduction in the myelinated giant fibers of the earthworm. Structure and function of the dorsal nodes in the median giant fiber." J Comp Neurol **168**(4): 505-531.

Gustafsson, M. V., X. Zheng, et al. (2005). "Hypoxia requires notch signaling to maintain the undifferentiated cell state." Dev Cell **9**(5): 617-628.

Haiko, P., T. Makinen, et al. (2008). "Deletion of vascular endothelial growth factor C (VEGF-C) and VEGF-D is not equivalent to VEGF receptor 3 deletion in mouse embryos." Mol Cell Biol **28**(15): 4843-4850.

Haines, J. D., G. Fragoso, et al. (2008). "p38 Mitogen-activated protein kinase regulates myelination." J Mol Neurosci **35**(1): 23-33.

Harris, J. J. and D. Attwell (2012). "The energetics of CNS white matter." J Neurosci **32**(1): 356-371.

Hartline, D. K. and D. R. Colman (2007). "Rapid conduction and the evolution of giant axons and myelinated fibers." Curr Biol **17**(1): R29-35.

Hayakawa, K., L. D. Pham, et al. (2011). "Vascular endothelial growth factor regulates the migration of oligodendrocyte precursor cells." J Neurosci **31**(29): 10666-10670.

Hazzalin, C. A., R. Le Panse, et al. (1998). "Anisomycin selectively desensitizes signalling components involved in stress kinase activation and fos and jun induction." Mol Cell Biol **18**(4): 1844-1854.

He, W., C. Ingraham, et al. (2001). "Multipotent stem cells from the mouse basal forebrain contribute GABAergic neurons and oligodendrocytes to the cerebral cortex during embryogenesis." J Neurosci **21**(22): 8854-8862.

He, X., S. Takahashi, et al. (2011). "Hypomyelination phenotype caused by impaired differentiation of oligodendrocytes in Emx1-cre mediated Cdk5 conditional knockout mice." Neurochem Res **36**(7): 1293-1303.

Hellstrom, M., L. K. Phng, et al. (2007). "Dll4 signalling through Notch1 regulates formation of tip cells during angiogenesis." Nature **445**(7129): 776-780.

High, F. A., M. M. Lu, et al. (2008). "Endothelial expression of the Notch ligand Jagged1 is required for vascular smooth muscle development." Proc Natl Acad Sci U S A **105**(6): 1955-1959.

Hindley, C., F. Ali, et al. (2012). "Post-translational modification of Ngn2 differentially affects transcription of distinct targets to regulate the balance between progenitor maintenance and differentiation." Development **139**(10): 1718-1723.

Hisaoka, T., Y. Nakamura, et al. (2010). "The forkhead transcription factors, Foxp1 and Foxp2, identify different subpopulations of projection neurons in the mouse cerebral cortex." Neuroscience **166**(2): 551-563.

Hodgkin, A. L. (1954). "A note on conduction velocity." J Physiol **125**(1): 221-224.

Hoskins, E. R. (1914). "On the vascularisation of the spinal cord of the pig." Anat. Rec. **8**: 371-391.

Hu, J. G., S. L. Fu, et al. (2004). "Differential gene expression in neural stem cells and oligodendrocyte precursor cells: a cDNA microarray analysis." J Neurosci Res **78**(5): 637-646.

Hu, J. G., Y. X. Wang, et al. (2012). "PDGF-AA mediates B104CM-induced oligodendrocyte precursor cell differentiation of embryonic neural stem cells through Erk, PI3K, and p38 signaling." J Mol Neurosci **46**(3): 644-653.

Huang, J. K. and R. J. Franklin (2012). "Current status of myelin replacement therapies in multiple sclerosis." Prog Brain Res **201**: 219-231.

Huillard, E., L. Ziercher, et al. (2010). "Disruption of CK2beta in embryonic neural stem cells compromises proliferation and oligodendrogenesis in the mouse telencephalon." Mol Cell Biol **30**(11): 2737-2749.

Ikeda, A., S. Ikeda, et al. (2001). "Neural tube defects and neuroepithelial cell death in Tulp3 knockout mice." Hum Mol Genet **10**(12): 1325-1334.

Isogai, S., M. Horiguchi, et al. (2001). "The vascular anatomy of the developing zebrafish: an atlas of embryonic and early larval development." Dev Biol **230**(2): 278-301.

Issa, R., A. AlQteishat, et al. (2005). "Expression of basic fibroblast growth factor mRNA and protein in the human brain following ischaemic stroke." Angiogenesis **8**(1): 53-62.

Iyer, N. V., L. E. Kotch, et al. (1998). "Cellular and developmental control of O2 homeostasis by hypoxia-inducible factor 1 alpha." Genes Dev **12**(2): 149-162.

Jagannathan, N. R., N. Tandon, et al. (1998). "Reversal of abnormalities of myelination by thyroxine therapy in congenital hypothyroidism: localized in vivo proton magnetic resonance spectroscopy (MRS) study." Brain Res Dev Brain Res **109**(2): 179-186.

Jessell, T. M. (2000). "Neuronal specification in the spinal cord: inductive signals and transcriptional codes." Nat Rev Genet **1**(1): 20-29.

Johnson, J. E., S. J. Birren, et al. (1990). "Two rat homologues of Drosophila achaete-scute specifically expressed in neuronal precursors." Nature **346**(6287): 858-861.

Jones, S. (2004). "An overview of the basic helix-loop-helix proteins." Genome Biol **5**(6): 226.

Kageyama, R., T. Ohtsuka, et al. (2005). "Roles of bHLH genes in neural stem cell differentiation." Exp Cell Res **306**(2): 343-348.

Kardalinou, E., N. Zhelev, et al. (1994). "Anisomycin and rapamycin define an area upstream of p70/85S6k containing a bifurcation to histone H3-HMG-like protein phosphorylation and c-fos-c-jun induction." Mol Cell Biol **14**(2): 1066-1074.

Karlsson, J., J. von Hofsten, et al. (2001). "Generating transparent zebrafish: a refined method to improve detection of gene expression during embryonic development." Mar Biotechnol (NY) **3**(6): 522-527.

Kessaris, N., M. Fogarty, et al. (2006). "Competing waves of oligodendrocytes in the forebrain and postnatal elimination of an embryonic lineage." Nat Neurosci **9**(2): 173-179.

Kessaris, N., F. Jamen, et al. (2004). "Cooperation between sonic hedgehog and fibroblast growth factor/MAPK signalling pathways in neocortical precursors." Development **131**(6): 1289-1298.

Kessaris, N., N. Pringle, et al. (2001). "Ventral neurogenesis and the neuron-glial switch." Neuron **31**(5): 677-680.

Khwaja, O. and J. J. Volpe (2008). "Pathogenesis of cerebral white matter injury of prematurity." Arch Dis Child Fetal Neonatal Ed **93**(2): F153-161.

Kim, H., J. Shin, et al. (2008). "Notch-regulated oligodendrocyte specification from radial glia in the spinal cord of zebrafish embryos." Dev Dyn **237**(8): 2081-2089.

Kimmel, C. B., W. W. Ballard, et al. (1995). "Stages of embryonic development of the zebrafish." Dev Dyn **203**(3): 253-310.

Kippert, A., K. Trajkovic, et al. (2008). "Identification of Tmem10/Opalin as a novel marker for oligodendrocytes using gene expression profiling." BMC Neurosci **9**: 40.

Kirby, B. B., N. Takada, et al. (2006). "In vivo time-lapse imaging shows dynamic oligodendrocyte progenitor behavior during zebrafish development." Nat Neurosci **9**(12): 1506-1511.

Kitada, M. and D. H. Rowitch (2006). "Transcription factor co-expression patterns indicate heterogeneity of oligodendroglial subpopulations in adult spinal cord." Glia **54**(1): 35-46.

Kondo, T. and M. Raff (2000). "The Id4 HLH protein and the timing of oligodendrocyte differentiation." EMBO J **19**(9): 1998-2007.

Kondo, Y. and I. D. Duncan (2009). "Transplantation of oligodendrocyte progenitor cells in animal models of leukodystrophies." Methods Mol Biol **549**: 175-185.

Krogh, A. (1919). "The rate of diffusion of gases through animal tissues, with some remarks on the coefficient of invasion." J Physiol **52**(6): 391-408.

Kuhlbrodt, K., B. Herbarth, et al. (1998). "Sox10, a novel transcriptional modulator in glial cells." J Neurosci **18**(1): 237-250.

Kuspert, M., A. Hammer, et al. (2011). "Olig2 regulates Sox10 expression in oligodendrocyte precursors through an evolutionary conserved distal enhancer." Nucleic Acids Res **39**(4): 1280-1293.

Langman, J. and C. C. Haden (1970). "Formation and migration of neuroblasts in the spinal cord of the chick embryo." J Comp Neurol **138**(4): 419-425.

Langseth, A. J., R. N. Munji, et al. (2010). "Wnts influence the timing and efficiency of oligodendrocyte precursor cell generation in the telencephalon." J Neurosci **30**(40): 13367-13372.

Leber, S. M., S. M. Breedlove, et al. (1990). "Lineage, arrangement, and death of clonally related motoneurons in chick spinal cord." J Neurosci **10**(7): 2451-2462.

Lee, E. C., D. Yu, et al. (2001). "A highly efficient Escherichia coli-based chromosome engineering system adapted for recombinogenic targeting and subcloning of BAC DNA." Genomics **73**(1): 56-65.

Lee, S. K., L. W. Jurata, et al. (2004). "Analysis of embryonic motoneuron gene regulation: derepression of general activators function in concert with enhancer factors." Development **131**(14): 3295-3306.

Lee, S. K., B. Lee, et al. (2005). "Olig2 and Ngn2 function in opposition to modulate gene expression in motor neuron progenitor cells." Genes Dev **19**(2): 282-294.

Lendahl, U., L. B. Zimmerman, et al. (1990). "CNS stem cells express a new class of intermediate filament protein." Cell **60**(4): 585-595.

Leung, S. F., M. W. Law, et al. (1992). "Efficacy of low-dose iodine-131 ablation of post-operative thyroid remnants: a study of 69 cases." Br J Radiol **65**(778): 905-909.

Leventhal, C., S. Rafii, et al. (1999). "Endothelial trophic support of neuronal production and recruitment from the adult mammalian subependyma." Mol Cell Neurosci **13**(6): 450-464.

Levison, S. W. and J. E. Goldman (1993). "Both oligodendrocytes and astrocytes develop from progenitors in the subventricular zone of postnatal rat forebrain." Neuron **10**(2): 201-212.

Lew, J., Q. Q. Huang, et al. (1994). "A brain-specific activator of cyclin-dependent kinase 5." Nature **371**(6496): 423-426.

Li, H., J. P. de Faria, et al. (2011). "Phosphorylation regulates OLIG2 cofactor choice and the motor neuron-oligodendrocyte fate switch." Neuron **69**(5): 918-929.

Li, H., Y. Lu, et al. (2007). "Olig1 and Sox10 interact synergistically to drive myelin basic protein transcription in oligodendrocytes." J Neurosci **27**(52): 14375-14382.

Li, H. and W. D. Richardson (2008). "The evolution of Olig genes and their roles in myelination." Neuron Glia Biol **4**(2): 129-135.

Li, Z., L. Yu, et al. (2001). "Identification of human, mouse and rat PPP1R14A, protein phosphatase-1 inhibitor subunit 14A, & mapping human PPP1R14A to chromosome 19q13.13-q13.2." Mol Biol Rep **28**(2): 91-101.

Ligon, K. L., J. A. Alberta, et al. (2004). "The oligodendroglial lineage marker OLIG2 is universally expressed in diffuse gliomas." J Neuropathol Exp Neurol **63**(5): 499-509.

Ligon, K. L., S. P. Fancy, et al. (2006). "Olig gene function in CNS development and disease." Glia **54**(1): 1-10.

Ligon, K. L., E. Huillard, et al. (2007). "Olig2-regulated lineage-restricted pathway controls replication competence in neural stem cells and malignant glioma." Neuron **53**(4): 503-517.

Ligon, K. L., S. Kesari, et al. (2006). "Development of NG2 neural progenitor cells requires Olig gene function." Proc Natl Acad Sci U S A **103**(20): 7853-7858.

Liu, R., J. Cai, et al. (2003). "Region-specific and stage-dependent regulation of Olig gene expression and oligodendrogenesis by Nkx6.1 homeodomain transcription factor." Development **130**(25): 6221-6231.

Liu, Z., X. Hu, et al. (2007). "Induction of oligodendrocyte differentiation by Olig2 and Sox10: evidence for reciprocal interactions and dosage-dependent mechanisms." Dev Biol **302**(2): 683-693.

Lobov, I. B., R. A. Renard, et al. (2007). "Delta-like ligand 4 (Dll4) is induced by VEGF as a negative regulator of angiogenic sprouting." Proc Natl Acad Sci U S A **104**(9): 3219-3224.

Lok, J., P. Gupta, et al. (2007). "Cell-cell signaling in the neurovascular unit." Neurochem Res **32**(12): 2032-2045.

Lord, E. M., L. Harwell, et al. (1993). "Detection of hypoxic cells by monoclonal antibody recognizing 2-nitroimidazole adducts." Cancer Res **53**(23): 5721-5726.

Louvi, A. and S. Artavanis-Tsakonas (2006). "Notch signalling in vertebrate neural development." Nat Rev Neurosci **7**(2): 93-102.

Lu, Q. R., T. Sun, et al. (2002). "Common developmental requirement for Olig function indicates a motor neuron/oligodendrocyte connection." Cell **109**(1): 75-86.

Lu, Q. R., D. Yuk, et al. (2000). "Sonic hedgehog--regulated oligodendrocyte lineage genes encoding bHLH proteins in the mammalian central nervous system." Neuron **25**(2): 317-329.

Luo, F., K. Burke, et al. (2014). "Cyclin-dependent kinase 5 mediates adult OPC maturation and myelin repair through modulation of Akt and GsK-3beta signaling." J Neurosci **34**(31): 10415-10429.

Lyons, D. A. and W. S. Talbot (2015). "Glial cell development and function in zebrafish." Cold Spring Harb Perspect Biol **7**(2): a020586.

Ma, S., H. J. Kwon, et al. (2013). "Radial glial neural progenitors regulate nascent brain vascular network stabilization via inhibition of Wnt signaling." PLoS Biol **11**(1): e1001469.

Maire, C. L., D. Buchet, et al. (2009). "Directing human neural stem/precursor cells into oligodendrocytes by overexpression of Olig2 transcription factor." J Neurosci Res **87**(15): 3438-3446.

Marshall, C. A. and J. E. Goldman (2002). "Subpallial dlx2-expressing cells give rise to astrocytes and oligodendrocytes in the cerebral cortex and white matter." J Neurosci **22**(22): 9821-9830.

Marshall, C. A., B. G. Novitch, et al. (2005). "Olig2 directs astrocyte and oligodendrocyte formation in postnatal subventricular zone cells." J Neurosci **25**(32): 7289-7298.

Marta, C. B., A. M. Adamo, et al. (1998). "Sustained neonatal hyperthyroidism in the rat affects myelination in the central nervous system." J Neurosci Res **53**(2): 251-259.

Marti, E., D. A. Bumcrot, et al. (1995). "Requirement of 19K form of Sonic hedgehog for induction of distinct ventral cell types in CNS explants." Nature **375**(6529): 322-325.

Masahira, N., H. Takebayashi, et al. (2006). "Olig2-positive progenitors in the embryonic spinal cord give rise not only to motoneurons and oligodendrocytes, but also to a subset of astrocytes and ependymal cells." Dev Biol **293**(2): 358-369.

Massari, M. E. and C. Murre (2000). "Helix-loop-helix proteins: regulators of transcription in eucaryotic organisms." Mol Cell Biol **20**(2): 429-440.

Mateo, J. L., D. L. van den Berg, et al. (2015). "Characterization of the neural stem cell gene regulatory network identifies OLIG2 as a multifunctional regulator of self-renewal." Genome Res **25**(1): 41-56.

Matsusue, Y., N. Horii-Hayashi, et al. (2014). "Distribution of corticosteroid receptors in mature oligodendrocytes and oligodendrocyte progenitors of the adult mouse brain." J Histochem Cytochem **62**(3): 211-226.

Mazumdar, J., W. T. O'Brien, et al. (2010). "O2 regulates stem cells through Wnt/beta-catenin signalling." Nat Cell Biol **12**(10): 1007-1013.

McKenzie, I. A., D. Ohayon, et al. (2014). "Motor skill learning requires active central myelination." Science **346**(6207): 318-322.

McMorris, F. A. and M. Dubois-Dalcq (1988). "Insulin-like growth factor I promotes cell proliferation and oligodendroglial commitment in rat glial progenitor cells developing in vitro." J Neurosci Res **21**(2-4): 199-209.

Mei, F., H. Wang, et al. (2013). "Stage-specific deletion of Olig2 conveys opposing functions on differentiation and maturation of oligodendrocytes." J Neurosci **33**(19): 8454-8462.

Meijer, D. H., M. F. Kane, et al. (2012). "Separated at birth? The functional and molecular divergence of OLIG1 and OLIG2." Nat Rev Neurosci **13**(12): 819-831.

Meijer, D. H., Y. Sun, et al. (2014). "An amino terminal phosphorylation motif regulates intranuclear compartmentalization of Olig2 in neural progenitor cells." J Neurosci **34**(25): 8507-8518.

Mekki-Dauriac, S., E. Agius, et al. (2002). "Bone morphogenetic proteins negatively control

oligodendrocyte precursor specification in the chick spinal cord." Development **129**(22): 5117-5130.

Miller, R. H., K. Dinsio, et al. (2004). "Patterning of spinal cord oligodendrocyte development by dorsally derived BMP4." J Neurosci Res **76**(1): 9-19.

Milo, R. and E. Kahana (2010). "Multiple sclerosis: geoepidemiology, genetics and the environment." Autoimmun Rev **9**(5): A387-394.

Miyamoto, N., T. Maki, et al. (2013). "Oxidative stress interferes with white matter renewal after prolonged cerebral hypoperfusion in mice." Stroke **44**(12): 3516-3521.

Miyamoto, Y., J. Yamauchi, et al. (2007). "Cdk5 regulates differentiation of oligodendrocyte precursor cells through the direct phosphorylation of paxillin." J Cell Sci **120**(Pt 24): 4355-4366.

Miyamoto, Y., J. Yamauchi, et al. (2008). "Cdk5 phosphorylation of WAVE2 regulates oligodendrocyte precursor cell migration through nonreceptor tyrosine kinase Fyn." J Neurosci **28**(33): 8326-8337.

Miyoshi, G., S. J. Butt, et al. (2007). "Physiologically distinct temporal cohorts of cortical interneurons arise from telencephalic Olig2-expressing precursors." J Neurosci **27**(29): 7786-7798.

Mizuguchi, R., M. Sugimori, et al. (2001). "Combinatorial roles of olig2 and neurogenin2 in the coordinated induction of pan-neuronal and subtype-specific properties of motoneurons." Neuron **31**(5): 757-771.

Mohyeldin, A., T. Garzon-Muvdi, et al. (2010). "Oxygen in stem cell biology: a critical component of the stem cell niche." Cell Stem Cell **7**(2): 150-161.

Moore, J. W., R. W. Joyner, et al. (1978). "Simulations of conduction in uniform myelinated fibers. Relative sensitivity to changes in nodal and internodal parameters." Biophys J **21**(2): 147-160.

Mozell, R. L. and F. A. McMorris (1991). "Insulin-like growth factor I stimulates oligodendrocyte development and myelination in rat brain aggregate cultures." J Neurosci Res **30**(2): 382-390.

Mukherjee, T., W. S. Kim, et al. (2011). "Interaction between Notch and Hif-alpha in development and survival of Drosophila blood cells." Science **332**(6034): 1210-1213.

Murre, C., P. S. McCaw, et al. (1989). "Interactions between heterologous helix-loop-helix proteins generate complexes that bind specifically to a common DNA sequence." Cell **58**(3): 537-544.

Nagase, T., M. Nagase, et al. (2005). "Angiogenesis within the developing mouse neural tube is dependent on sonic hedgehog signaling: possible roles of motor neurons." Genes Cells **10**(6): 595-604.

Naruse, M., E. Nakahira, et al. (2006). "Induction of oligodendrocyte progenitors in dorsal forebrain by intraventricular microinjection of FGF-2." Dev Biol **297**(1): 262-273.

Nielsen, J. A., D. Maric, et al. (2006). "Identification of a novel oligodendrocyte cell adhesion protein using gene expression profiling." J Neurosci **26**(39): 9881-9891.

Nishiyama, A., M. Komitova, et al. (2009). "Polydendrocytes (NG2 cells): multifunctional cells with lineage plasticity." Nat Rev Neurosci **10**(1): 9-22.

Noll, E. and R. H. Miller (1993). "Oligodendrocyte precursors originate at the ventral ventricular zone dorsal to the ventral midline region in the embryonic rat spinal cord." Development **118**(2): 563-573.

Novitch, B. G., A. I. Chen, et al. (2001). "Coordinate regulation of motor neuron subtype identity and pan-neuronal properties by the bHLH repressor Olig2." Neuron **31**(5): 773-789.

Ono, K., H. Takebayashi, et al. (2008). "Regional- and temporal-dependent changes in the differentiation of Olig2 progenitors in the forebrain, and the impact on astrocyte development in the dorsal pallium." Dev Biol **320**(2): 456-468.

Ozaki, H., A. Y. Yu, et al. (1999). "Hypoxia inducible factor-1alpha is increased in ischemic retina: temporal and spatial correlation with VEGF expression." Invest Ophthalmol Vis Sci **40**(1): 182-189.

Paes de Faria, J., N. Kessaris, et al. (2014). "New Olig1 null mice confirm a non-essential role for Olig1 in oligodendrocyte development." BMC Neurosci **15**: 12.

Panchision, D. M. (2009). "The role of oxygen in regulating neural stem cells in development and disease." J Cell Physiol **220**(3): 562-568.

Park, H. C. and B. Appel (2003). "Delta-Notch signaling regulates oligodendrocyte specification." Development **130**(16): 3747-3755.

Park, H. C., A. Mehta, et al. (2002). "olig2 is required for zebrafish primary motor neuron and oligodendrocyte development." Dev Biol **248**(2): 356-368.

Park, H. C., J. Shin, et al. (2004). "Spatial and temporal regulation of ventral spinal cord precursor specification by Hedgehog signaling." Development **131**(23): 5959-5969.

Pattyn, A., A. Vallstedt, et al. (2003). "Complementary roles for Nkx6 and Nkx2 class proteins in the establishment of motoneuron identity in the hindbrain." Development **130**(17): 4149-4159.

Pearce, L. R., D. Komander, et al. (2010). "The nuts and bolts of AGC protein kinases." Nat Rev Mol Cell Biol **11**(1): 9-22.

Perez Estrada, C., R. Covacu, et al. (2014). "Oxidative stress increases neurogenesis and oligodendrogenesis in adult neural progenitor cells." Stem Cells Dev **23**(19): 2311-2327.

Peti, W., A. C. Nairn, et al. (2013). "Structural basis for protein phosphatase 1 regulation and specificity." FEBS J **280**(2): 596-611.

Pistollato, F., H. L. Chen, et al. (2007). "Oxygen tension controls the expansion of human CNS precursors and the generation of astrocytes and oligodendrocytes." Mol Cell Neurosci **35**(3): 424-435.

Pollard, S. M., L. Conti, et al. (2006). "Adherent neural stem (NS) cells from fetal and adult forebrain." Cereb Cortex **16 Suppl 1**: i112-120.

Pombo, P. M., N. Ibarrola, et al. (1998). "Thyroid hormone regulates the expression of the MAL proteolipid, a component of glycolipid-enriched membranes, in neonatal rat brain." J Neurosci Res **52**(5): 584-590.

Preston, S. L. and F. A. McMorris (1984). "Adrenalectomy of rats results in hypomyelination of the central nervous system." J Neurochem **42**(1): 262-267.

Pringle, N. P. and W. D. Richardson (1993). "A singularity of PDGF alpha-receptor expression in the dorsoventral axis of the neural tube may define the origin of the oligodendrocyte lineage." Development **117**(2): 525-533.

Pringle, N. P., W. P. Yu, et al. (1996). "Determination of neuroepithelial cell fate: induction of the oligodendrocyte lineage by ventral midline cells and sonic hedgehog." Dev Biol **177**(1): 30-42.

Qi, Y., J. Cai, et al. (2001). "Control of oligodendrocyte differentiation by the Nkx2.2 homeodomain transcription factor." Development **128**(14): 2723-2733.

Qiu, M., K. Shimamura, et al. (1998). "Control of anteroposterior and dorsoventral domains of Nkx-6.1 gene expression relative to other Nkx genes during vertebrate CNS development." Mech Dev **72**(1-2): 77-88.

Rabadan, M. A., J. Cayuso, et al. (2012). "Jagged2 controls the generation of motor neuron and oligodendrocyte progenitors in the ventral spinal cord." Cell Death Differ **19**(2): 209-219.

Rafalski, V. A., P. P. Ho, et al. (2013). "Expansion of oligodendrocyte progenitor cells following SIRT1 inactivation in the adult brain." Nat Cell Biol **15**(6): 614-624.

Raff, M. C., K. L. Fields, et al. (1979). "Cell-type-specific markers for distinguishing and studying neurons and the major classes of glial cells in culture." Brain Res **174**(2): 283-308.

Ramirez-Bergeron, D. L., A. Runge, et al. (2006). "HIF-dependent hematopoietic factors regulate the development of the embryonic vasculature." Dev Cell **11**(1): 81-92.

Richardson, W. D., N. Kessaris, et al. (2006). "Oligodendrocyte wars." Nat Rev Neurosci **7**(1): 11-18.

Richardson, W. D., N. P. Pringle, et al. (1997). "Origins of spinal cord oligodendrocytes: possible developmental and evolutionary relationships with motor neurons." Dev Neurosci **19**(1): 58-68.

Richardson, W. D., H. K. Smith, et al. (2000). "Oligodendrocyte lineage and the motor neuron connection." Glia **29**(2): 136-142.

Rodriguez-Pena, A., N. Ibarrola, et al. (1993). "Neonatal hypothyroidism affects the timely expression of myelin-associated glycoprotein in the rat brain." J Clin Invest **91**(3): 812-818.

Roelink, H., J. A. Porter, et al. (1995). "Floor plate and motor neuron induction by different concentrations of the amino-terminal cleavage product of sonic hedgehog autoproteolysis." Cell **81**(3): 445-455.

Rojas, D. A., D. A. Perez-Munizaga, et al. (2007). "Cloning of hif-1alpha and hif-2alpha and mRNA expression pattern during development in zebrafish." Gene Expr Patterns **7**(3): 339-345.

Rowitch, D. H. (2004). "Glial specification in the vertebrate neural tube." Nat Rev Neurosci **5**(5): 409-419.

Rowitch, D. H., S. J. B, et al. (1999). "Sonic hedgehog regulates proliferation and inhibits differentiation

of CNS precursor cells." J Neurosci **19**(20): 8954-8965.

Sahlgren, C., M. V. Gustafsson, et al. (2008). "Notch signaling mediates hypoxia-induced tumor cell migration and invasion." Proc Natl Acad Sci U S A **105**(17): 6392-6397.

Samanta, J. and J. A. Kessler (2004). "Interactions between ID and OLIG proteins mediate the inhibitory effects of BMP4 on oligodendroglial differentiation." Development **131**(17): 4131-4142.

Schoch, H. J., S. Fischer, et al. (2002). "Hypoxia-induced vascular endothelial growth factor expression causes vascular leakage in the brain." Brain **125**(Pt 11): 2549-2557.

Schuller, U., V. M. Heine, et al. (2008). "Acquisition of granule neuron precursor identity is a critical determinant of progenitor cell competence to form Shh-induced medulloblastoma." Cancer Cell **14**(2): 123-134.

Sendtner, M., G. Pei, et al. (2000). "Developmental motoneuron cell death and neurotrophic factors." Cell Tissue Res **301**(1): 71-84.

Setoguchi, T. and T. Kondo (2004). "Nuclear export of OLIG2 in neural stem cells is essential for ciliary neurotrophic factor-induced astrocyte differentiation." J Cell Biol **166**(7): 963-968.

Shalaby, F., J. Rossant, et al. (1995). "Failure of blood-island formation and vasculogenesis in Flk-1-deficient mice." Nature **376**(6535): 62-66.

Shen, Q., S. K. Goderie, et al. (2004). "Endothelial cells stimulate self-renewal and expand neurogenesis of neural stem cells." Science **304**(5675): 1338-1340.

Shen, Q., Y. Wang, et al. (2008). "Adult SVZ stem cells lie in a vascular niche: a quantitative analysis of niche cell-cell interactions." Cell Stem Cell **3**(3): 289-300.

Siekmann, A. F. and N. D. Lawson (2007). "Notch signalling limits angiogenic cell behaviour in developing zebrafish arteries." Nature **445**(7129): 781-784.

Silbereis, J. C., H. Nobuta, et al. (2014). "Olig1 function is required to repress dlx1/2 and interneuron production in Mammalian brain." Neuron **81**(3): 574-587.

Sommer, L., Q. Ma, et al. (1996). "neurogenins, a novel family of atonal-related bHLH transcription factors, are putative mammalian neuronal determination genes that reveal progenitor cell

heterogeneity in the developing CNS and PNS." Mol Cell Neurosci **8**(4): 221-241.

Sorensen, I., R. H. Adams, et al. (2009). "DLL1-mediated Notch activation regulates endothelial identity in mouse fetal arteries." Blood **113**(22): 5680-5688.

Spassky, N., C. Olivier, et al. (2000). "Single or multiple oligodendroglial lineages: a controversy." Glia **29**(2): 143-148.

Sterzi, G. (1904). "Die Blutgefasse des Riickenmarks." Arb. anat. Inst. Wiesbaden. **24**: 3-364.

Studer, L., M. Csete, et al. (2000). "Enhanced proliferation, survival, and dopaminergic differentiation of CNS precursors in lowered oxygen." J Neurosci **20**(19): 7377-7383.

Suchting, S., C. Freitas, et al. (2007). "The Notch ligand Delta-like 4 negatively regulates endothelial tip cell formation and vessel branching." Proc Natl Acad Sci U S A **104**(9): 3225-3230.

Sun, T., H. Dong, et al. (2003). "Cross-repressive interaction of the Olig2 and Nkx2.2 transcription factors in developing neural tube associated with formation of a specific physical complex." J Neurosci **23**(29): 9547-9556.

Sun, T., Y. Echelard, et al. (2001). "Olig bHLH proteins interact with homeodomain proteins to regulate cell fate acquisition in progenitors of the ventral neural tube." Curr Biol **11**(18): 1413-1420.

Sun, T., N. P. Pringle, et al. (1998). "Pax6 influences the time and site of origin of glial precursors in the ventral neural tube." Mol Cell Neurosci **12**(4-5): 228-239.

Sun, Y., D. H. Meijer, et al. (2011). "Phosphorylation state of Olig2 regulates proliferation of neural progenitors." Neuron **69**(5): 906-917.

Suzuki, N., M. Fukushi, et al. (2012). "Teneurin-4 is a novel regulator of oligodendrocyte differentiation and myelination of small-diameter axons in the CNS." J Neurosci **32**(34): 11586-11599.

Takebayashi, H., T. Ohtsuki, et al. (2002). "Non-overlapping expression of Olig3 and Olig2 in the embryonic neural tube." Mech Dev **113**(2): 169-174.

Takebayashi, H., S. Yoshida, et al. (2000). "Dynamic expression of basic helix-loop-helix Olig family members: implication of Olig2 in neuron and oligodendrocyte differentiation and identification of a new member, Olig3." Mech Dev **99**(1-2): 143-148.

Takeshita, K., M. Satoh, et al. (2007). "Critical role of endothelial Notch1 signaling in postnatal angiogenesis." Circ Res **100**(1): 70-78.

Tammela, T., G. Zarkada, et al. (2011). "VEGFR-3 controls tip to stalk conversion at vessel fusion sites by reinforcing Notch signalling." Nat Cell Biol **13**(10): 1202-1213.

Tammela, T., G. Zarkada, et al. (2008). "Blocking VEGFR-3 suppresses angiogenic sprouting and vascular network formation." Nature **454**(7204): 656-660.

Tan, Y., J. Rouse, et al. (1996). "FGF and stress regulate CREB and ATF-1 via a pathway involving p38 MAP kinase and MAPKAP kinase-2." EMBO J **15**(17): 4629-4642.

Tanabe, Y., H. Roelink, et al. (1995). "Induction of motor neurons by Sonic hedgehog is independent of floor plate differentiation." Curr Biol **5**(6): 651-658.

Tang, D., J. Yeung, et al. (1995). "An isoform of the neuronal cyclin-dependent kinase 5 (Cdk5) activator." J Biol Chem **270**(45): 26897-26903.

Tang, X. M., P. Strocchi, et al. (1998). "Changes in the activity of cdk2 and cdk5 accompany differentiation of rat primary oligodendrocytes." J Cell Biochem **68**(1): 128-137.

Tang, X. M., P. Strocchi, et al. (1998). "Changes in the activity of cdk2 and cdk5 accompany differentiation of rat primary oligodendrocytes." J Cell Biochem **68**(1): 128-137.

Tavazoie, M., L. Van der Veken, et al. (2008). "A specialized vascular niche for adult neural stem cells." Cell Stem Cell **3**(3): 279-288.

Tekki-Kessaris, N., R. Woodruff, et al. (2001). "Hedgehog-dependent oligodendrocyte lineage specification in the telencephalon." Development **128**(13): 2545-2554.

Timsit, S., S. Martinez, et al. (1995). "Oligodendrocytes originate in a restricted zone of the embryonic ventral neural tube defined by DM-20 mRNA expression." J Neurosci **15**(2): 1012-1024.

Tomita, S., M. Ueno, et al. (2003). "Defective brain development in mice lacking the Hif-1alpha gene in neural cells." Mol Cell Biol **23**(19): 6739-6749.

Tripathi, R. B., L. E. Clarke, et al. (2011). "Dorsally and ventrally derived oligodendrocytes have similar

electrical properties but myelinate preferred tracts." J Neurosci **31**(18): 6809-6819.

Tsai, L. H., I. Delalle, et al. (1994). "p35 is a neural-specific regulatory subunit of cyclin-dependent kinase 5." Nature **371**(6496): 419-423.

Tung, J. J., I. W. Tattersall, et al. (2012). "Tips, stalks, tubes: notch-mediated cell fate determination and mechanisms of tubulogenesis during angiogenesis." Cold Spring Harb Perspect Med **2**(2): a006601.

Ulloa, F. and J. Briscoe (2007). "Morphogens and the control of cell proliferation and patterning in the spinal cord." Cell Cycle **6**(21): 2640-2649.

Ushkaryov, Y. A., A. G. Petrenko, et al. (1992). "Neurexins: synaptic cell surface proteins related to the alpha-latrotoxin receptor and laminin." Science **257**(5066): 50-56.

Vallstedt, A., J. M. Klos, et al. (2005). "Multiple dorsoventral origins of oligodendrocyte generation in the spinal cord and hindbrain." Neuron **45**(1): 55-67.

Vallstedt, A., J. Muhr, et al. (2001). "Different levels of repressor activity assign redundant and specific roles to Nkx6 genes in motor neuron and interneuron specification." Neuron **31**(5): 743-755.

Van't Veer, A., Y. Du, et al. (2009). "Brain-derived neurotrophic factor effects on oligodendrocyte progenitors of the basal forebrain are mediated through trkB and the MAP kinase pathway." J Neurosci Res **87**(1): 69-78.

Varia, M. A., D. P. Calkins-Adams, et al. (1998). "Pimonidazole: a novel hypoxia marker for complementary study of tumor hypoxia and cell proliferation in cervical carcinoma." Gynecol Oncol **71**(2): 270-277.

Varjosalo, M., S. Keskitalo, et al. (2013). "The protein interaction landscape of the human CMGC kinase group." Cell Rep **3**(4): 1306-1320.

Volpe, J. J. (2003). "Cerebral white matter injury of the premature infant-more common than you think." Pediatrics **112**(1 Pt 1): 176-180.

Vondran, M. W., P. Clinton-Luke, et al. (2010). "BDNF+/- mice exhibit deficits in oligodendrocyte lineage cells of the basal forebrain." Glia **58**(7): 848-856.

Walters, S. N. and P. Morell (1981). "Effects of altered thyroid states on myelinogenesis." J Neurochem

36(5): 1792-1801.

Wang, G. L., B. H. Jiang, et al. (1995). "Hypoxia-inducible factor 1 is a basic-helix-loop-helix-PAS heterodimer regulated by cellular O2 tension." Proc Natl Acad Sci U S A **92**(12): 5510-5514.

Wang, G. L. and G. L. Semenza (1993). "General involvement of hypoxia-inducible factor 1 in transcriptional response to hypoxia." Proc Natl Acad Sci U S A **90**(9): 4304-4308.

Wang, R., Y. W. Zhang, et al. (2006). "Transcriptional regulation of APH-1A and increased gamma-secretase cleavage of APP and Notch by HIF-1 and hypoxia." FASEB J **20**(8): 1275-1277.

Wang, S., J. Bates, et al. (2013). "Human iPSC-derived oligodendrocyte progenitor cells can myelinate and rescue a mouse model of congenital hypomyelination." Cell Stem Cell **12**(2): 252-264.

Wang, S., A. D. Sdrulla, et al. (1998). "Notch receptor activation inhibits oligodendrocyte differentiation." Neuron **21**(1): 63-75.

Wang, Y., M. Nakayama, et al. (2010). "Ephrin-B2 controls VEGF-induced angiogenesis and lymphangiogenesis." Nature **465**(7297): 483-486.

Warf, B. C., J. Fok-Seang, et al. (1991). "Evidence for the ventral origin of oligodendrocyte precursors in the rat spinal cord." J Neurosci **11**(8): 2477-2488.

Watterson, F. L. and J. F. Feeney (1946). "The development of the vascular pattern within the walls of the spinal cord of the chick embryo." Anat Rec **94**: 396.

Wegner, M. and C. C. Stolt (2005). "From stem cells to neurons and glia: a Soxist's view of neural development." Trends Neurosci **28**(11): 583-588.

Weidemann, A. and R. S. Johnson (2008). "Biology of HIF-1alpha." Cell Death Differ **15**(4): 621-627.

Weng, Q., Y. Chen, et al. (2012). "Dual-mode modulation of Smad signaling by Smad-interacting protein Sip1 is required for myelination in the central nervous system." Neuron **73**(4): 713-728.

Whitmarsh, A. J. and R. J. Davis (2000). "Regulation of transcription factor function by phosphorylation." Cell Mol Life Sci **57**(8-9): 1172-1183.

Williams, B. P., J. Read, et al. (1991). "The generation of neurons and oligodendrocytes from a common

precursor cell." Neuron **7**(4): 685-693.

Winkler, D. G., I. Park, et al. (1993). "Phosphorylation of Ser-42 and Ser-59 in the N-terminal region of the tyrosine kinase p56lck." Proc Natl Acad Sci U S A **90**(11): 5176-5180.

Wissmuller, S., T. Kosian, et al. (2006). "The high-mobility-group domain of Sox proteins interacts with DNA-binding domains of many transcription factors." Nucleic Acids Res **34**(6): 1735-1744.

Wolfer, A., T. Bakker, et al. (2001). "Inactivation of Notch 1 in immature thymocytes does not perturb CD4 or CD8T cell development." Nat Immunol **2**(3): 235-241.

Xiao, J., A. W. Wong, et al. (2010). "Brain-derived neurotrophic factor promotes central nervous system myelination via a direct effect upon oligodendrocytes." Neurosignals **18**(3): 186-202.

Xue, G. and B. A. Hemmings (2012). "Phosphorylation of basic helix-loop-helix transcription factor Twist in development and disease." Biochem Soc Trans **40**(1): 90-93.

Yamada, T., M. Placzek, et al. (1991). "Control of cell pattern in the developing nervous system: polarizing activity of the floor plate and notochord." Cell **64**(3): 635-647.

Yang, Y., H. Wang, et al. (2013). "Cyclin dependent kinase 5 is required for the normal development of oligodendrocytes and myelin formation." Dev Biol **378**(2): 94-106.

Yasuda, A., O. Tsuji, et al. (2011). "Significance of remyelination by neural stem/progenitor cells transplanted into the injured spinal cord." Stem Cells **29**(12): 1983-1994.

Yu, W. P., E. J. Collarini, et al. (1994). "Embryonic expression of myelin genes: evidence for a focal source of oligodendrocyte precursors in the ventricular zone of the neural tube." Neuron **12**(6): 1353-1362.

Yu, Y., Y. Chen, et al. (2013). "Olig2 targets chromatin remodelers to enhancers to initiate oligodendrocyte differentiation." Cell **152**(1-2): 248-261.

Yue, T., K. Xian, et al. (2006). "A critical role for dorsal progenitors in cortical myelination." J Neurosci **26**(4): 1275-1280.

Yuen, T. J., J. C. Silbereis, et al. (2014). "Oligodendrocyte-encoded HIF function couples postnatal myelination and white matter angiogenesis." Cell **158**(2): 383-396.

Zarubin, T. and J. Han (2005). "Activation and signaling of the p38 MAP kinase pathway." Cell Res **15**(1): 11-18.

Zeger, M., G. Popken, et al. (2007). "Insulin-like growth factor type 1 receptor signaling in the cells of oligodendrocyte lineage is required for normal in vivo oligodendrocyte development and myelination." Glia **55**(4): 400-411.

Zheng, X., S. Linke, et al. (2008). "Interaction with factor inhibiting HIF-1 defines an additional mode of cross-coupling between the Notch and hypoxia signaling pathways." Proc Natl Acad Sci U S A **105**(9): 3368-3373.

Zhou, Q. and D. J. Anderson (2002). "The bHLH transcription factors OLIG2 and OLIG1 couple neuronal and glial subtype specification." Cell **109**(1): 61-73.

Zhou, Q., G. Choi, et al. (2001). "The bHLH transcription factor Olig2 promotes oligodendrocyte differentiation in collaboration with Nkx2.2." Neuron **31**(5): 791-807.

Zhou, Q., S. Wang, et al. (2000). "Identification of a novel family of oligodendrocyte lineage-specific basic helix-loop-helix transcription factors." Neuron **25**(2): 331-343.

Zhu, X., R. A. Hill, et al. (2011). "Age-dependent fate and lineage restriction of single NG2 cells." Development **138**(4): 745-753.

Zhu, X., H. Zuo, et al. (2012). "Olig2-dependent developmental fate switch of NG2 cells." Development **139**(13): 2299-2307.

Zinck, R., M. A. Cahill, et al. (1995). "Protein synthesis inhibitors reveal differential regulation of mitogen-activated protein kinase and stress-activated protein kinase pathways that converge on Elk-1." Mol Cell Biol **15**(9): 4930-4938.